



HAL
open science

DC Microgrid optimized energy management and real-time control of power systems for grid-connected and off-grid operating modes

Wenshuai Bai

► **To cite this version:**

Wenshuai Bai. DC Microgrid optimized energy management and real-time control of power systems for grid-connected and off-grid operating modes. Electric power. Université de Technologie de Compiègne, 2021. English. NNT : 2021COMP2586 . tel-03313913

HAL Id: tel-03313913

<https://theses.hal.science/tel-03313913>

Submitted on 4 Aug 2021

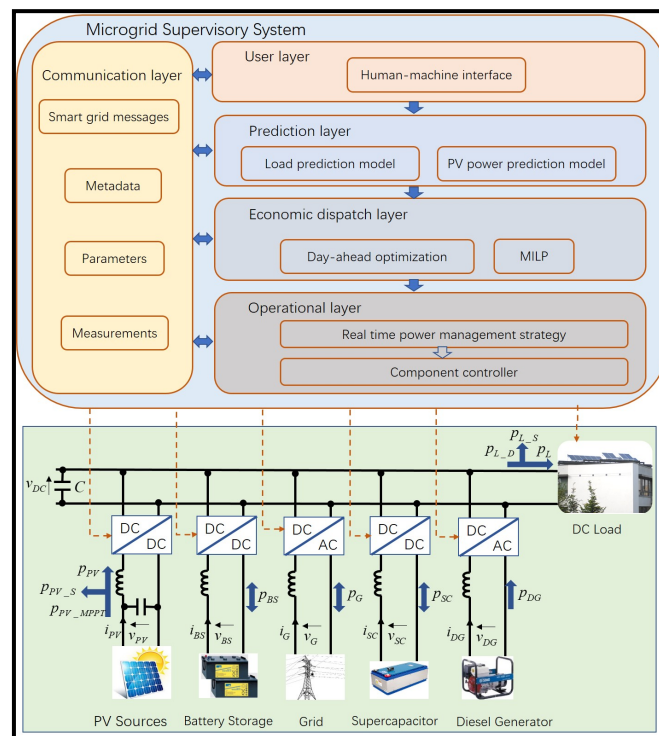
HAL is a multi-disciplinary open access archive for the deposit and dissemination of scientific research documents, whether they are published or not. The documents may come from teaching and research institutions in France or abroad, or from public or private research centers.

L'archive ouverte pluridisciplinaire **HAL**, est destinée au dépôt et à la diffusion de documents scientifiques de niveau recherche, publiés ou non, émanant des établissements d'enseignement et de recherche français ou étrangers, des laboratoires publics ou privés.

Par **Wenshuai BAI**

DC Microgrid optimized energy management and real-time control of power systems for grid-connected and off-grid operating modes

Thèse présentée
pour l'obtention du grade
de Docteur de l'UTC



Soutenue le 21 janvier 2021
Spécialité : Génie Électrique : Laboratoire Avenues - EA-7284

D2586

UNIVERSITÉ DE TECHNOLOGIE DE COMPIÈGNE

THESE

Pour obtenir le grade de

DOCTEUR

Spécialité : Génie Électrique

Wenshuai BAI

DC Microgrid optimized energy management and real-time control of power systems for grid-connected and off-grid operating modes

Laboratoire AVENUES, EA 7284

Soutenance le 21 Janv 2021 devant le jury composé de :

Rapporteurs : Prof. Mamadou Baïlo CAMARA, GREAH, Université Le Havre Normandie

Prof. Christophe SAUDEMONT, L2EP, HEI-YNCREA Lille

Examineurs : DR HDR Alexandre DE BERNARDINIS, SATIE, Université Gustave Eiffel

Prof. Christophe FORGEZ, Roberval, UTC Compiègne

Directeur de thèse : Prof. Manuela SECHILARIU, AVENUES, UTC Compiègne

Co-Directeur de thèse : Prof. Fabrice LOCMONT, AVENUES, UTC Compiègne

Université de Technologie de Compiègne - AVENUES -

Rue Roger Couttolenc, 60203 Compiègne

Abstract

The electric power system has been well developed for many years, which can give a well power supply for the load demand nowadays. However, with the increasing of the load demand and the increased awareness of the environmental protection, the renewable energy sources are proposed as the most promising energy sources. The most commonly used renewable energy is seriously affected by the natural environment, such as solar and wind energy. Thus, today's science and technology have sought a new solution, microgrid, which is a small-scale power and energy management system. In a microgrid, the multiply power sources, and multiply storages can be integrated, and the load demand can be managed by both the microgrid operator and the users. Thus, the physical components need to be reasonably controlled to well operate to satisfy users' load demands and public grid's requirements. Considering the user's convenience and the physical components' fast continuously regulation, the microgrid can be designed to a multi-layer supervisory system including physical layer, operational layer, economic dispatch layer, prediction layer, user layer and communication layer. In the communication layer, the microgrid can exchange information with the public grid. In addition, a power prediction model is also considered as the input information for the dispatching optimization in the microgrid. The microgrid can be built both with direct current (DC) bus and alternate current (AC) bus, and with different controllers or optimization theories. The DC microgrid has a higher efficiency than the AC microgrid because the photovoltaic sources and storage directly generate the DC power and most of the load demand can use DC power. Thus, this thesis focus on the research of the DC microgrid following two operation models: grid-connected mode, and off-grid mode including the islanded and isolated modes. In the previous research of our laboratory, the work focuses on the only the grid-connected or the off-grid mode. However, the problem of grid failure in grid-connected mode and low power supply reliability in off-grid mode should be resolved. Thus, the aim of this thesis is to propose a DC microgrid combining the advantages of the grid-connected or the off-grid mode, which named full DC microgrid. In the full DC microgrid, the renewable energy sources, storage, and public grid are included, and the back-up sources also applied to reduce the load shedding. In the full DC microgrid, a supervisory system is proposed to manage the power. The real-time power management in the operational layer of the supervisory system can keep the power balance and the power is managed based on the rules made according to the energy cost or tariff of every component, and the real-time load demand optimization is to manage the appliances by the microgrid operator and the users. In the optimization layer of the supervisory system, the day-ahead optimization is proposed to achieve the global minimal operation cost. The supervisory system and the full DC microgrid also can operate for 24 hours as the real case. The simulation results show that the full DC microgrid combines both advantages of the grid-connected and the off-grid mode to minimize the operating cost, the power in microgrid can be exchanged with the public grid, and the back-up sources is integrated to keep the load

demand. Then, the supervisory system considers the dynamic efficiency of the converter to solve the problem that the power quality of the microgrid is degraded due to the unstable DC bus voltage caused by the inaccurate power control. The simulation results show that considering the dynamic efficiency of the converter in the operational layer of the supervisory system, the fluctuation of the DC bus voltage can be reduced. However, considering the dynamic efficiency of the converter in the optimization layer of the supervisory system, the operation cost is increased because of the problem formulation of day-ahead optimization and the computation time of the formulated problem. Regarding the importance of the PV prediction for the day-ahead optimization, two prediction models are studied and compared to give a robust PV prediction power. The results are that the two models almost have the same results in the day-ahead optimization.

To sum up, this thesis focuses on the DC microgrid power and energy management. The proposed supervisory system and the full DC microgrid can give good reference for real applications.

In future work, a suitable problem formation to weigh the solution time of nonlinear optimization problems and the optimization effect of the system is suggested. Then, the simulation is applied to the experimental platform to check the actual difference between the experiment and the simulation, which will build a solid foundation for the future full DC microgrid construction.

Keywords: DC microgrid; grid-connected mode; off-grid mode; energy management; power management; supervisory system; optimization; non-linear constraints.

Acknowledgements

First of all, I would like to express my sincere gratitude to my supervisors, Prof. Manuela SECHILARIU and Prof. Fabrice LOCMET, for their good guidance and great efforts throughout the research and the writing of the thesis. Thanks to this teamwork and their well-organized working style, this thesis has advanced well according to the plan, which has permitted that the thesis work can be published in each stage. Thanks to Prof. Manuela SECHILARIU for the great advice and efforts in writing and revising of this thesis, as well as other publications. Thanks to Prof. Fabrice LOCMET for the help in the simulation operations.

I also express my very gratitude to Professor Mamadou Baïlo CAMARA and Professor Christophe SAUDEMONT, who have made detailed reports and remarks on my thesis, which help a lot in improving the quality of my thesis for both research content and presentation. Thanks also to Professor Alexandre DE BERNARDINIS, chairman of the thesis committee, and Professor Christophe FORGEZ for their interest in my work.

In addition, I would like to thank all the colleagues of the laboratory AVENUES and the department of Génie Urbain (GU): Jean-louis BATOZ, Nassima MOUHOUS-VOYNEAU, Nathalie MOLINES, Carine HENRIOT, Josiane GILLES, Lydie DELETTRE, Eduard ANTALUCA, Gilles MOREL, Fabien LAMARQUE, Hipolito MARTELL-FLORES, and Cristina PRONELLO, for the good ambiance during my PhD studies at UTC and in France.

I also thank my colleagues (PhD students) and friends: Hongwei WU, Changjie YIN, Raphael ROLIN, Amine BEN DAOUED, Ghada TAY, Jamila AOURIR, Soelarso SOELARSO and Saleh CHEIKH-MOHAMAD, for sharing the PhD and life experience, for discussions on culture and customs, as well as on the study.

I would like to thank my friends Peng DU, Caiyun LIU, Deyang ZHAO, Rui ZHANG, Lu WANG, CongCong MA, Jishuai LI, Xingyi WANG, Guoqiang WEI, Maiqi XIANG, Dong Ding, Kaidi PENG, and for their help during my PhD studies and daily life.

I am very grateful to my wife, Dian WANG, the care of my life, and deep love for me, which encourages me to face the work positively and successfully complete the doctoral project.

I would like to thank the China Scholarship Council (CSC) for offering the opportunity to support my PhD study and life in France. I will treasure the experiences both academic and personal in my life. Finally, a special bunch of thanks goes to my parents and my brother for all their love and encouragement to support me in finishing the PhD studies.

Table of Contents

Table of Contents	1
List of figures	4
List of tables	12
Abbreviations	14
Nomenclature	15
Publications associated with this PhD thesis	22
General introduction	24
Chapter I. Research background and thesis objective	28
I.1. Electric power system development	28
I.2. Economic dispatching optimization in microgrid	28
I.3. Objective of the thesis.....	33
I.4. Conclusion	35
Chapter II. DC microgrid with multiply operation modes	36
II.1. DC microgrid modeling.....	37
II.1.1. Microgrid system	38
II.1.2. PV sources.....	38
II.1.3. Public grid connection.....	39
II.1.4. Battery storage system	39
II.1.5. Diesel generator and supercapacitor	39
II.1.6. DC load	41
II.2. Microgrid supervisory overview	42
II.3. Tariff description	44
II.4. Economic dispatching optimization	45
II.4.1. Problem formulation	46
II.4.2. Optimization algorithm	54
II.5. Power management strategy	54

II.5.1. Grid-connected power management strategy	55
II.5.2. Off-grid power management strategy	57
II.5.3. Full microgrid power management strategy.....	60
II.5.4. Full microgrid power management strategy for 24 hours	64
II.6. Conclusion.....	69
Chapter III. Simulation results	70
III.1. Simulation verification.....	70
III.1.1. Simulation scenario for 9 hours' duration	70
III.1.2. Grid-connected simulation for 9 hours' duration	74
III.1.3. Off-grid simulation for 9 hours' duration.....	86
III.1.4. Full microgrid simulation for 9 hours' duration	107
III.1.5. Simulation scenario for 24 hours' duration	125
III.1.6. Full microgrid simulation for 24 hours' duration	129
III.2. Conclusion.....	143
Chapter IV. Optimization considering converter efficiency.....	144
IV.1. Description of converter modeling	144
IV.2. Power management strategy design.....	149
IV.3. Optimization considering converter dynamic efficiency	150
IV.3.1. Problem description.....	151
IV.3.2. Problem formulation.....	152
IV.4. Simulation verification.....	154
IV.4.1. Simulation scenario	154
IV.4.2. Simulation results	155
IV.4.3. Simulation analyzes.....	164
IV.5. Conclusion	165
Chapter V. PV power prediction model	166
V.1. Solar irradiation prediction model.....	167
V.1.1. Clear sky model	167
V.1.2. Météo France model	168

V.2. Supervisory system in a full DC microgrid.....	168
V.3. Simulation verification.....	168
V.3.1. Simulation scenario.....	169
V.3.2. Simulation results	170
V.3.3. Simulation analyzes	180
V.4. Conclusion.....	180
General conclusions and perspectives	182
References	186
Appendices	191
Appendix 1: Parameters of Solar-Fabrick series SF 130/2	192
Appendix 2: Parameters of Sonnenschein Solar: S12/6.6A.....	194
Appendix 3: Parameters of Maxwell 75V modules: BMOD0094 P075 B02	195
Appendix 4: Parameters of SDMO Technic 6500E AVR.....	200
Appendix 5: IGBT Semikron SKM 100GB063D	201

List of figures

Figure 1. Thesis structure.	26
Figure 2. DC Microgrid [53].	33
Figure 3. DC microgrid electrical scheme [53].	37
Figure 4. Microgrid multi-layer supervisory concept.....	42
Figure 5. The detail of the microgrid multi-layer supervisory concept.	43
Figure 6. Grid-connected microgrid power flow.....	46
Figure 7. Off-grid microgrid power flow.	49
Figure 8. Full microgrid power flow.	51
Figure 9. Grid-connected operational algorithm without economic optimization.....	55
Figure 10. Grid-connected operational algorithm with economic optimization.....	57
Figure 11. Off-grid operational algorithm without economic optimization.	58
Figure 12. Sub flow-chart of Figure 11.	58
Figure 13. Off-grid operational algorithm with economic optimization.	60
Figure 14. Sub-flow-chart of Figure 13.....	60
Figure 15. Full microgrid operational algorithm without economic optimization.	61
Figure 16. Sub flow-chart of Figure 15.	61
Figure 17. Full microgrid operational algorithm with economic optimization.	63
Figure 18. Sub flow-chart of Figure 17.	63
Figure 19. Full microgrid operational algorithm without economic optimization.	64
Figure 20. Sub flow-chart of operational power control and management algorithm.....	65
Figure 21. Sub flow-chart a and sub flow-chart b.	65
Figure 22. Full microgrid operational algorithm with economic optimization.	67
Figure 23. Full microgrid power management sub flow chart 1 in the operational layer.....	68
Figure 24. Sub flow-chart a and b of Figure 23.....	68
Figure 25. PV MPPT power and PV prediction power curves for May 8 th 2018.	71
Figure 26. PV MPPT power and PV prediction power curves for June 20 th 2018.....	72

Figure 27. PV MPPT power and PV prediction power curves for July 16 th 2018.....	72
Figure 28. Load demand power and load power prediction curves.....	73
Figure 29. The day-ahead economics optimization results (k_D) and BS SOC curves at grid-connected mode on May 8 th 2018.....	75
Figure 30. The day-ahead economics optimization results of power curves at grid-connected mode on May 8 th 2018.....	75
Figure 31. The ideal economics optimization results (k_D) and BS SOC curves at grid-connected mode on May 8 th 2018.....	76
Figure 32. The ideal economics optimization results of power curves at grid-connected mode on May 8 th 2018.....	77
Figure 33. DC bus voltage and BS SOC curves when $k_D = 1$ at grid-connected mode on May 8 th 2018.....	78
Figure 34. Power curves when $k_D = 1$ at grid-connected mode on May 8 th 2018.....	78
Figure 35. DC bus voltage and BS SOC curves when $k_D = 0.5$ at grid-connected mode on May 8 th 2018.....	79
Figure 36. Power curves when $k_D = 0.5$ at grid-connected mode on May 8 th 2018.	79
Figure 37. DC bus voltage and BS SOC curves when $k_D = 0$ at grid-connected mode on May 8 th 2018.....	80
Figure 38. Power curves when $k_D = 0$ at grid-connected mode on May 8 th 2018.....	80
Figure 39. The actual results of DC bus voltage and BS SOC curves at grid-connected mode on May 8 th 2018.....	81
Figure 40. The actual results of power curves at grid-connected mode on May 8 th 2018.	81
Figure 41. The ideal results of DC bus voltage and BS SOC curves at grid-connected mode on May 8 th 2018.....	82
Figure 42. The ideal results of power curves at grid-connected mode on May 8 th 2018.....	82
Figure 43. The total cost with constant DG power at off-grid mode on May 8 th 2018.....	88
Figure 44. The total cost with variable DG power at off-grid mode on May 8 th 2018.	88
Figure 45. The total cost with constant DG power at off-grid mode on June 20 th 2018.....	89
Figure 46. The total cost with variable DG power at off-grid mode on June 20 th 2018.	89
Figure 47. The total cost with constant DG power at off-grid mode on July 16 th 2018.	90

Figure 48. The total cost with variable DG power at off-grid mode on July 16 th 2018.....	90
Figure 49. The day-ahead economics optimization results (k_{DG}) and BS SOC curves at off-grid mode on May 8 th 2018.....	92
Figure 50. The day-ahead economics optimization results of power curves at off-grid mode on May 8 th 2018.....	92
Figure 51. The day-ahead economics optimization results (k_{DG}) and BS SOC curves at off-grid mode on May 8 th 2018.....	93
Figure 52. The day-ahead economics optimization results of power curves at off-grid mode on May 8 th 2018.....	94
Figure 53. The ideal economics optimization results (k_{DG}) and BS SOC curves at off-grid mode on May 8 th 2018.....	94
Figure 54. The ideal economics optimization results of power curves at off-grid mode on May 8 th 2018.....	95
Figure 55. The ideal economics optimization results (k_{DG}) and BS SOC curves at off-grid mode on May 8 th 2018.....	95
Figure 56. The ideal economics optimization results of power curves at off-grid mode on May 8 th 2018.....	96
Figure 57. DC bus voltage and BS SOC curves when $k_{DG} = 0$ at off-grid mode on May 8 th 2018.....	97
Figure 58. Power curves when $k_{DG} = 0$ in off-grid mode on May 8 th 2018.....	97
Figure 59. The actual results of DC bus voltage and BS SOC curves at off-grid mode on May 8 th 2018.....	98
Figure 60. The actual results of power curves at off-grid mode on May 8 th 2018.	99
Figure 61. The actual results of DC bus voltage and BS SOC curves at off-grid mode on May 8 th 2018.....	99
Figure 62. The actual results of power curves at off-grid mode on May 8 th 2018.	100
Figure 63. The ideal results of DC bus voltage and BS SOC curves at off-grid mode on May 8 th 2018.....	100
Figure 64. The ideal results of power curves at off-grid mode on May 8 th 2018.	101
Figure 65. The ideal results of DC bus voltage and BS SOC curves at off-grid mode on May 8 th 2018.....	101

Figure 66. The ideal results of power curves at off-grid mode on May 8 th 2018.	102
Figure 67. The day-ahead economics optimization results (k_D , k_{DG}) and BS SOC curves at full microgrid mode on May 8 th 2018.	109
Figure 68. The day-ahead economics optimization results of power curves at full microgrid mode on May 8 th 2018.	109
Figure 69. The day-ahead economics optimization results (k_D , k_{DG}) and BS SOC curves at full microgrid mode on May 8 th 2018.	110
Figure 70. The day-ahead economics optimization results of power curves at full microgrid mode on May 8 th 2018.	110
Figure 71. The ideal economics optimization results (k_D , k_{DG}) and BS SOC curves at full microgrid mode on May 8 th 2018.	111
Figure 72. The ideal economics optimization results of power curves at full microgrid mode on May 8 th 2018.	111
Figure 73. The ideal economics optimization results (k_D , k_{DG}) and BS SOC curves at full microgrid mode on May 8 th 2018.	112
Figure 74. The ideal economics optimization results of power curves at full microgrid mode on May 8 th 2018.	112
Figure 75. DC bus voltage and BS SOC curves when $k_D = 1$ and $k_{DG} = 0$ at full microgrid mode on May 8 th 2018.	113
Figure 76. Power curves when $k_D = 1$ and $k_{DG} = 0$ at full microgrid mode on May 8 th 2018.	114
Figure 77. DC bus voltage and BS SOC curves when $k_D = 0.5$ and $k_{DG} = 0$ at full microgrid mode on May 8 th 2018.	114
Figure 78. Power curves when $k_D = 0.5$ and $k_{DG} = 0$ at full microgrid mode on May 8 th 2018.	115
Figure 79. DC bus voltage and BS SOC curves when $k_D = 0$ and $k_{DG} = 0$ at full microgrid mode on May 8 th 2018.	115
Figure 80. Power curves when $k_D = 0$ and $k_{DG} = 0$ at full microgrid mode on May 8 th 2018.	116
Figure 81. The actual results of DC bus voltage and BS SOC curves at full microgrid mode on May 8 th 2018.	116

Figure 82. The actual results of power curves at full microgrid mode on May 8 th 2018.....	117
Figure 83. The actual results of DC bus voltage and BS SOC curves at full microgrid mode on May 8 th 2018.....	117
Figure 84. The actual results of power curves at full microgrid mode on May 8 th 2018.....	118
Figure 85. The ideal results of DC bus voltage and BS SOC curves at full microgrid mode on May 8 th 2018.....	118
Figure 86. The ideal results of power curves at full microgrid mode on May 8 th 2018.	119
Figure 87. The actual results of DC bus voltage and BS SOC curves at full microgrid mode on May 8 th 2018.....	119
Figure 88. The actual results of power curves at full microgrid mode on May 8 th 2018.....	120
Figure 89. PV MPPT power and PV prediction power curves for June 20 th 2018.....	126
Figure 90. Load power and load power prediction curves.	127
Figure 91. The day-ahead economics optimization results (k_D, k_{DG}) and BS SOC curves at full microgrid mode on June 20 th 2018.....	131
Figure 92. The day-ahead economics optimization results of power curves at full microgrid mode on June 20 th 2018.....	131
Figure 93. The day-ahead economics optimization results (k_D, k_{DG}) and BS SOC curves at full microgrid mode on June 20 th 2018.....	131
Figure 94. The day-ahead economics optimization results of power curves at full microgrid mode on June 20 th 2018.....	132
Figure 95. The ideal economics optimization results (k_D, k_{DG}) and BS SOC curves at full microgrid mode on June 20 th 2018.....	132
Figure 96. The ideal economics optimization results of power curves at full microgrid mode on June 20 th 2018.....	132
Figure 97. The ideal economics optimization results (k_D, k_{DG}) and BS SOC curves at full microgrid mode on June 20 th 2018.....	133
Figure 98. The ideal economics optimization results of power curves at full microgrid mode on June 20 th 2018.....	133
Figure 99. DC bus voltage and BS SOC curves when $k_D = 1$ and $k_{DG} = 0$ at full microgrid mode on June 20 th 2018.....	135

Figure 100. Power curves when $k_D = 1$ and $k_{DG} = 0$ at full microgrid mode on June 20 th 2018.	136
Figure 101. The actual results of DC bus voltage and BS SOC curves at full microgrid mode on June 20 th 2018.....	136
Figure 102. The actual results of power curves at full microgrid mode on June 20 th 2018....	137
Figure 103. The actual results of DC bus voltage and BS SOC curves at full microgrid mode on June 20 th 2018.....	137
Figure 104. The actual results of power curves at full microgrid mode on June 20 th 2018....	138
Figure 105. The ideal results of DC bus voltage and BS SOC curves at full microgrid mode on June 20 th 2018.....	138
Figure 106. The ideal results of power curves at full microgrid mode on June 20 th 2018.	138
Figure 107. The actual results of DC bus voltage and BS SOC curves at full microgrid mode on June 20 th 2018.....	139
Figure 108. The actual results of power curves at full microgrid mode on June 20 th 2018....	139
Figure 109. The boost/buck converter.	145
Figure 110. The single-phase full-bridge DC/AC converter.	145
Figure 111. Power loss classification in the converter.	146
Figure 112. The power loss in the PV boost converter.....	148
Figure 113. The power efficiency in the PV boost converter.....	149
Figure 114. The power loss model in power management strategy.	150
Figure 115. The optimized power flow with the power loss of converter.....	151
Figure 116. The power loss model in power management strategy.	153
Figure 117. The day-ahead economics optimization results k_D , k_{DG} and BS SOC curves at full microgrid mode on June 20 th , 2018 without converter loss.....	155
Figure 118. The day-ahead economics optimization results of power curves at full microgrid mode on June 20 th , 2018 without converter loss.....	156
Figure 119. The day-ahead economics optimization results k_D , k_{DG} and BS SOC curves at full microgrid mode on June 20 th , 2018 with converter loss.....	156
Figure 120. The day-ahead economics optimization results of power curves at full microgrid mode on June 20 th , 2018 with converter loss.....	157

Figure 121. The day-ahead economics optimization results of converter loss power curves at full microgrid mode on June 20 th , 2018.....	157
Figure 122. DC bus voltage and BS SOC curves of case 1 at full microgrid mode on June 20 th , 2018.....	158
Figure 123. Power curves of case 1 at full microgrid mode on June 20 th , 2018.	159
Figure 124. DC bus voltage and BS SOC curves of case 2 at full microgrid mode on June 20 th , 2018.....	159
Figure 125. Power curves of case 2 at full microgrid mode on June 20 th , 2018.	159
Figure 126. The converter loss power curves of case 2 at full microgrid mode on June 20 th , 2018.	160
Figure 127. DC bus voltage and BS SOC curves of case 3 at full microgrid mode on June 20 th , 2018.....	160
Figure 128. Power curves of case 3 at full microgrid mode on June 20 th , 2018.	160
Figure 129. The converter loss power curves of case 3 at full microgrid mode on June 20 th , 2018.	161
Figure 130. DC bus voltage and BS SOC curves of case 4 at full microgrid mode on June 20 th , 2018.....	161
Figure 131. Power curves of case 4 at full microgrid mode on June 20 th , 2018.	161
Figure 132. The converter loss power curves of case 4 at full microgrid mode on June 20 th , 2018.	162
Figure 133. DC bus voltage and BS SOC curves of case 5 at full microgrid mode on June 20 th , 2018.....	162
Figure 134. Power curves of case 5 at full microgrid mode on June 20 th , 2018.	162
Figure 135. The converter loss power curves of case 5 at full microgrid mode on June 20 th , 2018.	163
Figure 136. The supervisory system structure in a full DC microgrid with the power prediction model.....	168
Figure 137. The PV shedding cost comparison between the clear sky model and the Météo France model.....	173
Figure 138. The load shedding cost comparison between the clear sky model and the Météo France model.....	173

Figure 139. The total cost comparison between the clear sky model and the Météo France model.	173
Figure 140. The PV shedding cost comparison between the clear sky model and the Météo France model.	176
Figure 141. The load shedding cost comparison between the clear sky model and the Météo France model.	176
Figure 142. The total cost comparison between the clear sky model and the Météo France model.	176
Figure 143. The PV shedding cost comparison between the clear sky model and the Météo France model.	179
Figure 144. The load shedding cost comparison between the clear sky model and the Météo France model.	179
Figure 145. The total cost comparison between the clear sky model and the Météo France model.	179

List of tables

Table 1. Simulation parameter of the principal device.....	71
Table 2. TOU public grid energy tariffs.....	73
Table 3. Fixed energy tariffs.....	73
Table 4. Simulation scenarios.....	74
Table 5. Parameter.....	74
Table 6. Results summary for grid-connected mode on May 8 th 2018.....	83
Table 7. Results summary for grid-connected mode on June 20 th 2018.....	84
Table 8. Results summary for grid-connected mode on July 16 th 2018.	85
Table 9. Parameters for optimization in off-grid mode.	86
Table 10. Parameters for operational algorithm in off-grid mode.....	91
Table 11. Results summary for off-grid mode on May 8 th 2018.	103
Table 12. Results summary for off-grid mode on June 20 th 2018.	104
Table 13. Results summary for off-grid mode on July 16 th 2018.....	106
Table 14. Parameters for optimization at full microgrid mode.	107
Table 15. Parameters for the operational algorithm at full microgrid mode.	108
Table 16. Results summary for full microgrid mode on May 8 th 2018.	122
Table 17. Results summary for full microgrid mode on June 20 th 2018.	123
Table 18. Results summary for full microgrid mode for July 16 th 2018.	124
Table 19. 24 hours work hypothesis.....	126
Table 20. TOU public grid energy tariffs.....	127
Table 21. Fixed energy tariffs.....	128
Table 22. Period configuration.....	128
Table 23. Parameters for optimization at full microgrid mode.	129
Table 24. Parameters for the operational algorithm at full microgrid mode.	130
Table 25. Simulation cases without considering the day-ahead optimization results.	135
Table 26. Results summary for full microgrid mode June 20 th 2018.	140

Table 27. Simulation cases.	155
Table 28. Simulation results of the day-ahead optimization.	158
Table 29. Simulation results of the cases.	164
Table 30. Simulation cases.	169
Table 31. Simulation results of case 1 of the clear sky model.	170
Table 32. Simulation results of case 1 of the Météo France model.	172
Table 33. Simulation results of case 2 of the clear sky model.	174
Table 34. Simulation results of case 2 of the Météo France model.	175
Table 35. Simulation results of case 3 of the clear sky model.	177
Table 36. Simulation results of case 3 of the Météo France model.	178
Table 37. Simulation results of the cases.	180

Abbreviations

AC	Alternating Current
BS	Battery Storage
CPP	Critical Peak Pricing
CPU	Central Processing Unit
DC	Direct Current
DG	Diesel Generator
IGBT	Insulated Gate Bipolar Transistor
InC	Incremental Conductance
MILP	Mixed-integer linear programming
NOCT	Nominal Operating Cell Temperature
MPP	Maximum Power Point
MPPT	Maximum Power Point Tracking
O&M	Diesel Generator Operation and Maintenance
PC	Personal Computer
PCC	Point of Common Coupling
PI	Proportional-Integral Controller
PID	Proportional-Integral-Derivative Controller
PV	Photovoltaic
P&O	Perturb and Observe
RTP	Real-time Pricing
SC	Supercapacitor
STC	Standard Test Conditions
TOU	Time-of-Use Pricing

Nomenclature

a	Coefficients of the polynomial
AVR	Average difference of cost (c€)
AVR _{LDS}	Load shedding average difference of cost (c€)
AVR _{PVS}	Photovoltaic shedding average difference of cost (c€)
AVR _{TOTAL}	Total average difference of cost (c€)
b	Coefficients of the polynomial
B_1	Switching leg of the PV dedicated converter
B_2	Switching leg of the storage dedicated converter
B_3	Switching leg of the grid-connected dedicated converter
B_4	Switching leg of the grid-connected dedicated converter
B_5	Switching leg of the diesel generator dedicated converter
B_6	Switching leg of the diesel generator dedicated converter
B_7	Switching leg of the supercapacitor dedicated converter
c	Coefficients of the polynomial
C_{BS}	Battery storage cost (€)
C_{BS_REF}	Capacitor of battery storage (Ah)
C_{DC}	Bus capacitor (F)
C_{DG}	Diesel generator cost (€)
C_{DG_F}	Diesel generator fuel cost (€)
$C_{DG_O\&M}$	Diesel generator O&M cost (€)
C_G	Public grid cost (€)
C_{L_S}	DC load shedding cost (€)
C_{PV_S}	Photovoltaic shedding cost (€)

C_{SC}	Capacitor of supercapacitor (F)
C_{Total}	Total energy cost (€)
d	Duty cycle of transistor turn-on (%)
$E_{CV_LOSS_SUM}$	Energy loss sum of converters (kWh)
E_{LOAD}	Total energy consumption of load (kWh)
E_{SC}	Supercapacitor stored energy (kWh)
E_{SC_Rated}	Supercapacitor stored rated energy (kWh)
E_{SUPPLE}	Total supplied energy (kWh)
f	Switching frequency (Hz)
f_{DG}	Diesel generator voltage frequency (Hz)
$F1, F2, F3, F4, F5, F6, F7$	Piecewise functions
g_b	Beam solar radiation on earth (W/m ²)
g_{bg}	Beam radiation on a given sloped surface (W/m ²)
g_{dg}	Diffuse radiation on a given sloped surface (W/m ²)
g_{PRE}	Solar irradiation prediction (W/m ²)
g_{sc}	Extra-terrestrials solar radiation on earth (W/m ²)
g_{ig}	Total radiation on a surface (W/m ²)
G_{TEST}	Irradiation at standard test condition (W/m ²)
i_{AC_eff}	AC source effective current (A)
i_{BS}	Battery storage current (A)
\bar{i}_D	Average current flowing through diode (A)
i_{DG}	Diesel generator current (A)
i_{D_eff}	Effective current of diode (A)
i_G	Public grid current (A)
i_L	Load demand current (A)

i_{ph_eff}	Effective value of single-phase current (A)
i_{PV}	Photovoltaic current (A)
i_s	Source current (A)
i_{SC}	Supercapacitor charging or discharging current (A)
\bar{i}_T	Average current flowing through transistor (A)
i_{T_eff}	Effective current of transistor (A)
I_{DG_RATED}	Diesel generator rated output current (A)
k_D	Power distribution coefficient between public grid and battery storage
k_{DG}	Coefficient of DG start-up
k_{L_CRIT}	The minimum amount of load demand that must be attended
K_I	Integral gain of DC bus voltage controller
K_P	Proportional gain of DC bus voltage controller
m	Modulation index
n	Air mass coefficient
N_{PV}	Number of the PV panel
p	Power (W)
P_{AVAIL}	Total available DC microgrid power (W)
P_{BS}	Battery storage power (W)
P_{BS}	Battery storage power on the side of the microgrid DC bus (W)
$P_{BS_CV_LOSS}$	Power loss of converter connecting battery storage (W)
P_{BS_MAX}	Battery storage maximal power limit (W)
P_{comD}	Diode switching loss power (W)
P_{comT}	Transistor switching loss power (W)
P_{condD}	Diode conduction loss power (W)

P_{condT}	Transistor conduction loss power (W)
P_{DG}	Diesel generator output power (W)
P'_{DG}	Diesel generator output power on the side of the microgrid DC bus (W)
$P_{DG_CV_LOSS}$	Power loss of converter connecting diesel generator (W)
P_{DG_MAX}	Diesel generator maximum output power (W)
$P_{DG_ON_MAX}$	Diesel generator maximum output power (W) while diesel generator start-up
$P_{DG_ON_MIN}$	Diesel generator minimum output power (W) while diesel generator start-up
P_{DG_RATED}	Diesel generator rated output power (W)
P_G	Public grid power (W)
P'_G	Public grid power on the side of the microgrid DC bus (W)
P_{GF_Limit}	Public grid power fluctuation (V)
$P_{G_CV_LOSS}$	Power loss of converter connecting public grid (W)
P_{loss}	Loss power (W)
P_{loss_sum}	Loss power sum of converters (W)
P_L	DC load power (W)
P_{L_CRIT}	DC critical load power (W)
P_{L_D}	DC load demand power (W)
$P_{L_N_CRIT}$	DC non-critical load power (W)
P_{L_OPT}	DC load power after the load real-time optimization (W)
P_{L_S}	DC load shed power (W)
P_{PV}	Photovoltaic power (W)
P'_{PV}	Photovoltaic power on the side of the microgrid DC bus (W)
$P_{PV_CV_LOSS}$	Power loss of converter connecting photovoltaic (W)
P_{PV_MPPT}	Photovoltaic power by MPPT algorithm (W)

$P_{PV_MPPT_STC}$	PV maximum power at standard test condition (W)
P_{PV_S}	Photovoltaic shed power (W)
P_{SC}	Supercapacitor power (W)
P_{SC_MAX}	Supercapacitor maximal power limit (W)
Q_{rr}	Reverse recovery charge (C)
r_{CE}	Resistance between collector and emitter (Ω)
r_F	Resistance of diode (Ω)
r_L	Internal resistance of the inductor coil (Ω)
R_1	Equivalent series resistor of supercapacitor (Ω)
R_2	Equivalent series resistor of supercapacitor (Ω)
S_{AVR}	Percentage of AVR and the average cost of the Météo France model (%)
S_{AVR_LDS}	Percentage of AVR and the average load shedding cost of the Météo France model (%)
S_{AVR_PVS}	Percentage of AVR and the average photovoltaic shedding cost of the Météo France model (%)
S_{AVR_TOTAL}	Percentage of AVR and the average total cost of the Météo France model (%)
SOC_{BS}	State charge of batteries storage (%)
SOC_{SC}	State charge of supercapacitor (%)
SOC_{BS_0}	Initial state of charge of batteries storage (%)
SOC_{BS_MAX}	Upper limit of state charge of batteries storage (%)
SOC_{BS_MIN}	Lower limit of state charge of batteries storage (%)
SOC_{SC_0}	Initial state of charge of supercapacitor storage (%)
$SOC_{SC_MAX_MAX}$	Maximum value of the maximum state charge of supercapacitor (%)
$SOC_{SC_MAX_MIN}$	Minimum value of the maximum state charge of supercapacitor (%)
$SOC_{SC_MIN_MAX}$	Maximum value of the minimum state charge of supercapacitor (%)
$SOC_{SC_MIN_MIN}$	Minimum value of the minimum state charge of supercapacitor (%)

t	Continues time (s)
t_0	Initial time instant (s)
t_F	Final time instant (s)
t_{DG_OFF}	The diesel generator off time (s)
t_{DG_ON}	The diesel generator on time (s)
T	Atmospheric transmittance for short wave solar irradiance
T_{BS}	Battery storage energy tariff (€/kWh)
T_{DG_F}	Diesel generator power production tariff (€/kWh)
$T_{DG_OFF_LIM}$	The time constraints when the DG is turned off (s)
$T_{DG_ON_MAX}$	The time constraints when the DG is turned on (s)
$T_{DG_O\&M}$	Diesel generator average O&M cost per hour (€/h)
T_G	Public grid energy tariff (€/kWh)
T_{L_S}	DC load shedding tariff (€/kWh)
T_{PV_S}	Photovoltaic shedding energy tariff (€/kWh)
T_{SC}	Supercapacitor energy tariff (€/kWh)
T_{SC_MIN}	Supercapacitor minimal time limit (minute)
U_n	Nominal voltage of transistor (V)
v_{BS}	Batteries storage voltage (V)
v_{DC}	DC bus voltage (V)
v_{DC}^*	DC bus voltage control reference (V)
v_{DG}	Diesel generator voltage (V)
v_G	Public grid voltage (V)
v_{PV}	Photovoltaic Voltage (V)
v_{SC}	Supercapacitor voltage (V)
v_{SC_0}	The initial voltage of supercapacitor (V)

V_{SC_Rated}	Supercapacitor rated voltage (V)
V_{cc}	Direct voltage applied to diode when opening (V)
V_{CE0}	Threshold voltage of voltage drop between the collector and the emitter of the transistor (V)
V_{DG_RATED}	Diesel generator rated output voltage (V)
V_{F0}	Threshold voltage of diode forward voltage drop (V)
Δp	Compensation power by the public grid, BS, DG, and SC
Δt	Time interval between two samples
β	Slope angle between the plane and horizontal
γ	Surface azimuth angle
γ_s	Temperature coefficient of PV power
δ	Declination of the sun at solar noon
η_{GLOBAL}	Global efficiency (%)
η_{PV}	Conversion efficiency connecting photovoltaic (%)
θ	Angle of incidence between the beam irradiance on the surface and the normal to the surface
θ_{AIR_PRE}	Air temperature prediction
θ_{AIR_TEST}	Air temperature at standard test condition
θ_{PV_PRE}	PV cell temperature prediction
θ_z	Local zenith angle
σ_{V_BUS}	Root mean square of DC bus voltage
φ	Local latitude
φ_{ph}	Phase angle between current and voltage
ω	Solar hour angle

Publications associated with this PhD thesis

Publications in journals with review committees and indexed in Scopus and WoS

1. **W. Bai**, M. Sechilariu, and F. Locment: "DC Microgrid System Modeling and Simulation Based on a Specific Algorithm for Grid-Connected and Islanded Modes with Real-Time Demand-Side Management Optimization." *Applied Sciences* 10.7 (2020): 2544, Impact Factor 2.217, WoS, Scopus, doi.org/10.3390/app10072544
2. **W. Bai**, H. Wu, M. Sechilariu, F. Locment: "Power management of a full DC microgrid for building self-consumption applications", *Lecture Notes in Electrical Engineering*, vol. 697, pp. 177-189, Springer Ed., 2020, Scopus, DOI:10.1007/978-3-030-56970-9_14; article selected and published following the international conference ELECTRIMACS 2019
3. H. Wu, **W. Bai**, F. Locment, M. Sechilariu: "Optimal power dispatching in the DC microgrid with clear sky irradiance model", *Lecture Notes in Electrical Engineering*, vol. 615, pp. 497-509, Springer Ed., 2020, DOI: 10.1007/978-3-030-37161-6_38; article selected and published following the international conference ELECTRIMACS 2019

Presentations at international conferences/congresses with proceedings

1. **W. Bai**, M. Sechilariu, F. Locment: "On-grid/off-grid DC microgrid optimization and demand response management", *EPE'20 ECCE Europe (22nd European Conference on Power Electronics and Applications)*, pp.1-6, Lyon, France (virtual conference), 7th-11th September 2020; Scopus, ISI WoS
2. **W. Bai**, H. Wu, M. Sechilariu, F. Locment: "Power management of a full DC microgrid for building self-consumption applications", *ELECTRIMACS 2019 (International conference on theory and application of modeling and simulation in electrical power engineering including electric machines, power electronic converters and power systems)*, pp.1-6, Salerno, Italy, 21st-23rd May 2019
3. H. Wu, **W. Bai**, F. Locment, M. Sechilariu: "Optimal power dispatching in the DC microgrid with clear sky irradiance model", *ELECTRIMACS 2019 (International conference on theory and application of modeling and simulation in electrical power engineering including electric machines, power electronic converters and power systems)*, pp.1-6, Salerno, Italy, 21st-23rd May 2019

Presentations at national conferences/congresses with proceedings

1. **W. Bai**, H. Wu, M. Sechilariu, F. Locment : "Gestion de l'énergie d'un micro-réseau DC complet pour créer des applications d'autoconsommation", SEEDS-JCGE 2019 (Conférence des Jeunes Chercheurs en Génie Électrique, Ile d'Oléron, 11-14 juin 2019)

General introduction

Electric power system has a long history since the first electrical appliances came. With the development of the electrical appliances, the power supply is getting big, robust and advance. An electric power system is integrated with power generation, power transmission, and power distribution. The power generation is now mainly separately into renewable and non-renewable energy. Although non-renewable energy is the main power generation, the advantages of the renewable energy is more attractive for users, grid operator, grid builder and environment. As it is known to all, the scale of the electric power system provides inertia to be robust for the regulator and safety, and the uneven distribution of the regional energy can be solved. All the power generation and power transmission supply power for the electrical appliances.

Nowadays, the installed power generation capacity growth rate of the renewable energy is greater than the ones of the non-renewable energy. The advantage of renewable energy is environmental-friendly, such as photovoltaic (PV) panels and wind turbines. On the other hand, these renewable sources can be installed near the load demand to reduce the power loss in power transmission. Then, some project, such as intelligent home, intelligent official building, and intelligent city, can be driven by electric power system integrated with buildings and renewable energy. The distributed generator of the renewable energy greatly increases the penetration rate. Thus, distributed renewable energy generation is reducing the growth of non-renewable energy. Also, the cost decreasing of the PV panel is the one reason to increase the renewable power generation. However, the renewable energy is not easy to be used as the traditional power source, because the intermitted power generation is caused by the local weather condition.

Microgrid is a concept to miniaturized grid with distributed energy sources, distributed storage, and intelligent power management including communication system. Furthermore, microgrid is known as the economical and creative way to upgrade from the tradition power grid to the smart grid because the multiply microgrid can be connected with power and information exchange. In a microgrid, the power management and control are the most important part to achieve the power balance, because the intermitted power generation of the renewable energy sources increases the complexity of the power management and control in the microgrid. Furthermore, the uncertain load demand is also a factor to challenge the reliability of the microgrid. In modern load demand management, the appliances in microgrid are designed to be controlled by both the user and microgrid operator, which give the possibility to achieve the intelligent load demand management.

In a microgrid, there are many types of controller to be chosen. The reliable and fast controller with the acceptable overshoot of the current and voltage is pursued. The classic controller, proportional-integral-derivative (PID) controller, is used as easy way to control power according to a reference value.

The droop controller is most used because it can be used without communication system in a microgrid. More advanced is model predictive controller, a process controller considering an optimization objective in a time horizon.

The power management in a microgrid is the center part, which should consider the safety of electronic devices and the rational usage of power. In traditional power grid, the power management is regarded as the operation by the grid operator. Thus, the power regulation speed cannot be fast. In the modern power grid, the regulation is the combination of automatic regulation and manual regulation. In the future power grid, the power grid will be fully automatic regulation supported by management theory, the artificial intelligence will provide more possibility to achieve a better power management in future power grid.

In a microgrid, the optimization technology is mostly used. For example, the optimization in power generation and load demand, the optimization in the overall operation cost, the optimization in environment, the optimization in power loss of a microgrid, etc. The optimization can be suitable for different microgrids. In alternating current (AC) microgrid, the optimization to reduce the operation cost should consider both reactive power and active power; in direct current (DC) microgrid, the reactive power is not considered. In the grid-connected operation model of a microgrid, the public grid power source should be considered; however, in the off-grid operation model, the public grid is not included. Thus, the optimization should be modified for the specified microgrid.

The optimization technology is a specific type of mathematical problem. The basic characteristics of this type of problem are well-defined objective and constraints. From a mathematical point of view, optimization objective can be divided into single objective and multiple objectives and the mathematical optimization problems can be divided into convex optimization and non-convex optimization. And there are many methods to solve the proposed optimization, such as pure mathematical methods, various search algorithms, etc.

The aim of this thesis is to build a power and energy management system, which is called supervisory system, for a full DC microgrid considering the grid-connected mode and off-grid mode, respecting to the power and time constraints to protect the power quality, the equipment safe and life, and to keep the communication with the public grid for regulation of shaving the peak and valley. In the DC microgrid supervisory system there are many problems need to be considered, for example, the PV intermitted power generation, the uncertain of the power prediction for the economic dispatching optimization, the physical characteristics of the physical components in the DC microgrid, the non-linear constraints in the power converters, etc. In order to better meet the load demand, a well-designed load demand optimization need to be integrated. The results are expected that the supervisory system can well manage the power flow in real-time and give a long-term energy schedule for well meeting load demand and increase the usage of the renewable energy to reduce the overall operating cost.

The thesis is organized in five chapters as shown in Figure 1. After the general introduction, in Chapter I firstly, the development of the electric power system is introduced to be as the background of the microgrid. Then, the economic dispatching optimization in microgrid is provided. Optimization problems and types of problems in microgrid are introduced. At last, the objective of the thesis is given.

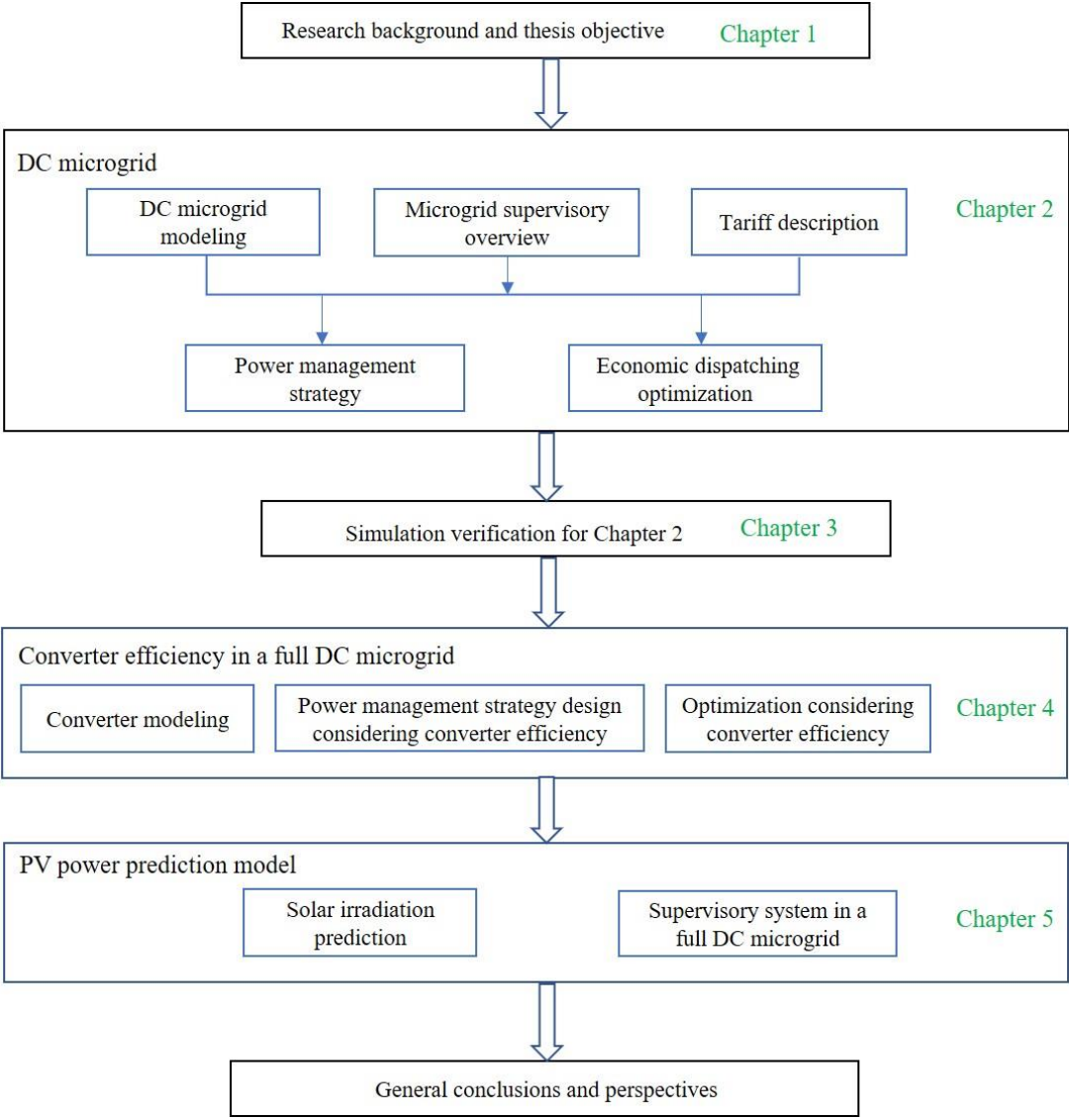


Figure 1. Thesis structure.

In Chapter II, firstly, the DC microgrid modeling is given. Then, the advanced microgrid power management system, i.e. supervisory system, is introduced. In the designing process of the supervisory system, the tariff of every component is required. Thus, this chapter introduces the tariffs considered in microgrid. Thereafter, the economic dispatching optimization in the DC microgrid is proposed and the optimization problem is separately formulated for the grid-connected model, off-grid model, full microgrid model, and the full microgrid model in 24 hours, and the optimization algorithms are presented. Then, the power management strategy to achieve an instantaneous power balance considering a rule-based power flow rule is proposed according to the tariff of every component in the DC microgrid. At the same time, the power management strategy for grid-connected model, off-grid model, full

microgrid model, and the full microgrid model in 24 hours are respectively given. In chapter III, the simulation results are given to prove the effectiveness of the supervisory system.

Based on the study of the supervisory system in Chapter II and III, Chapter IV proposed an optimization based on the non-linear constraints of the converter efficiency. The description of the converter modeling is given in the first part. Then, the power management strategy design is introduced. The optimization problem description and problem formulation considering the converter dynamic efficiency are proposed. At last, the simulation is designed to valid the proposed optimization problem.

At the beginning of the chapter V, the PV power prediction model is introduced with its function in the microgrid supervisory system. The solar irradiation prediction is a key factor to calculate the PV power prediction. Thus, two solar irradiation prediction models are introduced, which are simple to calculate and free-access. Then, the two models are introduced into the supervisory system to valid the effectiveness and give a comparison. The simulation results show that the two models can provide effective solar irradiation prediction and almost have the same simulation results in the microgrid.

General conclusions and perspectives of the research of this thesis are given in the end.

Chapter I. Research background and thesis objective

1.1. Electric power system development

In the 19th century, the first power system was operated to open the history of power supply. Since then, the electric power system has gone through a big development, which means a more mature and wider range of services. Now, the modern power system is very complicated to integrate power generators, power transmission, and power distribution with a power protection system to be more reliable to the inertia of a wide range connection. In addition, the number and the power consumption of electrical appliances are distributed increasing to demand more electric energy and the world sustainable development gives guidance to advocate renewable energy [1, 2]. However, the high permeability installed renewable energy will lead to instability of the public power system due to the intermitted power generation of renewable energy sources influenced by the local weather condition [3, 4]. A smart grid based on a communication system, intelligent energy management, and multiple distributed renewable generators, will become more efficient and reliable than traditional public power grid systems [5, 6]. Hence, the smart grid represents a revolution of the whole power system. However, it is impossible and expensive to upgrade directly traditional power system to a smart grid. At this moment, microgrid, a small range intelligent power system flexibly integrated with multi-source [7, 8], multi-storage, and local demand-side management in multiple operational modes, becomes a good enough technology to gradually transit to smart grid [9, 10].

1.2. Economic dispatching optimization in microgrid

A supervisory system for a microgrid is integrated with an information collection system, prediction system, optimization system, economic dispatch system, user application system, and communication system. The economic dispatch, based on the optimization system, is important in a power system to achieve the lowest microgrid operation cost with respect to other objectives of power dispatch such as the usage rate of renewable energy, the power quality, the power loss, etc. [11, 12].

Economic dispatching optimization is structured by a series of optimization problems based on operation research including deterministic and stochastic optimization [13, 14]. Most economic dispatching optimization is built into two layers: lower layer and upper layer [15, 16]. The lower layer concerns the power balance between demand and supply, reliable protection of microgrid with local controller-based mostly on proportional-integral (PI) control, droop control, and model predictive

control theory [17, 18]. The PI is a classical and simple control method. The droop control is commonly applied to a generator for primary frequency control. Model predictive controller, a process controller, can be used to achieve a determined control purpose in the local microgrid control with a system model and cost function. The upper layer concentrates on the microgrid economic dispatch problem, which can be formulated to a different type of problem such as linear problem, non-linear problem, mixed-integer linear problem, mixed-integer non-linear problem, Nash equilibrium problem, etc. The formulated problems of the upper layer are mostly based on multiple time scales, which need an accuracy and time-save load and power prediction model.

Under deterministic optimization, [19] proposes a novel optimization technique using a linear programming method to solve the optimal scheduling problem of distributed energy resources including battery energy storage systems. The proposed optimization technique has a dual objective function of economics and peak-shaving. A mixed-integer algorithm is used in [20, 21] to ensure energy cost reduction and reliability. Separately, in [20], the optimization focuses on the PV storage system, in [21], a flexible microgrid controller is designed and implemented through mixed-integer linear programming (MILP) optimization.

Considering the renewable energy variability and forecast uncertainty, robust optimization is regarded as a proper method for the problem formulation by considering the worst case. In [22], the authors propose a strategy using a two-stage decision process combined with a receding horizon approach. The first-stage decision variables are determined using a cutting-plane algorithm to solve a robust unit commitment; the second stage solves the final dispatch commands using a three-phase optimal power flow. In [23], a novel two-stage min-max-min robust optimal dispatch model is presented, and the column-and-constraint generation algorithm is implemented to efficiently obtain a robust dispatching plan for the microgrid, which minimizes the daily operating cost in the worst-case scenario. The reference [24] also proposes to use a robust optimization-based formulation. However, robust optimization methodologies have an important drawback. By the very nature of the methodology, robust optimal solutions are highly conservative, aiming to hedge against all possible worst-case realizations of the uncertainty. In some cases, this can lead to solutions that are too conservative [25]. A robust optimization based on worst cases may sometimes over pessimistically emphasize the problems so that the feasible region is reduced and resulting in an ineffective solution [26].

Stochastic optimization is a method that generates and uses random variables. In [27] the authors proposed a multi-carrier generation scheduling scheme that is formulated as a scenario-based nonlinear and stochastic optimization model based on a rolling horizon strategy. It is a mixed-integer nonlinear programming problem, which can be implemented with the freely available YALMIP toolbox in the MATLAB software and solved using the BONMIN solver. In [28], a hybrid stochastic/robust optimization model is proposed to minimize the expected net cost, this formulation can be solved by MILP.

In the aspect of the optimization object of microgrid, the single-object and the multi-object optimization can be used according to the user's needs. In [29], an alternative approach based on multi-objective optimization is proposed in order to maximize the "collective benefits" of a group of players. As such, the problem is formulated as multi-objective optimization and solved using a modified approach based on goal programming to ensure the Pareto optimality of the overall solution. In [30], an optimization problem with multiple objectives including economics, power quality, and security requirements, is solved by the optimization algorithm of chaotic group search optimizer with multiple producers.

Considering an AC/DC microgrid, the optimization problem is formulated based on different system models, and it is more complex to consider the reactive power in the AC microgrid. In [31] an economic dispatch problem for total operation cost minimization in DC microgrids is formulated. The optimization problem is solved in a heuristic method. The reference [32] proposes a multi-level energy management system for DC microgrids operations to ensure system reliability, power quality, speed of response, and control accuracy. In [33], a two-stage framework is introduced for active power real-time dispatch in islanded AC microgrids. In [34, 35], an optimization problem is formulated for an AC/DC hybrid microgrid economic dispatch.

In the aspect of the period of optimization, a multi-time scale can be used in the economics optimization of microgrid; it includes real-time, short-time, and long-time period. Due to the low-inertia nature of islanded AC microgrid, reliable control for active power real-time dispatch becomes a key issue for system operation [33]. Real-time pricing (RTP) is one of the new forms of agreement between the customers and the supplier, which allows real-time demand response [31]. The objective of [31] is to minimize the total operating cost in one optimization cycle in the context of RTP. In [36], a two-time-scale stochastic optimization dispatch schedule for PV based microgrid using demand-side management programs is proposed with day-ahead scheduling and real-time scheduling. In [26], the authors propose a bi-layer multi-time coordination method with the days-ahead schedule layer and the real-time dispatch layer. In the days ahead schedule layer, generating units are committed and relaxed bidirectional reserve boundaries are predicted for the next day [26]. In the real-time dispatch layer, generation output is dynamically adjusted and the reserve is dispatched using a successive approximation based on real-time data [26]. A multiple time-scale optimization scheduling including day-ahead and short-time for an islanded microgrid is studied in [37]. The day-ahead generation scheduling takes into account the minimum operational cost and the maximum load satisfaction as objective function [37]. Short-term optimal dispatch is based on minimizing the adjustment of day-ahead scheduling and giving priority to the use of renewable energy [37].

Considering the primary dynamic controller performance, the dynamic economic dispatch is an ideal method to improve controller performance. The reference [38] proposes a novel distributed approach to solve a new dynamic economic dispatch problem in which environmental cost function and ramp rate constraints are taken into consideration in an islanded microgrid. Then, a novel fully distributed

algorithm is proposed to address the dynamic economic dispatch problem based on the alternating direction method of multipliers and distributed consensus theory of the multi-agent system. In [39], the economic dispatch problem employs a dynamic performance controller based on PID control for improved performance by using an augmented Lagrange-based approach.

Considering the multi-microgrid and single microgrid, the economic dispatch method will be different. Single microgrid only considers single microgrid economics dispatch optimization. The microgrid economics dispatch optimization of multi-microgrid is more complex and useful than that of a single microgrid. In [40], a comprehensive real-time interactive energy management system framework for the utility and multiple electrically coupled microgrids. The introduced distributed economic dispatch strategy used in [40] can be easily configured in systems with multiple microgrids interconnection having different owners. In [29], the authors propose a methodology based on multi-objective optimization for optimal pricing and dispatch of energy resources in a multi-microgrid environment. The reference [41] proposes an operation model for multi-microgrid within the distribution system to achieve a higher operation economy. Motivated by the cooperative game theory, a number of individual microgrids are treated as one grand coalition and are scheduled via a centralized economic dispatch approach with the aim of minimizing global cost.

Regarding the aspects of centralized and decentralized economic dispatch, conventionally economic dispatch of all distributed generators is solved by centralized control with optimization algorithms or distributed control with consensus algorithms [42-44]. To improve the reliability, scalability, and economy of microgrid, a fully decentralized economic power-sharing strategy is proposed in [42]. In [45], the challenge to apply the consensus-based method is to meet the power balance constraint without the centralized facility, since the value of power mismatch is hard to be obtained for a distributed control system. To solve the problem, [45] proposes the method to combine the frequency control methods with the consensus protocol from graph theory to develop the distributed economics dispatch control method. Decentralized economic operation schemes have several advantages when compared with the traditional centralized management system for microgrids [46]. Specifically, decentralized schemes are more flexible, less computationally intensive, and easier to implement without relying on communication infrastructure [46].

More theories from other disciplines, such as economics, mathematics, industrial, are used in economics dispatch of a microgrid.

In [24], the authors present a problem of generation scheduling of self-generation power plant in energy-intensive industries microgrid with wind power, which uses a robust optimization-based formulation to obtain the feasible range and then decouples a multiperiod scheduling problem the based on feasible range into a series of single period economic dispatch problems. In [35], a two-layer control scheme is proposed for maintaining the frequency and the optimal economic operation of hybrid AC/DC microgrids, in which the implementation of the lower layer control presents an iterative solution for the

decentralized dispatch in real-time; the operations of AC and DC sections at the upper layer are coordinated by regulating the interlinking converters power exchange. In [47] an enhanced multi-period dispatch model for microgrids is described, in which frequency-aware islanding constraints are established to ensure microgrids with the capability to ride through unplanned islanding events and a two-stage solution strategy is proposed to remove the nonlinearity. In [48], the authors present a hierarchical distributed model predictive control regarding the large-scale, geographically dispersed, for standalone wind/solar/battery power generation system. The upper layer utilizes an iterative distributed control strategy to realize the coordination of the power dispatch. The lower layer utilizes the supervisory predictive control to realize both the economic and property to track the controller reference. In [49] an economic dispatch scheme is formulated using a predictive optimization policy called receding horizon control. The proposed power dispatch framework is able to incorporate multi-step ahead forecasts of wind power and energy price, and an innovative intelligent forecast model is presented using the radial-basis functional network. The article [50] investigates the economic dispatch problem of microgrids in a distributed fashion. To address this issue, a delay-free-based distributed algorithm is presented to optimally assign the whole energy demand among local generation units with the objective of minimizing the aggregated operation cost. In [51], a data-driven energy management solution based on a Bayesian optimization algorithm for a single grid-connected home microgrid is presented. The proposed solution formulates the optimization problem without a closed-form objective function expression and solves it using the Bayesian optimization algorithm-based data-driven framework. The article [45] introduces a new consensus-based control scheme for distributed power systems to solve the distributed economic dispatch problem. In [45], PI frequency controller and neural network frequency controller with the consensus protocol from graph theory are employed to develop the distributed economic dispatch control method. Consensus-based methods can be used to reach an agreement on the incremental costs in a large distributed system, which is a lack of control center.

The two main problems in the microgrid economic dispatching optimization are how to build the electricity tariff modeling and how to give economic dispatching optimization when the microgrid is operating. To give the electricity tariff of every component needs to consider many factors, such as geographic location, equipment cost, local government policy, etc. To achieve an economic dispatching optimization when the microgrid is operating needs the proper problem formulation by using proper optimization theory.

The day-ahead optimization, short-time optimization, robust optimization, stochastic optimization, and Markov decision processes belong to offline optimization where complete information is assumed. On the opposite, online optimization is a field of optimization theory that deals with optimization problems having no or incomplete knowledge of the future. The reference [52] presents a distributed algorithm for online energy management in networked microgrids with a high penetration of distributed energy resources. The online algorithm provides a less conservative schedule than the robust optimization-based approach.

In order to compromise the computation complexity and the accuracy of the optimization problem, the problem formulation is important to be simplified, such as to transfer non-linear constraints to linear constraints, to use smoothing or approximated function.

1.3. Objective of the thesis

Decentralized generation grows significantly, and grid-connected system is proposed in most applications. However, the intermittent and unpredictable nature of renewable energy sources, such as wind turbine and PV sources, remains an issue for their integration into the public grid resulting in, fluctuations of voltage and/or frequency, harmonic pollution, difficult load management. Urban areas have great potential for intensive development of these renewable energy sources. To increase their integration level and obtain a robust power grid, the smart grid could solve problems of peak consumption, optimal energy, demand response, and dynamic tariffs. The smart grid is being designed primarily to exchange information on grid needs and availability, and to help balancing powers via avoiding undesirable injection and performing peak shaving. Concerning ancillary services (grid technical regulations), for better decentralization of production, microgrids play an important role. A microgrid, seen as an off-grid / grid-connected system, includes a multi-source system consisting of renewable and traditional energy sources, storage systems, and adjustable loads. A controller is used to interact with the smart grid; it provides voltage control, power balancing, load shedding, and takes into account the constraints of the public grid provided by smart grid communication. At an urban scale, the building-integrated DC microgrid (Figure 2) provides a solution for the self-supply of buildings and controlled grid interaction.

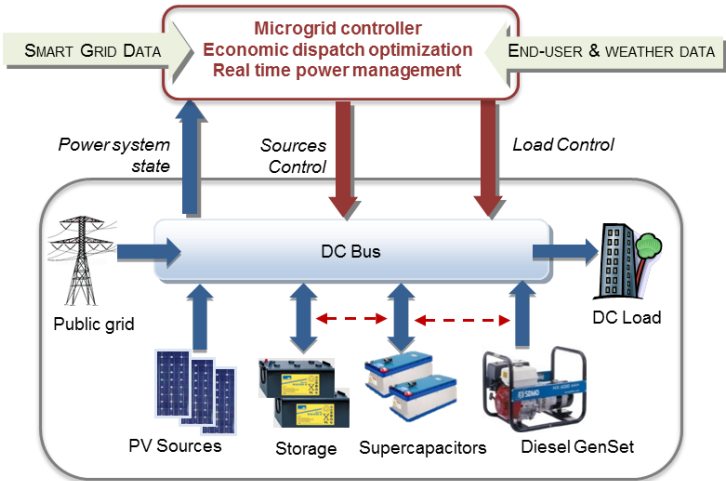


Figure 2. DC Microgrid [53].

The objective of this research is to design and develop an intelligent energy management system that optimizes power transfer in microgrid, adapts to conditions imposed by the public grid through the smart grid bus communication, and takes into account the various constraints in order to minimize the

energy consumption from the public grid and to make full use of local production. The main application is represented by commercial and office buildings.

The controller is designed as five subsystems structure: forecast, communication, economic dispatch, demand-side management, and operational. It is able to exchange data with the smart grid, takes into account forecast of power production and load consumption, storage capability, grid power limitations, dynamic grid tariffs, dynamic efficiency of converters, to optimize the load shedding, and handles instantaneous power balancing based on optimized powers flow. This interface between the smart grid and the proposed microgrid offers strategies that ensure, at the same time, local power balancing, local power flow optimization, and response to grid issues such as peak shaving and avoiding undesired injections.

The microgrid components consists of a set of PV panels, a battery storage (BS) system, a diesel generator (DG), a suit of supercapacitors (SC), a connection with public grid, a local building as the DC load.

The research, through this thesis, aims to study, design and develop intelligent control strategies using a predictive control approach which optimizes efficiently operation while satisfying constraints. Based on forecast data, dynamic efficiency of converters, and using non-linear optimization, predictive power flow is obtained off-line and on-line, which leads to a predictive control parameter for real-time power balancing. This predictive control parameter is the interface between the economic dispatch subsystem and the operational subsystem.

The operational subsystem handles instantaneous power balancing in the power system by applying the predictive control parameter and load shedding optimization and ensures self-correcting capability.

Both grid-connected and off-grid operating modes will be explored. In grid-connected mode, the microgrid controller should respond to grid issues such as peak shaving and avoiding undesired injections. During off-grid mode, the microgrid controller should be able to minimize diesel generator fuel.

The main scientific issue is the difficulty of day-ahead optimization due to the risk of mismatch between predictions and real-time operating conditions, on the one hand, and the need to take into account the constraints imposed by the public grid, on the other hand.

The first step is to study a centralized multi-layer supervisory system to achieve optimal power management in DC microgrid, which achieves the self-consumption for the building's electrical applications to reach the maximal usage rate of renewable energy while respecting the public grid constraints. The multiply operation modes are integrated. The constraints of PV sources, the public grid, the BS, the DG, and the SC are also considered, meanwhile, a real-time load optimization method is applied.

The second step is to study the non-linear optimization required for the consideration of the dynamic efficiency of static power converters in the power balancing equation.

Therefore, the research work goal is to implement the constraints of the power balancing equation, implying the dynamic efficiency of static power converters [54], firstly in the economic dispatching subsystem and secondly in the real-time control. This work is realized for grid-connected microgrid and separately for off-grid microgrid.

The third step focus on PV prediction model, which determines the accuracy of the day-ahead optimization, which influences the real-time power controlling. Thus, the PV prediction is important in the power management. However, the problem is that it is very difficult to get an accurate PV prediction model on day-ahead because of the intermitted PV generated power influenced by the uncertainty of the local weather. The aim of the third step is to find or propose an accurate enough PV prediction mode, which can be used in local computer with limited solving time.

1.4. Conclusion

This thesis briefly descripts the electric power system development. Then, the economic dispatching optimization in microgrid is introduced including the optimization studies for different topology microgrid, for multiple time scales, etc. Furthermore, the thesis objective is detailly given, and the main steps of the thesis are provided.

This thesis focus on the power control strategy and optimization of the local DC microgrid in grid-connected and off-grid operation models. The constraints of the DC microgrid and the characteristics of the components need to be concluded. The power quality should be maintained, and several objectives, such as minimize costs and maximize utilization of the renewable energy source, minimize the power loss in the local DC microgrid, need to be considered. However, there are many problems to be considered, such as the natural severe varies of the renewable energy sources, the non-linear of the components and power converters in the DC microgrid.

Chapter II. DC microgrid with multiply operation modes

The microgrid is an advanced electric power system that integrates multi-source and storage to give a better service for different load demand [55, 56]. However, it is complex to give an appropriate power management considering the natural characteristics of every component in the microgrid, such as the natural rapid and dramatic varies of the PV generated power, the low dynamic of the DG while its start-up, etc. [57, 58]. Compared with AC power grid, DC power grid can reduce control complexity without frequency adjustment while improving system efficiency because the PV generated power and most of storage and load are DC native, which motivates the studies of the DC microgrid [59-61].

In the previous research of our laboratory, the DC microgrid is designed to separate into two operation mode: grid-connected and off-grid mode. The grid-connected operation mode is based on the real case without considering the back-up source; the isolated operation mode which belongs to off-grid operation mode is built according to the independent microgrid without connection with the public grid; thus, it is more suitable for remote village or remote island [62, 63]. In fact, a full DC microgrid design should consider the grid-connected and off-grid mode at the same time; the public grid is used to exchange power with the DC microgrid to reduce the operation cost of the DC microgrid and the smart grid, and the long-term support back-up sources are also considered to prevent the critical load shedding when the public grid failure happens [64].

In this chapter, two DC microgrids are built to separately operate in grid-connected and off-grid operation modes, and then a DC microgrid is built considering the advantages of the grid-connected and off-grid operation modes, named full microgrid operation mode. The microgrid supervisory system [65, 66] is proposed for the grid-connected, off-grid, and the full microgrid operation modes. The real-time power management strategy is regarded to be achieve real-time power balance and the power priority rule is used according to the tariff of every component; and the day-ahead optimization is also considered to make power system can achieve pre-schedule and to reduce the total operational cost. In this chapter three microgrids are built and compared separately in the grid-connected, off-grid, and the full microgrid operation modes. The DC microgrid modeling is given in the Section II.1. The microgrid supervisory system is described in section II.2. In Section II.3, the tariff methods are introduced. In II.4., the day-ahead optimization for economic dispatching is separately proposed for the three microgrid operation modes, and the optimization algorithm is chosen. In Section II.5, the power management strategy is introduced to support the three operation modes. The conclusions of this chapter are given in Section II.6.

II.1. DC microgrid modeling

The physical components of a DC microgrid are shown in Figure 3. It consists of PV sources, a BS system, a public grid single-phase connection, a DG, an SC, and a DC load. All parts are connected to the common DC bus of the microgrid by a seven-leg power converter (B_1, B_2, \dots, B_7) and a set of inductors and capacitors to ensure compatibility among the components. B_1 is the leg connecting the PV with the DC bus, B_2 is the converter connecting the BS with the DC bus, B_3 and B_4 are the legs connecting the public grid with the DC bus, B_5 and B_6 are the legs connecting the DG with the DC bus, B_7 is the leg connecting the SC with the DC bus. The DC load directly connects to the DC bus.

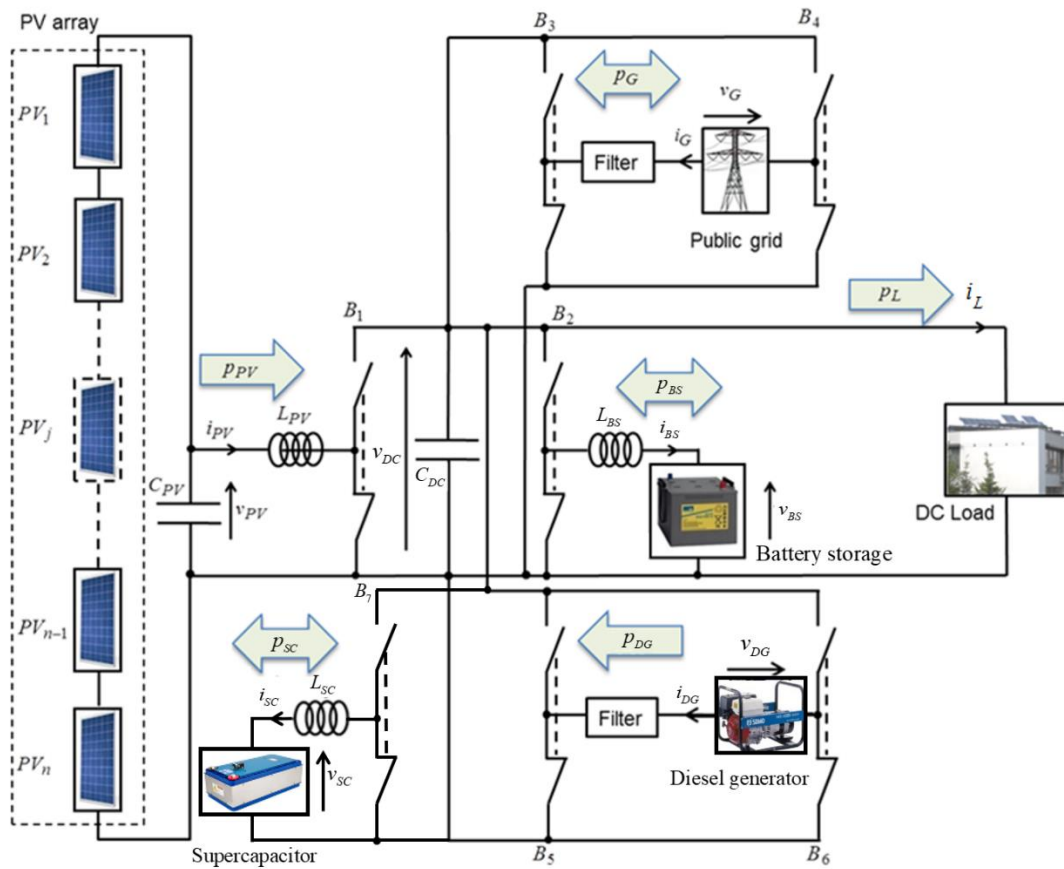


Figure 3. DC microgrid electrical scheme [53].

The PV sources consist of several PV panels, the PV generated power directly supplies the DC load through the DC bus for the maximal usage rate of renewable energy. If the PV generated power cannot support the DC load, the BS and the public grid would supply the DC load; if the PV, BS, and the public grid cannot provide enough power to the DC load, the non-critical load would be shed; if the critical load need to be shed, the DG would start as the back-up source; if the DC load still cannot be supported by the microgrid, the excessive load would be shed. If there is too much PV generated power to support the DC load, the BS and the public grid would absorb the rest of the PV generated power; if the BS and

the public grid would absorb cannot absorb the rest power, the PV can be shed to keep the power balance in the DC microgrid.

II.1.1. Microgrid system

For keeping the power balance and common DC bus voltage stable, a PI controller is introduced to calculate the power to be compensated by the public grid and BS. The power balance expressed by the equations (2. 1), (2. 2), and(2. 3) are introduced to keep the common DC bus voltage v_{DC} at the reference voltage noted by v_{DC}^* :

$$\Delta p = p_{PV} - p_L - p_{PI} \quad (2. 1)$$

$$p_{PI} = K_p (v_{DC}^* - v_{DC}) + K_I \int (v_{DC}^* - v_{DC}) \quad (2. 2)$$

$$\Delta p = p_{BS} + p_G - p_{DG} + p_{SC} \quad (2. 3)$$

where p_{PV} is the power of PV sources, p_L is the DC load power, K_p and K_I are the PI controller coefficients, Δp is the compensation power by the public grid, BS, DG, and SC, p_G is the public grid power, which represents the power injection when p_G is positive and power supply when p_G is negative; p_{BS} is the storage power that represents BS charging when p_{BS} is positive and BS discharging when p_{BS} is negative; p_{DG} is the DG supply power which is only 0 or positive; and p_{SC} is the SC power that represents SC charging when p_{SC} is positive and SC discharging when p_{SC} is negative.

II.1.2. PV sources

The PV model comes from [67], where a mathematical modelling of PV is introduced. To obtain the most economic benefits, the PV should be driven by a maximum power point tracking (MPPT) method [68].

To reach the maximum power point (MPP), searching algorithms are required, and the most used are perturb and observe (P&O) algorithm and incremental conductance (InC) algorithm. When the PV power is greater than the microgrid consumption, the system will be not stable, and the devices will be broken if out of their tolerations. Thus, a limit controller is proposed in [68], whose goal is to operate PV shedding, in case the PV power generation is over the consumption of the microgrid.

$$P_{PV} = P_{PV_MPPT} - P_{PV_S} \quad (2. 4)$$

where P_{PV_MPPT} is the MPPT power of PV at the standard test conditions (STC), P_{PV_S} is the shedding power of PV.

II.1.3. Public grid connection

The public grid is a large-scale and complex electric power system. In a microgrid, it is seen as a source that can supply and absorb power. The public grid power equipment must be protected from the overload by giving the power limitations for injection and supply as in the equation (2. 5):

$$-P_{G_MAX} \leq p_G(t) \leq P_{G_MAX} \quad (2. 5)$$

where p_G is the public grid power, which represents the power injection when p_G is positive and power supply when p_G is negative. The public grid power injection is limited by P_{G_MAX} . The public grid power supply is limited by $-P_{G_MAX}$. Therefore, when the public grid power injection and grid power supply are limited, it is required to operate the load shedding or PV shedding when the public grid reaches its limitations.

II.1.4. Battery storage system

The BS can supply and absorb power to keep the microgrid power balance. Owing to low cost and high recycling rate, lead-acid battery is the most used in a small power microgrid; however, although more expensive but more efficient, lithium-ion is also a worldwide used battery technology. To avoid overcharging and over-discharging, it is necessary to limit its state of charge soc_{BS} . The soc_{BS} is calculated according to the equation (2. 6), where C_{BS_REF} is the battery capacity, v_{BS} is the BS voltage, and soc_{BS} is limited between two limits, SOC_{BS_MIN} and SOC_{BS_MAX} , as in the equation (2. 7). The power p_{BS} is the BS power that represents BS charging when p_{BS} is positive and BS discharging when p_{BS} is negative. The BS charging and discharging powers are limited by P_{BS_MAX} and $-P_{BS_MAX}$ respectively, as in the equation (2. 8).

$$soc_{BS}(t + \Delta t) = soc_{BS}(t) + \frac{100\%}{3600C_{BS_REF}v_{BS}} \int_t^{t+\Delta t} p_{BS}(t)dt \quad (2. 6)$$

$$SOC_{BS_MIN} \leq soc_{BS}(t) \leq SOC_{BS_MAX} \quad (2. 7)$$

$$-P_{BS_MAX} \leq p_{BS}(t) \leq P_{BS_MAX} \quad (2. 8)$$

II.1.5. Diesel generator and supercapacitor

The DG is a backup source that can provide long-term support for microgrid. However, the DG start-up stage presents a slow dynamic behavior. Therefore, during the period of the DG starting up, an SC is suggested to compensate for the power balance because of its fast response and high-power density [58]. There are two operation modes of the DG to be considered, duty cycle mode and load following. At the

duty cycle mode, the DG is turn on in the constant period to provide its maximal power to supply the load demand and to charge the BS; at the load-following mode, the DG is turned on to only supply the load demand. In fact, the DG operates at a lower power of the load following mode than the power of the duty cycle mode in the daytime of the weekday, it is meaning that the DG has a low efficiency at load-following mode. So, the duty cycle mode is better than the load following mode because the DG only works when it can output a high power and the BS is regarded as the power storage can be recharged by the DG to reduce the operation time of the DG. Thus, it is assumed the DG works at duty cycle mode as in [69], where the duty cycle mode is proved to be better than a load-following mode, and one-hour is proposed as a good trade-off between fuel consumption and start-up frequency.

When the DG is turned off, the DG power p_{DG} is 0. When the DG is turned on, the DG power p_{DG} is limited by maximal DG supply power P_{DG_MAX} as given in the equation (2. 9), which is chosen as the same level of the PV power and the load demand power. Due to the slow dynamic behavior of the DG start-up stage, the DG cannot support the microgrid until it satisfies the conditions expressed by the equation (2. 10), which also can prevent the converter from being broken by the peak power of the DG start-up stage. During the period between DG start-up and DG stable state given by the equation (2. 10), the SC compensates the microgrid to keep its power balance. In the duty cycle mode, the time constraints when the DG is turned on is shown in the equation (2. 11), the time constraints when the DG is turned off is provided in the equation (2. 12).

$$0 \leq p_{DG}(t) \leq P_{DG_MAX} \quad (2. 9)$$

$$\begin{cases} 310V < v_{DG} < 340V \\ 48Hz < f_{DG} < 52Hz \end{cases} \quad (2. 10)$$

$$t_{DG_ON} \leq T_{DG_ON_MAX} \quad (2. 11)$$

$$t_{DG_OFF} \geq T_{DG_OFF_LIM} \quad (2. 12)$$

where the v_{DG} is the DG voltage, f_{DG} is DG voltage frequency in the equation (2. 10), t_{DG_ON} is the DG on time, t_{DG_OFF} is the DG off time, $T_{DG_ON_MAX}$ is the time constraints when the DG is turned on, $T_{DG_OFF_LIM}$ is the time constraints when the DG is turned off.

The SC power p_{SC} is limited to its maximal SC charging power P_{SC_MAX} and maximal SC discharging power $-P_{SC_MAX}$ as in the equation (2. 13). The energy of SC E_{SC} is calculated according to SC capacitance C_{SC} and SC voltage v_{SC} as expressed by the equation (2. 14). The $E_{SC}(t)$ and E_{SC_Rated} provide the $soc_{SC}(t)$, which can be simplified as in the equation (2. 15).

$$-P_{SC_MAX} \leq p_{SC}(t) \leq P_{SC_MAX} \quad (2. 13)$$

$$E_{SC} = \frac{C_{SC} \cdot v_{SC}^2}{2} \quad (2.14)$$

$$soc_{SC}(t) = \frac{E_{SC}(t)}{E_{SC_Rated}} = \frac{\frac{C_{SC} v_{SC}^2(t)}{2}}{\frac{C_{SC} v_{SC_Rated}^2}{2}} = \frac{v_{SC}(t)}{v_{SC_Rated}} 100\% \quad (2.15)$$

As to the SC model given in [58], the SC is natural self-discharging. It should be recharged at a certain time to keep its lowest energy for DG start-up compensation and it is also necessary to define the SC recharge period. So, soc_{SC} limitations are provided: $SOC_{SC_MIN_MIN}$, $SOC_{SC_MIN_MAX}$, $SOC_{SC_MAX_MIN}$, and $SOC_{SC_MAX_MAX}$. When PV power is enough for load demand power, the recharging start-time and recharging end-time are respectively the time when soc_{SC} reaches $SOC_{SC_MAX_MIN}$ and $SOC_{SC_MAX_MAX}$. The soc_{SC} minimal limitation for the SC is $SOC_{SC_MIN_MIN}$ and the soc_{SC} minimal limitation for DG start-up compensation is $SOC_{SC_MIN_MAX}$. When PV power is insufficient for load demand power, the recharging start-time is the time when soc_{SC} reaches $SOC_{SC_MIN_MAX}$ which can keep the SC energy supporting the DG start-up.

II.1.6. DC load

The DC load, whose power changes according to the demand of buildings, is electrical appliances of buildings. Therefore, in order to operate the demand side management, *i.e.* to allow a load shedding optimization, it is necessary to assign the priority of each electrical appliance, to define the time duration of load shedding, to define the power based on the real electrical appliances and critical loads. The purpose is to define the load power closing to the real load power by applying a load shedding real-time optimization [70], which is formulated to the load optimization problem based on the knapsack problem and solved by MILP with IBM CPLEX [71]. The load power p_L and the load shedding power p_{L_S} are given respectively by the equations (2.16) and (2.17), where p_{L_OPT} is the load power after the load real-time optimization, p_{AVAIL} is the total available DC microgrid power, and p_{L_D} is the load demand power.

$$p_L = \begin{cases} p_{L_OPT} & \text{if } p_{AVAIL} < p_{L_D} \\ p_{L_D} & \text{if } p_{AVAIL} \geq p_{L_D} \end{cases} \quad (2.16)$$

$$p_{L_S} = p_{L_D} - p_L \quad (2.17)$$

The coefficient k_{L_CRIT} represents the percentage rate defined by the end-user as the minimum amount of load demand that must be attended; it is defined by the critical load p_{L_CRIT} and the equation

(2. 18) where p_{L_CRIT} is the minimum power of load demand that must be always attended; p_{L_D} equals to the sum of p_{L_CRIT} and $p_{L_N_CRIT}$ provided in the equation (2. 19) where the non-critical load $p_{L_N_CRIT}$ is the maximum power of load demand that can be shed.

$$k_{L_CRIT} = p_{L_CRIT} / p_{L_D}, k_{L_CRIT} \in [0\%, 100\%] \quad (2. 18)$$

$$p_{L_D} = p_{L_CRIT} + p_{L_N_CRIT} \quad (2. 19)$$

II.2. Microgrid supervisory overview

The proposed multi-layer supervisory structure can integrate different layers that operate in different scale time. The purpose of the microgrid supervisory is to interact with the smart grid and the end-user and to be able to receive metadata from external sources, meanwhile, to keep the instantaneous power balance in the microgrid. The multi-layer supervisory structure is based on several previous works of the AVENUES laboratory, depicted in detail in [72-76].

Figure 4 and Figure 5 present the concept of the multi-layer supervisory system. In the measurement block, the instant state of charge of BS soc_{BS} and of SC soc_{SC} are respectively estimated by using the equations (2. 6) and (2. 15) with the instant measurement data p_{BS} and v_{SC} .

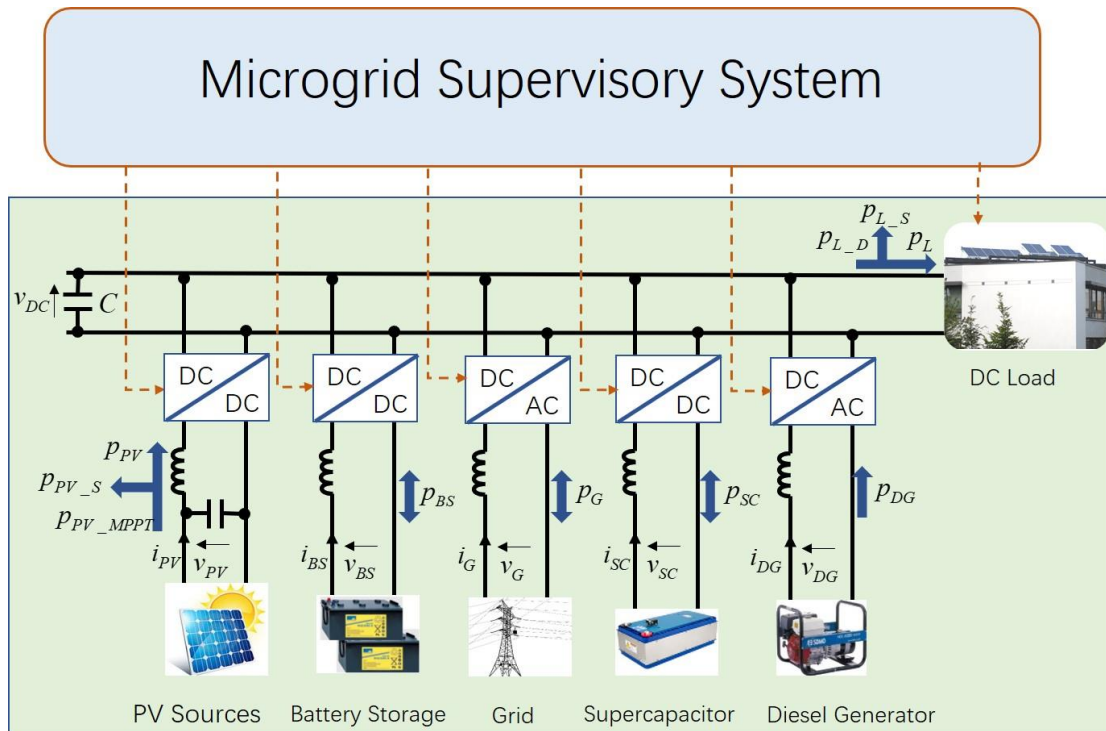


Figure 4. Microgrid multi-layer supervisory concept.

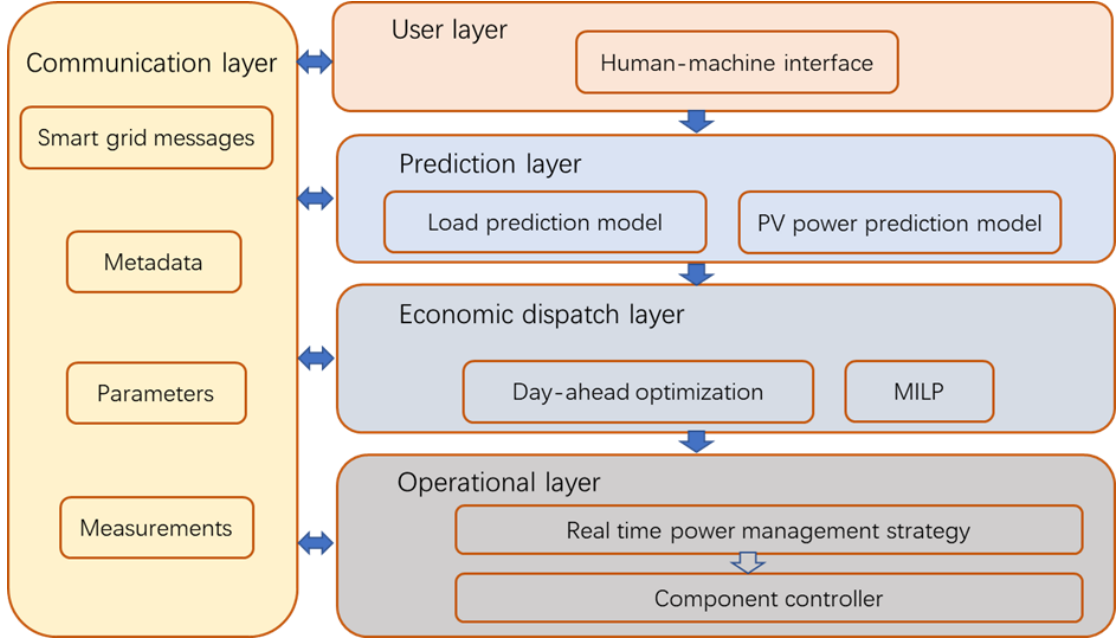


Figure 5. The detail of the microgrid multi-layer supervisory concept.

The parameters block includes the group of parameters related to the microgrid and their physical limitations. The metadata block receives the forecast data. The smart grid messages block represents the communication with the public grid, exchanging information about the maximum power that can be sent towards the public grid and the maximum power that can be used from the public grid to supply the microgrid system P_{G_MAX} .

The human-machine interface is responsible for the interaction with the end-user, allowing the end-user to personalize the microgrid environment to suit individual needs.

The prediction layer is responsible for the interpretation of the metadata; it comprises the calculation of the PV power and load power predictions. The load power prediction p_{L_PRE} is generally calculated by the operator of the public grid. In this research, the p_{PV_PRE} is calculated based on the g_{PRE} and θ_{AIR_PRE} prediction by using the method given in [68], where the PV panel temperature prediction θ_{PV_PRE} is estimated by the equation (2. 20), the p_{PV_PRE} is calculated according to the equation (2. 21).

$$\theta_{PV_PRE} = \theta_{AIR_PRE} + g_{PRE} \frac{NOCT - \theta_{AIR_TEST}}{G_{TEST}} \quad (2. 20)$$

$$P_{PV_PRE} = P_{PV_MPPT_STC} + \frac{g_{PRE}}{1000} [1 + \gamma_s (\theta_{PV_PRE} - 25)] N_{PV} \quad (2. 21)$$

where nominal operating cell temperature ($NOCT$) is PV cells temperature at standard test condition, θ_{AIR_TEST} is the air temperature at standard test condition, G_{TEST} is the solar irradiation at standard test condition, N_{PV} is the number of the PV panel, γ_s is the temperature coefficient of PV power.

The economic dispatch layer optimizes the usage of the renewable sources, storage and the power exchanged with the public grid and the DG usage in multiple operation modes. The main goal of this economic dispatch layer is to reduce the global energy cost, taking into account the information exchanged with the prediction layer, the information received through the smart grid message, the settings defined by the end-user and the system parameters to perform the optimization.

Working in the grid-connected mode, the economic dispatch layer aims to minimize the energy cost by following the optimized trend of usage of the BS and public grid. This optimal control vector noted k_D is calculated based on the optimal BS and public grid power evolutions.

Working in the off-grid mode, the economic dispatch layer aims to minimize the energy cost by following the optimized usage of the BS and the DG. The optimization respecting the constraints imposed by the off-grid mode, the resulting power flow obtained based on the optimal BS and DG power evolutions, is used to calculate the distribution coefficient k_{DG} showing when DG has to operate. Therefore, the off-grid optimal control vector noted k_{DG} is responsible for defining the trade-off between BS power and DG power during the running of the operational layer.

When the microgrid works in the full microgrid mode, both coefficients, k_D and k_{DG} , are calculated in the optimization layer to give a trend to optimize the power dispatch among BS power, public grid power, and DG power.

The operational layer is responsible for keeping the instant power balance and the DC bus voltage stabilization.

II.3. Tariff description

The static and particularly the dynamic pricing could allow the demand side response to play a more active role to help balance power supply and demand and to reduce the public grid stress. Some approaches to increase the demand side participation are the time-of-use pricing (TOU), the RTP, and the critical peak pricing (CPP).

TOU tariffs derived from wholesale energy prices can encourage customers to take advantage of the price variations to schedule their electricity use. In a TOU pricing scheme, a group of prices is fixed in advance and they apply to different predefined intervals of a calendar day, where the electricity prices are differentiated by patterns and the rates [77].

The RTP [77-79] tends to be more complex than the TOU because the RTP changes the tariff in a period of minutes. The CPP [80-82] allows the distribution grid operator to occasionally increase the tariff for a limited number of hours given the consumption peak. Users with a flat load profile or with high consumption during low price periods, *i.e.* off-peak hours, are going to have the greatest benefits

from the RTP. But even some users demand peaks match the high price periods during peak hours, they could also have some benefits because of the reduction of the tariff during peak hours when others could shift some load to off-peak hours, even if this tariff would still be considerably greater than off-peak periods.

Since the optimal load shedding is performed inside of the microgrid supervisory system, instead of giving the partial control of the user's appliances to the distribution grid operator, the operator is only responsible for defining the maximum amount of power that can be taken from the grid and the microgrid supervisory system will ensure to respect this condition, performing a load shedding or using backup sources to supply the demanded load power.

The other energy sources' tariffs are chosen arbitrarily but following the rule presented in the equations (2. 22) and (2. 23) for the grid-connected and off-grid modes, respectively. This rule is designed to prioritize the load supply and the usage of renewable sources; for those reasons, the cost for load shedding and PV shedding are the highest ones.

$$T_{BS} \ll T_G < T_{PV_S} < T_{L_S} \quad (2. 22)$$

$$T_{BS} < T_{SC} \ll T_{DG_F} < T_{PV_S} < T_{L_S} \quad (2. 23)$$

where T_{BS} and T_{SC} are roughly set to be fixed energy tariff according to their lifespan, T_{PV_S} is set as a penalization for the shedding PV power, T_{L_S} is set to be the highest cost to protect the load demand as fixed shedding penalization tariff and T_{DG_F} is simply set as a DG fixed fuel tariff to be easily used.

II.4. Economic dispatching optimization

The economic dispatch layer of the supervisory described in Figure 5 aims to optimize the energy usage by using all predictions data while taking into account the information exchanged with the smart grid and the end-user. Its goal is to reduce the energy cost for the end-users.

The following part of this study describes the optimization problem formulation for grid-connected mode, the off-grid mode, and full microgrid mode. The solver, MILP, is used to solve the formulated problem. The output of the optimization is the power flows of sources and load translated into the distribution coefficients k_D and k_{DG} regarded as predictive control variables, which are responsible for the communication with the operational algorithm to ensure the optimal operation.

It is assumed that the optimization is performed day-ahead, i.e. once before the day operation by using a dataset from Météo France and a load consumption prediction.

II.4.1. Problem formulation

II.4.1.1. Grid-connected microgrid problem formulation

For on grid-connected mode the DC microgrid has a point of common coupling (PCC) with the public grid, have the capacity to exchange power with the public grid in a bidirectional way, buying and selling energy to the grid. The DG is not supposed to run in grid-connected mode. The detailed grid-connected microgrid power flow can be seen in Figure 6.

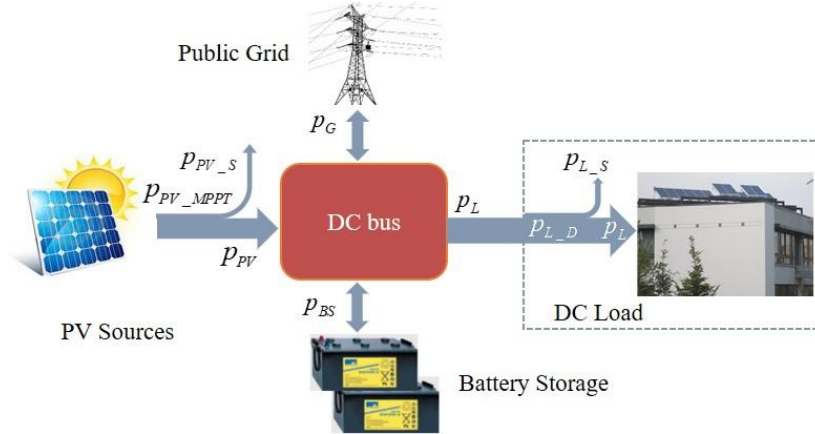


Figure 6. Grid-connected microgrid power flow.

The power flow presented in Figure 6 shows two fully controllable sources, BS and public grid connection, as well as other two partially controllable components, PV and load. The fully controllable sources are used to ensure stability on the bus, given its capacity to inject and remove energy from the bus.

The proposed problem formulation is based on the operation characteristics and constraints presented on (2. 1), (2. 2), (2. 3), (2. 4), (2. 5), (2. 6), (2. 7), (2. 8), (2. 17), (2. 18), and (2. 19) The DC bus voltage stability is then ensured by the power balance constraint presented in (2. 24). The controller dynamic of microgrid is not considered at this stage.

$$p_{PV_MPPT}(t) - p_{PV_S}(t) = p_{L_D}(t) - p_{L_S}(t) + p_{BS}(t) + p_G(t) \quad (2. 24)$$

The total cost to be minimized by the optimization algorithm is described in (2. 25).

$$C_{TOTAL} = C_{BS} + C_G + C_{PV_S} + C_{L_S} \quad (2. 25)$$

where C_{PV_S} is the PV shedding energy cost presented in (2. 26), C_{L_S} is the load shedding energy cost following (2. 27), and C_{BS} is the BS energy cost given by (2. 28), and C_G is the public grid energy cost described in (2. 29).

The PV energy cost is calculated according to the amount of PV shedding power and its tariff in (2. 26). The load energy cost is achieved according to the amount of load shedding power and its tariff in

(2. 27). The BS cost is described in (2. 28), and total public grid energy costs C_G is presented in (2. 29). The C_G maybe a negative cost representing the fact that when the energy is injected into the public grid to sell power to decrease the overall cost.

$$C_{PV_S} = \frac{1}{3.6 \times 10^6} \sum_{t_i=t_0}^{t_F} T_{PV_S}(t_i) \cdot \Delta t \cdot p_{PV_S}(t_i) \quad (2. 26)$$

$$C_{L_S} = \frac{1}{3.6 \times 10^6} \sum_{t_i=t_0}^{t_F} T_{L_S}(t_i) \cdot \Delta t \cdot p_{L_S}(t_i) \quad (2. 27)$$

$$C_{BS} = \frac{1}{3.6 \times 10^6} \sum_{t_i=t_0}^{t_F} T_{BS}(t_i) \cdot \Delta t \cdot |p_{BS}(t_i)| \quad (2. 28)$$

$$C_G = \frac{1}{3.6 \times 10^6} \sum_{t_i=t_0}^{t_F} T_G(t_i) \cdot \Delta t \cdot (-p_G(t_i)) \quad (2. 29)$$

Considering a continuous operation of the system into a finite horizon, the time t is defined in (2. 30). The optimization algorithm provides the optimal energy cost of the day.

$$t_i = \{t_0, t_0 + \Delta t, t_0 + 2\Delta t, \dots, t_F\} \quad (2. 30)$$

where the time interval between two samples is defined as Δt and the initial and final time being respectively t_0 and t_F .

The whole optimal power dispatching problem is formulated as in (2. 31) and (2. 32).

Variables :

$$\begin{aligned} p_{PV}(t_i) &\in [0 \quad p_{PV_MPPT}(t_i)] \\ p_{PV_S}(t_i) &\in [0 \quad p_{PV_MPPT}(t_i)] \\ p_L(t_i) &\in [0 \quad p_{L_D}(t_i)] \\ p_{L_S}(t_i) &\in [0 \quad p_{L_CRIT}(t_i)] \\ p_{BS}(t_i) &\in [-p_{BS_MAX} \quad p_{BS_MAX}] \\ soc_{BS}(t_i) &\in [SOC_{BS_MIN} \quad SOC_{BS_MAX}] \\ p_G(t_i) &\in [-P_{G_MAX} \quad P_{G_MAX}] \end{aligned} \quad (2. 31)$$

$$\begin{aligned}
& \min C_{TOTAL} = C_{BS} + C_G + C_{PV_S} + C_{L_S} \\
& \text{s.t.} \left\{ \begin{aligned}
& p_{PV}(t_i) + p_{DG}(t_i) = p_L(t_i) + p_{BS}(t_i) + p_G(t_i) \\
& p_{PV}(t_i) = p_{PV_MPPT}(t_i) - p_{PV_S}(t_i) \\
& p_L(t_i) = p_{L_D}(t_i) - p_{L_S}(t_i) \\
& \text{if } p_{PV_MPPT}(t_i) \geq p_{L_D}(t_i) \text{ then } \begin{cases} p_G(t_i) \geq 0 \\ p_S(t_i) \geq 0 \end{cases} \\
& \text{if } p_{PV_MPPT}(t_i) \leq p_{L_D}(t_i) \text{ then } \begin{cases} p_G(t_i) \leq 0 \\ p_S(t_i) \leq 0 \end{cases} \\
& \text{if } soc_{BS}(t_i) < SOC_{BS_MAX} \text{ then } p_{PV_S}(t_i) = 0 \\
& \text{if } soc_{BS}(t_i) > SOC_{BS_MIN} \text{ then } p_{L_S}(t_i) = 0 \\
& p_{L_S}(t_i) \leq (1 - k_{L_CRIT}) \cdot p_L(t_i) \\
& soc_{BS}(t_i) = SOC_{BS_0} + \frac{1}{3600 \cdot v_S \cdot C_{REF}} \sum_{t_i=t_0}^{t_F} p_{BS}(t_i) \Delta t \\
& |p_G(t_i) - p_G(t_{i-1})| \leq P_{GF_Limit} \\
& t_i = \{t_0, t_0 + \Delta t, t_0 + 2\Delta t, \dots, t_F\}
\end{aligned} \right. \quad (2.32)
\end{aligned}$$

where P_{GF_Limit} is the power limit for the public grid power fluctuation.

Due to the different operation period between economic dispatch layer and operational layer, the optimization results in the economic dispatch layer, which is directly introduced into the operational layer will lead to the power unbalance in DC bus; therefore, the economic optimization coefficients k_D are given to introduce the economic optimization results into the operational layer and to decouple the system operation between economic dispatch layer and operational layer. The k_D are calculated according to (2.33).

$$k_D = p_{BS} / (p_{BS} + p_G), k_D \in [0, 1] \quad (2.33)$$

where k_D is the division value between the BS and the sum of the BS and the public grid.

II.4.1.2. Off-grid microgrid problem formulation

The DC microgrid operating in off-grid mode uses DG instead of the public grid connection as a back-up source. Its goal is to supply the load under the multi-source rated power capacity with the power balance at a minimum energy cost while minimizing the usage of DG. The detailed power flow of the off-grid microgrid can be seen in Figure 7.

The proposed problem formulation is based on the operation characteristics and constraints presented already in (2.1), (2.2), (2.3), (2.4), (2.6), (2.7), (2.8), (2.9), (2.17), (2.18), and (2.19). Note that the constraints of SC are not considered in the optimization problem formulation, because, on the one hand, it is only used to compensate the real-time start-up of the DG, on the other hand, regarding

the self-discharge of the SC, one of the most evident SC characteristics, it increases too much the complexity of the optimization problem formulation.

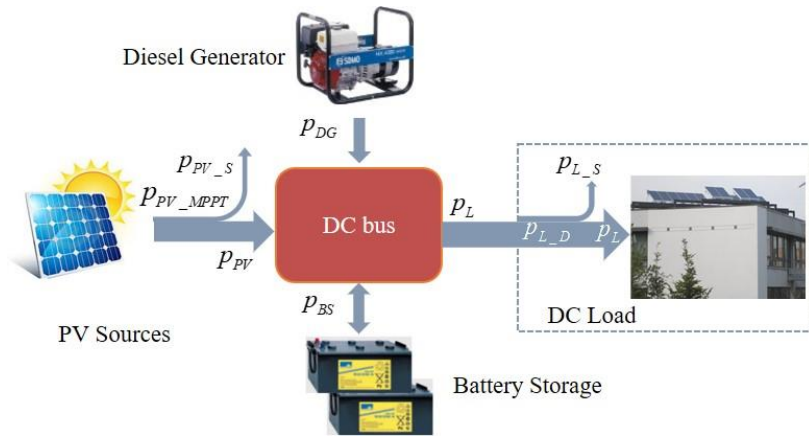


Figure 7. Off-grid microgrid power flow.

The optimization problem formulation has to consider the instantaneous power balance given by (2. 34), as well as the minimization of the total energy cost given by (2. 35).

$$p_{PV}(t) + p_{DG}(t) = p_L(t) + p_{BS}(t) \quad (2. 34)$$

$$C_{TOTAL} = C_{DG} + C_{PV_S} + C_{L_S} + C_{BS} \quad (2. 35)$$

where C_{TOTAL} is the total energy cost, and C_{DG} is the DG energy cost given by (2. 38), which is the sum of the DG fixed fuel cost C_{DG_F} and the DG operating and maintaining cost $C_{DG_O\&M}$ respectively provided by (2. 36) and (2. 37).

$$C_{DG_F} = \frac{1}{3.6 \times 10^6} \sum_{t_i=t_0}^{t_f} T_{DG_F}(t_i) \cdot \Delta t \cdot p_{DG}(t_i) \quad (2. 36)$$

$$C_{DG_O\&M} = \frac{1}{3.6 \times 10^3} \sum_{t_i=t_0}^{t_f} T_{DG_O\&M}(t_i) \cdot \Delta t \cdot (p_{DG}(t_i) > 0) \quad (2. 37)$$

$$C_{DG} = C_{DG_F} + C_{DG_O\&M} \quad (2. 38)$$

where T_{DG_F} is the tariff of the DG fuel, $T_{DG_O\&M}$ is the tariff of the DG operation and maintenance.

During the operation of the off-grid DC microgrid, it is assumed that:

- the load shedding is not allowed when BS has enough power;
- the non-critical load may be shed when there is not enough power in BS;
- the PV shedding is not permitted when the microgrid can consume its production.

The whole optimal power dispatching problem is formulated as follows (2. 39) and (2. 40).

Variables :

$$\begin{aligned}
p_{PV}(t_i) &\in [0 \quad p_{PV_MPPT}(t_i)] \\
p_{PV_S}(t_i) &\in [0 \quad p_{PV_MPPT}(t_i)] \\
p_L(t_i) &\in [0 \quad p_{L_D}(t_i)] \\
p_{L_S}(t_i) &\in [0 \quad p_{L_CRIT}(t_i)] \\
p_{BS}(t_i) &\in [-p_{BS_MAX} \quad p_{BS_MAX}] \\
SOC_{BS}(t_i) &\in [SOC_{BS_MIN} \quad SOC_{BS_MAX}] \\
p_{DG}(t_i) &\in \{0\} \cup [p_{DG_ON_MIN} \quad p_{DG_ON_MAX}]
\end{aligned} \tag{2.39}$$

$$\begin{aligned}
\min C_{TOTAL} &= C_{BS} + C_{DG} + C_{PV_S} + C_{L_S} \\
s.t. \left\{ \begin{aligned}
&p_{PV}(t_i) + p_{DG}(t_i) = p_L(t_i) + p_{BS}(t_i) \\
&p_{PV}(t_i) = p_{PV_MPPT}(t_i) - p_{PV_S}(t_i) \\
&p_L(t_i) = p_{L_D}(t_i) - p_{L_S}(t_i) \\
&\text{if } p_{PV_MPPT}(t_i) \geq p_{L_D}(t_i) \text{ then } p_{BS}(t_i) \geq 0 \\
&\text{if } p_{PV_MPPT}(t_i) \leq p_{L_D}(t_i) \text{ and } p_{DG}(t_i) = 0 \text{ then } p_{BS}(t_i) \leq 0 \\
&\text{if } SOC_{BS}(t_i) > SOC_{BS_MIN} \text{ then } p_{L_S}(t_i) = 0 \\
&p_{L_S}(t_i) \leq (1 - k_{L_CRIT}) \cdot p_L(t_i) \\
&\text{if } SOC_{BS}(t_i) < SOC_{BS_MAX} \text{ and } p_{DG}(t_i) = 0 \text{ then } p_{PV_S}(t_i) = 0 \\
&SOC_{BS}(t_i) = SOC_{BS_0} + \frac{1}{3600 \cdot v_s \cdot C_{REF}} \sum_{t_i=t_0}^{t_F} p_{BS}(t_i) \Delta t \\
&p_{DG}(t_i) = p_{DG}(t_{i-1}) \text{ if } rem(t_i / dt_{DG}) \neq 0 \\
&t_i = \{t_0, t_0 + \Delta t, t_0 + 2\Delta t, \dots, t_F\}
\end{aligned} \right. \tag{2.40}
\end{aligned}$$

Normally, the time constraint for the DG should be formulated according to the equation (2. 11) and (2. 12), at the time, the time counters for t_{DG_ON} and t_{OFF_ON} should be formulated due to the DG operates in the duty cycle mode. However, it is too complex for a solver and gives a big solution space to search, so, the time constraint for the DG is simplified to be the constraints shown in the equation (2. 40).

In the equation (2. 40), the operating mode of the DG can be changed as well as the period dt_{DG} , and the operation power of DG is formulated to be a constant value, which is chosen between DG minimum output power (W) while DG start-up $p_{DG_ON_MIN}$ and DG maximum output power (W) while DG start-up $p_{DG_ON_MAX}$, during its period. When $p_{DG_ON_MIN}$ equal to $p_{DG_ON_MAX}$, the DG must operate at a certain constant power in the whole optimization process. When $p_{DG_ON_MIN}$ is less than $p_{DG_ON_MAX}$, the operation power of the DG can be different between $p_{DG_ON_MIN}$ and $p_{DG_ON_MAX}$ in the whole optimization process. So, how to choose the better constant DG power value or the better range of values for the DG operation power can be an important problem. The constant DG power value is a stricter constraint than the range of values for the DG operation power. So, it is more likely that the

inappropriate setting of the constant DG power value lets the optimization problem to be not optimal, even be infeasible when the DG operates at a constant power.

The k_{DG} is introduced in (2. 41) based on the same reason as the k_D to decouple the system operation between the economic dispatch layer and operational layer because of the different operation periods.

$$k_{DG} = \begin{cases} 1 & \text{if } p_{DG} > 0 \\ 0 & \text{others} \end{cases} \quad (2. 41)$$

where k_{DG} can be 1 representing the DG should be turned on, 0 representing the DG should be turned off.

II.4.1.3. Full microgrid problem formulation

The full DC microgrid operates with the public grid and, if necessary, with the DG as a back-up source to balance the power flow. The DC bus can exchange power with BS and public grid but also can be supplied by the DG when the DC load is much higher than the PV generated power. The detailed power flow of the full microgrid can be seen in Figure 8.

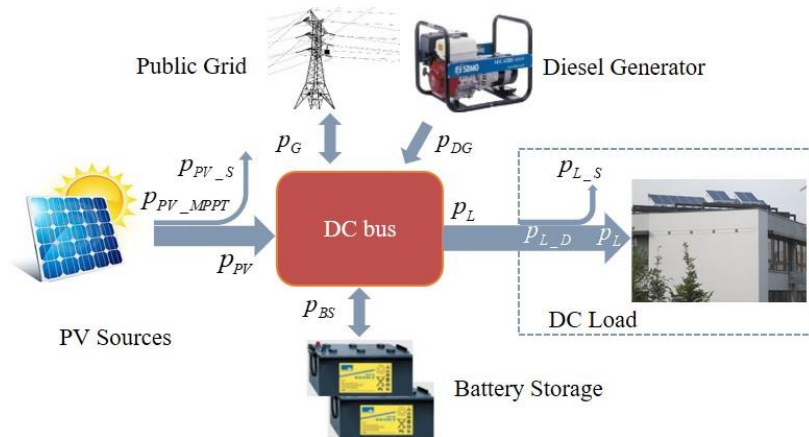


Figure 8. Full microgrid power flow.

The proposed problem formulation is based on the operation characteristics and constraints presented on (2. 1), (2. 2), (2. 3), (2. 4), (2. 5), (2. 6), (2. 7), (2. 8), (2. 9), (2. 17), (2. 18), and (2. 19).

The optimization problem formulation has to consider the instantaneous power balance given by (2. 42), as well as the minimization of the total energy cost given by (2. 43).

$$p_{PV}(t) + p_{DG}(t) = p_L(t) + p_{BS}(t) + p_G(t) \quad (2. 42)$$

$$C_{TOTAL} = C_{DG} + C_{PV_S} + C_{L_S} + C_{BS} + C_G \quad (2. 43)$$

In the operation of the full DC microgrid, it is assumed that all the operating conditions and constraints formulated for grid-connected and off-grid modes are respected.

The completely optimal power dispatching problem is formulated as in (2. 44) and (2. 45).

Variables :

$$\begin{aligned}
p_{PV}(t_i) &\in [0 \quad p_{PV_MPPT}(t_i)] \\
p_{PV_S}(t_i) &\in [0 \quad p_{PV_MPPT}(t_i)] \\
p_L(t_i) &\in [0 \quad p_{L_D}(t_i)] \\
p_{L_S}(t_i) &\in [0 \quad p_{L_CRIT}(t_i)] \\
p_{BS}(t_i) &\in [-P_{BS_MAX} \quad P_{BS_MAX}] \\
SOC_{BS}(t_i) &\in [SOC_{BS_MIN} \quad SOC_{BS_MAX}] \\
p_G(t_i) &\in [-P_{G_MAX} \quad P_{G_MAX}] \\
p_{DG}(t_i) &\in \{0\} \cup [p_{DG_ON_MIN} \quad p_{DG_ON_MAX}]
\end{aligned} \tag{2. 44}$$

$$\begin{aligned}
\min C_{TOTAL} &= C_{BS} + C_G + C_{DG} + C_{PVS} + C_{LS} \\
s.t. &\left\{ \begin{aligned}
&p_{PV}(t_i) + p_{DG}(t_i) = p_L(t_i) + p_{BS}(t_i) + p_G(t_i) \\
&p_{PV}(t_i) = p_{PV_MPPT}(t_i) - p_{PV_S}(t_i) \\
&p_L(t_i) = p_{L_D}(t_i) - p_{L_S}(t_i) \\
&\text{if } p_{PV_MPPT}(t_i) \geq p_{L_D}(t_i) \text{ then } \begin{cases} p_G(t_i) \geq 0 \\ p_S(t_i) \geq 0 \end{cases} \\
&\text{if } p_{PV_MPPT}(t_i) \leq p_{L_D}(t_i) \text{ and } p_{DG}(t_i) = 0 \text{ then } \begin{cases} p_G(t_i) \leq 0 \\ p_S(t_i) \leq 0 \end{cases} \\
&\text{if } p_{DG}(t_i) > 0 \text{ then } p_G(t_i) = 0 \\
&\text{if } SOC_{BS}(t_i) > SOC_{BS_MIN} \text{ then } p_{L_S}(t_i) = 0 \\
&p_{L_S}(t_i) \leq (1 - k_{L_CRIT}) \cdot p_L(t_i) \\
&\text{if } SOC_{BS}(t_i) < SOC_{BS_MAX} \text{ and } p_{DG}(t_i) = 0 \text{ then } p_{PV_S}(t_i) = 0 \\
&SOC_{BS}(t_i) = SOC_{BS_0} + \frac{1}{3600 \cdot v_S \cdot C_{REF}} \sum_{t_i=t_0}^{t_F} p_{BS}(t_i) \Delta t \\
&|p_G(t_i) - p_G(t_{i-1})| \leq P_{GF_Limit} \\
&p_{DG}(t_i) = p_{DG}(t_{i-1}) \text{ if } rem(t_i / dt_{DG}) \neq 0 \\
&t_i = \{t_0, t_0 + \Delta t, t_0 + 2\Delta t, \dots, t_F\}
\end{aligned} \right. \tag{2. 45}
\end{aligned}$$

II.4.1.4. Full microgrid problem formulation for 24 hours

The problem formulation for 24 hours is given below considering the different PV power and load demand conditions during the 24 hours for the microgrid continuous operation. The detailed power flow of the full microgrid can be seen in Figure 8.

The completely optimal power dispatching problem is formulated as in (2. 46), (2. 47), and (2. 48).

$$\begin{aligned}
& \min C_{TOTAL} = C_{BS} + C_G + C_{DG} + C_{PVS} + C_{LS} \\
& s.t. \left\{ \begin{array}{l}
p_{PV}(t_i) + p_{DG}(t_i) = p_L(t_i) + p_{BS}(t_i) + p_G(t_i) \\
p_{PV}(t_i) = p_{PV_MPPT}(t_i) - p_{PV_S}(t_i) \\
p_L(t_i) = p_{L_D}(t_i) - p_{L_S}(t_i) \\
\text{if } p_{DG}(t_i) > 0 \text{ then } p_G(t_i) = 0 \\
\text{if } SOC_{BS}(t_i) > SOC_{BS_MIN} \text{ then } p_{L_S}(t_i) = 0 \\
\text{if } SOC_{BS}(t_i) < SOC_{BS_MAX} \text{ and } p_{DG}(t_i) = 0 \text{ then } p_{PV_S}(t_i) = 0 \\
SOC_{BS}(t_i) = SOC_{BS_0} + \frac{1}{3600 \cdot v_S \cdot C_{REF}} \sum_{t_i=t_0}^{t_F} p_{BS}(t_i) \Delta t \\
|p_G(t_i) - p_G(t_{i-1})| \leq P_{GF_Limit} \\
p_{DG}(t_i) = p_{DG}(t_{i-1}) \text{ if } rem(t_i / dt_{DG}) \neq 0 \\
t_i = \{t_0, t_0 + \Delta t, t_0 + 2\Delta t, \dots, t_F\}
\end{array} \right. \quad (2.46)
\end{aligned}$$

where the power balance constraints, the power fluctuation constraints of the public grid, and the cycle power constraints of the DG are shown.

Two additional constraints groups are shown here below:

additional constraints group 1:

$$s.t. \left\{ \begin{array}{l}
\text{if } p_{PV_MPPT}(t_i) \geq p_{L_D}(t_i) \text{ then } \begin{cases} p_G(t_i) \geq 0 \\ p_S(t_i) \geq 0 \end{cases} \\
\text{if } p_{PV_MPPT}(t_i) \leq p_{L_D}(t_i) \text{ and } p_{DG}(t_i) = 0 \text{ then } \begin{cases} p_G(t_i) \leq 0 \\ p_S(t_i) \leq 0 \end{cases} \\
p_{L_S}(t_i) \leq (1 - k_{L_CRIT}) \cdot p_L(t_i)
\end{array} \right. \quad (2.47)$$

additional constraints group 2:

$$s.t. p_{L_S}(t_i) \leq (1 - k_{L_CRIT}) \cdot p_L(t_i) \quad (2.48)$$

The additional constraints group 1 includes the constraint for the load shedding power and the constraints to rule to the BS and the public grid have the same power direction, i.e. the BS and the public grid cannot directly exchange power. The additional constraints group 2 only constrains the load shedding power; thus, the BS and the public grid can exchange power under the additional constraints group 2.

Due to the different operation period between economic dispatch layer and operational layer, the optimization results in the economic dispatch layer, which is directly introduced into the operational layer will lead to the power unbalance in DC bus, therefore, the economic optimization coefficients k_D and k_{DG} are given to introduce the economic optimization results into the operational layer and to decouple the system operation between economic dispatch layer and operational layer. The k_D and k_{DG} are calculated according to (2.49) and (2.50) respectively.

$$k_D = p_{BS} / (p_{BS} + p_G), k_D \in [-\infty, 1] \quad (2.49)$$

$$k_{DG} = \begin{cases} 1 & \text{if } p_{DG} > 0 \\ 0 & \text{others} \end{cases} \quad (2.50)$$

where k_D is the power distribution rate between the BS and the public grid, which is negative only when the load demand is low and the available power of the public grid is high in the night, when k_D is positive, both of public grid and BS can work at the same power direction, charging the microgrid or discharging by the microgrid, when k_D is negative, the public grid and BS can work at the different power direction, the public grid is selling power while the BS is charging; k_{DG} represents whether the DG is turned on or not, when k_{DG} is 1 representing the DG is turned on, 0 representing the DG is turned off.

II.4.2. Optimization algorithm

This chapter proposes to use the MILP method, which is also able to optimize the whole day but is restricted to a linear formulation of the problem. Indeed, in [74], the authors have described some work aiming to define the most suitable optimization algorithm to be used with the proposed microgrid architecture and energy management strategies. Two different approaches, differential evolution and MILP, are presented to solve the optimal self-scheduling problem and ensure a minimum energy cost to the end-user given a day-ahead prediction horizon; then, these methods are compared with the rule-based method, which is a real-time optimization. The proposed problem formulation describes the problem only with linear constraints and as a convex function. The MILP, being more direct than an artificial intelligence approach and more reliable than a rule-based approach, has proved to have the best trade-off between computational time and energy cost among the proposed algorithms.

II.5. Power management strategy

The operational layer is responsible for ensuring power balance in real-time as well as respect the system's limits under uncertain weather conditions and load demand power. At the beginning of each algorithm's iteration the newest value of the optimal control vector, received from the optimization algorithm, also the real measurements and the fixed parameters are read. The load optimization happens according to equation (2.16). The compensation power Δp is calculated according to equation (2.1) and then, based on the resulting power flow and the newest control vector value, the tradeoff between BS and either public grid or DG is defined to supply Δp in multiple operation modes to keep the power balanced and ensure voltage stability.

In grid-connected mode, the power exchanged with the public grid or BS in a bidirectional way is a decision taken following the economic optimization coefficient k_D . In off-grid mode, the decision of DG starting is given by introducing the economic optimization coefficient k_{DG} . In full microgrid mode, both the conditions, happen in grid-connected mode and off-grid mode, need to be considered. The proposed power management strategies are shown following in three main operation modes. In each operation mode, there are two conditions to be distinguished into the mode without the usage of economic optimization and with the usage of economic optimization.

II.5.1. Grid-connected power management strategy

The operational algorithm used during grid-connected operation is introduced in two ways: grid-connected mode without economic optimization, grid-connected mode with economic optimization.

II.5.1.1. Grid-connected power management strategy without economic optimization

In grid-connected mode without economic optimization, the power management strategy is presented in Figure 9. The load optimization runs in every iteration of the power management strategy to decide the optimal load power according to the available power.

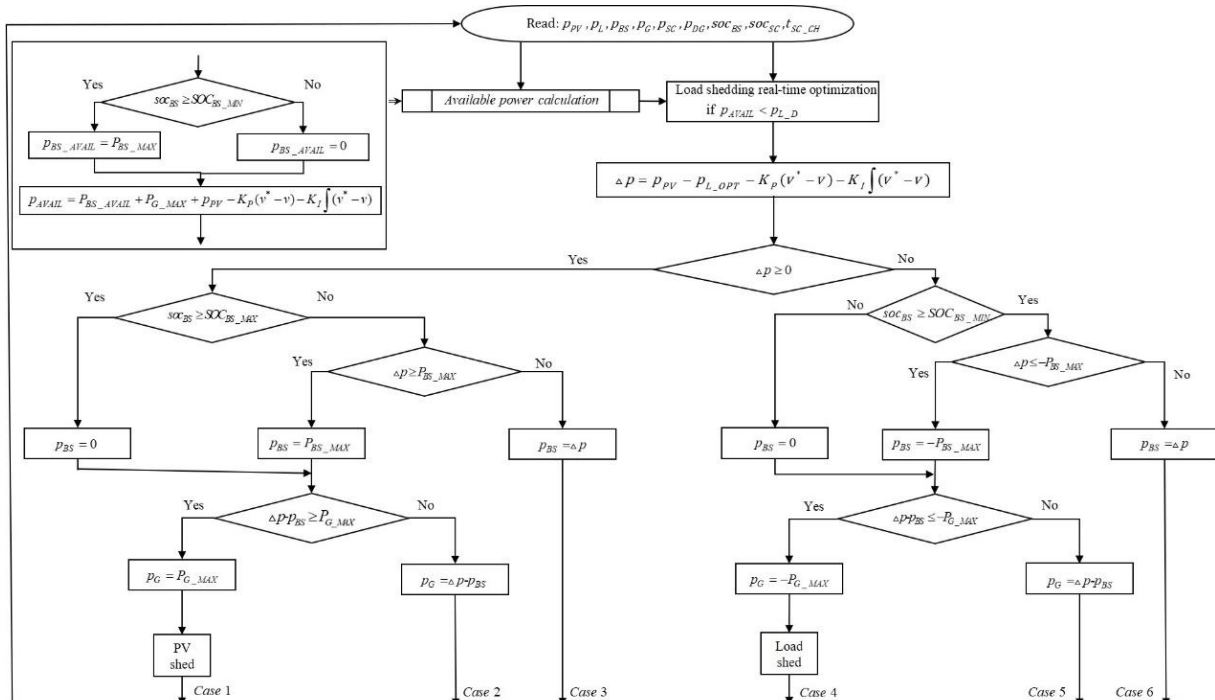


Figure 9. Grid-connected operational algorithm without economic optimization.

II.5.1.1.1. Case 1, 2, 3

The case 1, case 2, and case 3 happen when Δp is positive representing that the power of PV supply is more than the power sum of load demand and common DC bus compensated, meanwhile, p_L is more than its critical load. In these cases, Δp can be distributed by the BS and public grid. The power management takes into account the assumption that BS has a higher priority than the public grid in the power compensation of the microgrid. When BS and public grid are both limited to their limitations, the PV shedding happens in case 1. The BS and public grid can support the Δp in case 2 and case 3 under their limitations.

II.5.1.1.2. Case 4, 5, 6

Case 4, case 5, and case 6 happen when Δp is negative. In these cases, Δp can be distributed to the BS and public grid. The BS has always the high priority than the public grid in the power compensation of the microgrid. When BS and public grid are both limited to their limitations, the load shedding happens in case 4, and the load power is supposed to be decided in the load optimization part before the case 4. Mostly, load shedding in case 4 is not in operation unless the error happens in the load optimization part.

II.5.1.2. Grid-connected power management strategy with economic optimization

In grid-connected mode with economic optimization, the power management strategy is presented in Figure 10. The load optimization runs in every iteration of the power management strategy to decide the optimal load power according to the available power. When k_D equals 1, the operational algorithm is the same as the one in II.5.1.

II.5.1.2.1. Case 1, 2, 3

The most parts of this operational algorithm are the same as the operational algorithm in II.5.1.1.1. The different part is the introduction of the economic optimization coefficient k_D . The Δp can be distributed to the BS and public grid as the coefficient k_D in case 3, when the public grid is limited, the necessary power will be compensated by the BS to avoid the PV shedding in case 2. When the BS is also limited, the PV shedding happens to balance power in case 1.

II.5.1.2.2. Case 4, 5, 6

The most parts of this operational algorithm are the same as the operational algorithm in II.5.1.1.2. The different parts are the economic optimization coefficient k_D , is introduced. The Δp can be

distributed to the BS and public grid as the coefficient k_D in case 6, when the public grid is limited, the necessary power will be compensated by the BS to avoid the load shedding in case 5. When the BS is also limited, the load shedding happens to balance power in case 4.

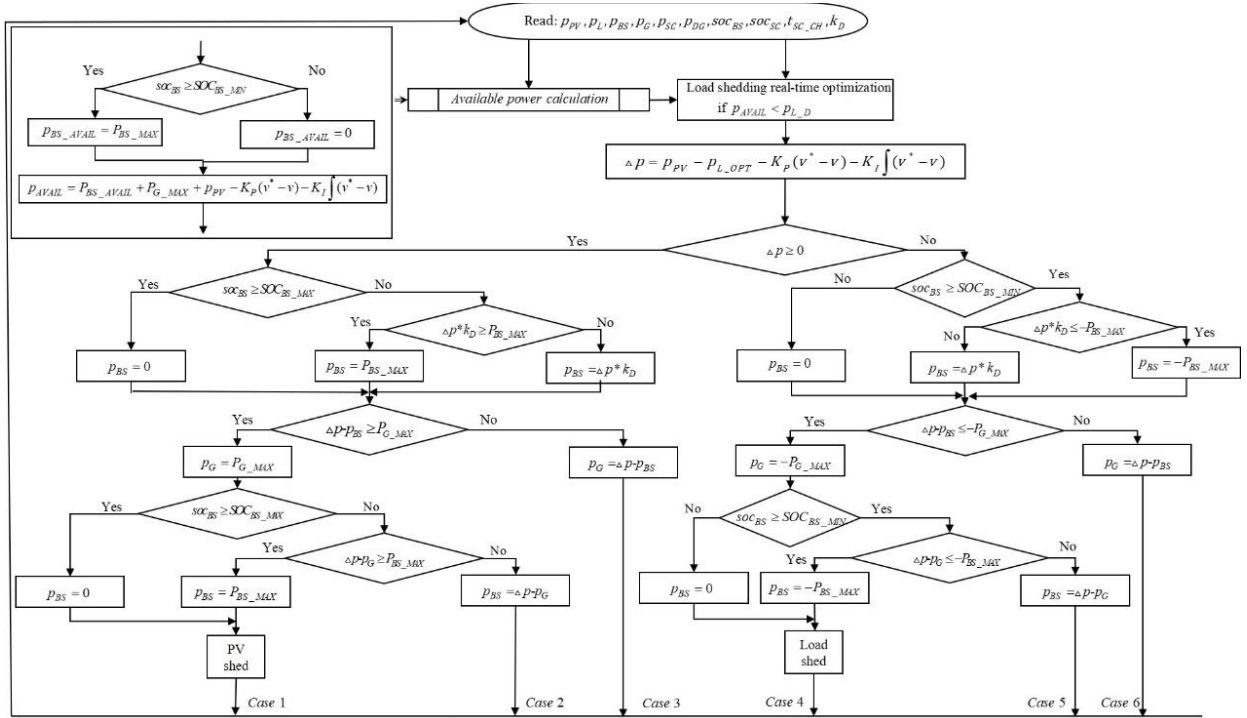


Figure 10. Grid-connected operational algorithm with economic optimization.

II.5.2. Off-grid power management strategy

The operational algorithm used during operation in off-grid mode is presented in two ways: off-grid mode without economic optimization, off-grid mode with economic optimization. The DG and SC controls are integrated into the operational algorithm.

II.5.2.1. Off-grid power management strategy without economic optimization

In off-grid mode without economic optimization, the power management strategy is presented in Figure 11 and Figure 12. The load optimization also runs in every iteration of the power management strategy to decide the optimal load power according to the available power.

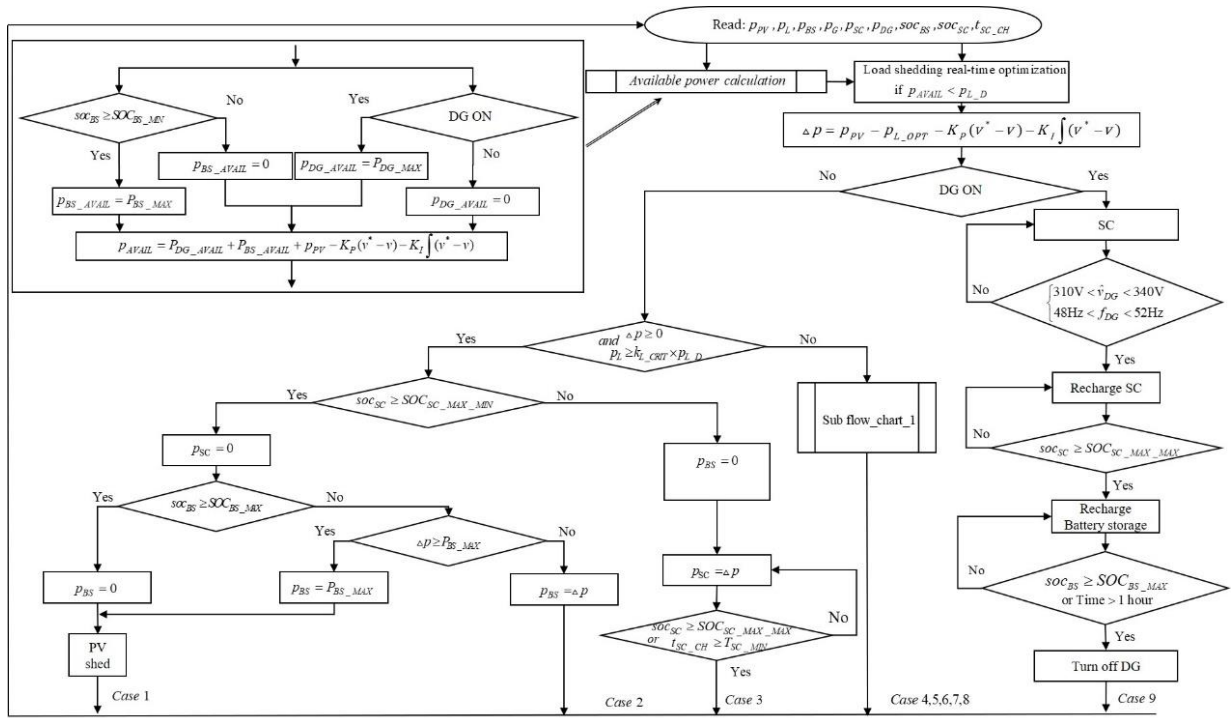


Figure 11. Off-grid operational algorithm without economic optimization.

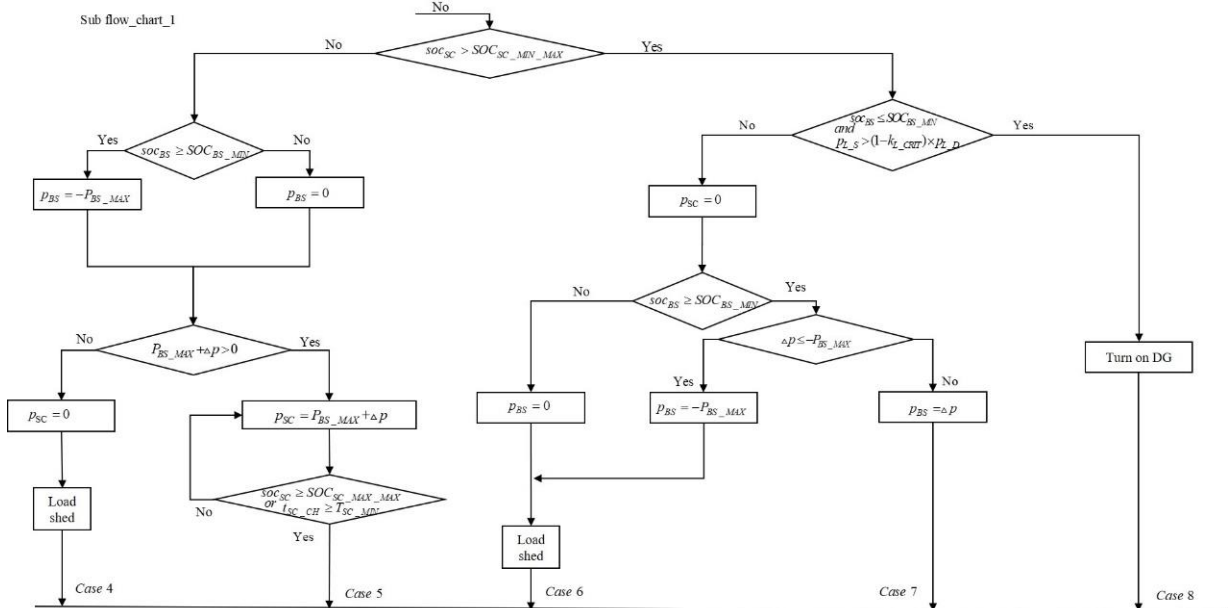


Figure 12. Sub flow-chart of Figure 11.

II.5.2.1.1. Case 1, 2, 3

The case 1, case 2, and case 3 happen when Δp is positive representing that the power of PV supply is more than the power sum of load demand and common DC bus compensated, meanwhile, p_L is more than its critical load. In case 1, and case 2, Δp can be distributed by the BS. When BS is limited to its limitations, the PV shedding happens in case 1. The BS can support the Δp in case 2 under its limitations. The SC recharging is triggered by the soc_{SC} in case 3. When the SC starts recharging, the

Δp is the SC recharging power. The SC cannot stop recharging until soc_{SC} reaches the $SOC_{SC_MAX_MAX}$ or the SC recharging time, t_{SC_CH} , is more than its minimum value T_{SC_MIN} . The two conditions also keep the SC working at a period to avoid the converters working at low efficiency.

II.5.2.1.2. Case 4, 5, 6, 7, 8

The case 4, case 5, case 6, case 7, and case 8 happen when Δp is negative, or p_L is less than its critical load. The start-time of SC recharging is decided by soc_{SC} . When soc_{SC} is less than $SOC_{SC_MIN_MAX}$, the SC starts recharging. The BS can support the SC recharging and p_{L_D} under their limitations in case 5. The SC cannot stop recharging until soc_{SC} is more than $SOC_{SC_MAX_MAX}$ or the SC recharging time, t_{SC_CH} , is more than its minimum value T_{SC_MIN} . The load shedding happens in case 4 or case 6. The BS can support p_{L_D} in case 7.

When soc_{SC} is less than SOC_{BS_MIN} and p_L is less than its critical load, the DG is turned on in case 8.

II.5.2.1.3. Case 9

When the DG is turned on, the SC starts discharging to compensate for the power of the sluggish dynamic of the DG until the DG can supply the stable power expressed in (2. 10). When the DG can supply the stable power, it starts charging the SC and supplying Δp to keep the power balance of the microgrid until the SC finishes charging. Then the DG stops charging the SC, and it starts charging the battery and supplying Δp to keep the power balance of the microgrid till the battery finishes charging. When the BS finishes charging or the DG reaches its duty cycle, the DG is turned off.

II.5.2.2. Off-grid power management strategy with economic optimization

In off-grid mode with economic optimization, the power management strategy is presented in Figure 13 and Figure 14. The load optimization also runs in every iteration of the power management strategy to decide the optimal load power according to the available power. The economic optimization coefficient k_{DG} is introduced in the operational algorithm. When k_{DG} equals 0, the operational algorithm is the same as the one in II.5.2.1.

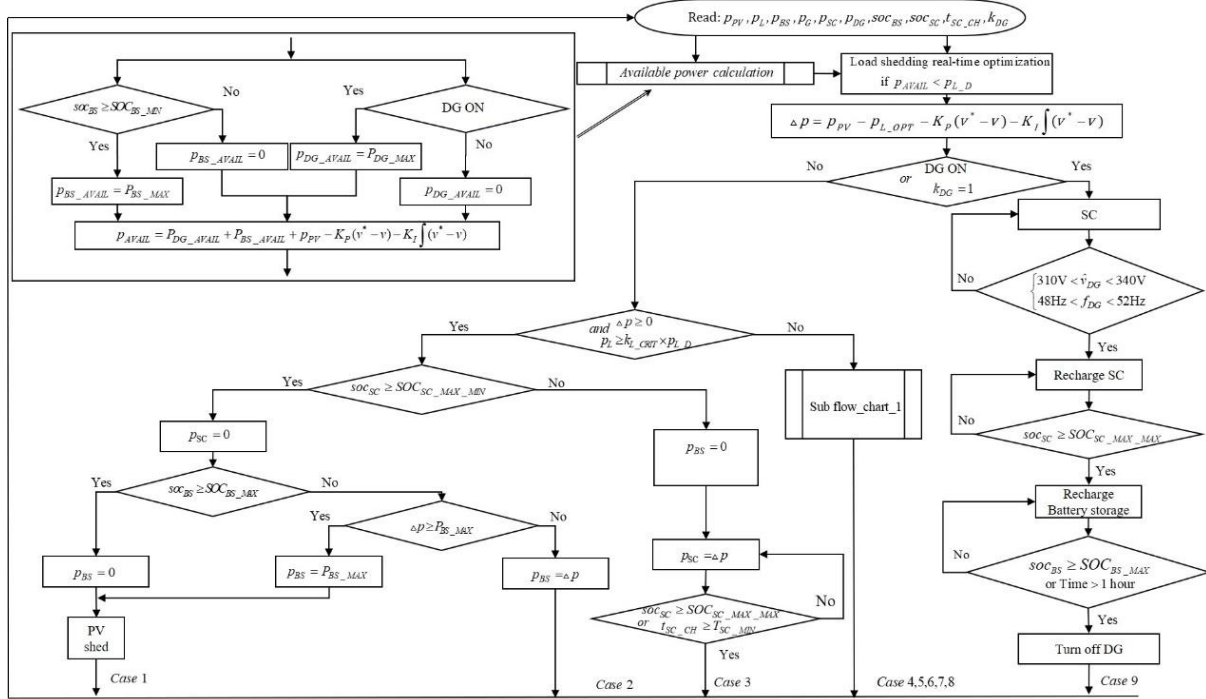


Figure 13. Off-grid operational algorithm with economic optimization.

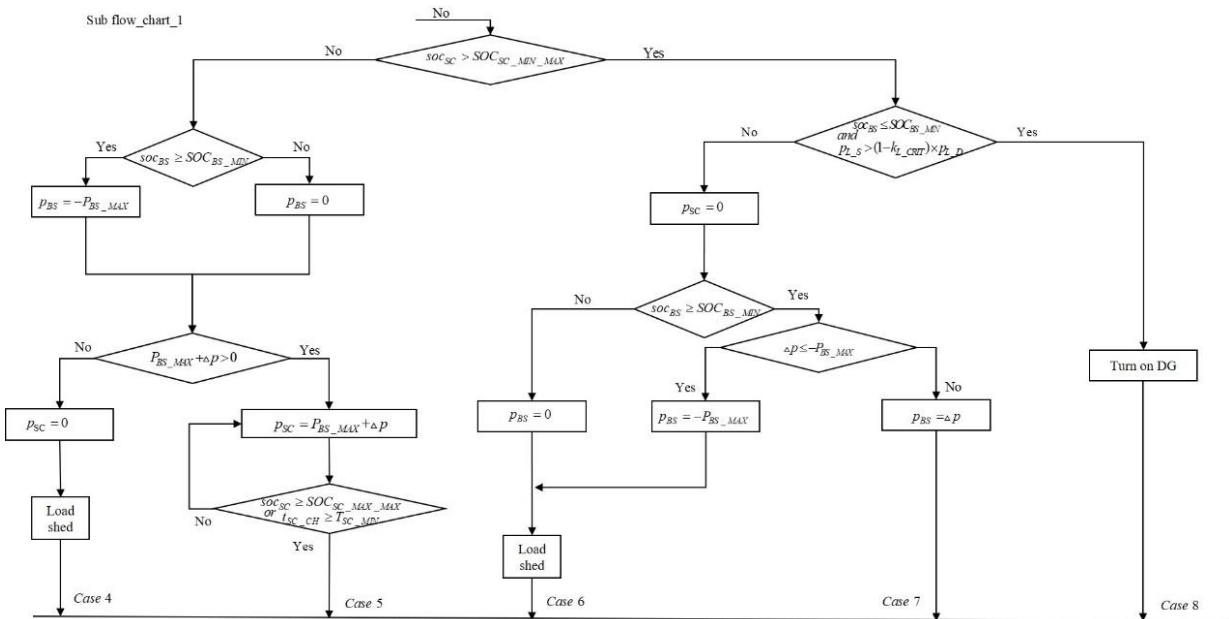


Figure 14. Sub-flow-chart of Figure 13.

II.5.3. Full microgrid power management strategy

The operational algorithm used during full microgrid operation is introduced in two ways: full microgrid mode without economic optimization, full microgrid mode with economic optimization.

II.5.3.1. Full microgrid power management strategy without economic optimization

The power management strategy is presented in Figure 15 and Figure 16. The load optimization also runs in every iteration of the power management strategy to decide the optimal load power according to the available power.

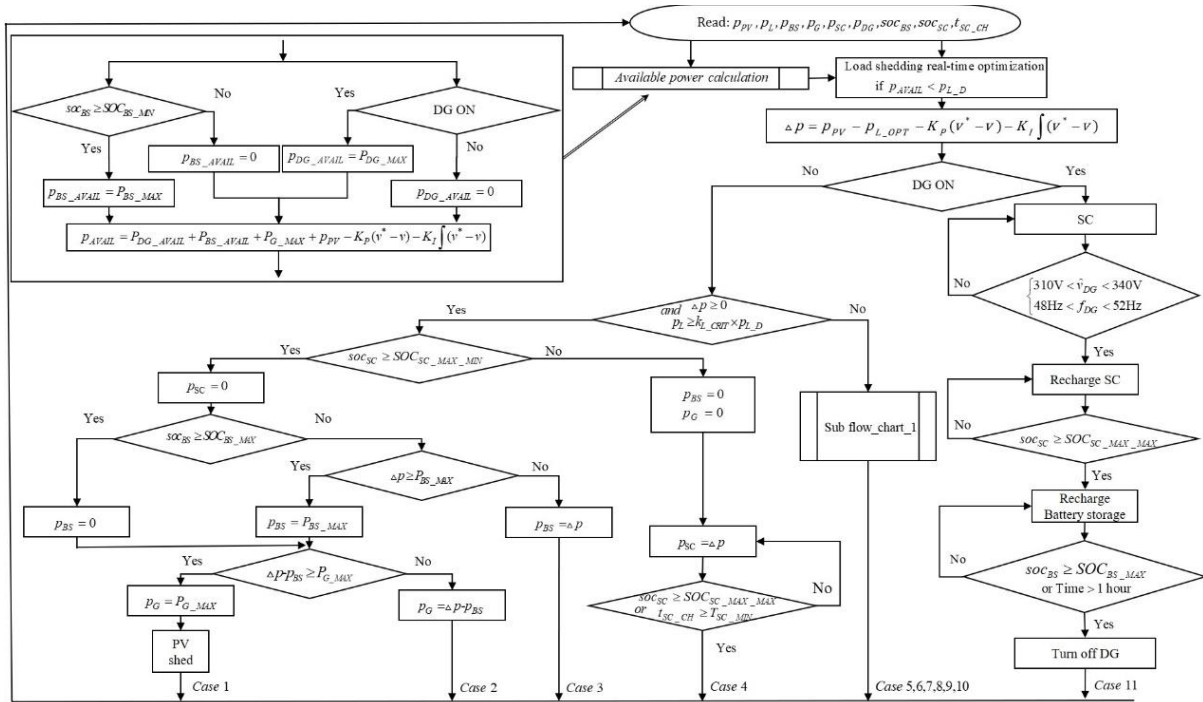


Figure 15. Full microgrid operational algorithm without economic optimization.

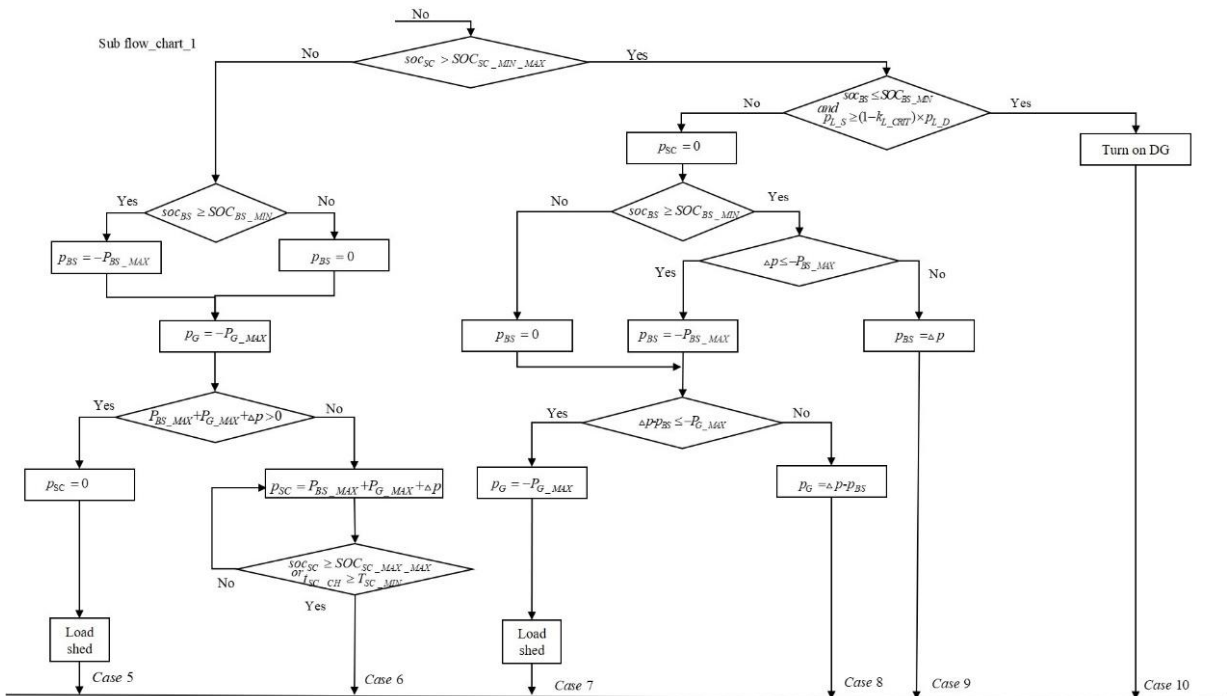


Figure 16. Sub flow-chart of Figure 15.

II.5.3.1.1. Case 1, 2, 3, 4

The case 1, case 2, case 3, and case 4 happen when Δp is positive representing that the power of PV supply is more than the power sum of load demand and common DC bus compensated, meanwhile, p_L is more than its critical load. In case 1, case 2, and case 3, Δp can be distributed by the BS and public grid. The BS has a higher priority than the public grid in the power compensation of the microgrid. When BS and public grid are both limited to their limitations, the PV shedding happens in case 1. The BS and public grid can support the Δp in case 2 and case 3 under their limitations. The SC recharging is triggered by the soc_{SC} in case 4. When the SC starts recharging, the Δp is the SC recharging power. The SC cannot stop recharging until soc_{SC} reaches the $SOC_{SC_MAX_MAX}$ or the SC recharging time, t_{SC_CH} , is more than its minimum value T_{SC_MIN} . The two conditions also keep the SC working at a period to avoid the converters working at low efficiency.

II.5.3.1.2. Case 5, 6, 7, 8, 9, 10

The case 5, case 6, case 7, case 8, case 9, and case 10 happen when Δp is negative, or p_L is less than its critical load. The start-time of SC recharging is decided by soc_{SC} . When soc_{SC} is less than $SOC_{SC_MIN_MAX}$, the SC starts recharging. The BS and public grid can support the SC recharging and p_{L_D} under their limitations in cases 5 and 6. The load shedding happens in case 5. The SC cannot stop recharging until soc_{SC} is more than $SOC_{SC_MAX_MAX}$ or the SC recharging time, t_{SC_CH} , is more than its minimum value T_{SC_MIN} . In case 7, case 8, case 9 and case 10, Δp can be distributed to the BS and public grid. The BS has a high priority than the public grid in the power compensation of the microgrid. When BS and public grid are both limited to their limitations, the load shedding happens in case 7.

When soc_{SC} is less than SOC_{BS_MIN} and p_L is less than its critical load, the DG is turned on in case 10. The BS and public grid can support the Δp in case 8 and case 9 under their limitations.

II.5.3.1.3. Case 11

When the DG is turned on, the SC starts discharging to compensate for the power of the sluggish dynamic of the DG till the DG can supply the stable power expressed in (2. 10). When the DG can supply the stable power, it starts charging the SC and supplying Δp to keep the power balance of the microgrid till the SC finishes charging. Then the DG stops charging the SC, and it starts charging the battery and supplying Δp to keep the power balance of the microgrid till the battery finishes charging. When the battery finishes charging or the DG reaches its duty cycle, the DG is turned off.

II.5.3.2. Full microgrid power management strategy with economic optimization

The power management strategy is presented in Figure 17 and Figure 18. The load optimization also runs in every iteration of the power management strategy to decide the optimal load power according to the available power. The economic optimization coefficient k_D and k_{DG} are introduced in the operational algorithm. When k_D equals to 1, and k_{DG} equals to 0, the operational algorithm is the same as the one in II.5.3.1.

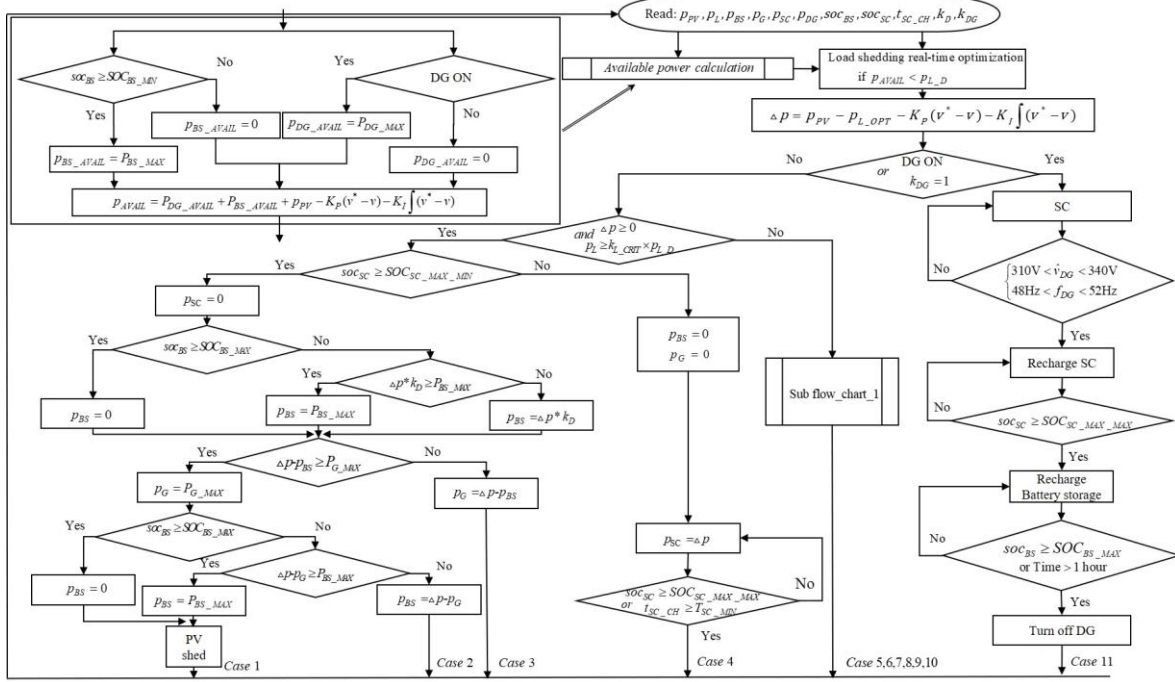


Figure 17. Full microgrid operational algorithm with economic optimization.

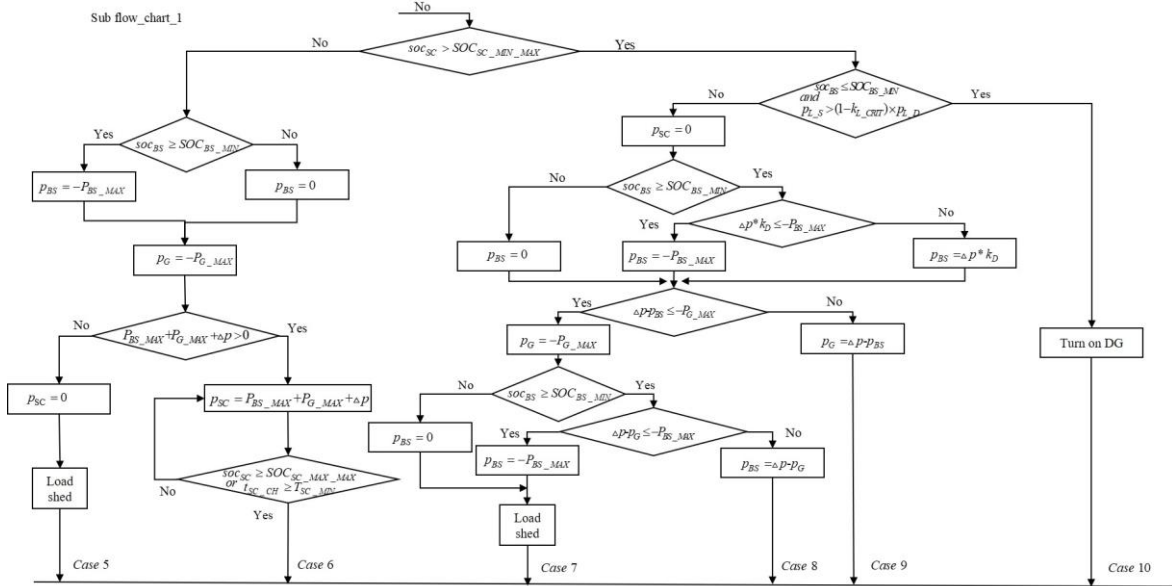


Figure 18. Sub flow-chart of Figure 17.

II.5.4. Full microgrid power management strategy for 24 hours

The operational algorithm used during full microgrid operation for 24 hours is introduced in two ways: full microgrid mode without economic optimization, full microgrid mode with economic optimization.

II.5.4.1. Full microgrid power management strategy without economic optimization

The algorithm for power control operating simultaneously with the power management is presented in Figure 19, Figure 20, and Figure 21. The available power block is given in Figure 18. The power management is introduced with the power control flow-chart to provide a high running rate for real-time power management and complex computation is avoided due to the computation time. Therefore, the power of the described full DC microgrid can be balanced in real-time by running the proposed algorithm. In order to present an optimal load demand management, this algorithm for power control and power management integrates a load optimization algorithm, which can run in real-time to decide the optimal load management. In order to forbid the BS directly sell power to the public grid, the power management is designed respecting the rules following, the public grid can sell power to support the load demand, the BS, and the SC, the public grid can only buy the PV generated power.

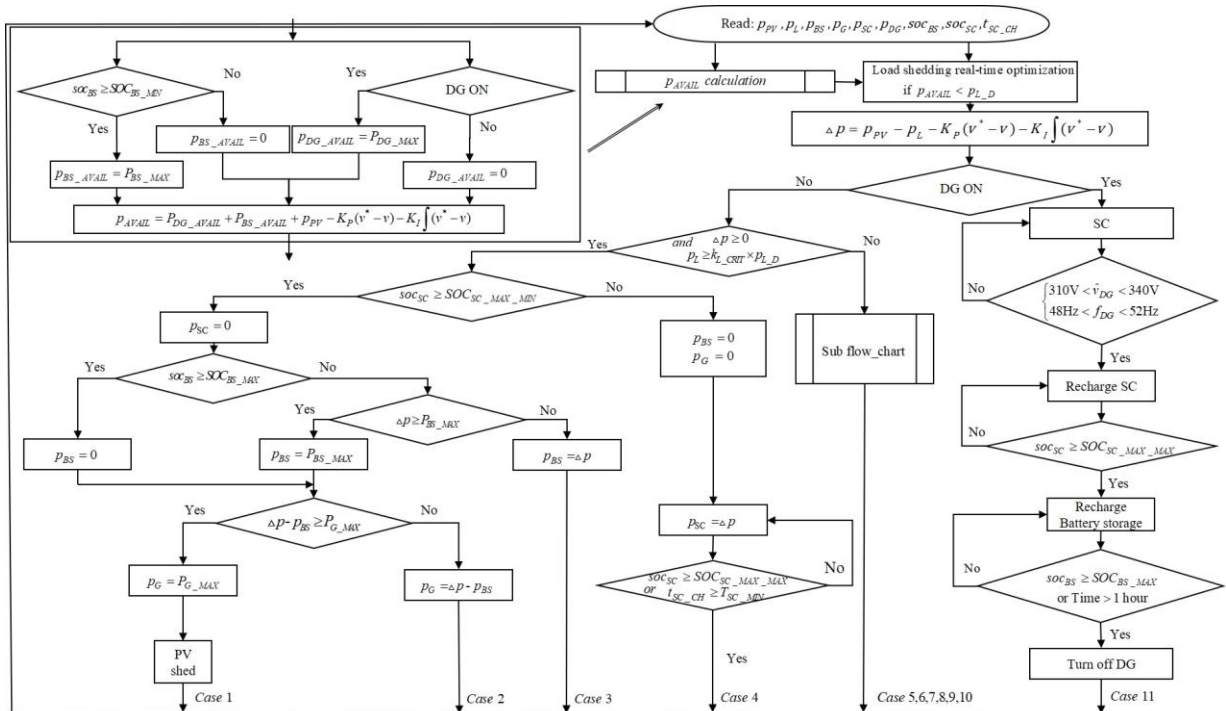


Figure 19. Full microgrid operational algorithm without economic optimization.

In Figure 19, Figure 20, and Figure 21, the input of the algorithm is the power measurement value and real-time estimated value; the output is the controller references values for the PV sources, the BS, the public grid, the DG, and the SC. In Figure 21, there are two sub-flow-charts, a and b, which can

operate at different time periods. The load optimization runs in real-time according to the (2. 16). The available power is calculated according to the BS available power p_{BS_AVAIL} , the DG available power p_{DG_AVAIL} , the public grid available power, and the common DC compensated power (Figure 19). The public grid available power equals to p_{G_MAX} . The proposed power management consists of 11 cases that are detailed in the following sections.

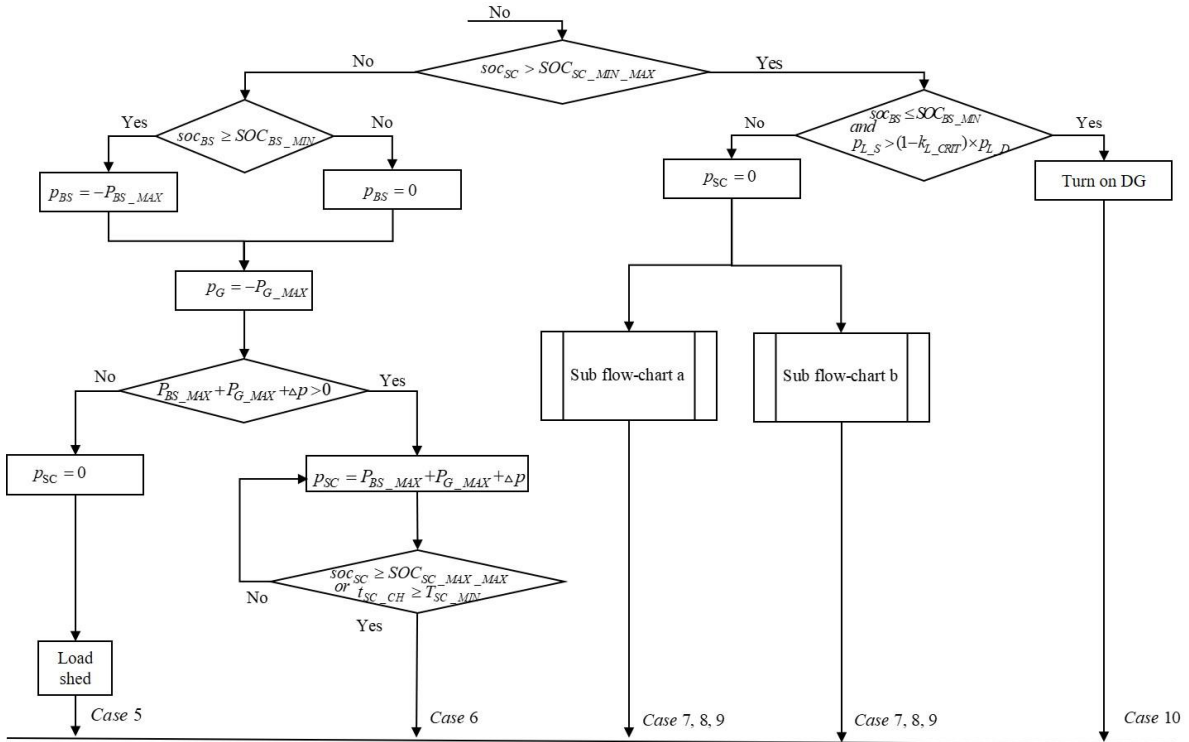


Figure 20. Sub flow-chart of operational power control and management algorithm.

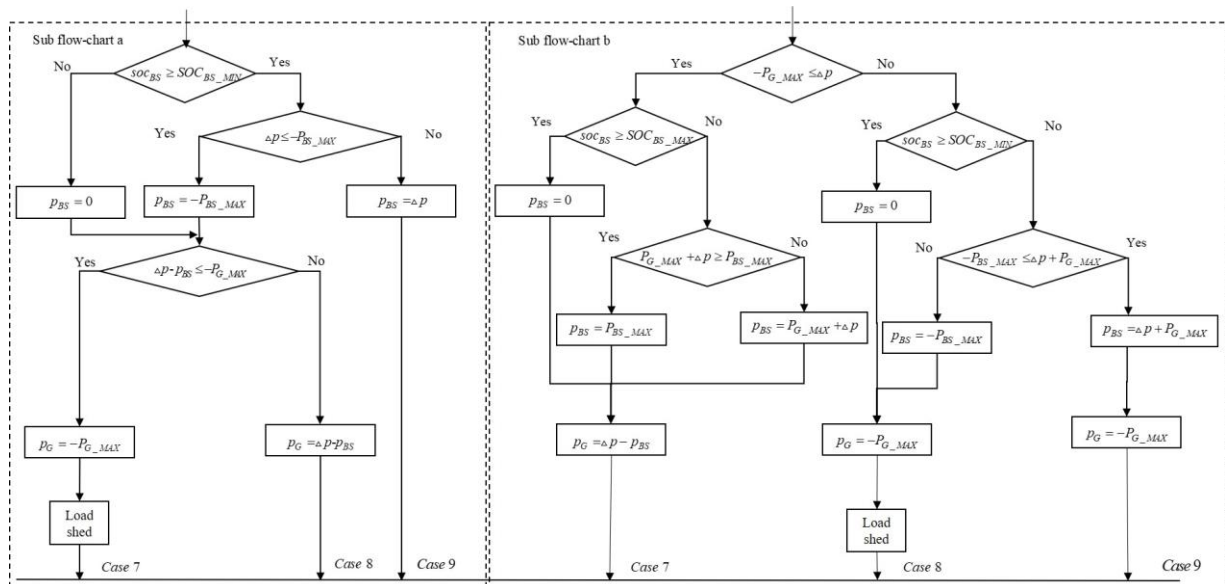


Figure 21. Sub flow-chart a and sub flow-chart b.

II.5.4.1.1. Case 1, 2, 3, 4

The case 1, case 2, case 3, and case 4 happen when Δp is positive representing that the power of PV supply is more than the power sum of load demand and common DC bus compensated, meanwhile, p_L is more than its critical load. In case 1, case 2, and case 3 Δp can be distributed by the BS and public grid. The BS has a higher priority than the public grid in the power compensation of the microgrid. When the BS and public grid are both limited to their limitations, the PV shedding happens in case 1. The BS and public grid can support the Δp in case 2 and case 3 under their limitations. The SC recharging is triggered by the soc_{SC} in case 4. When the SC starts recharging, the Δp is the SC recharging power. The SC cannot stop recharging until soc_{SC} reaches the $SOC_{SC_MAX_MAX}$ or the SC recharging time, t_{SC_CH} , is more than its minimum value T_{SC_MIN} . The two conditions also keep the SC working at period to avoid the converters working at low efficiency.

II.5.4.1.2. Case 5, 6, 7, 8, 9, 10

The case 5, case 6, case 7, case 8, case 9, and case 10 happen when Δp is negative, or p_L is less than its critical load. The start-time of SC recharging is decided by soc_{SC} . When soc_{SC} is less than $SOC_{SC_MIN_MAX}$, the SC starts recharging. The BS and public grid can support the SC recharging and p_{L_D} under their limitations in cases 5 and 6. The load shedding happens in case 5 when the BS and public grid can support the p_{L_D} . The SC cannot stop recharging until soc_{SC} is more than $SOC_{SC_MAX_MAX}$ or the SC recharging time, t_{SC_CH} , is more than its minimum value T_{SC_MIN} . In case 7, case 8 and case 9 of the sub-flow-chart a in Figure 21, Δp can be distributed to the BS and public grid in case 8 and 9. The BS has high priority than the public grid in the power compensation of the microgrid. When BS and public grid are both limited to their limitations, the load shedding happens in case 7. In case 7, case 8 and case 9 of the sub flow-chart b in Figure 21, when the public grid can supply Δp , the rest of the public grid power can charge the BS in case 7; when the public grid cannot supply Δp , Δp can be also distributed to the BS and public grid, and the public grid has high priority than the BS in the power compensation of the microgrid in case 9; when BS and public grid are both limited to their limitations, the load shedding happens in case 8.

When soc_{SC} is less than SOC_{BS_MIN} and p_L is less than its critical load, the DG is turned on in case 10. The BS and public grid can support the Δp in case 8 and case 9 under their limitations.

II.5.4.1.3. Case 11

When the DG is turned on, the SC starts discharging to compensate for the power of the sluggish dynamic of the DG until the DG can supply the stable power expressed in (2. 10). When the DG can

supply the stable power, it starts charging the SC and supplying Δp to keep the power balance of the microgrid until the SC finishes charging. Then the DG stops charging the SC, and it starts charging the BS and supplying Δp to keep the power balance of the microgrid until the BS finishes charging. When the BS finishes charging or the DG reaches its duty cycle, the DG is turned off.

II.5.4.2. Full microgrid power management strategy with economic optimization

The proposed full microgrid power management strategy with economic optimization is introduced in the flow chart structured in Figure 22, Figure 23, and Figure 24, which is a rule-based method. The k_D and k_{DG} calculated in the energy management are introduced in the real-time power management strategy.

In Figure 22, it can be seen that the proposed power management strategy consists of 11 cases, the real-time load power optimization is integrated. When Δp is positive or equals to 0 and the load power is greater than its critical load or equals to its critical load, the case 1, 2, 3, 4 can happen. In case 1, PV shedding happens because the BS and the public grid are limited. In case 2, 3 the BS and the public grid can support Δp . In case 4, the SC is recharging by Δp because soc_{SC} reaches $SOC_{SC_MAX_MIN}$, the SC can stop recharging when soc_{SC} is less than $SOC_{SC_MAX_MAX}$ or recharging time t_{SC_CH} reaches its maximal recharging time T_{SC_MAX} . The case 5, 6, 7, 8, 9, 10 can happen when Δp is negative or the critical load is shedding. The case 11 shows the process while the DG is turned on.

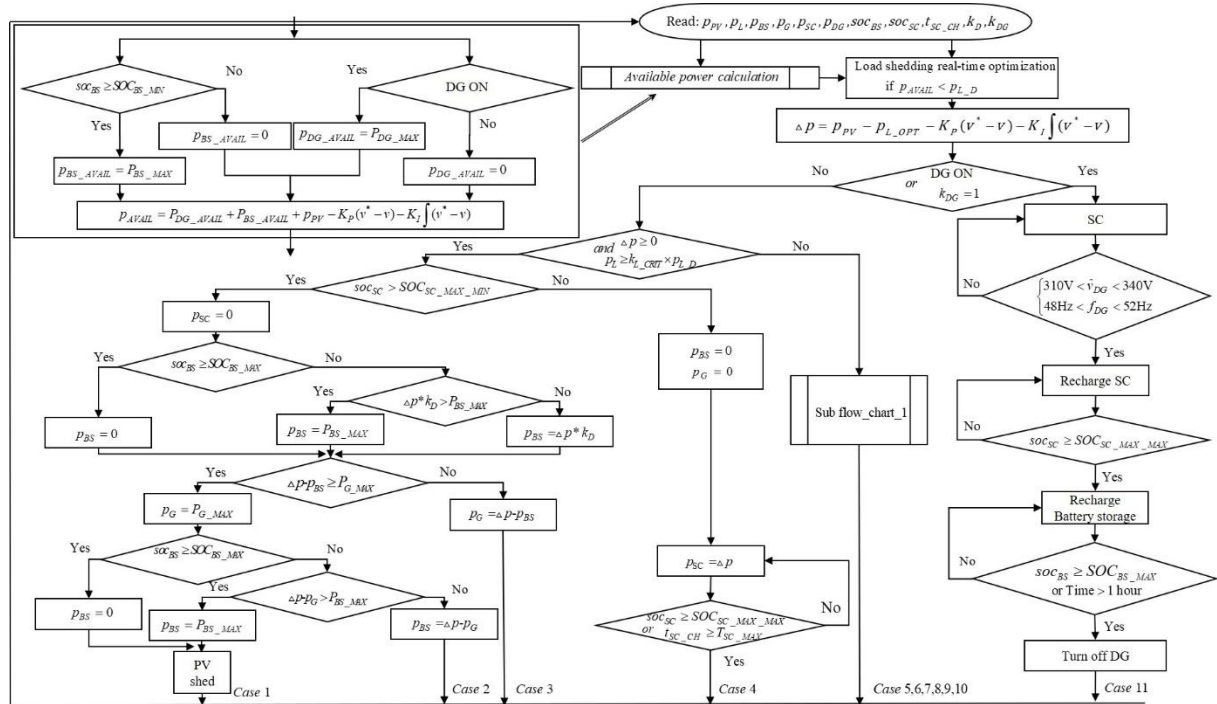


Figure 22. Full microgrid operational algorithm with economic optimization.

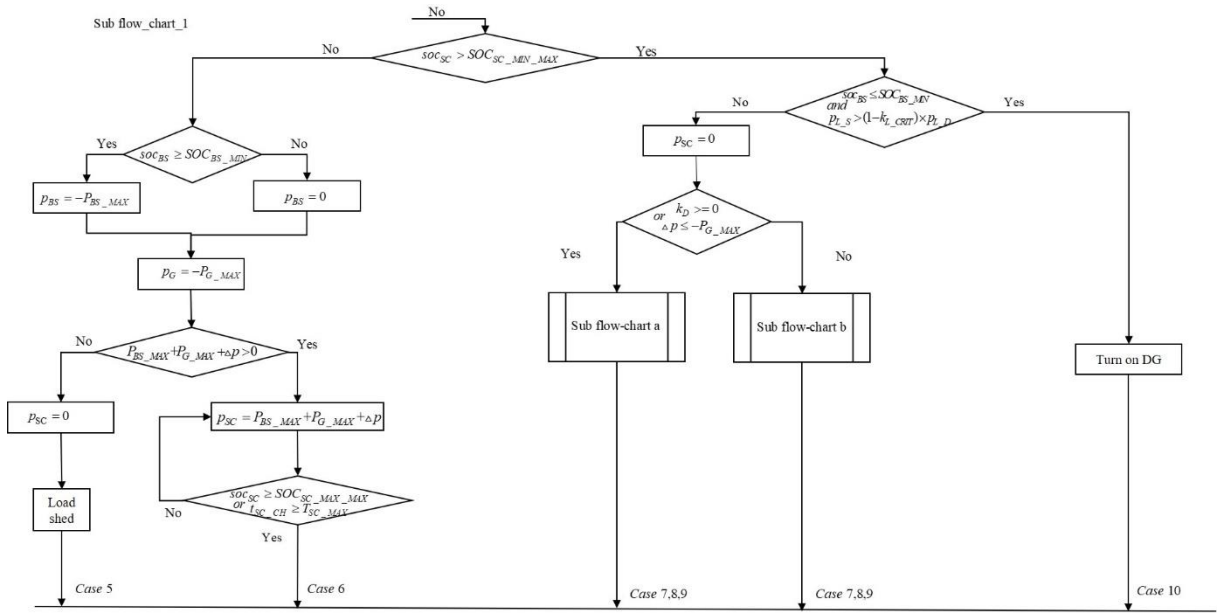


Figure 23. Full microgrid power management sub flow chart 1 in the operational layer.

In Figure 23, the detailed process of the case 5, 6, 7, 8, 9, 10 can be seen. The case 5, 6 can happen when soc_{SC} reaches $SOC_{SC_MIN_MAX}$, the load shedding happens in case 5 because there is no more in the BS and the public grid to support Δp , the SC is recharging in case 6. There are two flow charts, sub-flow-chart a and b describing in cases 7, 8, 9. The sub-flow-chart a can be chosen according to the condition when k_D is positive or 0 and Δp is less or equals to $-P_{PG_MAX}$, the sub-flow-chart b can be chosen in the opposite condition. In the sub-flow-chart a, the BS and the public grid can supply power to the microgrid. In the sub-flow-chart b, the public grid can support the BS and the microgrid by selling power. The start-up signal is sent in case 10 when soc_{BS} is less or equals to SOC_{BS_MIN} and the critical load is shedding.

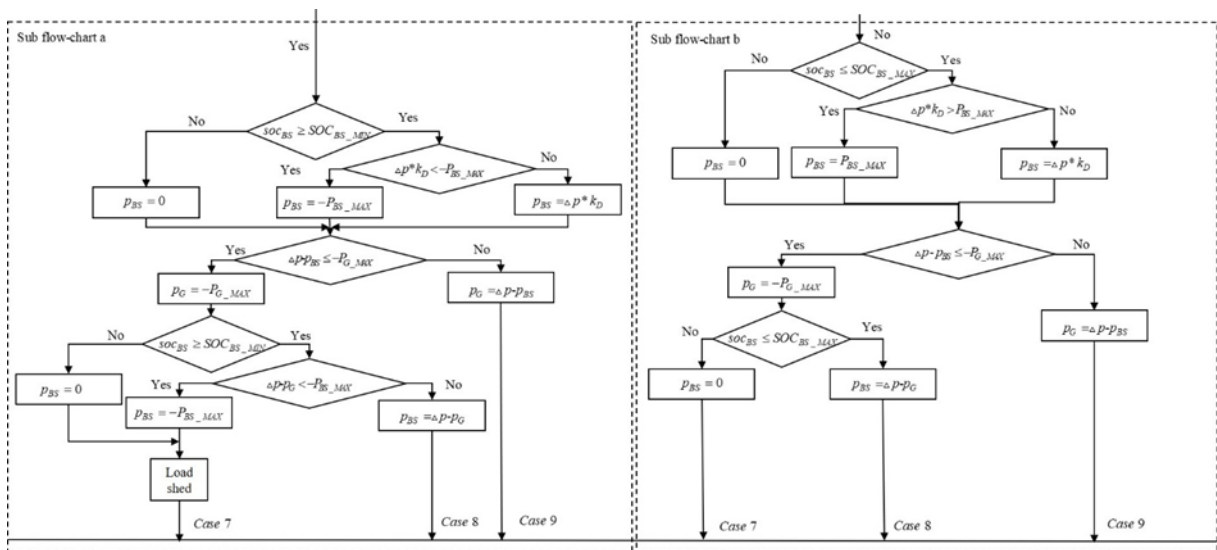


Figure 24. Sub flow-chart a and b of Figure 23.

In Figure 24, the detailed flow chart of cases 7, 8, 9 is shown. In case 7 of sub-flow-chart a, the load shedding happens because the BS and the public grid cannot support Δp , in case 8, 9 of sub-flow-chart a, the BS and the public grid can support Δp . In case 7 of sub-flow-chart b, the public grid only supply Δp , in case 8, 9 of sub-flow-chart b, the public grid can support Δp and the BS.

II.6. Conclusion

In order to integrate the advantages of the grid-connected and off-grid operation modes of a DC microgrid, this chapter proposes the full microgrid operation mode. A special supervisory system including the real-time power management strategy and day-ahead optimization for microgrid economic dispatching is proposed for the proposed full DC microgrid.

In this chapter, firstly, the DC microgrid modeling is introduced including the multi-source, and multi-storage, and load demand. Secondly, the economic dispatching optimization algorithm is presented after problem formulation. The full DC microgrid problem formulation is obtained by combining grid-connected microgrid problem formulation and off-grid microgrid problem formulation. Then, full DC microgrid power management strategy is proposed by considering the advantages and shortages grid-connected power management strategy and off-grid power management strategy.

In the following chapter the simulation results are presented.

Chapter III. Simulation results

The simulation for chapter II is done following. This chapter first presents grid-connected simulation, off-grid simulation, and full microgrid simulation for 9 hours' duration, then presents full microgrid simulation for 24 hours' duration. The simulation results show the superiority of the proposed full DC microgrid supervisory system.

III.1. Simulation verification

Simulations tests are carried out to validate the optimization formulation problem in the economic dispatching layer and to validate the proposed power management strategy under the optimization problem formulation. The economic optimization in the economic dispatching layer is performed in the day-ahead.

There are two simulation time periods: 9 hours' duration and 24 hours' duration. Under each simulation period, the results in the economic dispatching layer is shown, the real-time simulation results in the operational layer by using the day-ahead optimization results from the economic dispatching layer is compared with the real-time simulation results in the operational layer without consideration the day-ahead optimization results.

The results and the comparison analyze are presented in three operating modes, grid-connected DC microgrid, off-grid DC microgrid, and full DC microgrid, as well as for three different weather conditions in each operating mode.

III.1.1. Simulation scenario for 9 hours' duration

To solve the optimization problem of the economic dispatching, the MILP solver is applied. The weather data set from three different days, i.e. May 8th 2018, June 20th 2018, and July 16th 2018, under different weather conditions, the sunny weather, cloudy weather, and thunderstorm weather, corresponding to the three types of solar radiation, can give a good simulation verification. The PV prediction power curves can be calculated according to the equations (2. 20) and (2. 21) with solar irradiation data prediction obtained from the Météo France website. The load power is scaled according to the real daily load demand data in the university building from the local electrical company ENEDIS. In the load power, the power curve is the sum of all the appliances of the university building, then, the load power is scaled from the same profile of the real load demand power. The load shedding real-time optimization [70] is used in the following simulation.

Table 1 shows the simulation parameters' values of the principal devices, which are applied in the simulation. The PV sources consist of 14 PV panels with 125W MPPT power under STC per panel as shown in appendix 1. The BS consists of 5 batteries with 6.6Ah per battery in appendix 2. The load power is assumed to be 49 controllable appliances for verifying the load real-time optimization algorithm. It is based on the experience that the load demand respects to a duty-cycle regular change, the load prediction power is assumed to be a little different from the real load power, and the maximal load demand power is set to 1500W. The rated voltage of SC is 75V as given in appendix 3. The maximal power limit of DG as described in appendix 4 is set to 1500W to satisfy the load demand.

Table 1. Simulation parameter of the principal device

Element	Parameter	Number
PV	125W	14
BS	6.6Ah	5
Public grid	~	1
Load	1500W	49
SC	75V	1
DG	1500W	1

The PV MPPT power and hourly PV prediction power for three days are separately shown in Figure 25, Figure 26, and Figure 27.

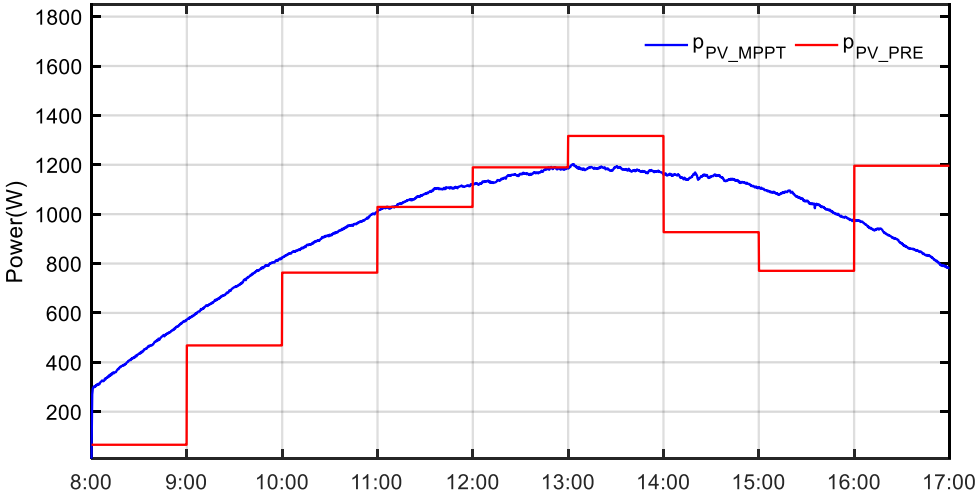


Figure 25. PV MPPT power and PV prediction power curves for May 8th 2018.

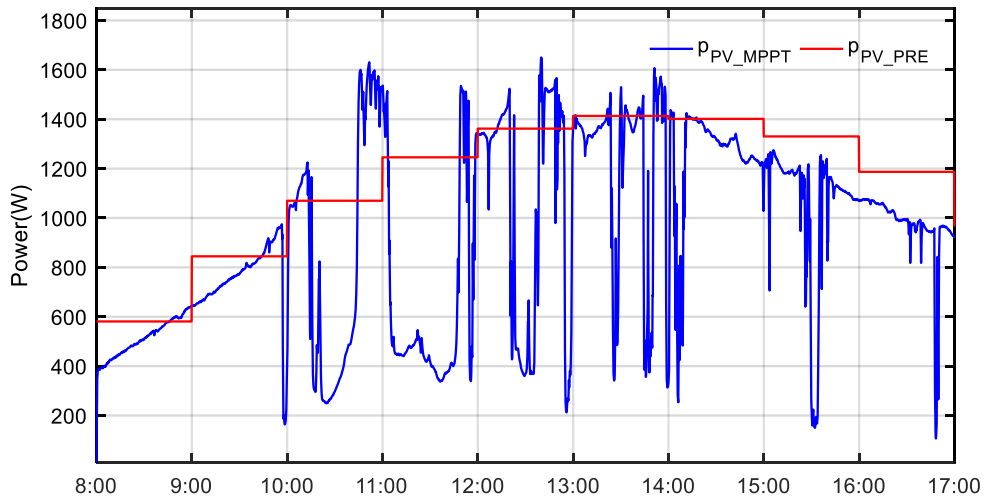


Figure 26. PV MPPT power and PV prediction power curves for June 20th 2018.

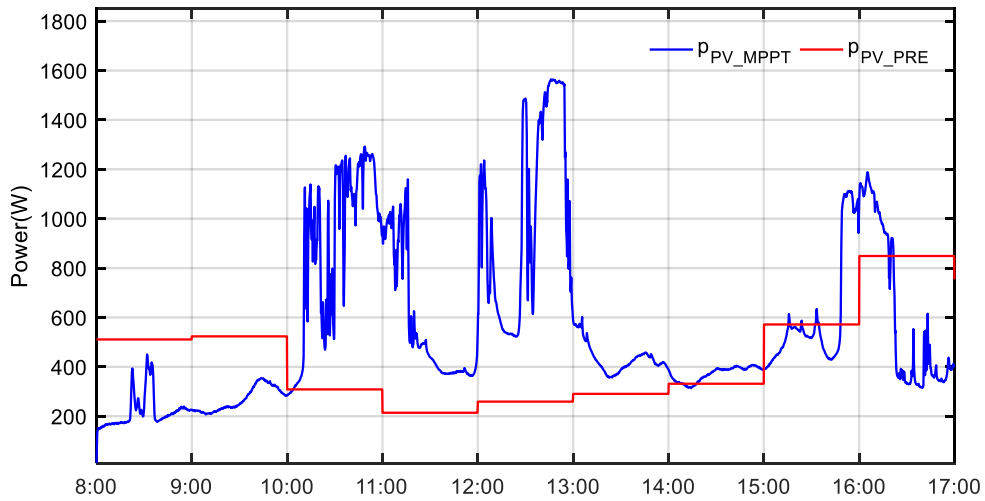


Figure 27. PV MPPT power and PV prediction power curves for July 16th 2018.
The load demand power and load power prediction curves are given in Figure 28.

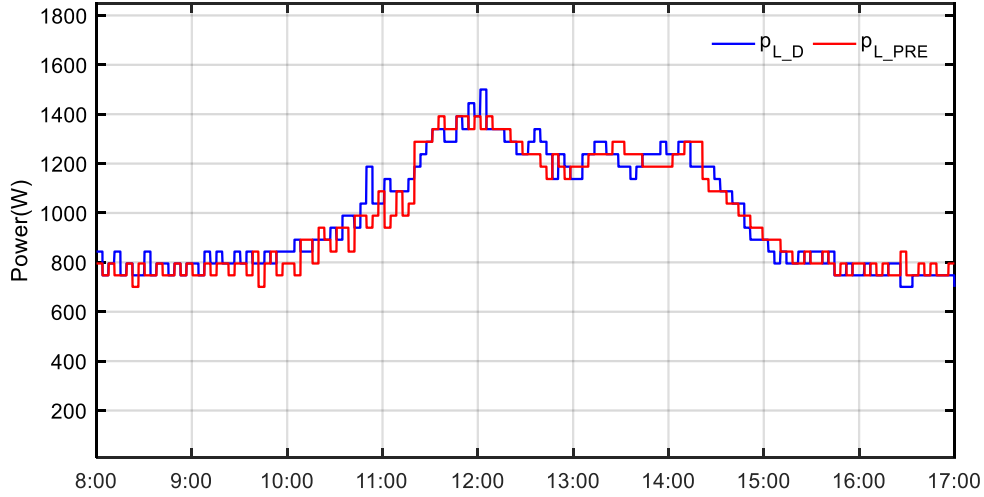


Figure 28. Load demand power and load power prediction curves.

The enterprise tariff of the public grid is given according to the TOU method in Table 2, the high tariff of peak hours is in the period from 10:00 to 12:00, the low tariff of normal hours is in the rest time of the 9 hours.

Table 2. TOU public grid energy tariffs

Public grid	TOU energy tariffs (€/kWh)		
	08:00-10:00	10:00-12:00	12:00-17:00
T_G	0.1	0.7	0.1

with T_G being the public grid exchanging imposed tariffs for supply and injection.

Table 3 presents the numerical values of the fixed energy tariffs considered in this work based on the rule presented in chapter II. 3. The average DG operation and maintenance (O&M) tariff $T_{DG_O\&M}$ including oil change cost and the replacement cost of several elements: pre-cleaner, air cleaner, low-profile air cleaner, fuel filter, and the spark plug [69] are also considered, the $T_{DG_O\&M}$ is assumed to be 0.63 €/h.

Table 3. Fixed energy tariffs

Fixed energy tariffs (€/kWh)	
BS T_{BS}	0.05
PV shed T_{PV_S}	1.5
Load shed T_{L_S}	1.8
DG T_{DG_F}	1.2
SC T_{SC}	0.3

In Table 4, the simulation scenarios are shown with the three operation modes, grid-connected mode, off-grid mode, and full microgrid mode. In every operation mode, the day-ahead optimization and real-time simulation are separately done. Then, in the day-ahead optimization, the optimization is designed by using the PV and load prediction power compared with the optimization by using the real PV and load power to eliminate the interference of the uncertain of power prediction.

Table 4. Simulation scenarios

Simulation scenarios		
Grid-connected mode, off-grid mode, and full microgrid mode.	Day-ahead optimization	Optimization with the PV and load prediction power
		Optimization with the real PV and load power
	Real-time simulation	Real-time result without day-ahead optimization
		Real-time result with day-ahead optimization

III.1.2. Grid-connected simulation for 9 hours' duration

To solve the grid-connected optimization problem of the economic dispatching, the MILP solver is applied. The 9 hours' duration weather data set from three different days, May 8th 2018, June 20th 2018, and July 16th 2018, under different weather conditions have been introduced in III.1.1. The load power and load prediction power has been provided in III.1.1. The tariff of every electrical component in the grid-connected mode has been given in III.1.1.

The grid-connected DC microgrid parameters used for the optimization dispatch layer and the operational algorithm of the operational layer are presented in Table 5.

Table 5. Parameter

Parameters	Values	Parameters	Values
P_{BS_MAX}	1000W	P_{PV_STC}	1750W
SOC_{BS_MIN}	20%	C_{BS_REF}	6.6Ah
SOC_{BS_MAX}	80%	P_{G_MAX}	200W
SOC_{BS_0}	50%		

In this study, the capacity of the BS and the power limits of the public grid are chosen in order to be able to illustrate and to demonstrate some features of the system considering the BS behavior and the public grid, such as maximum limit reached, PV shedding happened, and load shedding happened. The difference between the parameters in the optimization dispatch layer and the parameters in the operational algorithm is that the public grid power fluctuation P_{GF_Limit} is only considered in the optimization dispatch layer, the DC bus reference voltage v_{DC}^* is only considered in the operational layer because the characteristic of the DC bus controller is not considered in the optimization dispatch layer.

In order to avoid the DC microgrid paralysis in the operational layer and the infeasible solution in the optimization dispatch layer, all the load demand power is assumed to be non-critical load in both of the layers. SOC_{BS_0} is the initial BS state of charge, P_{PV_STC} is the MPPT power under STC.

III.1.2.1. Optimization results

Based on PV and load prediction power profiles of May 8th 2018, the day-ahead economics optimization results are shown in Figure 29 and Figure 30. Δt is 10 seconds as the weather data's sampling.

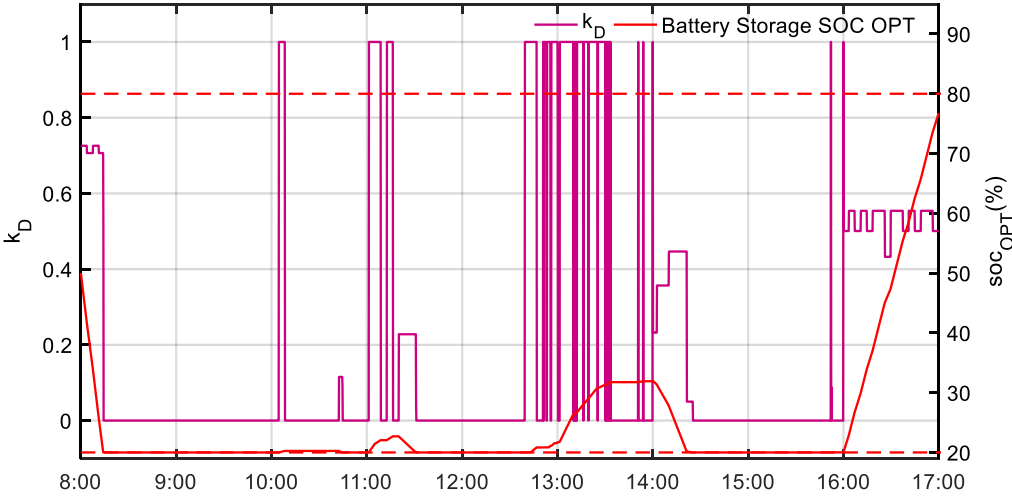


Figure 29. The day-ahead economics optimization results (k_D) and BS SOC curves at grid-connected mode on May 8th 2018.

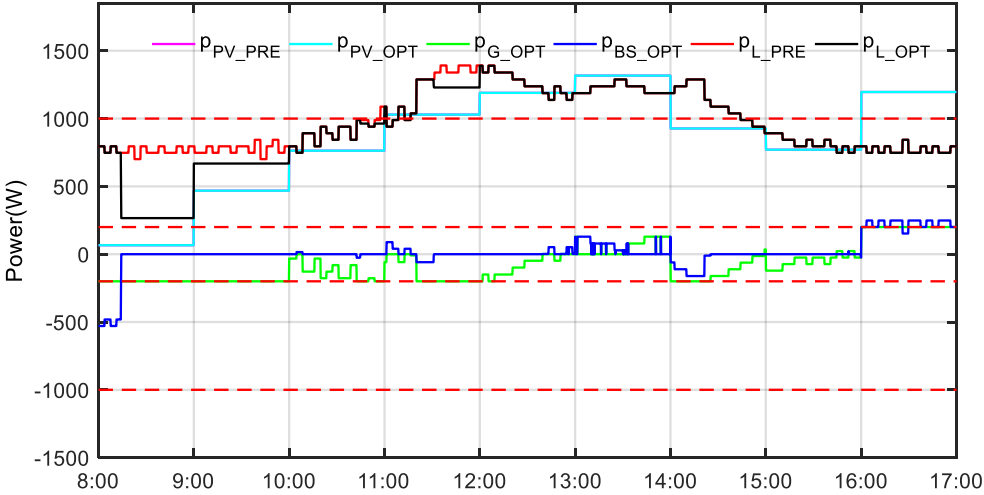


Figure 30. The day-ahead economics optimization results of power curves at grid-connected mode on May 8th 2018.

In Figure 29 and Figure 30, at the beginning of the optimization results, the PV power is less than the load demand power, the public grid and BS try their best to supply the load demand power; when the soc_{BS} reaches soc_{BS_MIN} , the load shedding can happen to keep the power balance of the microgrid; from 10:00 to 16:00, the PV power is close to the load demand, the public grid can sell or buy power from the microgrid and the BS can be charging and discharging; at the end of the optimization, the PV power is more than the load demand power, so the public grid can buy the PV power, at the same time, the BS can be charging. The results above are the day-ahead optimization results, which means the 9 hours' duration day-ahead optimization, thus the power distribution is different from the instant optimization base on the component tariff.

In the day-ahead optimization, it is natural that the prediction error exists between the prediction power and real power of the PV and load due to the complexity to model the uncertain weather condition and uncertain human behaviors. Thus, the day-ahead optimization suffers the prediction error, which causes the uncertain optimization results when the PV and load prediction power are used. Thus, in the day-ahead optimization, the real PV and load power profiles are used to replace the PV and load power prediction profiles to eliminate the prediction error between the prediction and the real value, which can be a reference to the results by using the prediction value. The economics optimization results by using real PV and load power profiles are shown in Figure 31 and Figure 32. Δt is 10 seconds as the weather data's sampling.

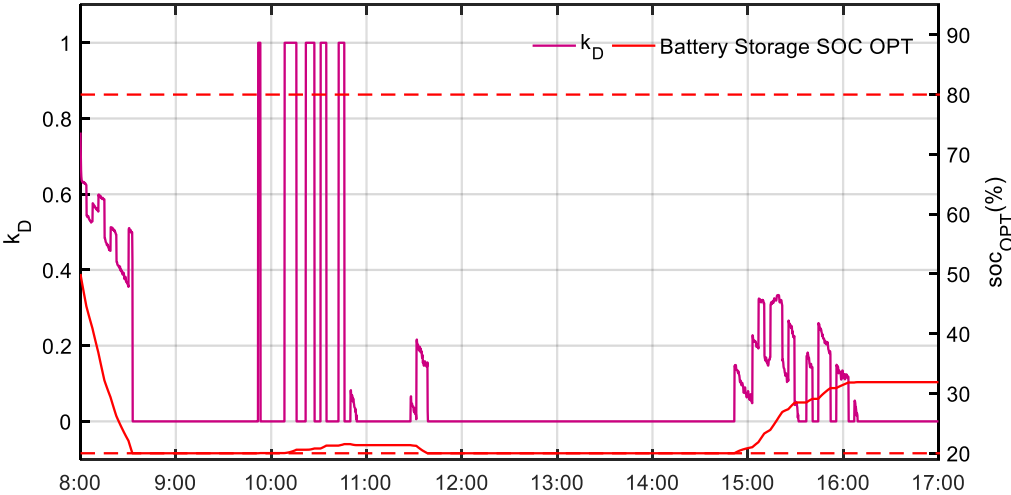


Figure 31. The ideal economics optimization results (k_D) and BS SOC curves at grid-connected mode on May 8th 2018.

In Figure 31 and Figure 32, the PV and load prediction power profiles are replaced by the real PV and load power profiles measurements and respectively considered for May 8th 2018. It can be seen that the results by using the real PV and load power profiles probably has the same trend as the results by using the PV and load prediction power profiles; however, the PV in the day-ahead optimization results

have more shedding power than the ideal economics optimization in 8:00 to 10:00, which is influenced by the difference between PV and load prediction power profiles, and real PV and load power profiles.

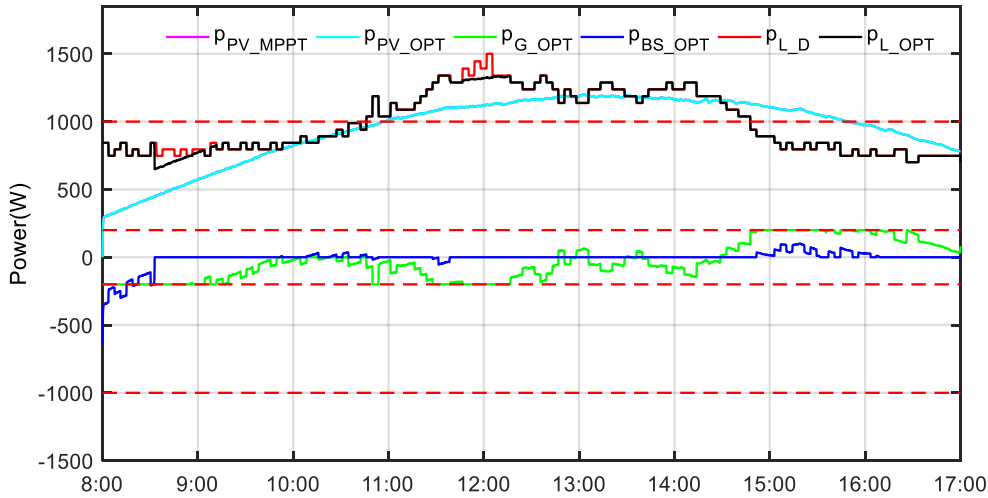


Figure 32. The ideal economics optimization results of power curves at grid-connected mode on May 8th 2018.

III.1.2.2. Real-time simulation results

The following section considers the real-time simulation results of the operational layer. In order to validate the effectiveness of the day-ahead optimization, the real-time simulation result by using the day-ahead optimization will be compared with the real-time simulation result without considering the day-ahead optimization results.

III.1.2.2.1 Real-time result without day-ahead optimization

Without considering the day-ahead optimization results, the cases under the power management strategy proposed in II.5.1.1. should be used, which are also special cases in II.5.1.2. when k_D equal to 1. Thus, in order to give a better comparison, the cases when k_D equal to 0.5, or 0 are also simulated.

The results when k_D equal to 1, 0.5, or 0 are separately shown in Figure 33 and Figure 34, Figure 35, and Figure 36, Figure 37, and Figure 38.

In Figure 33 and Figure 34 the BS has a higher priority than the public grid to compensate for the power difference between p_{PV_MPPT} and p_{L_D} . At the beginning of the optimization results, the PV power is less than the load demand power, the BS has the higher priority to supply the load demand power; when the SOC_{BS} reaches SOC_{BS_MIN} , the public grid try to supply the load demand power; when both of the public grid and the BS are limited, the load shedding can happen to keep the power balance of the microgrid; from 10:00 to 16:00, the PV power is close to the load demand, the public grid can sell or buy power from the microgrid and the BS can be charging and discharging; at the end of the

optimization, the PV power is more than the load demand power, so the BS has the higher priority to absorb the excess PV power; when the soc_{BS} reaches SOC_{BS_MAX} , the public grid can buy the PV power; when both of the public grid and the BS are limited, the PV shedding can happen to keep the power balance of the microgrid.

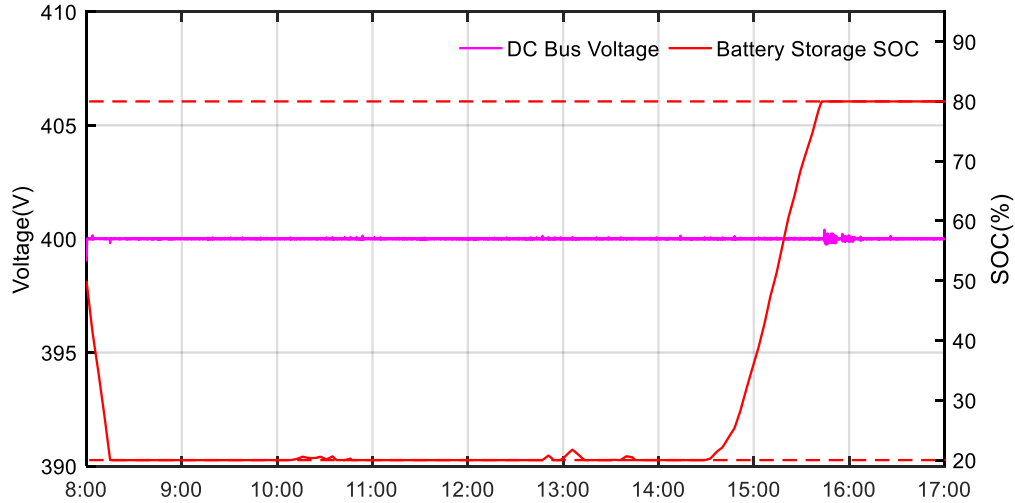


Figure 33. DC bus voltage and BS SOC curves when $k_D = 1$ at grid-connected mode on May 8th 2018.

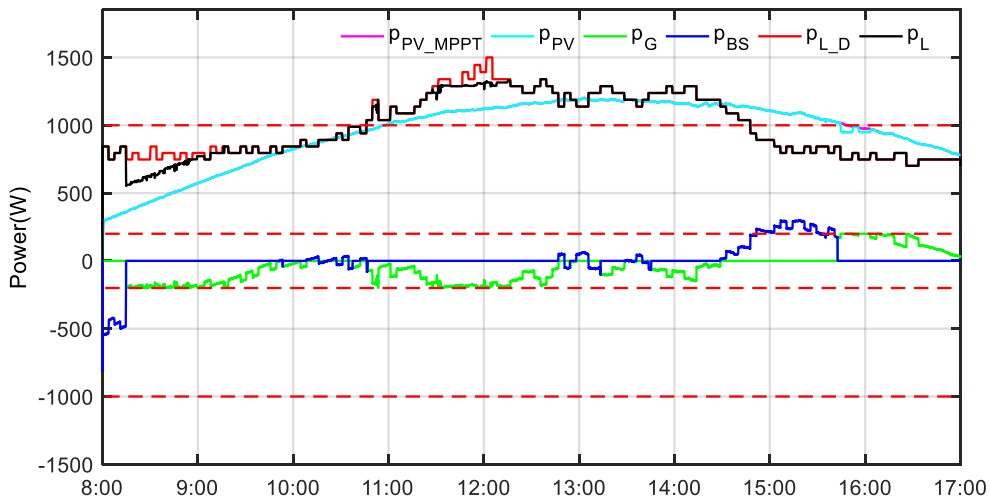


Figure 34. Power curves when $k_D = 1$ at grid-connected mode on May 8th 2018.

In Figure 35 and Figure 36 both the BS and the public grid have the same priority to compensate for the power difference between p_{PV_MPPT} and p_{L_D} .

In Figure 35 and Figure 36 at the beginning of the optimization results, the PV power and is less than the load demand power, the public grid and the BS has the same priority to supply the load demand power; when one of the public grid and the BS is limited, the other tries to supply the load demand

power; when both of the public grid and the BS are limited, the load shedding can happen to keep the power balance of the microgrid; from 10:00 to 16:00, the PV power is close to the load demand, the public grid can sell or buy power from the microgrid and the BS can be charging and discharging; at the end of the optimization, the PV power is more than the load demand power, so when one of the public grid and the BS is limited, the other tries to absorb the PV power; when both of the public grid and the BS are limited, the PV shedding can happen to keep the power balance of the microgrid.

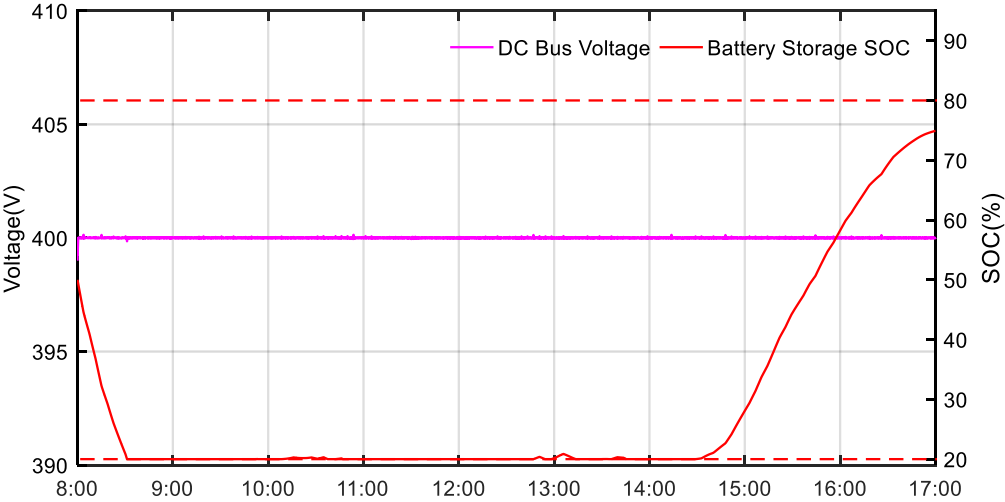


Figure 35. DC bus voltage and BS SOC curves when $k_D = 0.5$ at grid-connected mode on May 8th 2018.

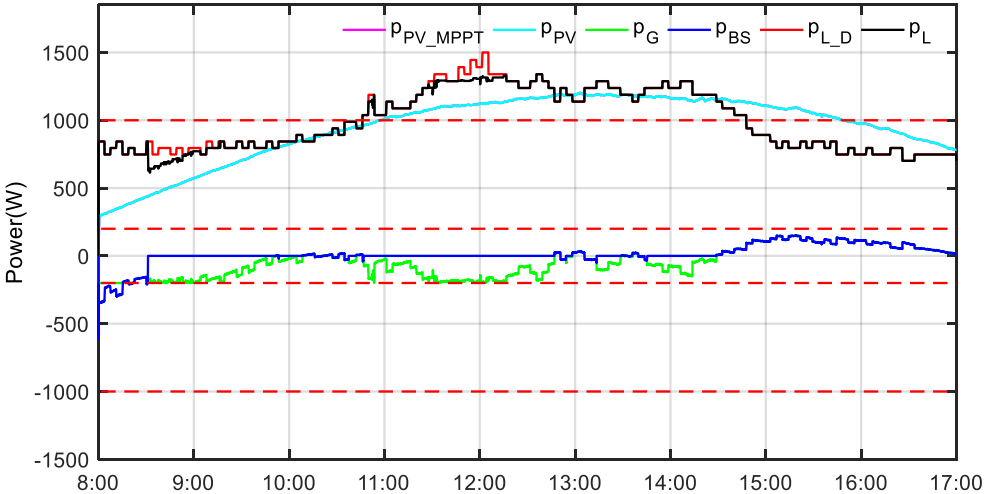


Figure 36. Power curves when $k_D = 0.5$ at grid-connected mode on May 8th 2018.

In Figure 37 and Figure 38, the public grid has a higher priority than the BS to compensate for the power difference between p_{PV_MPPT} and p_{L_D} .

In Figure 37 and Figure 38, at the beginning of the optimization results, the PV power is greater than the load demand power, the public grid has the higher priority to supply the load demand power; when

the public grid is limited, the BS tries to charge the load demand power; when both of the public grid and the BS are limited, the load shedding can happen to keep the power balance of the microgrid; from 10:00 to 16:00, the PV power is close to the load demand, the public grid can sell or buy power from the microgrid and the BS can be charging and discharging; at the end of the optimization, the PV power is more than the load demand power, so the public grid has the higher priority to absorb the excess PV power; when the public grid is limited, the BS can be charging by the PV power; when both of the public grid and the BS are limited, the PV shedding can happen to keep the power balance of the microgrid.

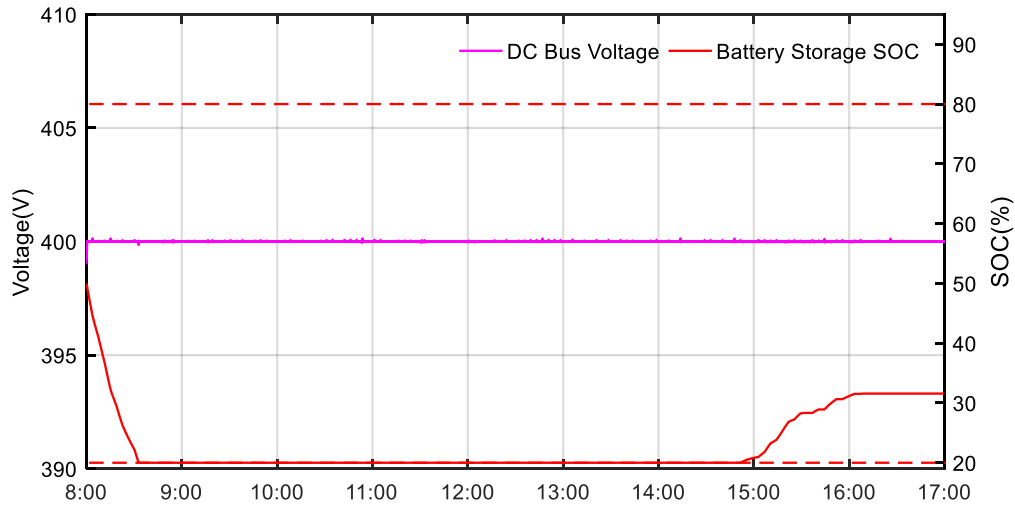


Figure 37. DC bus voltage and BS SOC curves when $k_D = 0$ at grid-connected mode on May 8th 2018.

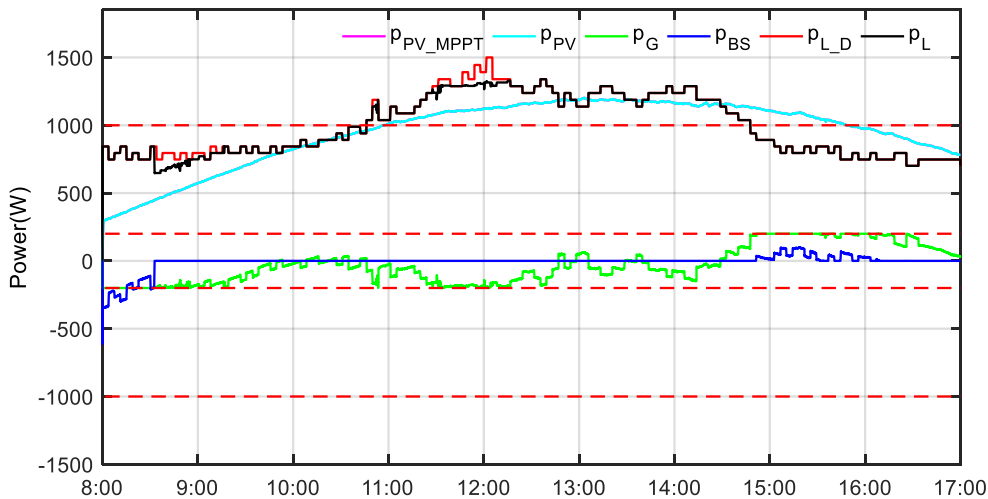


Figure 38. Power curves when $k_D = 0$ at grid-connected mode on May 8th 2018.

III.1.2.2.2 Real-time results with day-ahead optimization

Considering the day-ahead optimization results, the cases under the power management strategy proposed in II.5.1.2. should be used. The optimization coefficient k_D can introduce the day-ahead optimization results in the economic dispatching layer.

The real-time operational simulation results of the DC microgrid by using the day-ahead economics optimization results are shown in Figure 39 and Figure 40.

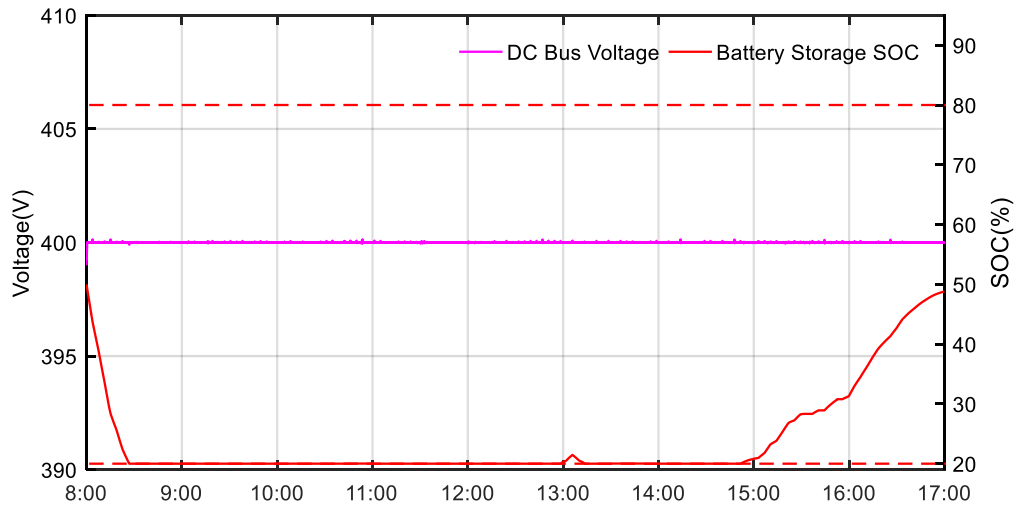


Figure 39. The actual results of DC bus voltage and BS SOC curves at grid-connected mode on May 8th 2018.

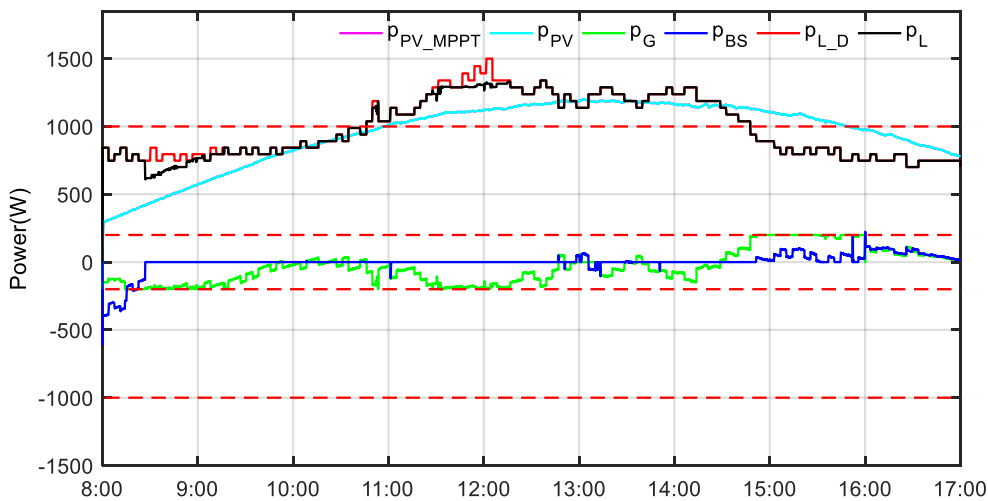


Figure 40. The actual results of power curves at grid-connected mode on May 8th 2018.

In Figure 39 and Figure 40, the day-ahead economics optimization results are introduced in the real-time operational layer, it can be seen that the power ratio between the public grid and the BS can not be a constant value. At the beginning of the real-time simulation, the BS is charging more power because of the higher PV power.

The ideal real-time operational simulation results of the DC microgrid by using the ideal economics optimization results under the real PV and load power profiles are shown in Figure 41 and Figure 42.

In Figure 41 and Figure 42, the ideal economics optimization results are introduced in a real-time operational layer, it can be seen that the ideal power management of the DC microgrid.

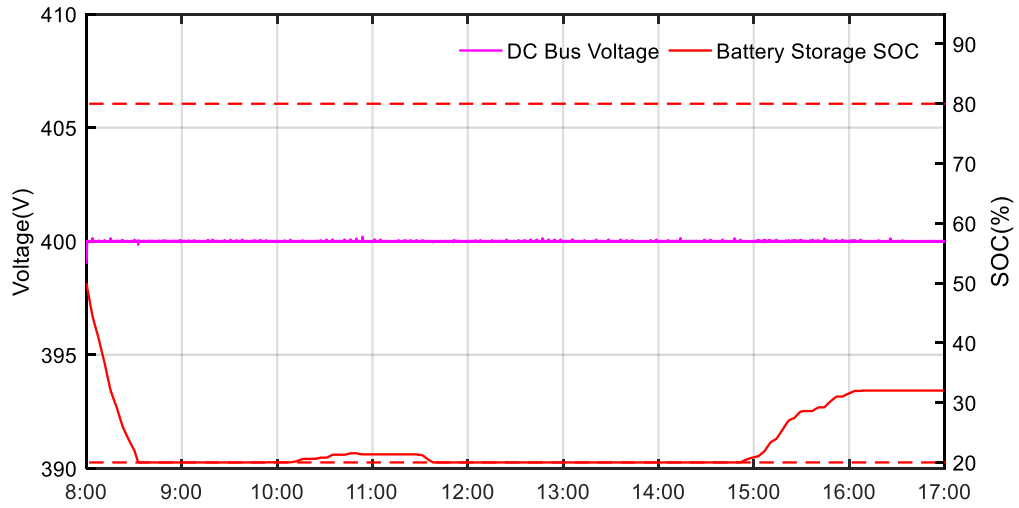


Figure 41. The ideal results of DC bus voltage and BS SOC curves at grid-connected mode on May 8th 2018.

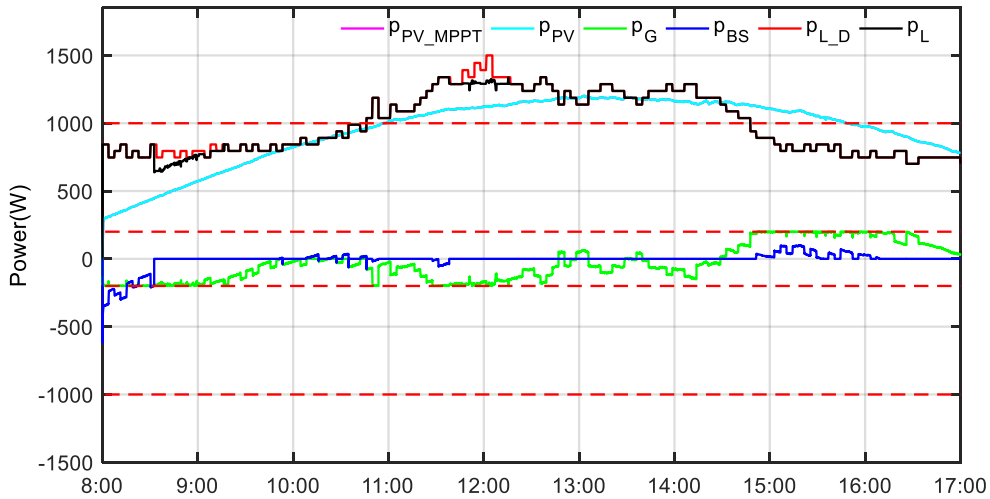


Figure 42. The ideal results of power curves at grid-connected mode on May 8th 2018.

III.1.2.3. Grid-connected simulation results comparison and analysis

This section presents some tables that list the energy cost of every component from the above simulation results including the optimization results given in III.1.2.1. and the real-time operational results given in III.1.2.2.

The summary of the simulation results for grid-connected mode on May 8th 2018 are shown in Table 6.

In Table 6, there are seven conditions listing, the conditions when k_d equals to 1, 0.5, or 0 are the real-time simulation results in the operational layer. The conditions of MILP results are the day-ahead optimization results in the economics dispatching layer by using the prediction power profiles of PV

and load. The conditions of operational results are the real-time simulation results in the operational layer by using the MILP results based on prediction power profiles of PV and load. The conditions of ideal MILP results are the ideal optimization results in the economics dispatching layer by using real recorded PV and load power profiles to replace the prediction power profiles of PV and load; it is an ideal case because the real power profiles are considered without any uncertainties, i.e. 100% accuracy. The conditions of ideal operational results are the real-time simulation results in the operational layer by using the ideal MILP results. In fact, the MILP problem formulation can be close to the operational layer model. However, the MILP cannot formulate a problem which is exactly the same to the operational layer due to complexity of the operational layer. Thus, the ideal MILP results and the ideal operational results are not exactly the same.

Table 6. Results summary for grid-connected mode on May 8th 2018.

Day-ahead optimization	NO		
Condition in real-time simulation	$k_D = 1$	$k_D = 0.5$	$k_D = 0$
The sum of C_{BS} and C_G (c€)	15.89	15.86	13.24
C_{PV_S} (c€)	1.57	0	0
C_{L_D} (c€)	26.63	18.11	17.27
C_{TOTAL} (c€)	44.09	33.97	30.52

Table 6 bis. Results summary for grid-connected mode on May 8th 2018.

Day-ahead optimization	YES			
Condition	MILP results	Operational results	Ideal MILP results	Ideal Operational results
The sum of C_{BS} and C_G (c€)	25.17	14.17	14.65	14.13
C_{PV_S} (c€)	0	0	0	0
C_{L_D} (c€)	101.04	20.16	11.91	15.75
C_{TOTAL} (c€)	126.21	34.32	26.56	29.88

To evaluate the day-ahead optimization performance, the ideal operational results after using ideal MILP results are regarded as a reference to compare with the real operational results after using real MILP results.

By comparing the results given in Table 6, it can be seen that the total cost under the condition when k_D equals to 1, 0.5, or 0, and operational results is higher than the total cost under the condition of ideal

operational results, because the accuracy of PV and load power prediction has a big influence on power dispatching. Normal, the phenomenon that the total cost under the condition of operational results is less than the total cost under the condition when k_D equals to 1, 0.5, or 0 should happen, which can give a positive proof that the optimization in the economics dispatching layer can make a good function to reduce the total cost in the real-time operational simulation in the operational layer. The huge difference between the prediction power and the real power as shown in Figure 25, Figure 26, and Figure 27 leads to a non-optimal power management results in the real-time operational layer. However, the low difference between the operational results and ideal operational results, which represent the perfect optimization reference, shows that the defined optimization work well.

In order to give better evidence to prove the effectiveness of the optimization and real-time power management strategy, other two weather data are applied in the grid-connected DC microgrid.

The simulation results for grid-connected mode on June 20th 2018 are shown in Table 7.

Table 7. Results summary for grid-connected mode on June 20th 2018.

Day-ahead optimization	NO		
Condition in real-time simulation	$k_D = 1$	$k_D = 0.5$	$k_D = 0$
The sum of C_{BS} and C_G (c€)	19.68	14.20	9.58
C_{PV_S} (c€)	19.79	4.21	0
C_{L_D} (c€)	133.52	143.21	155.53
C_{TOTAL} (c€)	172.99	161.62	165.11

Table 7 bis. Results summary for grid-connected mode on June 20th 2018.

Day-ahead optimization	YES			
Condition	MILP results	Operational results	Ideal MILP results	Ideal Operational results
The sum of C_{BS} and C_G (c€)	-20.89	11.93	23.70	22.60
C_{PV_S} (c€)	0	0	0	0
C_{L_D} (c€)	62.09	158.51	93.75	101.15
C_{TOTAL} (c€)	41.20	170.44	117.45	123.74

By the comparisons before, it can be seen that the total cost under the condition when k_D equals to 1, 0.5, or 0, and operational results is higher than the total cost under the condition of ideal operational results, which prove that optimization work well to reduce the total cost. And the cause of the difference

between the total cost under the condition of operational results and ideal operational results is the accuracy of PV and load power prediction has big influence on power dispatching.

The simulation results for grid-connected mode on July 16th 2018 is shown in Table 8.

By the comparisons before, it can be seen that the total cost under the condition of ideal operational results less than the other results, meaning that the power optimization can work and reduce the total cost of microgrid. And, the operational results is worse than the ideal operational results mostly by the reason of the bad accuracy of PV power prediction, which is also the reason why the total cost under the condition when k_D equals to 1, 0.5, or 0, and operational results is more than the total cost under the condition of ideal operational results.

Table 8. Results summary for grid-connected mode on July 16th 2018.

Day-ahead optimization	NO		
Condition in real-time simulation	$k_D = 1$	$k_D = 0.5$	$k_D = 0$
The sum of C_{BS} and C_G (c€)	26.58	24.76	22.84
C_{PV_S} (c€)	0	0	0
C_{L_D} (c€)	479.90	475.73	483.93
C_{TOTAL} (c€)	506.48	500.49	506.77

Table 8 bis. Results summary for grid-connected mode on July 16th 2018.

Day-ahead optimization	YES			
Condition	MILP results	Operational results	Ideal MILP results	Ideal Operational results
The sum of C_{BS} and C_G (c€)	39.76	22.85	32.74	30.96
C_{PV_S} (c€)	0	0	0	0
C_{L_D} (c€)	606.59	483.83	438.90	450.81
C_{TOTAL} (c€)	646.36	506.68	471.64	481.77

In conclusion, the real-time power management in the operational layer without the economics optimization in the economics dispatching layer cannot achieve the purpose of the optimal real-time power management. The accuracy of PV and load power predictions has big influence on the economics optimization. In particular, the uncertainty of weather will lead to uncertainty in the results of economic optimization because PV power generation highly depends on the weather condition. The economics

optimization in the economics dispatching layer can reduce the total cost of the power flow of DC microgrid in grid-connected mode considering the increased accuracy of PV and load power prediction.

III.1.3. Off-grid simulation for 9 hours' duration

To solve the off-grid optimization problem of the economic dispatching, the MILP solver is applied. The weather data set from the same three different days, i.e. May 8th 2018, June 20th 2018, and July 16th 2018, introduced in III.1.1, are used. The load power and load prediction power has been provided in III.1.1. The tariff of every electrical component in the grid-connected mode has been given in III.1.1.

The off-grid DC microgrid parameters used for the optimization dispatch layer are presented in Table 9.

Table 9. Parameters for optimization in off-grid mode.

Parameters	Values	Parameters	Values
P_{BS_MAX}	1000W	P_{DG_MAX}	1500W
SOC_{BS_MIN}	20%	$P_{DG_ON_MAX}$	$(0, P_{DG_MAX}]$
SOC_{BS_MAX}	80%	$P_{DG_ON_MIN}$	$(0, P_{DG_ON_MAX}]$
SOC_{BS_0}	50%	dt_{DG}	1200s
C_{REF}	6.6Ah	k_{L_CRIT}	80%
P_{PV_STC}	1750W		

In Table 9, the parameters of the BS and PV are the same as the parameters in the grid-connected mode; there is no parameter about SC in the optimization because the SC is not considered; the duty cycle of the DG is fixed as 1200s to be simplified according to the time constraints of the DG start-up and turning off. In the optimization of the economics dispatching layer, the DG power is limited between $P_{DG_ON_MIN}$ and $P_{DG_ON_MAX}$ when the DG is turned on. The $P_{DG_ON_MAX}$ is chosen between 0 and P_{DG_MAX} , the $P_{DG_ON_MIN}$ is chosen between 0 and $P_{DG_ON_MAX}$. The k_{L_CRIT} is set as 80% to provide the condition for turning on the DG.

The parameters $P_{DG_ON_MIN}$ and $P_{DG_ON_MAX}$ are very important in the economics dispatching layer, which give a big influence on the optimization results, the appropriate $P_{DG_ON_MIN}$ and $P_{DG_ON_MAX}$ do not mean the lowest total cost of the optimization results in the economics dispatching layer, which actual means that the optimization results in the economics dispatching layer can give the best schedule for future power management in the real-time operational layer, in other word the power management in the real-time operational layer can achieve the lowest total cost by using optimization results in the economics dispatching layer. However, it is uncertainty and not easy to find the appropriate $P_{DG_ON_MIN}$

and $P_{DG_ON_MAX}$ because the problem formulation in the economics dispatching layer is simple due to the computation and the accuracy of power prediction is not so high. Thus, we assumed that the appropriate $P_{DG_ON_MIN}$ and $P_{DG_ON_MAX}$ are the values when the total cost of optimization results in the economics dispatching layer is the lowest.

In order to choose the appropriate $P_{DG_ON_MIN}$ and $P_{DG_ON_MAX}$, we make two assumptions; one is to assume that $P_{DG_ON_MIN}$ equals to $P_{DG_ON_MAX}$, and to take the $P_{DG_ON_MIN}$ and $P_{DG_ON_MAX}$ when the lowest total cost appears as the appropriate value; the other is to assume that $P_{DG_ON_MIN}$ does not equal to $P_{DG_ON_MAX}$, and the appropriate $P_{DG_ON_MIN}$ and $P_{DG_ON_MAX}$ appear when the lowest total cost happens based on the range at the middle of the appropriate $P_{DG_ON_MIN}$ of the assumption 1.

Based on the two assumptions above, we propose to use a simple method to determine the two values, $P_{DG_ON_MAX}$ and $P_{DG_ON_MIN}$ in two ways, a constant DG power and a range of DG power. There are two steps in this method; firstly, to search the appropriate constant DG power value in the DG's power range between 0 and P_{DG_MAX} ; secondly, to search the appropriate power range of DG by using the appropriate constant DG power value above as the middle value.

For example, to find the appropriate constant DG power and the range of DG power on May 8th 2018, firstly, to set the $P_{DG_ON_MAX}$ and $P_{DG_ON_MIN}$ to be the same values based on the assumption 1, the $P_{DG_ON_MAX}$ and $P_{DG_ON_MIN}$ can change from 0 W to P_{DG_MAX} based on the step 50 W, then to solve these optimization problems, to take the constant value while the minimum total price is achieved as the appropriate constant DG power value, 800W is the appropriate constant DG power shown in Figure 43; secondly, to solve several optimization problems based on the power range between $P_{DG_ON_MAX}$ and $P_{DG_ON_MIN}$ widen with 800W as the center value, to take the first range while the minimum total price appears as the appropriate power range for the DG, the range from 300W to 1300W is the appropriate power range on May 8th 2018 in Figure 44.

In Figure 43, it can be seen that the constant DG power is chosen from the 0 to P_{DG_MAX} , only the "Optimal" and "OptimalTol" solution of the optimization results in the economics dispatching layer is shown, so from results in Figure 43, it is sure that the lowest total cost appears when the constant DG is 800W, thus 800W are considered as the appropriate constant DG power.

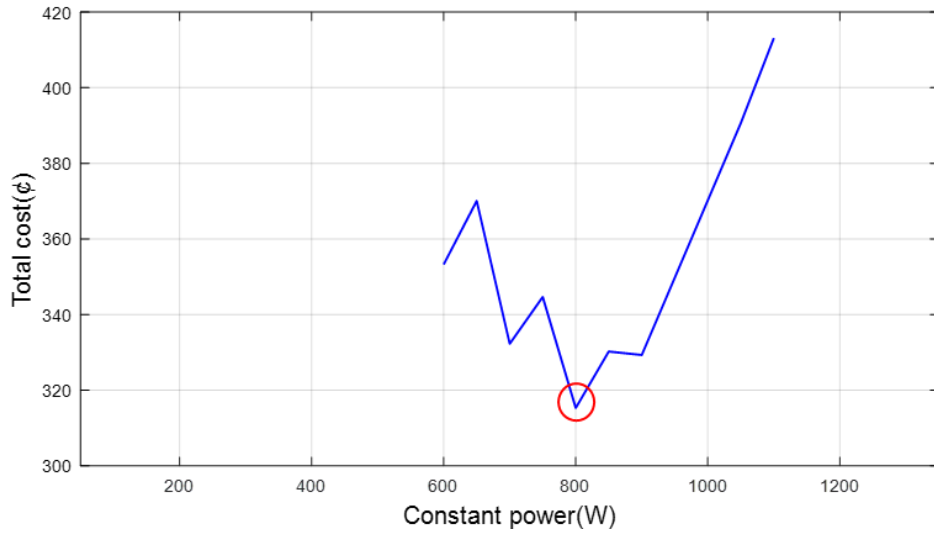


Figure 43. The total cost with constant DG power at off-grid mode on May 8th 2018.

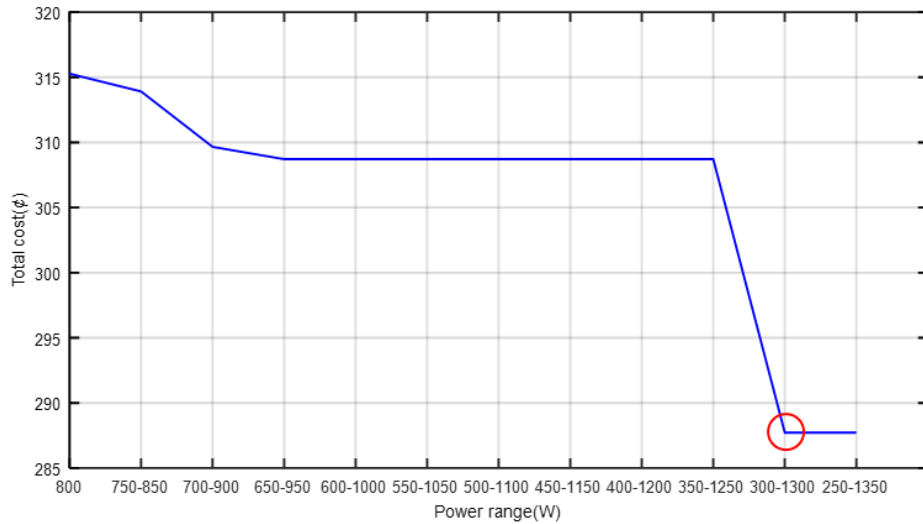


Figure 44. The total cost with variable DG power at off-grid mode on May 8th 2018.

In Figure 44, it can be seen that the variable DG power is chosen at middle of the appropriate constant DG power, only the “Optimal” and “OptimalTol” solution of the optimization results in the economics dispatching layer are shown, so from results in Figure 36, it is sure that the lowest total cost appears when the variable DG is from 300W to 1300W, thus we take the range from 300W to 1300W as the appropriate variable DG power. According to the same method depicted on the weather data on May 8th 2018, the appropriate constant power on June 20th 2018 is 200W in Figure 45; the appropriate power range on June 20th 2018 is from 150W to 250W in Figure 46.

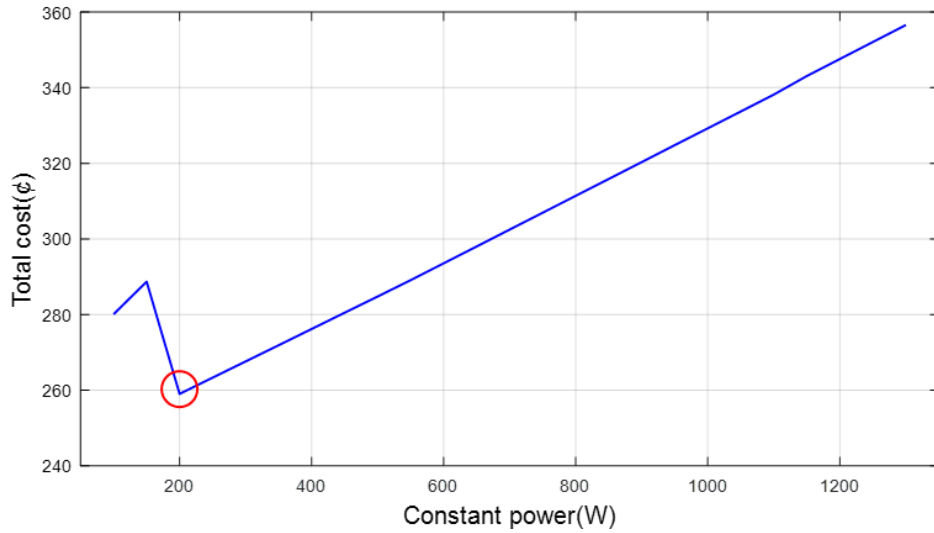


Figure 45. The total cost with constant DG power at off-grid mode on June 20th 2018.

In Figure 45, it can be seen that the constant DG power is chosen from the 0 to P_{DG_MAX} , only the “Optimal” and “OptimalTol” solution of the optimization results in the economics dispatching layer is shown, so from results in Figure 45, it is sure that the lowest total cost appears when the constant DG is 200W, thus 200W are considered as the appropriate constant DG power.

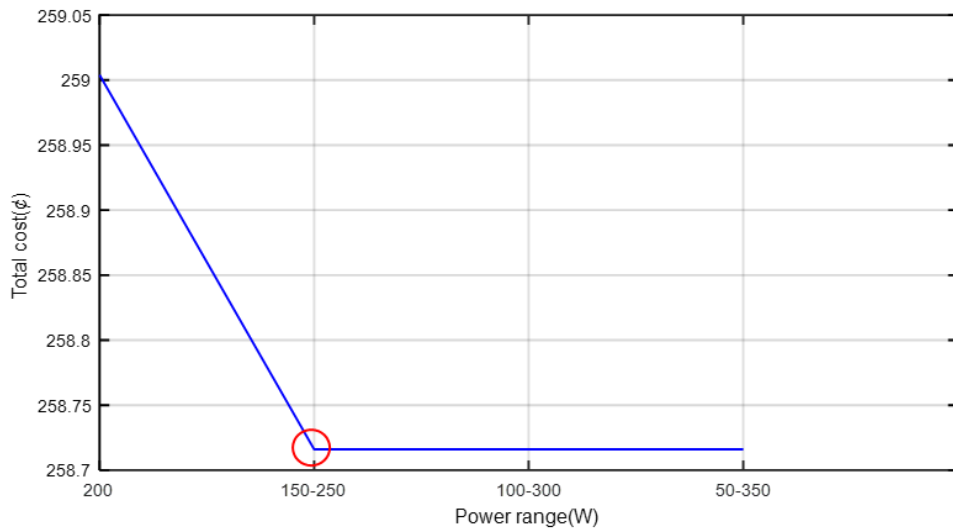


Figure 46. The total cost with variable DG power at off-grid mode on June 20th 2018.

In Figure 46, it can be seen that the variable DG power is chosen at middle of the appropriate constant DG power, only the “Optimal” and “OptimalTol” solution of the optimization results in the economics dispatching layer are shown, so from results in Figure 46, it is sure that the lowest total cost appears when the variable DG is from 150W to 250W, thus we take the range from 150W to 250W as the appropriate variable DG power. According to the same method depicted on the weather data on May 8th 2018, the appropriate constant power on July 16th 2018 is 900W in Figure 47; the appropriate power range on July 16th 2018 is from 600W to 1200W in Figure 48.

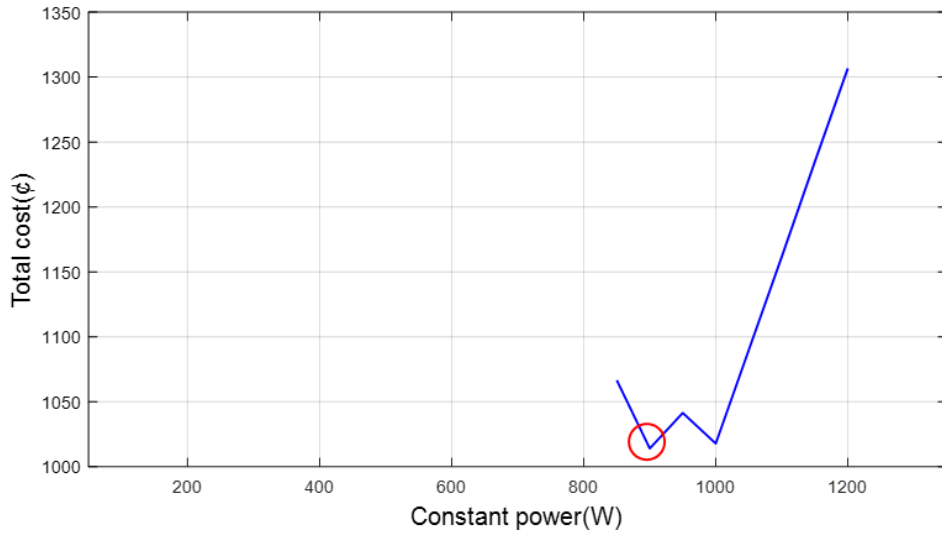


Figure 47. The total cost with constant DG power at off-grid mode on July 16th 2018.

In Figure 47, it can be seen that the constant DG power is chosen from the 0 to P_{DG_MAX} , only the “Optimal” and “OptimalTol” solution of the optimization results in the economics dispatching layer is shown, so from results in Figure 39, it is sure that the lowest total cost appears when the constant DG is 900W, thus 900W are considered as the appropriate constant DG power.

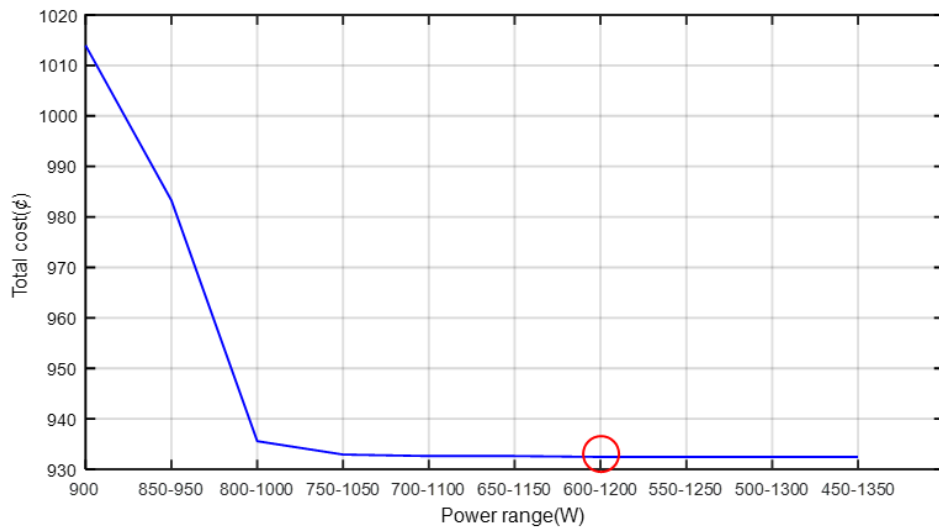


Figure 48. The total cost with variable DG power at off-grid mode on July 16th 2018.

In Figure 48, it can be seen that the variable DG power is chosen at middle of the appropriate constant DG power, only the “Optimal” and “OptimalTol” solution of the optimization results in the economics dispatching layer is shown, so from results in Figure 48, it is sure that the lowest total cost appears when the variable DG is from 600W to 1200W, thus we take the range from 600W to 1200W as the appropriate variable DG power.

The off-grid DC microgrid parameters used for the operational algorithm of the operational layer is presented in Table 10.

Table 10. Parameters for operational algorithm in off-grid mode.

Parameters	Values	Parameters	Values
P_{BS_MAX}	1000W	v_{SC_Rated}	75V
SOC_{BS_MIN}	20%	$SOC_{SC_MAX_MAX}$	85%
SOC_{BS_MAX}	80%	$SOC_{SC_MAX_MIN}$	75%
SOC_{BS_0}	50%	$SOC_{SC_MIN_MAX}$	45%
C_{REF}	6.6Ah	$SOC_{SC_MIN_MIN}$	35%
P_{PV_STC}	1750W	SOC_{SC_0}	75%
v_{DC}^*	400V	P_{DG_MAX}	1500W
P_{SC_MAX}	1500W	$T_{DG_ON_MAX}$	3600s
T_{SC_MIN}	180s	$T_{DG_OFF_LIM}$	1200s
C_{SC}	94F	k_{L_CRIT}	80%

In Table 10, the detailed SC and DG parameters are be set; the function of SC is to compensate the power deficiency while DG start-up, so the maximum limits of SC and DG are the same; the voltage of DC bus is introduced as 400 V to make DC power exchanged in microgrid efficient by reducing the power loss in a power transmission, the k_{L_CRIT} is introduced to limit the load power more than 80% of P_{L_D} .

III.1.3.1. Optimization results

The day-ahead economics optimization results for May 8th 2018 by using PV and load prediction power profiles under the appropriate constant DG power 800W are shown in Figure 49 and Figure 50.

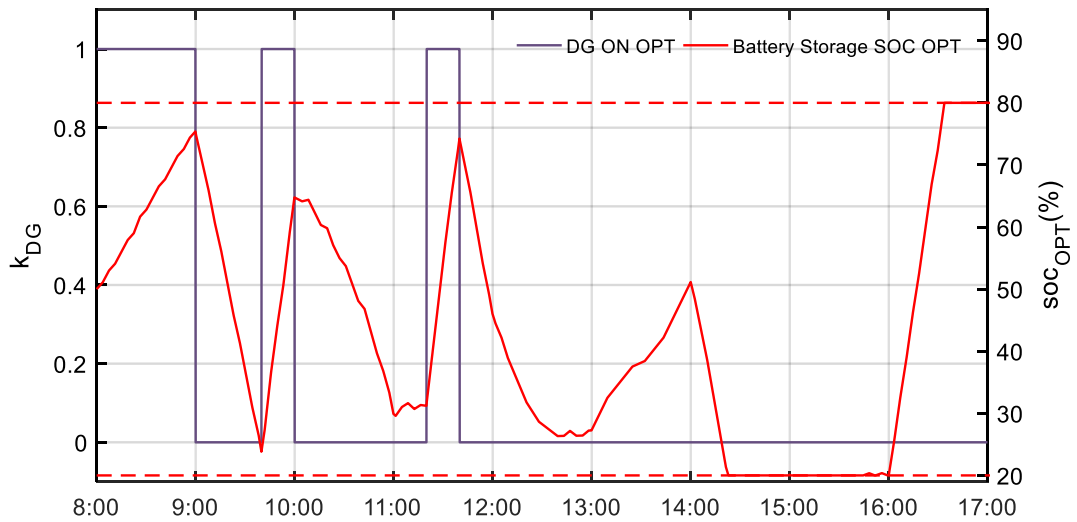


Figure 49. The day-ahead economics optimization results (k_{DG}) and BS SOC curves at off-grid mode on May 8th 2018.

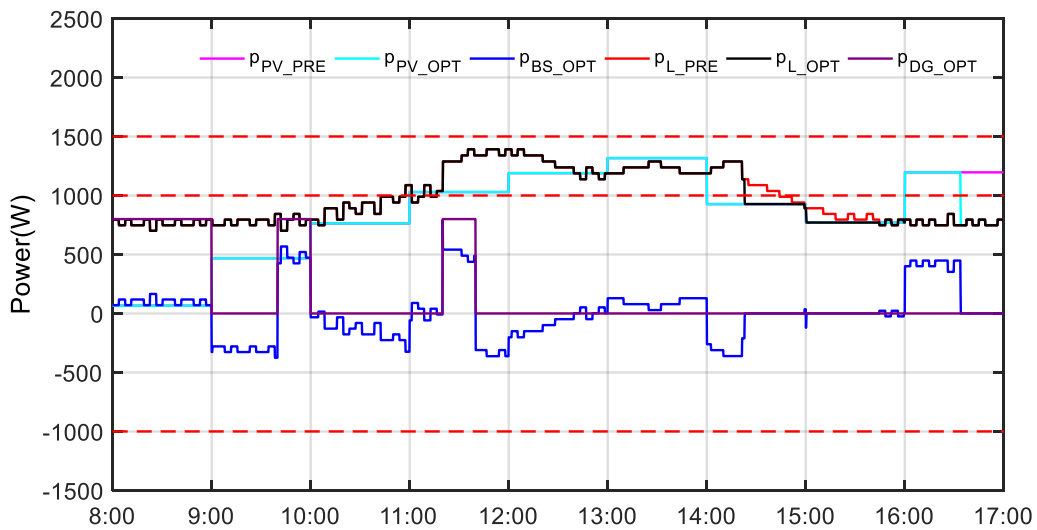


Figure 50. The day-ahead economics optimization results of power curves at off-grid mode on May 8th 2018.

In Figure 49 and Figure 50, the PV and load prediction power profiles are used, the day-ahead optimization results are shown under the appropriate constant DG power; in the beginning of the optimization results, the PV power is less than the load demand power, the DG is turned on to supply the load demand power, and the BS is charging by the rest of the DG power due to the DG operating at the constant power in the duty cycle; at 9:00, the DG is turned off, the BS is discharging to support the load demand power; then the DG is turned on at 9:40; from 10:00 to 16:00, the PV power is close to the load demand, the DG is turned on at 11:20 to support the microgrid and the BS can be charging and discharging; at the end of the optimization, the PV power is more than the load demand power, so the

DG is always off, at the same time, the BS can be charging; when the soc_{BS} reaches SOC_{BS_MAX} , the PV shedding happens to keep the power balance of the microgrid.

The day-ahead economics optimization results on May 8th 2018 by using PV and load prediction power profiles under the appropriate DG power range from 300W to 1300W are shown in Figure 51 and Figure 52. In Figure 51 and Figure 52, the PV and load prediction power profiles are used, the day-ahead optimization results are shown under the appropriate DG power range; at the beginning of the optimization results, the PV power is less than the load demand power, the DG is turned on to supply the load demand power and the BS in the duty cycle; at 8:20, the DG is turned off, the BS is discharging to support the load demand power; then the DG is turned on at 8:40 and 9:40; from 10:00 to 16:00, the PV power is close to the load demand, the DG is turned on at 11:40 to support the microgrid and the BS can be charging and discharging; at the end of the optimization, the PV power is more than the load demand power, so the DG is always off, at the same time, the BS can be charging; when the soc_{BS} reaches SOC_{BS_MAX} , the PV shedding happens to keep the power balance of the microgrid.

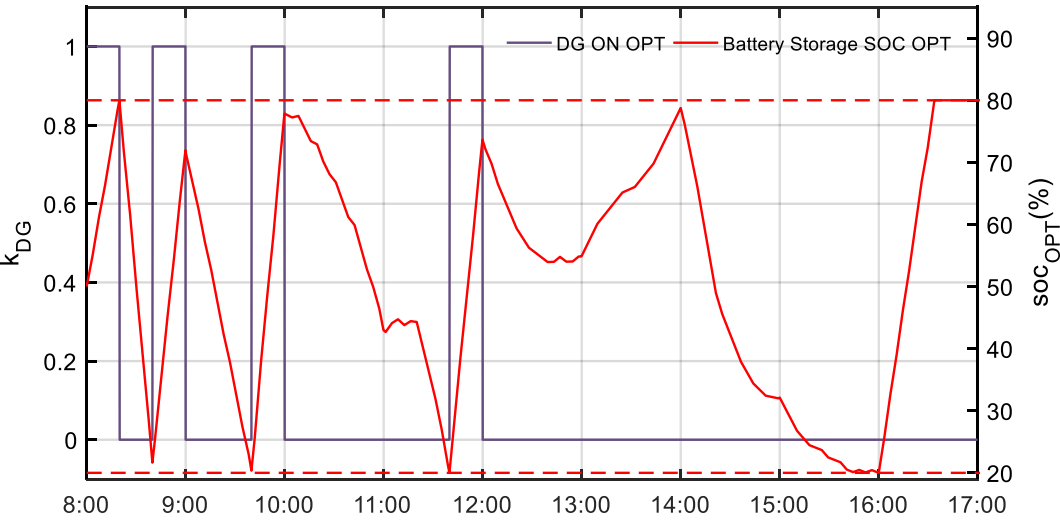


Figure 51. The day-ahead economics optimization results (k_{DG}) and BS SOC curves at off-grid mode on May 8th 2018.

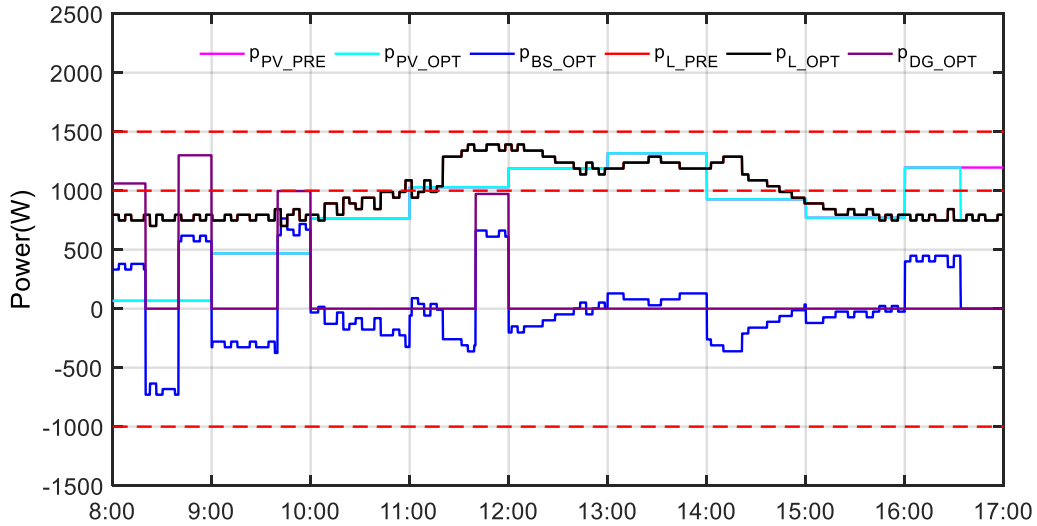


Figure 52. The day-ahead economics optimization results of power curves at off-grid mode on May 8th 2018.

The ideal economics optimization results on May 8th 2018 by using real PV and load power profiles under the appropriate constant DG power 700W are shown in Figure 53 and Figure 54.

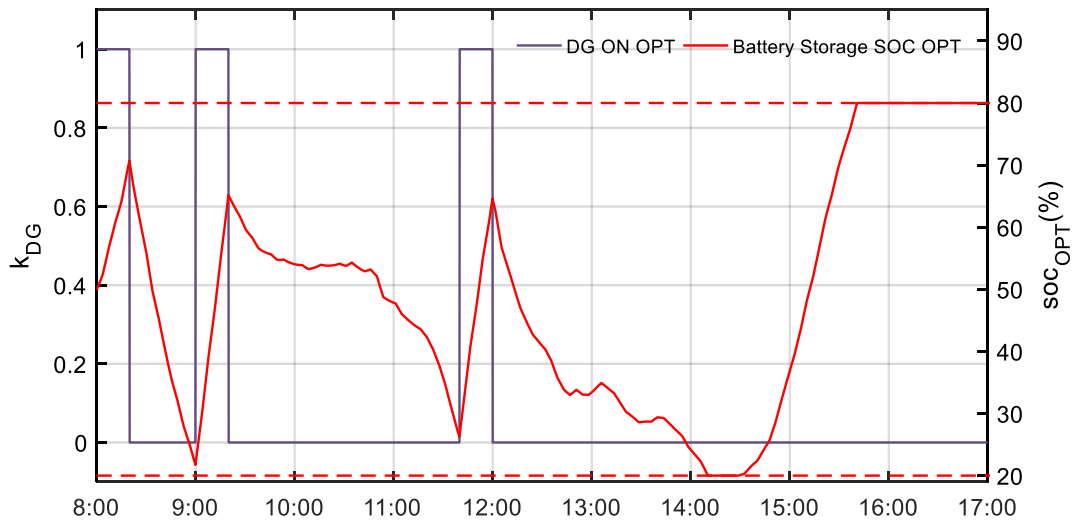


Figure 53. The ideal economics optimization results (k_{DG}) and BS SOC curves at off-grid mode on May 8th 2018.

In Figure 53 and Figure 54, the real PV and load power profiles are used, the ideal day-ahead optimization results are shown under the appropriate constant DG power; in the beginning of the optimization results, the PV power is less than the load demand power, the DG is turned on to supply the load demand power and the BS at the constant power in the duty cycle; at 8:20, the DG is turned off, the BS is discharging to support the load demand power; then the DG is turned on at 9:00; from 10:00 to 16:00, the PV power is close to the load demand, the DG is turned on at 11:40 to support the microgrid and the BS can be charging and discharging; at the end of the optimization, the PV power is more than

the load demand power, so the DG is always off, at the same time, the BS can be charging; when the soc_{BS} reaches soc_{BS_MAX} , the PV shedding happens to keep the power balance of the microgrid.

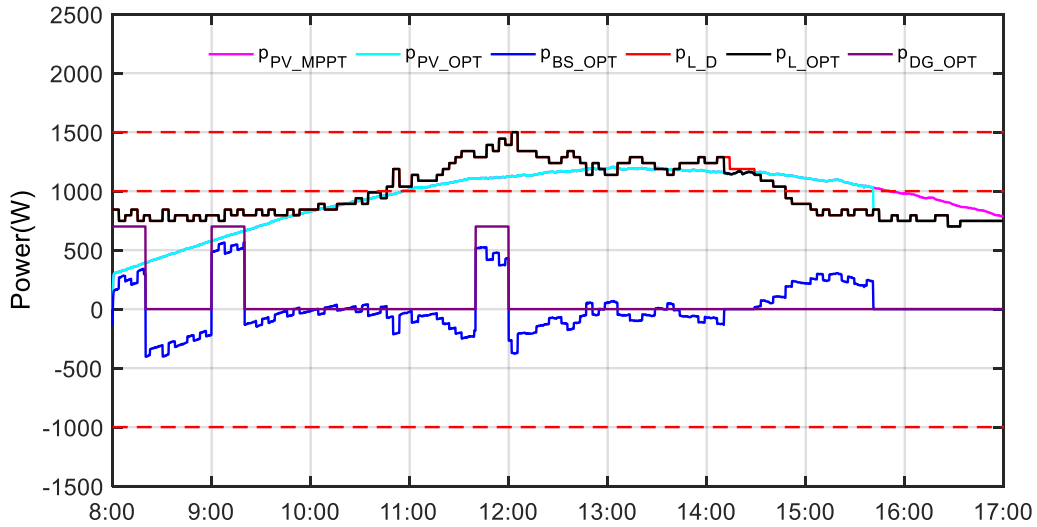


Figure 54. The ideal economics optimization results of power curves at off-grid mode on May 8th 2018.

The ideal economics optimization results on May 8th 2018 by using real PV and load power profiles under the appropriate DG power range from 650W to 750W are shown in Figure 55 and Figure 56.

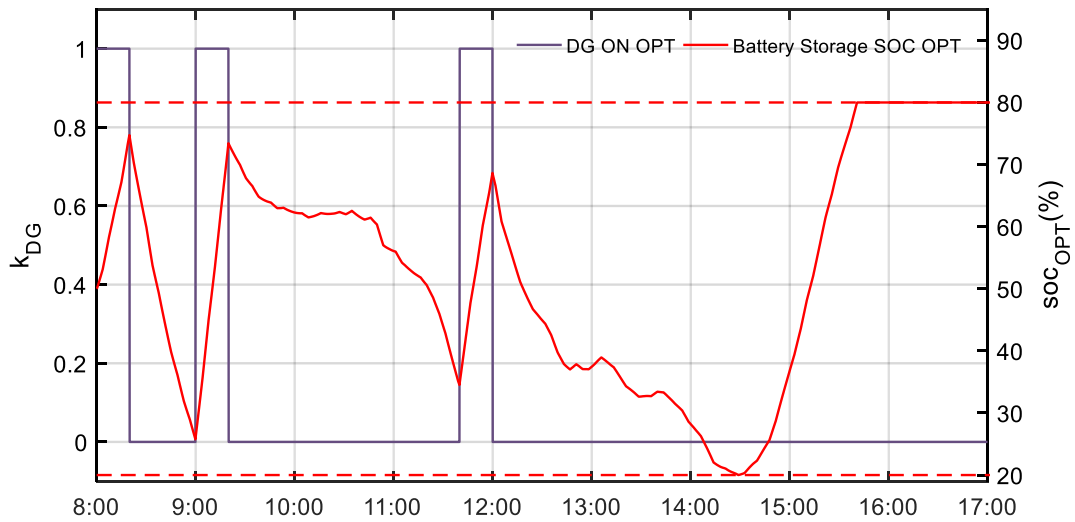


Figure 55. The ideal economics optimization results (k_{DG}) and BS SOC curves at off-grid mode on May 8th 2018.

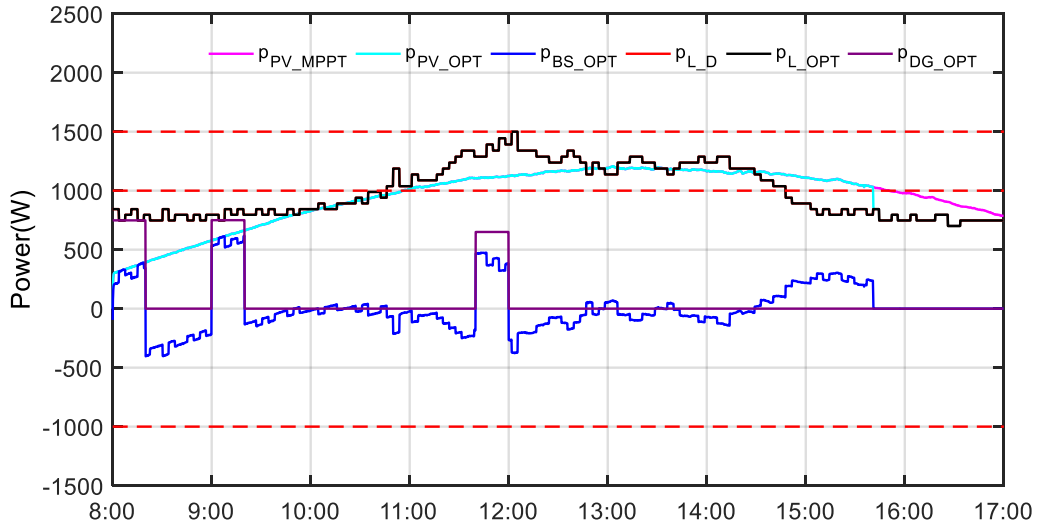


Figure 56. The ideal economics optimization results of power curves at off-grid mode on May 8th 2018.

In Figure 55 and Figure 56, the real PV and load power profiles are used, the ideal day-ahead optimization results are shown under the appropriate DG power range; at the beginning of the optimization results, the PV power is less than the load demand power, the DG is turned on to supply the load demand power and the BS in the duty cycle; at 8:20, the DG is turned off, the BS is discharging to support the load demand power; then the DG is turned on at 9:00; from 10:00 to 16:00, the PV power is close to the load demand, the DG is turned on at 11:40 to support the microgrid and the BS can be charging and discharging; at the end of the optimization, the PV power is more than the load demand power, so the DG is always off, at the same time, the BS can be charging; when the soc_{BS} reaches soc_{BS_MAX} , the PV shedding happens to keep the power balance of the microgrid.

III.1.3.2. Real-time simulation results

The following results consider the real-time simulation results of the operational layer. In order to validate the effectiveness of the day-ahead optimization, the real-time simulation result by using the day-ahead optimization will be compared with the real-time simulation result without considering the day-ahead optimization results.

III.1.3.2.1 Real-time result without optimization

Without considering the day-ahead optimization results, the cases under the power management strategy proposed in II.5.2.1. should be used, which are also the special cases in II.5.2.2. when k_{DG} equal to 0. The cases when k_{DG} equal to 1 have no meaning because the DG is always turned on in the duty cycle.

The results when k_{DG} equal to 0 are shown in Figure 57 and Figure 58.

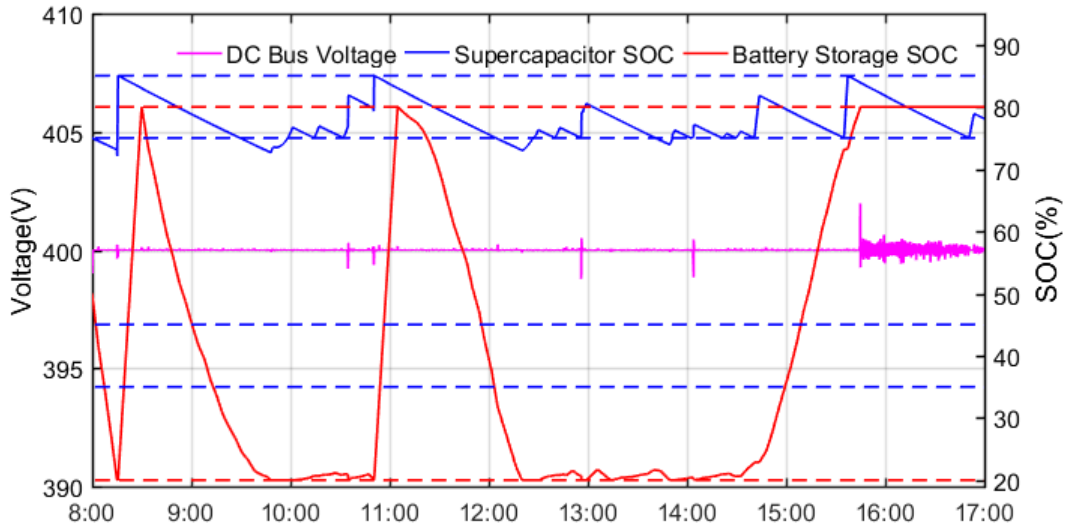


Figure 57. DC bus voltage and BS SOC curves when $k_{DG} = 0$ at off-grid mode on May 8th 2018.

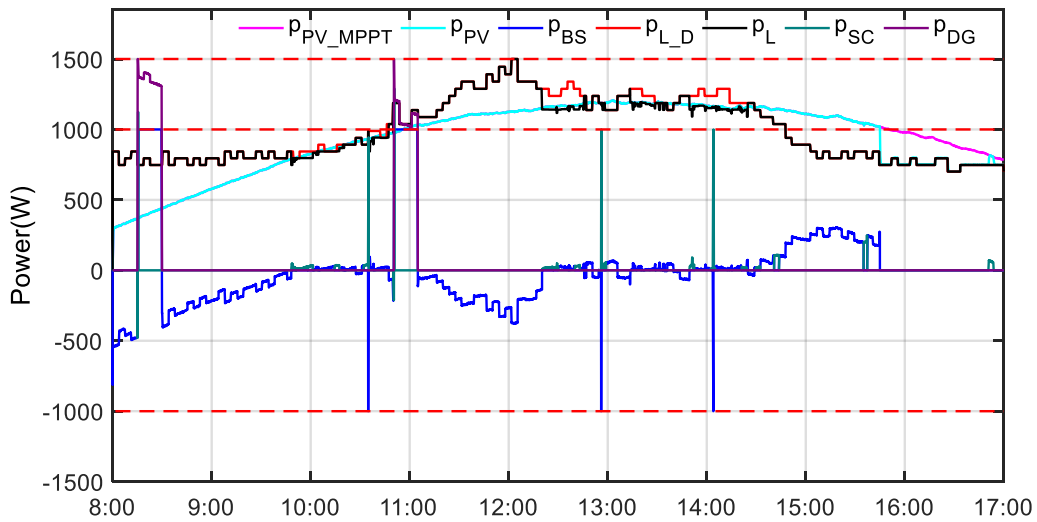


Figure 58. Power curves when $k_{DG} = 0$ in off-grid mode on May 8th 2018.

In Figure 57 and Figure 58, the DG and BS are the controllable sources to support the microgrid, the SC is only used to compensate the start-up of the DG, the BS has higher priority than the DG to compensate the power difference between p_{PV_MPPT} and p_{L_D} . In the beginning of the optimization results, the PV power is less than the load demand power, the BS has the higher priority to supply the load demand power; when the soc_{BS} reaches soc_{BS_MIN} , the non-critical load can shed, if the critical need to be shed, the DG is turned on to supply the load demand power and charge the SC and BS at 8:20; from 10:00 to 16:00, the PV power is close to the load demand, the DG supports the microgrid at 10:50 and the BS can be charging and discharging, the SC is recharging at 10:35, 12:55 and 14:05 to keep enough power to support the DG start-up; at the end of the optimization, the PV power is more

than the load demand power, so the BS is charging by the excess PV power; when the soc_{BS} reaches SOC_{BS_MAX} , the PV shedding can happen to keep the power balance of the microgrid.

III.1.3.2.2 Real-time results with day-ahead optimization

Considering the day-ahead optimization results, the cases under the power management strategy proposed in II.5.2.2. should be used. The optimization coefficient k_D can introduce the day-ahead optimization results in the economic dispatching layer. There are two real-time operational simulations by using the day-ahead economics optimization results under the appropriate constant DG power and the appropriate DG power range showing following; in the same time, there are two real-time operational simulations by using the ideal economics optimization results under the appropriate constant DG power and the appropriate DG power range showing following.

The real-time operational simulation results of the DC microgrid by using the day-ahead economics optimization results under the appropriate constant DG power are shown in Figure 59 and Figure 60.

In Figure 59 and Figure 60, the day-ahead economics optimization results under the appropriate constant DG power are introduced in the real-time operational layer, it can be seen that the DG is turned on five times. At the end of the real-time simulation, the DG is off, the BS is charging to reach SOC_{BS_MAX} , and PV shedding happens because of the high PV power.

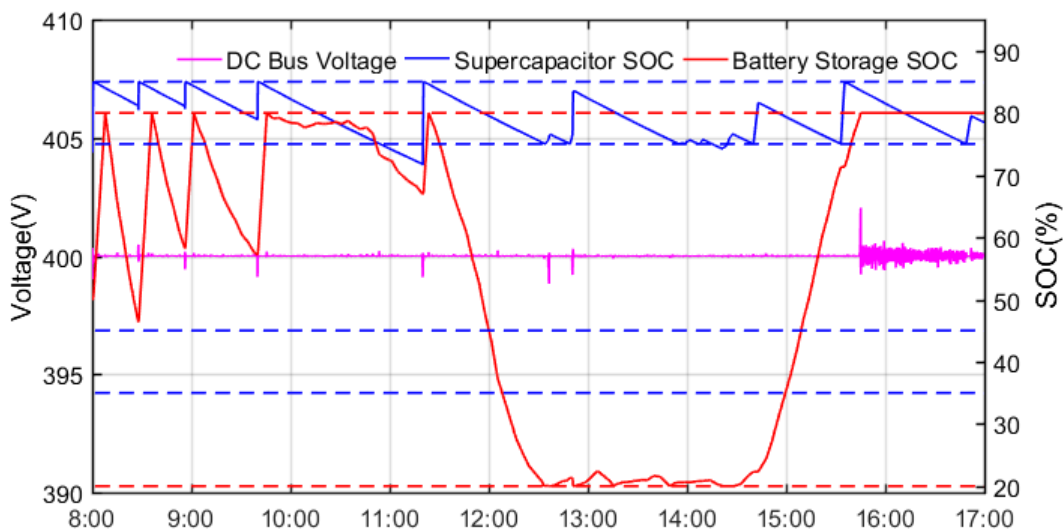


Figure 59. The actual results of DC bus voltage and BS SOC curves at off-grid mode on May 8th 2018.

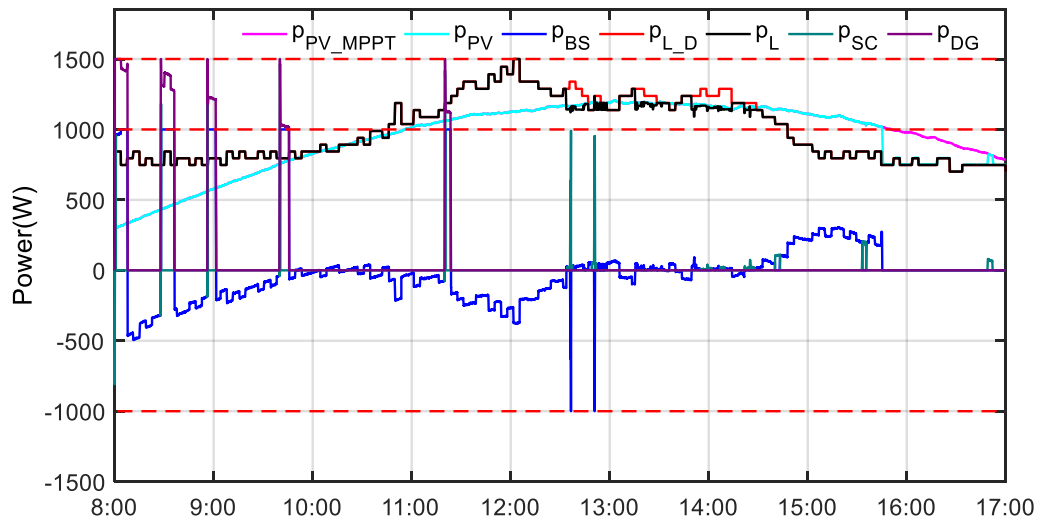


Figure 60. The actual results of power curves at off-grid mode on May 8th 2018.

The real-time operational simulation results of the DC microgrid by using the day-ahead economics optimization results under the appropriate DG power range are shown in Figure 61 and Figure 62. In Figure 61 and Figure 62, the day-ahead economics optimization results under the appropriate DG power range are introduced in the real-time operational layer, it can be seen that the DG is turned on four times. At the end of the real-time simulation, the DG is off, the BS is charging to reach SOC_{BS_MAX} , and PV shedding happens because of the high PV power.

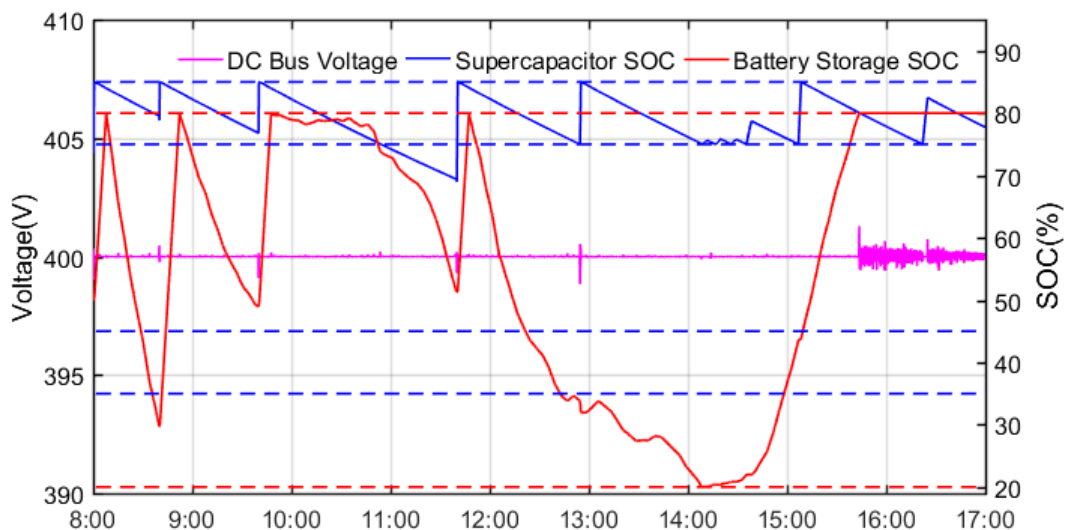


Figure 61. The actual results of DC bus voltage and BS SOC curves at off-grid mode on May 8th 2018.

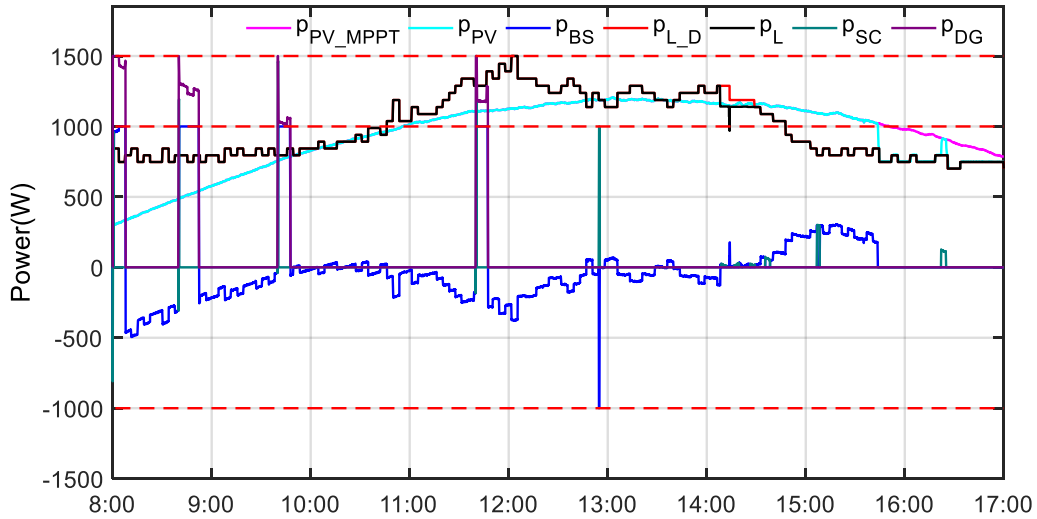


Figure 62. The actual results of power curves at off-grid mode on May 8th 2018.

To compare the two cases before, it can be seen that the results under the appropriate DG power range is better than the results under the appropriate constant DG power in the point of load demand.

The real-time operational simulation results of the DC microgrid by using the ideal economics optimization results under the appropriate constant DG power are shown in Figure 63 and Figure 64.

In Figure 63 and Figure 64, the ideal economics optimization results under the appropriate constant DG power are introduced in the real-time operational layer, it can be seen that the DG is turned on three times. At the end of the real-time simulation, the DG is off, the BS is charging to reach SOC_{BS_MAX} , and PV shedding happens because of the high PV power. In the simulation results, there almost no PV shedding.

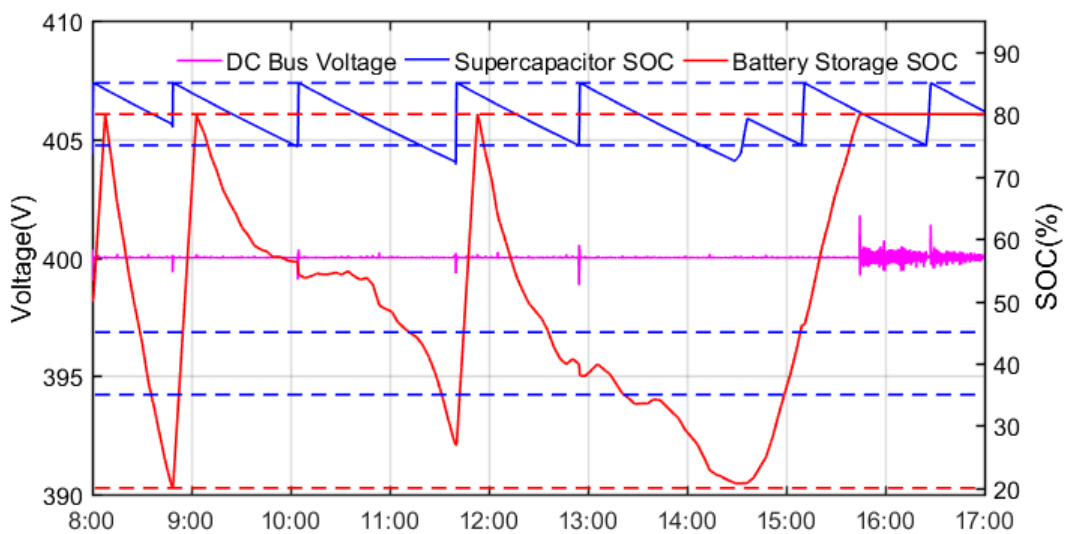


Figure 63. The ideal results of DC bus voltage and BS SOC curves at off-grid mode on May 8th 2018.

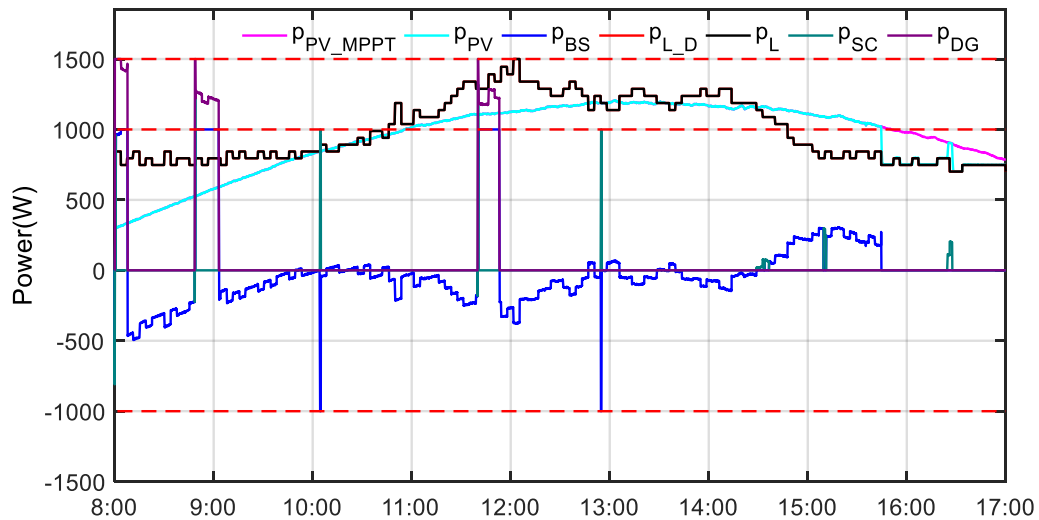


Figure 64. The ideal results of power curves at off-grid mode on May 8th 2018.

The real-time operational simulation results of the DC microgrid by using the ideal economics optimization results under the appropriate DG power range are shown in Figure 65 and Figure 66.

In Figure 65 and Figure 66, the ideal economics optimization results under the appropriate DG power range are introduced in the real-time operational layer, it can be seen that the DG is turned on three times. At the end of the real-time simulation, the DG is off, the BS is charging to reach SOC_{BS_MAX} , and PV shedding happens because of the high PV power. In the simulation results, there almost no PV shedding.

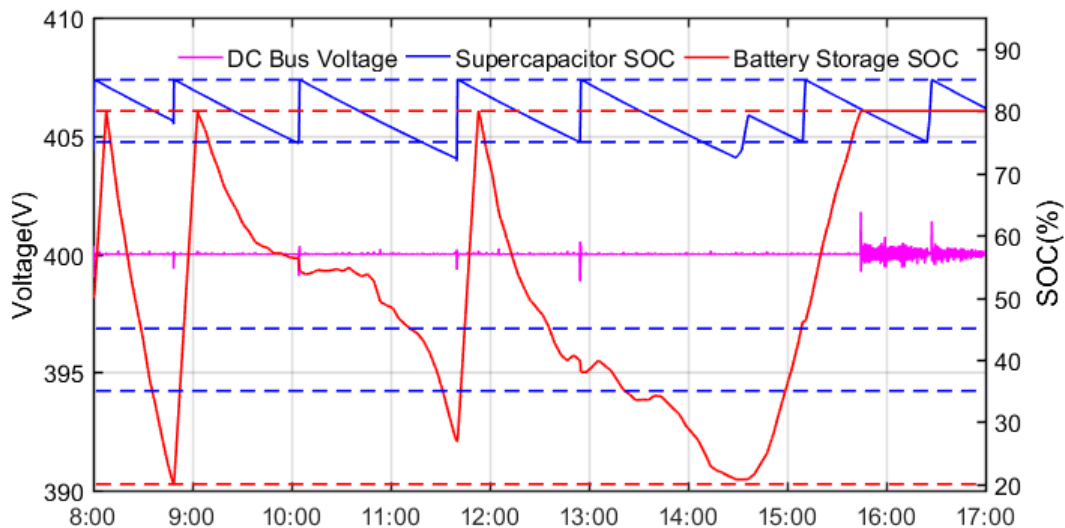


Figure 65. The ideal results of DC bus voltage and BS SOC curves at off-grid mode on May 8th 2018.

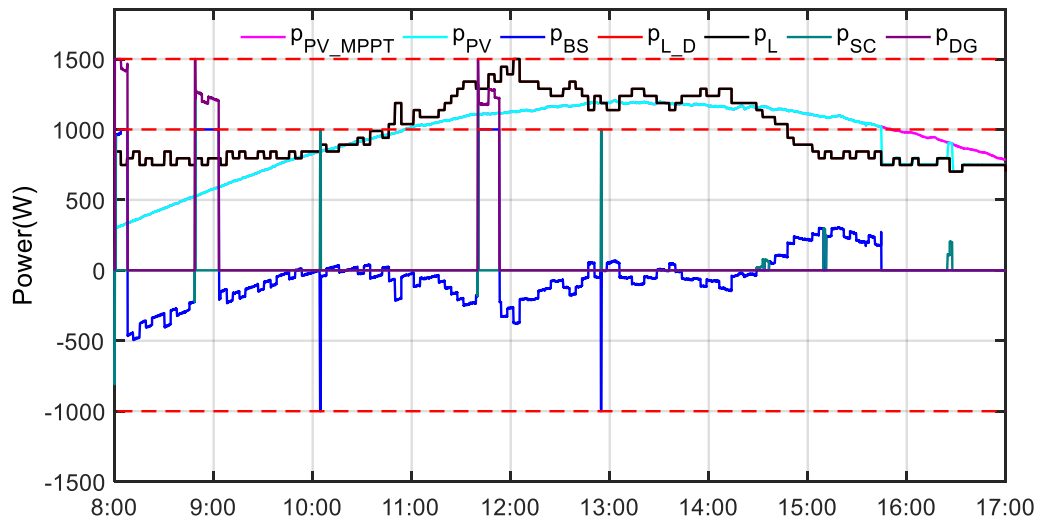


Figure 66. The ideal results of power curves at off-grid mode on May 8th 2018.

To compare the two real-time operational results above, the power by using the ideal economics optimization results can be more appropriately managed than the power by using the real economics optimization results because there is no power prediction difference between the ideal economics optimization results and real-time operational results and the real power profiles are used to replace the prediction power profiles in the ideal economics optimization.

III.1.3.3. Off-grid simulation results comparison and analysis

Now, it is necessary to give a table that lists the cost of every component from the above simulation results including the optimization results in III.1.3.1. and the real-time operational results in III.1.3.2. The simulation results for off-grid mode on May 8th 2018 is shown in Table 11.

Table 11. Results summary for off-grid mode on May 8th 2018.

Day-ahead optimization	NO	YES			
		Constant DG		Variable DG	
Condition	$k_{DG}=0$	MILP results	Operational results	Ideal MILP results	Ideal Operational results
C_G (c€)	6.87	2.94	6.92	2.94	7.54
C_{PV_S} (c€)	28.53	28.08	28.31	28.08	28.78
C_{L_D} (c€)	28.09	19.68	19.16	0	4.84
C_{DG} (c€)	102.48	264.55	109.66	256.68	124.27
C_{SC} (c€)	1.71	--	1.81	--	1.78
C_{TOTAL} (c€)	167.69	315.27	165.87	287.71	167.23

Table 11 bis. Results summary for off-grid mode on May 8th 2018.

Day-ahead optimization	YES			
	Constant DG		Variable DG	
Condition	Ideal MILP results	Ideal Operational results	Ideal MILP results	Ideal Operational results
C_G (c€)	2.00	7.63	2.00	7.63
C_{PV_S} (c€)	31.43	28.07	31.43	28.07
C_{L_D} (c€)	2.87	0.01	0	0.01
C_{DG} (c€)	146.59	127.58	148.50	127.58
C_{SC} (c€)	--	1.84	--	1.84
C_{TOTAL} (c€)	182.90	165.15	181.94	165.15

In Table 11, there are nine conditions listing. The condition when k_{DG} equals to 0 is the real-time simulation result in the operational layer. The conditions of ideal MILP results and ideal operational results are respectively the ideal optimization results in the economics dispatching layer and the real-time simulation results in the operational layer by using real recorded PV and load power profiles to ignore the power prediction accuracy. The conditions of MILP results and operational results are respectively the day-ahead optimization results in the economics dispatching and real-time simulation

results in the operational layer by using the real PV and load prediction power profiles. The appropriate constant DG power and DG power range are considered in the simulation.

By the comparisons in Table 11, it can be seen that the total cost under the condition when k_{DG} equals to 0, and operational results is higher than the total cost under the condition of ideal operational results because the accuracy of PV and load power prediction has a big influence on power dispatching. The total cost under the condition of operational results is less than the total cost under the condition when k_{DG} equals to 0, which can give a positive proof that the optimization in the economics dispatching layer can make a good function to reduce the total cost in the real-time operational simulation in the operational layer. The total cost with variable DG power is less than the results with constant DG power under the condition of MILP results due to the loose constraints for DG power. What's more, the total cost under the condition of operational results by using appropriate DG power range is greater than the total cost under the condition of operational results by using appropriate constant DG power, because there is more power from the DG to support the microgrid and the load shedding power is reduced under the condition of operational results by using appropriate DG power range.

In order to give better evidence to prove the effectiveness of the optimization and real-time power management strategy, other two weather data are applied in the off-grid DC microgrid.

The simulation results for off-grid mode on June 20th 2018 are shown in Table 12.

Table 12. Results summary for off-grid mode on June 20th 2018.

Day-ahead optimization	NO	YES			
		Constant DG		Variable DG	
Condition	$k_{DG}=0$	MILP results	Operational results	MILP results	Operational results
C_G (c€)	13.54	2.45	14.15	2.45	14.15
C_{PV_S} (c€)	96.54	227.79	86.31	227.63	86.31
C_{L_D} (c€)	0.77	0	6.75	0	6.75
C_{DG} (c€)	243.50	28.75	238.48	28.62	238.48
C_{SC} (c€)	1.99	--	2.06	--	2.06
C_{TOTAL} (c€)	356.36	259.00	347.77	258.71	347.77

Table 12 bis. Results summary for off-grid mode on June 20th 2018.

Day-ahead optimization	YES			
	Constant DG		Variable DG	
Condition	Ideal MILP results	Ideal Operational results	Ideal MILP results	Ideal Operational results
C_G (c€)	7.03	13.14	7.61	13.80
C_{PV_S} (c€)	100.69	111.41	70.99	117.34
C_{L_D} (c€)	0	6.65	0.17	6.23
C_{DG} (c€)	293.59	258.95	248.71	265.41
C_{SC} (c€)	--	2.21	--	2.19
C_{TOTAL} (c€)	401.31	392.37	327.49	404.99

By the comparisons in Table 12, the total cost under the condition when k_{DG} equals to 0, and operational results is less than the total cost under the condition of ideal operational results which is different from the results on May 8th 2018 because the variation of the ideal PV power is so violent compared to the variation of the PV power prediction that the DG is turned on too often. The total cost under the condition of operational results is less than the total cost under the condition when k_{DG} equals to 0, which can give a positive proof that the optimization in the economics dispatching layer can make a good function to reduce the total cost in the real-time operational simulation in the operational layer. The total cost with variable DG power is less than the results with constant DG power under the condition of MILP results due to the loose constraints for DG power. What's more, the total cost under the condition of ideal operational results is greater than the total cost under the condition of operational results, because the DG supports more power to the microgrid and the load shedding power is reduced under the condition of ideal operational results.

The simulation results for off-grid mode on July 16th 2018 is shown in Table 13.

Table 13. Results summary for off-grid mode on July 16th 2018.

Day-ahead optimization	NO	YES			
		Constant DG		Variable DG	
Condition	$k_{DG}=0$	MILP results	Operational results	MILP results	Operational results
C_G (c€)	23.08	0.10	24.38	0.98	24.40
C_{PV_S} (c€)	22.00	18.48	26.95	0	21.54
C_{L_D} (c€)	59.65	26.40	27.07	0	25.76
C_{DG} (c€)	611.00	969.00	640.22	931.46	661.10
C_{SC} (c€)	2.19	--	2.31	--	2.61
C_{TOTAL} (c€)	717.94	1013.99	720.95	932.45	735.42

Table 13 bis. Results summary for off-grid mode on July 16th 2018.

Day-ahead optimization	YES			
	Constant DG		Variable DG	
Condition	Ideal MILP results	Ideal Operational results	Ideal MILP results	Ideal Operational results
C_G (c€)	3.89	24.32	4.05	24.32
C_{PV_S} (c€)	11.09	0	0	0
C_{L_D} (c€)	0	33.25	0	33.25
C_{DG} (c€)	740.52	612.80	730.72	612.80
C_{SC} (c€)	--	2.56	--	2.56
C_{TOTAL} (c€)	755.52	672.96	734.78	672.96

By the comparisons in Table 13, it can be seen that the total cost under the condition when k_{DG} equals to 0, and operational results is higher than the total cost under the condition of ideal operational results because the accuracy of PV and load power prediction has a big influence on power dispatching. The total cost under the condition of operational results is less than the total cost under the condition when k_{DG} equals to 0, which can give a positive proof that the optimization in the economics dispatching layer can make a good function to reduce the total cost in the real-time operational simulation in the operational layer. The total cost with variable DG power is less than the results with constant DG power under the condition of MILP results due to the loose constraints for DG power. What's more, the total cost under the condition of operational results by using appropriate DG power range is greater than the

total cost under the condition of operational results by using appropriate constant DG power, because there is more power from the DG to support the microgrid and the load shedding power is reduced under the condition of operational results by using appropriate DG power range.

In conclusion, the real-time power management in the operational layer without the economics optimization in the economics dispatching layer cannot achieve the purpose of the optimal real-time power management. The accuracy of PV and load power predictions has a big influence on the economics optimization. In particular, the uncertainty of weather will lead to uncertainty in the results of economic optimization. Especially, the total cost becomes more sensitive to the weather condition in the off-grid mode because the high tariff of DG leads to a high total cost. The economics optimization in the economics dispatching layer can reduce the total cost of the power flow of DC microgrid and reduce the load shedding power in off-grid mode.

III.1.4. Full microgrid simulation for 9 hours' duration

To solve the full microgrid optimization problem of the economic dispatching, the MILP solver is applied. The weather data set from three different days, May 8th 2018, June 20th 2018, and July 16th 2018 under different weather conditions have been introduced in III.1.1. The load power and load prediction power has been provided in III.1.1. The tariff of every electrical component in the full microgrid mode has been given in III.1.1.

The full DC microgrid parameters used for the optimization dispatch layer are presented in Table 14.

Table 14. Parameters for optimization at full microgrid mode.

Parameters	Values	Parameters	Values
P_{BS_MAX}	1000W	P_{DG_MAX}	1500W
SOC_{BS_MIN}	20%	$P_{DG_ON_MAX}$	$(0, P_{DG_MAX}]$
SOC_{BS_MAX}	80%	$P_{DG_ON_MIN}$	$(0, P_{DG_ON_MAX}]$
SOC_{BS_0}	50%	dt_{DG}	1200s
C_{REF}	6.6Ah	k_{L_CRIT}	80%
P_{PV_STC}	1750W	P_{GF_Limit}	20W / s
P_{G_MAX}	200W		

In Table 14, the parameters are the same as the parameters in the economics dispatching layer of the grid-connected and off-grid mode above. The DG power limited between $P_{DG_ON_MIN}$ and $P_{DG_ON_MAX}$ when the DG is turned on is the same as the constraints in the economics dispatching layer of the off-

grid mode. The $P_{DG_ON_MAX}$ is chosen between 0 and P_{DG_MAX} , the $P_{DG_ON_MIN}$ is chosen between 0 and $P_{DG_ON_MAX}$. The k_{L_CRIT} is set as 80% to provide the condition for turning on the DG.

The calculation of the parameters $P_{DG_ON_MIN}$ and $P_{DG_ON_MAX}$ are the same as the parameters in the economics dispatching layer of the off-grid mode. Thus, the appropriate $P_{DG_ON_MIN}$ and $P_{DG_ON_MAX}$ power can be got as the same method depicted in the economics dispatching layer of the off-grid mode

The full DC microgrid parameters used for the operational algorithm of the operational layer is presented in Table 15.

Table 15. Parameters for the operational algorithm at full microgrid mode.

Parameters	Values	Parameters	Values
P_{BS_MAX}	1000W	V_{SC_Rated}	75V
SOC_{BS_MIN}	20%	$SOC_{SC_MAX_MAX}$	85%
SOC_{BS_MAX}	80%	$SOC_{SC_MAX_MIN}$	75%
SOC_{BS_0}	50%	$SOC_{SC_MIN_MAX}$	45%
C_{REF}	6.6Ah	$SOC_{SC_MIN_MIN}$	35%
P_{PV_STC}	1750W	SOC_{SC_0}	75%
V_{DC}^*	400V	P_{DG_MAX}	1500W
P_{SC_MAX}	1500W	$T_{DG_ON_MAX}$	3600s
T_{SC_MIN}	180s	$T_{DG_OFF_LIM}$	1200s
C_{SC}	94F	k_{L_CRIT}	80%
P_{G_MAX}	200W		

In Table 15, the parameters are the same as the parameters in the operational layer of the grid-connected and off-grid mode above.

III.1.4.1. Optimization results

The day-ahead economics optimization results on May 8th 2018 by using PV and load prediction power profiles under the appropriate constant DG power 1050W are shown in Figure 67 and Figure 68.

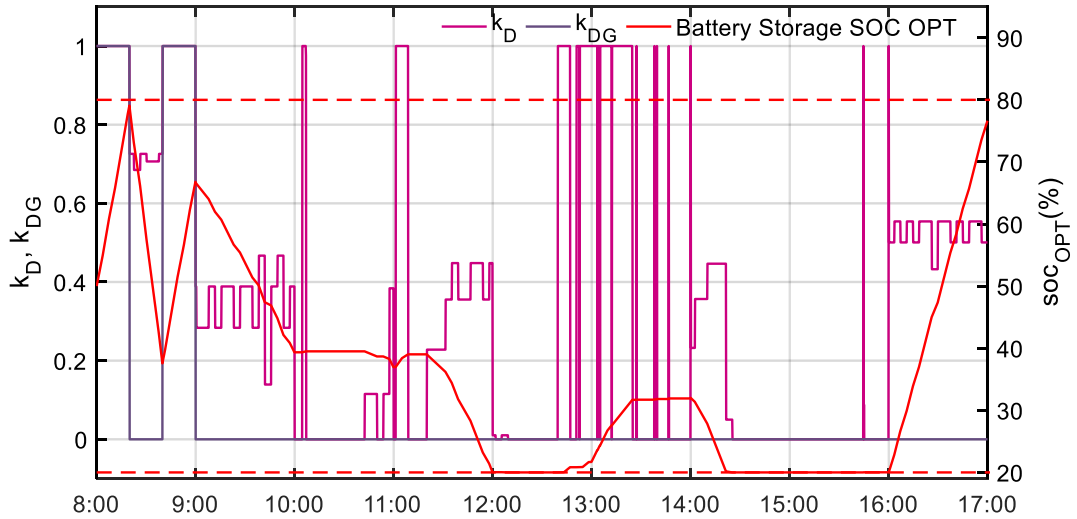


Figure 67. The day-ahead economics optimization results (k_D , k_{DG}) and BS SOC curves at full microgrid mode on May 8th 2018.

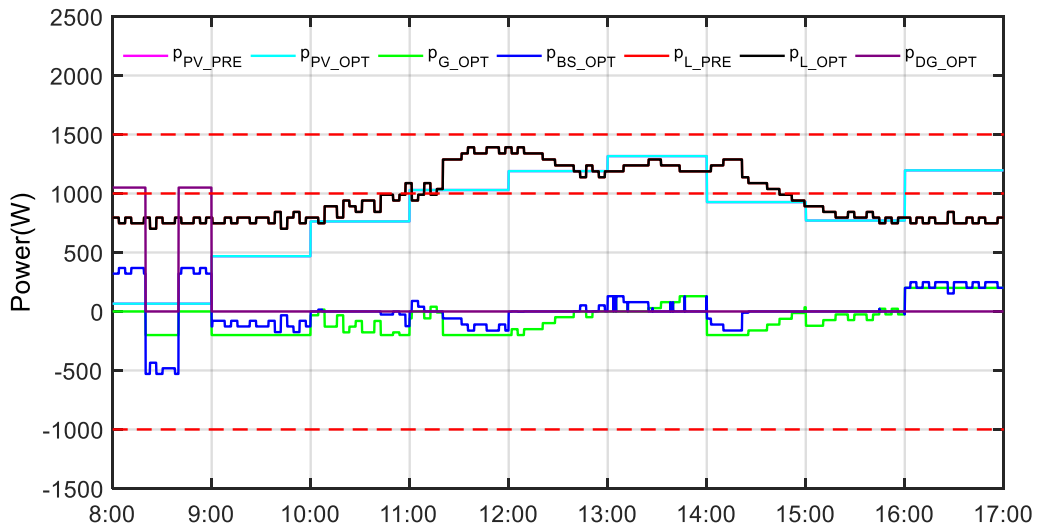


Figure 68. The day-ahead economics optimization results of power curves at full microgrid mode on May 8th 2018.

In Figure 67 and Figure 68, the PV and load prediction power profiles are used, the day-ahead optimization results are shown under the appropriate constant DG power; at the beginning of the optimization results, the PV power is less than the load demand power, the DG is turned on to supply the load demand power, and the BS is charging by the rest of the DG power due to the DG operating at the constant power in the duty cycle; at 8:20, the DG is turned off, the BS and the public grid provide power to support the load demand power; then the DG is turned on at 8:40; from 10:00 to 16:00, the PV power is close to the load demand, the BS can be charging and discharging and the public grid can sell and buy power from the microgrid; at the end of the optimization, the PV power is more than the load

demand power, and the public grid can buy power from the microgrid, the microgrid can keep the power balance.

The day-ahead economics optimization results on May 8th 2018 by using PV and load prediction power profiles under the appropriate DG power range from 1000W to 1100W are shown in Figure 69 and Figure 70.

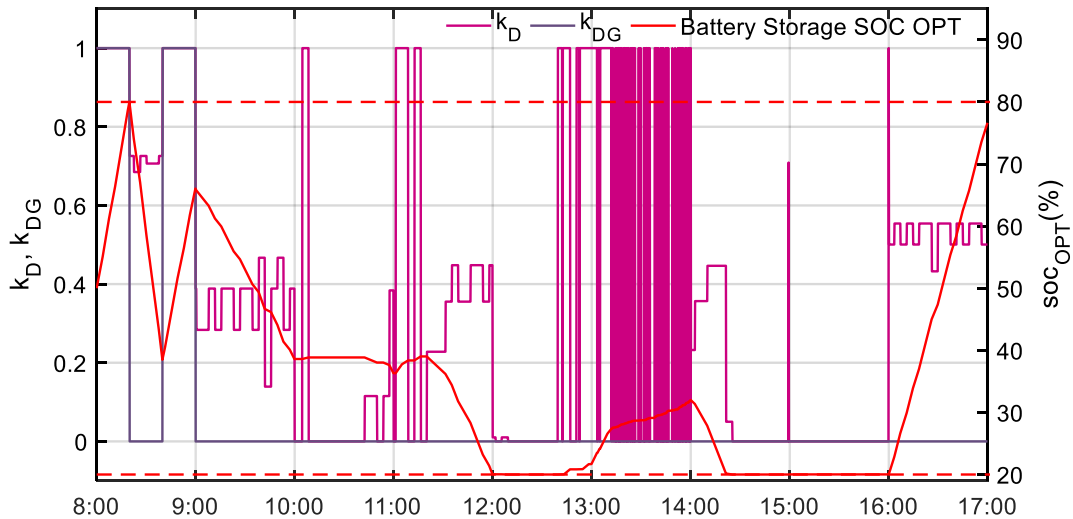


Figure 69. The day-ahead economics optimization results (k_D , k_{DG}) and BS SOC curves at full microgrid mode on May 8th 2018.

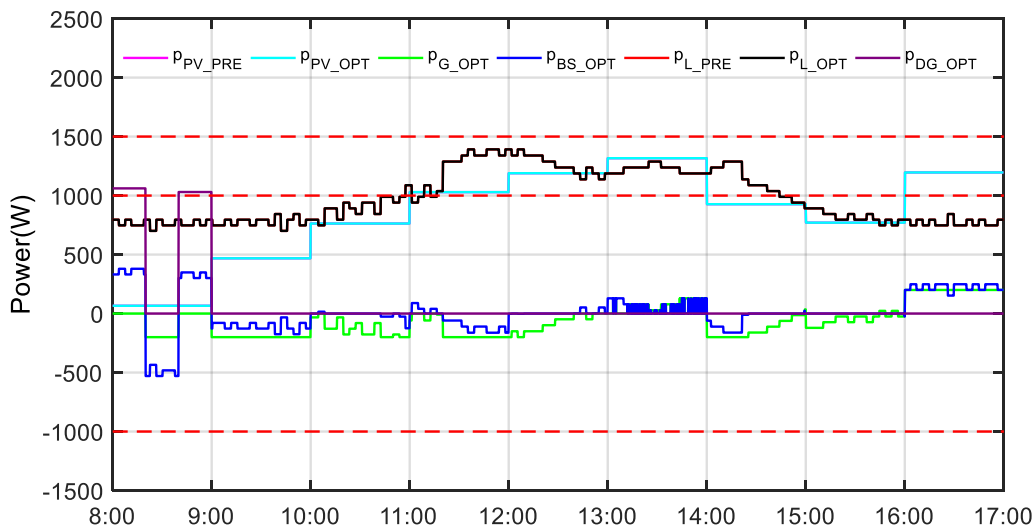


Figure 70. The day-ahead economics optimization results of power curves at full microgrid mode on May 8th 2018.

In Figure 69 and Figure 70, the PV and load prediction power profiles are used, the day-ahead optimization results are shown under the appropriate DG power range, which is almost the same as the

results in Figure 67 and Figure 68. The power values of the DG are not the same, and the variation of the k_{DG} in the period from 13:00 to 14:00 is not the same.

The ideal economics optimization results on May 8th 2018 by using real PV and load power profiles under the appropriate constant DG power 350W are shown in Figure 71 and Figure 72.

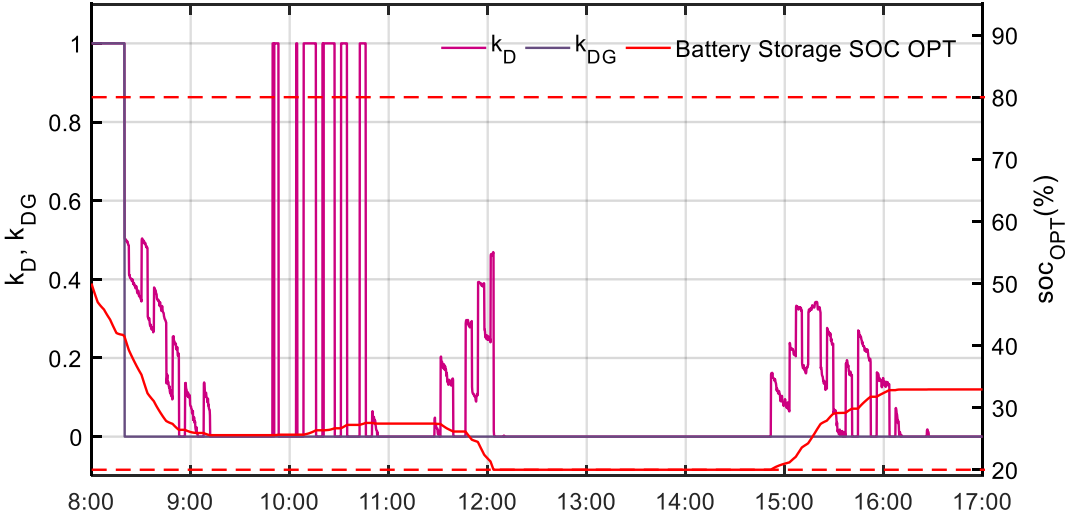


Figure 71. The ideal economics optimization results (k_D , k_{DG}) and BS SOC curves at full microgrid mode on May 8th 2018.

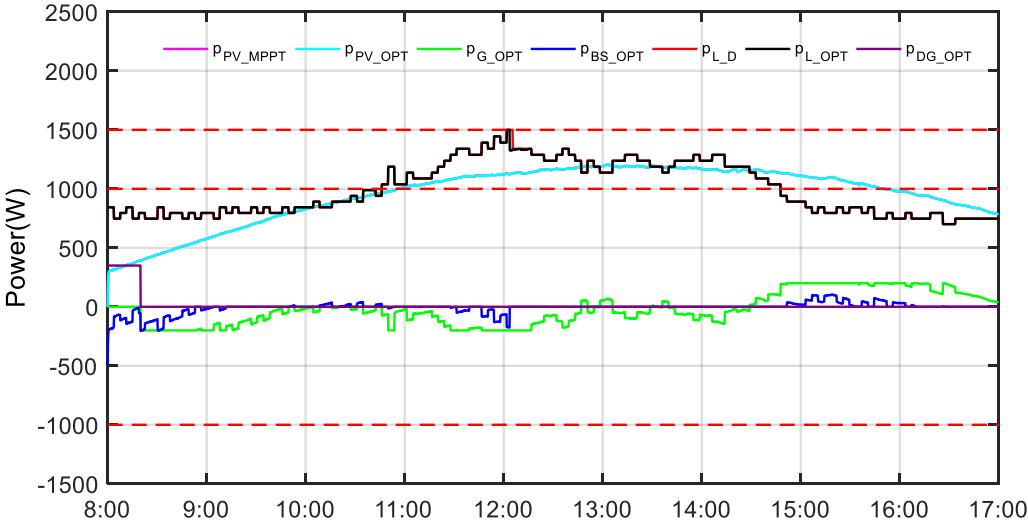


Figure 72. The ideal economics optimization results of power curves at full microgrid mode on May 8th 2018.

In Figure 71 and Figure 72, the real PV and load power profiles are used, the ideal day-ahead optimization results are shown under the appropriate constant DG power; at the beginning of the optimization results, the PV power is less than the load demand power, the DG is turned on to supply the load demand power and the BS at the constant power in the duty cycle; at 8:20, the DG is turned off,

then the BS is discharging and the public grid is selling power to support the load demand power; from 10:00 to 16:00, the PV power is close to the load demand, the BS can be charging and discharging, and the public grid can sell and buy power from the microgrid, and there is a little load power shedding; at the end of the optimization, the PV power is more than the load demand power, so the DG is always off, at the same time, the BS can be charging, the microgrid can sell power to the public grid.

The ideal economics optimization results on May 8th 2018 by using real PV and load power profiles under the appropriate DG power range from 300W to 400W are shown in Figure 73 and Figure 74.

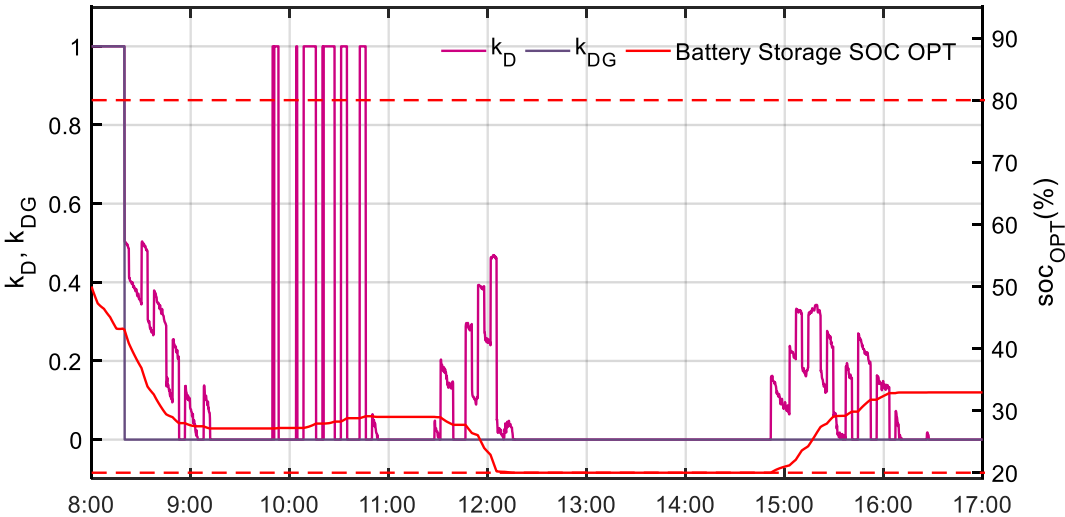


Figure 73. The ideal economics optimization results (k_D , k_{DG}) and BS SOC curves at full microgrid mode on May 8th 2018.

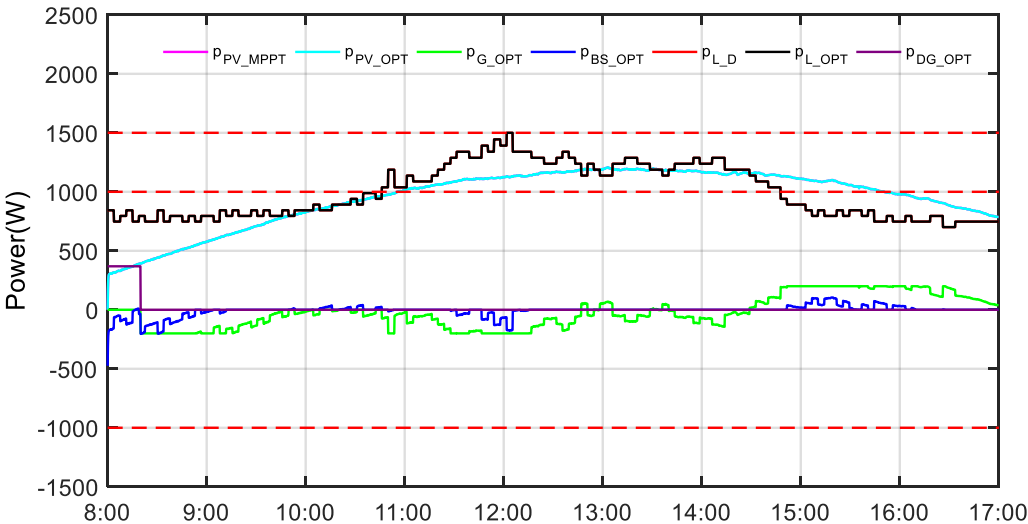


Figure 74. The ideal economics optimization results of power curves at full microgrid mode on May 8th 2018.

In Figure 73 and Figure 74, the real PV and load power profiles are used, the ideal day-ahead optimization results are shown under the appropriate DG power range, which is almost the same as the results in Figure 71 and Figure 72. The difference is the PV shedding at noon which does not happen in Figure 73 and Figure 74.

III.1.4.2. Real-time simulation results

The following simulation would consider the real-time simulation results of the operational layer. In order to validate the effectiveness of the day-ahead optimization, the real-time simulation result by using the day-ahead optimization will be compared with the real-time simulation result without considering the day-ahead optimization results.

III.1.4.2.1 Real-time result without optimization

Without considering the day-ahead optimization results, the cases under the power management strategy proposed in II.5.3.1. should be used, which are also special cases in II.5.3.2. when k_D equal to 1 and k_{DG} equal to 0. Thus, in order to give a better comparison, the cases when k_D equal to 0.5, or 0 and k_{DG} equal to 0 are also simulated. The results when k_D equal to 1 and k_{DG} equal to 0 are shown in Figure 75 and Figure 76. In Figure 75 and Figure 76, the public grid, the BS, and the DG are the controllable sources to support the microgrid, the SC is only used to compensate the start-up of the DG, the public grid and the BS have higher priority than the DG to compensate the power difference between P_{PV_MPPT} and P_{L_D} . The DG is turned on at 8:15. The SC is recharging at 9:45, 10:10, 10:20, 10:30, 12:50, 13:30, 14:50, and 16:05. The load shedding happens at 10:50 and 11:20. The PV shedding happens at 15:50.

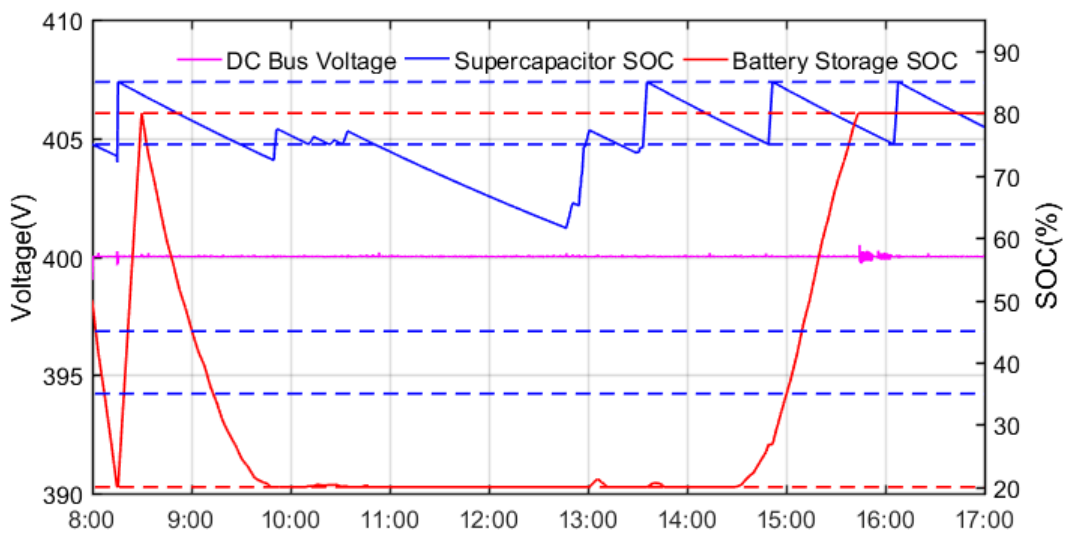


Figure 75. DC bus voltage and BS SOC curves when $k_D = 1$ and $k_{DG} = 0$ at full microgrid mode on May 8th 2018.

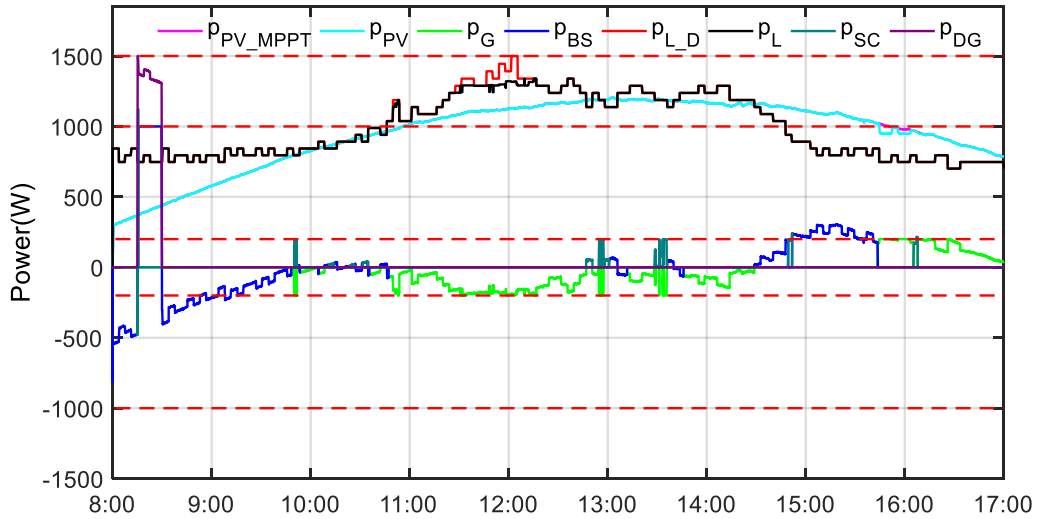


Figure 76. Power curves when $k_D = 1$ and $k_{DG} = 0$ at full microgrid mode on May 8th 2018.

The results when k_D equal to 0.5 and k_{DG} equal to 0 are shown in Figure 77 and Figure 78. In Figure 77 and Figure 78, the public grid, the BS, and the DG are the controllable sources to support the microgrid, the SC is only used to compensate the start-up of the DG, the public grid and the BS have higher priority than the DG to compensate the power difference between p_{PV_MPPT} and p_{L_D} . The DG is turned on at 8:32. The SC is recharging at 9:55, 12:45, 12:55, 13:05, 14:30, 15:05, and 16:20. There is no load shedding and PV shedding.

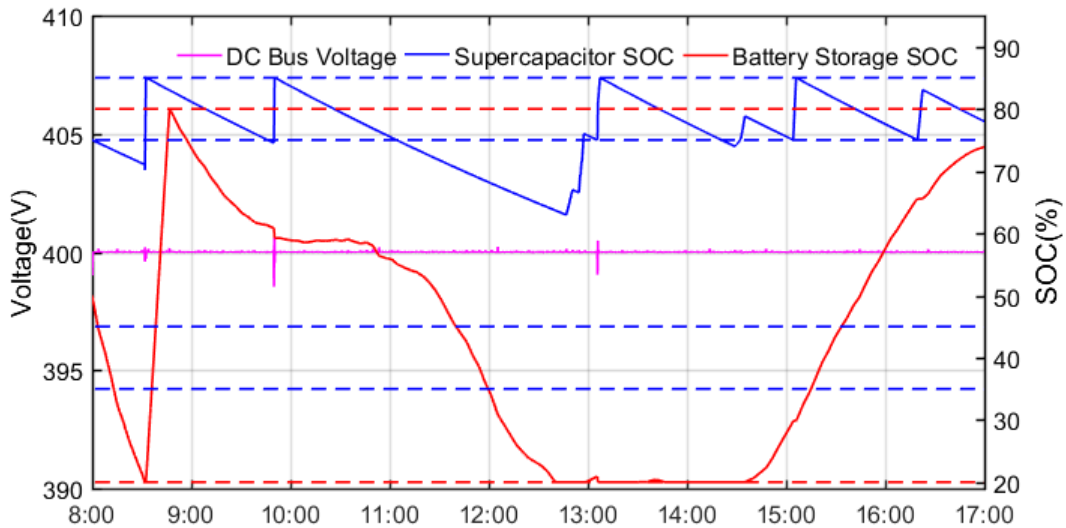


Figure 77. DC bus voltage and BS SOC curves when $k_D = 0.5$ and $k_{DG} = 0$ at full microgrid mode on May 8th 2018.

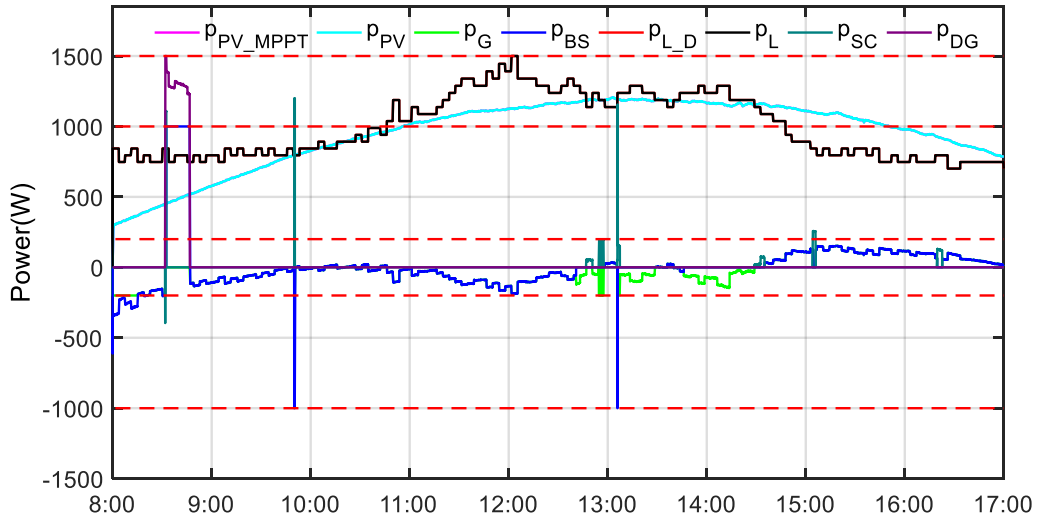


Figure 78. Power curves when $k_D = 0.5$ and $k_{DG} = 0$ at full microgrid mode on May 8th 2018.

The results when k_D equal to 0 and k_{DG} equal to 0 are shown in Figure 79 and Figure 80. In Figure 79 and Figure 80, the DG is turned on at 8:32; the SC is recharging at 9:55, 12:45, 12:55, 14:30, 15:05, and 16:20, there is no load shedding and PV shedding.

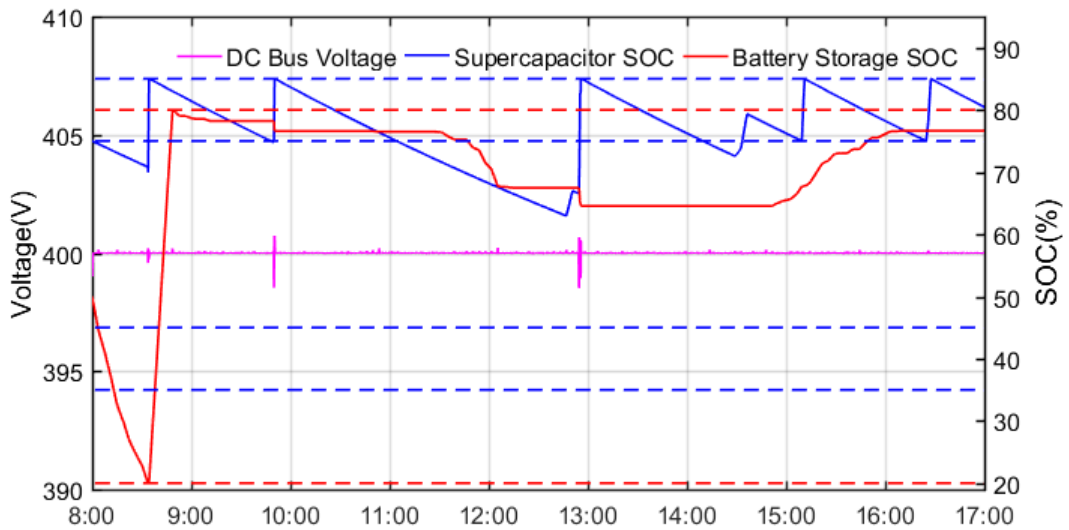


Figure 79. DC bus voltage and BS SOC curves when $k_D = 0$ and $k_{DG} = 0$ at full microgrid mode on May 8th 2018.

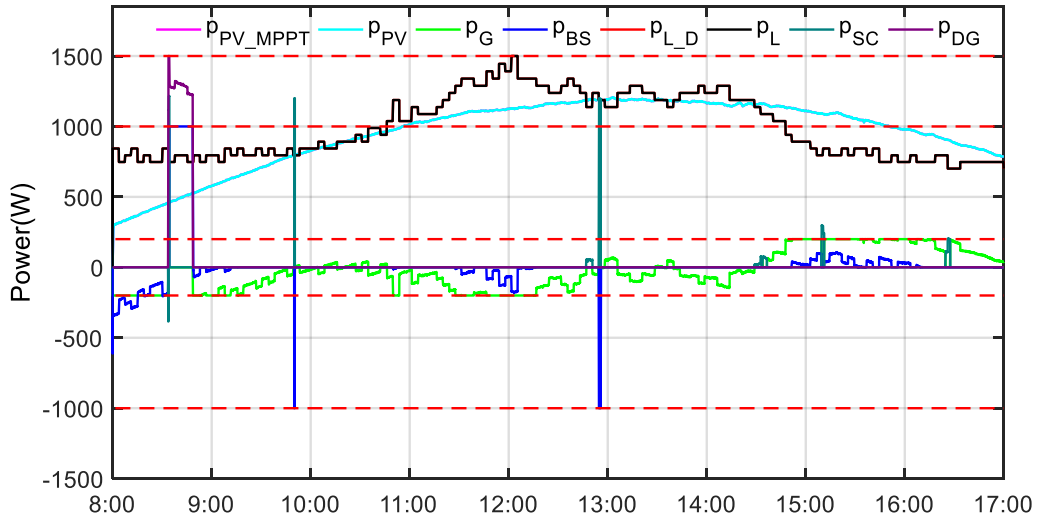


Figure 80. Power curves when $k_D = 0$ and $k_{DG} = 0$ at full microgrid mode on May 8th 2018.

III.1.4.2.2 Real-time results with day-ahead optimization

Considering the day-ahead optimization results, the cases under the power management strategy proposed in II.5.3.2. should be used. The optimization coefficient k_D and k_{DG} can introduce the day-ahead optimization results in the economic dispatching layer. There are two real-time operational simulations by using the day-ahead economics optimization results under the appropriate constant DG power and the appropriate DG power range showing following; in the same time, there are two real-time operational simulations by using the ideal economics optimization results under the appropriate constant DG power and the appropriate DG power range showing following.

The real-time operational simulation results of the DC microgrid by using the day-ahead economics optimization results under the appropriate constant DG power are shown in Figure 81 and Figure 82.

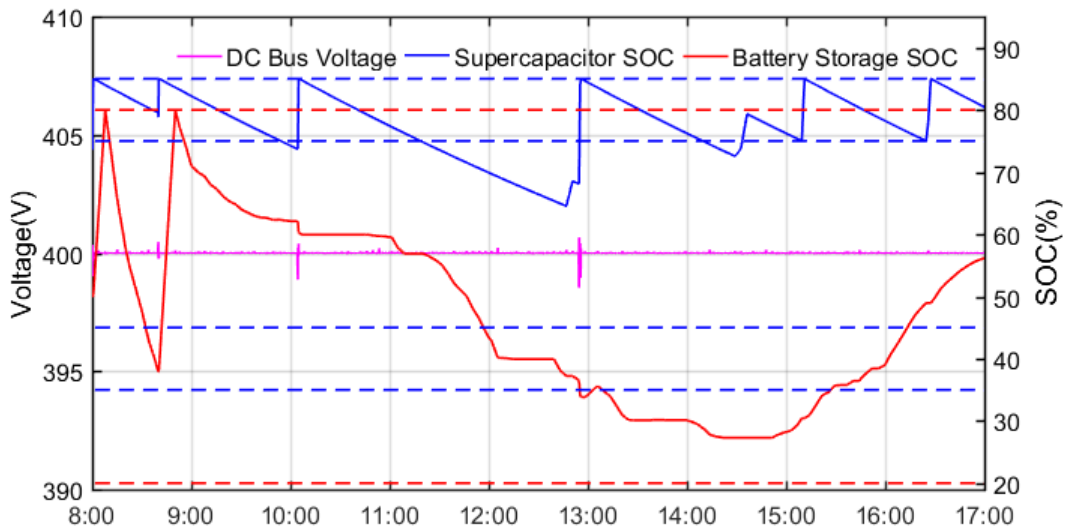


Figure 81. The actual results of DC bus voltage and BS SOC curves at full microgrid mode on May 8th

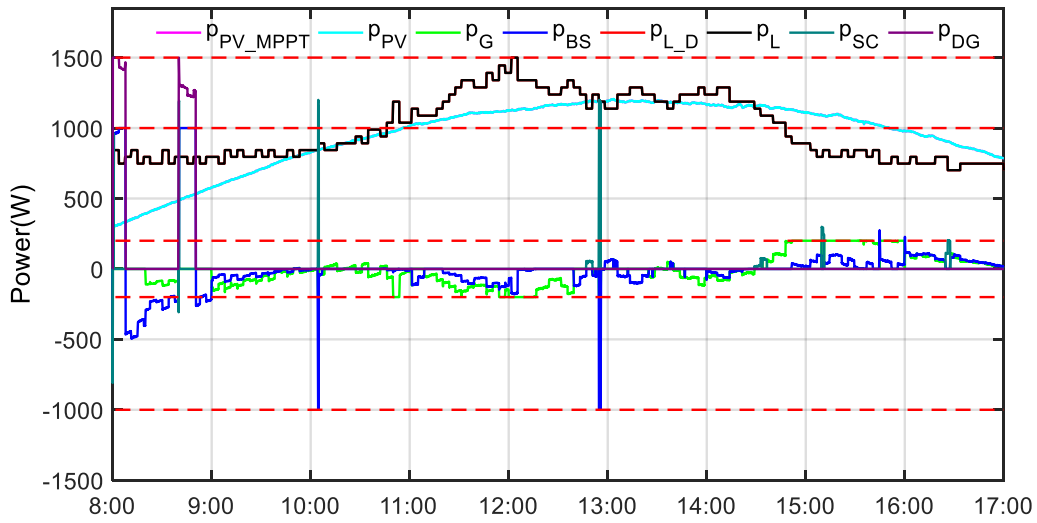


Figure 82. The actual results of power curves at full microgrid mode on May 8th 2018.

In Figure 81 and Figure 82, the day-ahead economics optimization results under the appropriate constant DG power are introduced in the real-time operational layer, it can be seen that the DG is turned on twice. In the rest of the real-time simulation, the DG is off, the BS is charging and discharging, the public is selling and buying power from the microgrid, the SC is recharging six times, and there are no PV shedding and load shedding.

The real-time operational simulation results of the DC microgrid by using the day-ahead economics optimization results under the appropriate DG power range are shown in Figure 83 and Figure 84.

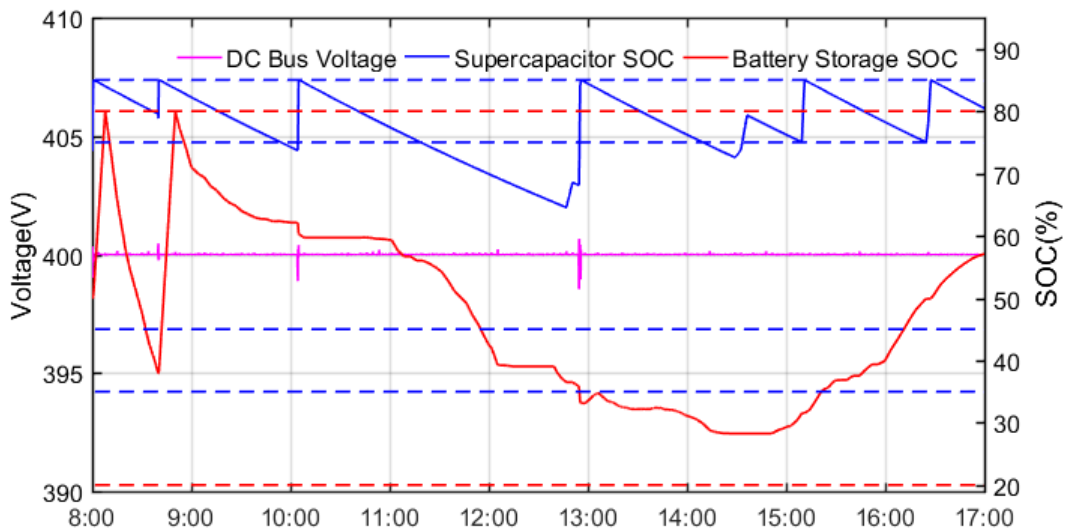


Figure 83. The actual results of DC bus voltage and BS SOC curves at full microgrid mode on May 8th 2018.

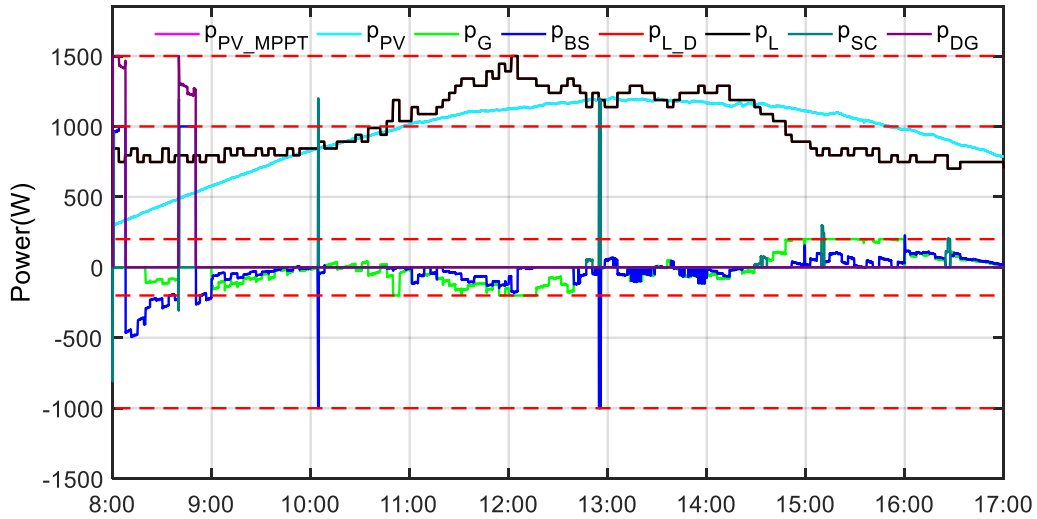


Figure 84. The actual results of power curves at full microgrid mode on May 8th 2018.

In Figure 83 and Figure 84, the day-ahead economics optimization results under the appropriate DG power range are introduced in the real-time operational layer, it can be seen that the DG is turned on twice. In the rest of the real-time simulation, the DG is off, the BS is charging and discharging, the public is selling and buying power from the microgrid, the SC is recharging six times, and there are no PV shedding and load shedding.

To compare the two results before, it can be seen that the results under the appropriate DG power range are the same as the results under the appropriate constant DG power.

The real-time operational simulation results of the DC microgrid by using the ideal economics optimization results under the appropriate constant DG power are shown in Figure 85 and Figure 86.

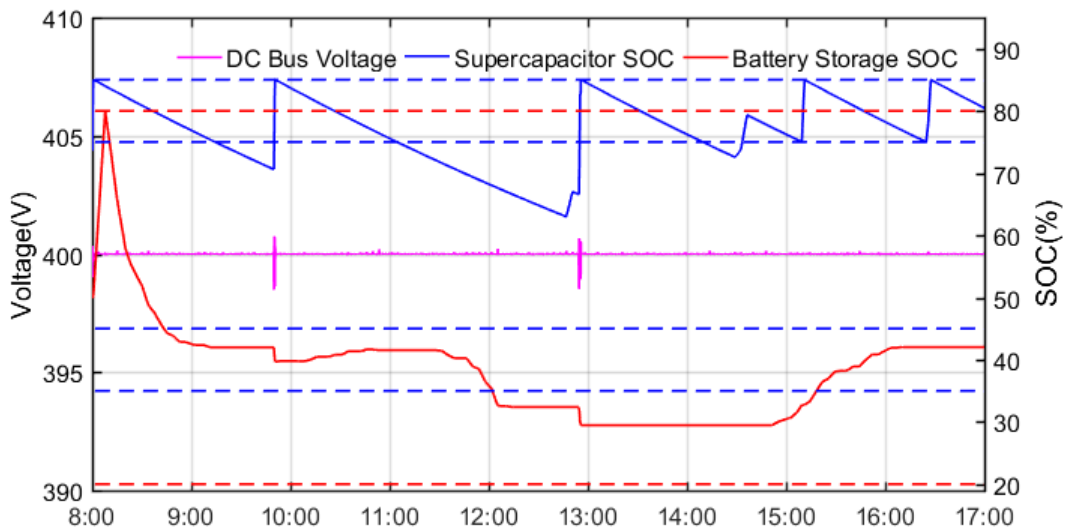


Figure 85. The ideal results of DC bus voltage and BS SOC curves at full microgrid mode on May 8th 2018.

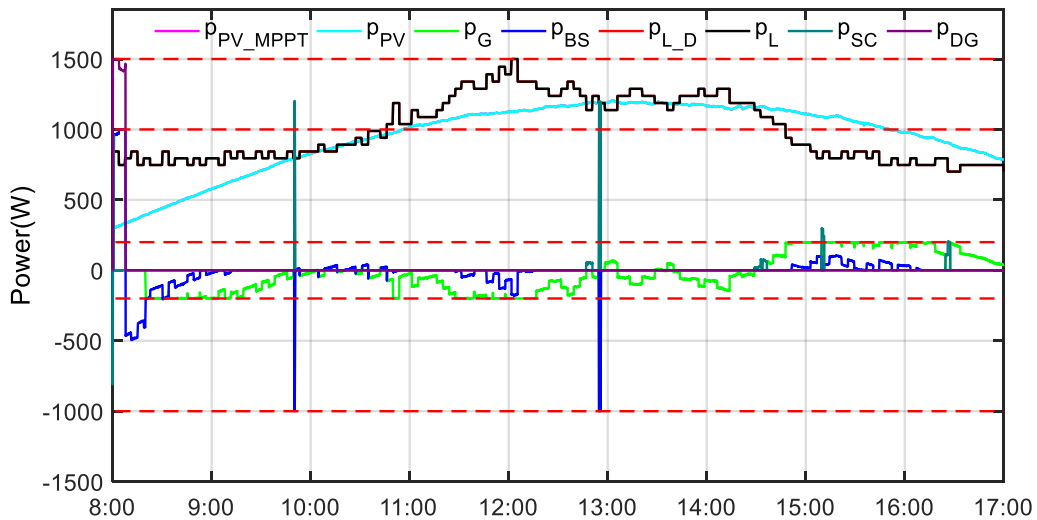


Figure 86. The ideal results of power curves at full microgrid mode on May 8th 2018.

In Figure 85 and Figure 86, the ideal economics optimization results under the appropriate constant DG power are introduced in the real-time operational layer, it can be seen that the DG is turned on only once. In the rest of the real-time simulation, the DG is off, the BS is charging and discharging, the public is selling and buying power from the microgrid, the SC is recharging six times, and there are no PV shedding and load shedding.

The real-time operational simulation results of the DC microgrid by using the ideal economics optimization results under the appropriate DG power range are shown in Figure 87 and Figure 88.

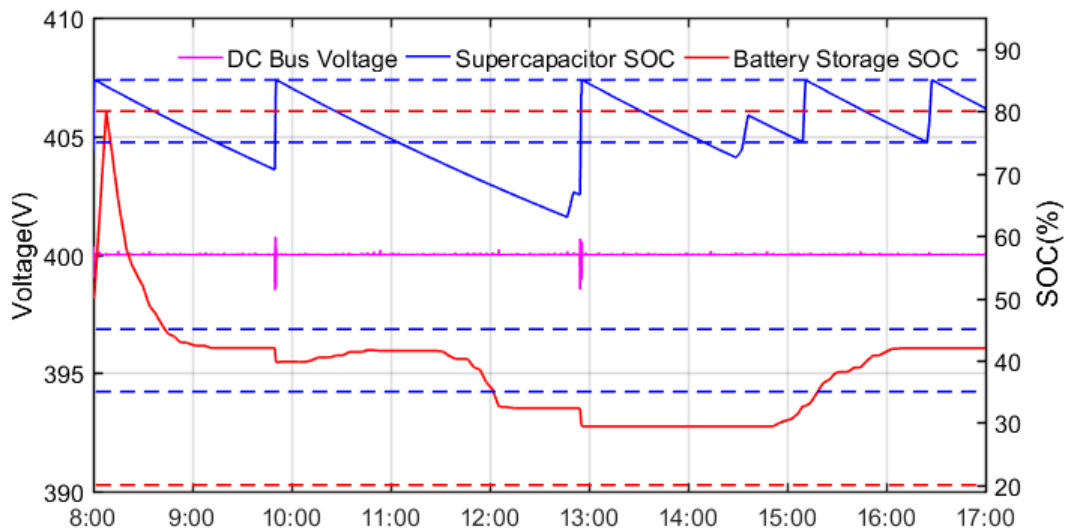


Figure 87. The actual results of DC bus voltage and BS SOC curves at full microgrid mode on May 8th 2018.

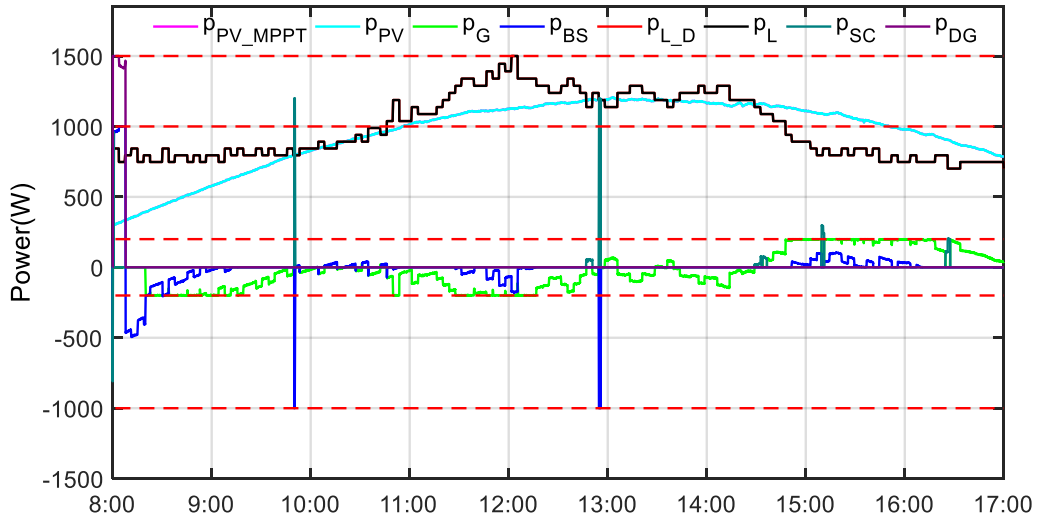


Figure 88. The actual results of power curves at full microgrid mode on May 8th 2018.

In Figure 87 and Figure 88, the ideal economics optimization results under the constant DG power range are introduced in the real-time operational layer, it can be seen that the DG is also turned on only once. In the rest of the real-time simulation, the DG is off, the BS is charging and discharging, the public is selling and buying power from the microgrid, the SC is recharging six times, and there are no PV shedding and load shedding.

To compare the two results before, it also can be seen that the results under the appropriate DG power range are the same as the results under the appropriate constant DG power.

III.1.4.3. Full microgrid simulation results comparison and analysis

Now, it is necessary to give a table that lists the cost of every component from the above simulation results including the optimization results in III.1.4.1. and the real-time operational results in III.1.4.2. The simulation results for full microgrid mode on May 8th 2018 is shown in Table 16.

In Table 16, there are eleven conditions listing. The condition when k_{DG} equals to 0 and k_D equals to 1, 0.5 or 0 are the real-time simulation results in the operational layer. The conditions of ideal MILP results and ideal operational results are respectively the ideal optimization results in the economics dispatching layer and the real-time simulation results in the operational layer by using real recorded PV and load power profiles to replace the PV and load power profile to ignore the power prediction accuracy. The conditions of MILP results and operational results are respectively the day-ahead optimization results in the economics dispatching and real-time simulation results in the operational layer by using the real PV and load prediction power profiles. The appropriate constant DG power and DG power range are considered in the simulation.

By the comparisons in Table 16, it can be seen that the total cost under the condition when k_{DG} equals to 0 and k_D equals to 1, 0.5 or 0, and operational results is higher than the total cost under the condition of ideal operational results, because the accuracy of PV and load power prediction has a big influence on power dispatching. The total cost under the condition of operational results is less than the total cost under the condition when k_{DG} equals to 0 and k_D equals to 1, however, which is higher than the total cost under the condition when k_{DG} equals to 0 and k_D equals to 0.5 and 0, which can give a positive proof that the optimization in the economics dispatching layer can make a little good function to reduce the total cost in the real-time operational simulation in the operational layer because of the low PV power prediction accuracy. The total cost with variable DG power is less than the results with constant DG power under the condition of MILP results due to the loose constraints for DG power. What's more, the total cost under the condition of operational results' by using appropriate DG power range is also less than the total cost under the condition of operational results by using appropriate constant DG power.

In order to give better evidence to prove the effectiveness of the optimization and real-time power management strategy, other two weather data are applied in the off-grid DC microgrid.

Table 16. Results summary for full microgrid mode on May 8th 2018.

Day-ahead optimization	NO			YES	
				Constant DG	
Condition	$k_D = 1,$ $k_{DG} = 0$	$k_D = 0.5,$ $k_{DG} = 0$	$k_D = 0,$ $k_{DG} = 0$	MILP results	Operati onal results
The sum of C_{BS} and C_G (c€)	15.80	11.98	14.74	23.60	12.09
C_{PV_S} (c€)	1.71	0	0	0	0
C_{L_D} (c€)	9.60	0.01	0.01	0	0.01
C_{DG} (c€)	55.63	54.37	53.72	125.47	67.65
C_{SC} (c€)	1.64	1.66	1.72	--	1.79
C_{TOTAL} (c€)	84.41	68.04	70.20	149.08	81.55

Table 16 bis. Results summary for full microgrid mode on May 8th 2018.

Day-ahead optimization	YES		YES			
	Variable DG		Constant DG		Variable DG	
Condition	MIL P results	Opera tional results	Ideal MILP results	Ideal Operatio nal results	Ideal MILP results	Ideal Operatio nal results
The sum of C_{BS} and C_G (c€)	23.84	11.90	13.50	14.67	13.50	14.67
C_{PV_S} (c€)	0	0	0	0	0	0
C_{L_D} (c€)	0	0.01	1.11	0.01	0	0.01
C_{DG} (c€)	125.1 2	67.65	34.70	30.87	35.44	30.87
C_{SC} (c€)	--	1.79	--	1.74	--	1.74
C_{TOTAL} (c€)	148.9 6	81.36	49.32	47.30	48.95	47.30

The simulation results for full microgrid mode on June 20th 2018 is shown in Table 17.

Table 17. Results summary for full microgrid mode on June 20th 2018.

Day-ahead optimization	NO			YES	
				Constant DG	
Condition	$k_D = 1,$ $k_{DG} = 0$	$k_D = 0.5,$ $k_{DG} = 0$	$k_D = 0,$ $k_{DG} = 0$	MILP results	Operational results
The sum of C_{BS} and C_G (c€)	9.19	14.95	9.19	-20.95	12.63
C_{PV_S} (c€)	30.71	27.06	18.30	61.89	13.94
C_{L_D} (c€)	5.31	0.05	0.01	0	4.29
C_{DG} (c€)	210.90	184.34	188.90	0	180.48
C_{SC} (c€)	1.97	1.91	1.86	--	1.96
C_{TOTAL} (c€)	258.11	228.31	218.28	40.93	213.33

Table 17 bis. Results summary for full microgrid mode on June 20th 2018.

Day-ahead optimization	YES		YES			
	Variable DG		Constant DG		Variable DG	
Condition	MILP results	Operational results	Ideal MILP results	Ideal Operational results	Ideal MILP results	Ideal Operational results
The sum of C_{BS} and C_G (c€)	- 20.95	12.65	10.28	13.18	19.11	20.28
C_{PV_S} (c€)	61.89	13.94	0	3.69	0	1.87
C_{L_D} (c€)	0	3.99	0.10	5.40	0	0.01
C_{DG} (c€)	0	180.48	147	139.60	134.71	136.57
C_{SC} (c€)	--	1.96		1.87	--	1.90
C_{TOTAL} (c€)	40.93	213.05	157.38	163.76	153.82	160.66

By the comparisons in Table 17, the total cost under the condition when k_{DG} equals to 0 and k_D equals to 1, 0.5 or 0, and operational results is higher than the total cost under the condition of ideal

operational results, because the accuracy of PV and load power prediction has a big influence on power dispatching. The total cost under the condition of operational results is less than the total cost under the condition when k_D equals to 1, 0.5 or 0, which can give a positive proof that the optimization in the economics dispatching layer can make a good function to reduce the total cost in the real-time simulation in the operational layer. The total cost with variable DG power is less than the results with constant DG power under the condition of ideal MILP results due to the loose constraints for DG power. What's more, the total cost under the condition of ideal operational results is less than the total cost under the condition of operational results because of the ideal prediction power.

The simulation results for full microgrid mode on July 16th 2018 is shown in Table 18. By the comparisons in Table 18, it can be seen that the total cost under the condition when k_{DG} equals to 0 and k_D equals to 1, and operational results is higher than the total cost under the condition of ideal operational results, because the accuracy of PV and load power prediction has a big influence on power dispatching, the exception is the total cost under the condition when k_{DG} equals to 0 and k_D equals to 0.5 or 0 is less than the total cost under the condition of ideal operational results because of the low PV power leading to a big more frequency start-up of the DG. The total cost under the condition of operational results is less than the total cost under the condition when k_{DG} equals to 0 and k_D equals to 1, which can give a positive proof that the optimization in the economics dispatching layer can make a good function to reduce the total cost in the real-time operational simulation in the operational layer.

Table 18. Results summary for full microgrid mode for July 16th 2018.

Day-ahead optimization	NO			YES	
				Variable DG	
Condition	$k_D = 1,$ $k_{DG} = 0$	$k_D = 0.5,$ $k_{DG} = 0$	$k_D = 0,$ $k_{DG} = 0$	MILP results	Operational results
The sum of C_{BS} and C_G (c€)	23.63	32.59	31.37	12.86	23.81
C_{PV_S} (c€)	5.85	0	0.26	9.04	5.31
C_{L_D} (c€)	8.43	2.26	3.64	0	13.04
C_{DG} (c€)	641.25	518.86	519.62	737	568.54
C_{SC} (c€)	2.20	2.20	2.21	--	2.35
C_{TOTAL} (c€)	681.38	555.93	557.11	758.90	613.06

Table 18 bis. Results summary for full microgrid mode on July 16th 2018.

Day-ahead optimization	YES		YES			
	Variable DG		Constant DG		Variable DG	
Condition	MILP results	Operational results	Ideal MILP results	Ideal Operational results	Ideal MILP results	Ideal Operational results
The sum of C_{BS} and C_G (c€)	16.42	24.03	10.49	26.74	22.65	30.40
C_{PV_S} (c€)	0	5.31	3.27	3.287	0	5.43
C_{L_D} (c€)	0	12.77	0	20.55	0.01	6.40
C_{DG} (c€)	723.3 2	567.2 2	566.4 7	557.9 7	488.0 2	546.1 2
C_{SC} (c€)	--	2.36	--	2.42	--	2.37
C_{TOTAL} (c€)	739.7 5	611.7 0	580.2 4	610.9 8	510.7 0	590.7 5

The total cost with variable DG power is less than the results with constant DG power under the condition of MILP results due to the loose constraints for DG power. What's more, the total cost under the condition of operational results by using appropriate DG power range is less than the total cost under the condition of operational results by using appropriate constant DG power due to the loose constraints for DG power.

In conclusion, the real-time power management of the operational layer without the economics optimization of the economics dispatching layer cannot achieve the purpose of optimal real-time power management. The accuracy of PV and load power predictions has a big influence on the economics optimization as the conclusion in III.6.2.3 and III.6.3.3. In particular, the uncertainty of weather will lead to uncertainty in the results of economic optimization. The economics optimization in the economics dispatching layer can reduce the total cost of the power flow of DC microgrid and reduce the load shedding power in full microgrid mode.

III.1.5. Simulation scenario for 24 hours' duration

To solve the optimization problem of the economic dispatching for 24 hours, the MILP solver which is the same as the 9 hours' simulation before is applied. The 24 hours' weather data set from June 20th 2018 can give a good simulation verification.

The 24 hours work hypothesis based on a university is shown in Table 19 with five time periods. During 0:00-6:00 and 22:00-24:00 it is assumed that the load demand power, and the public grid can

exchange power with the BS due to the fact that the low power tariff in the public grid. During 6:00-8:00, the PV energy production is different according to the seasons, the PV can produce more power in summer than the power in winter. During 8:00-17:00, the load demand varies according to the energy demand of the university building, mostly the peak consumption appears at noon. During 17:00-22:00 the load demand for tertiary buildings is low but for residential buildings are very high so that the public grid is highly stressed. Thus, it is assumed that the public grid cannot exchange power with the BS during 6:00-22:00 to prevent the BS buys and sells power from and to the public grid for extra money.

Table 19. 24 hours work hypothesis.

Time period	Description
0:00-6:00	Low load demand
6:00-8:00	Different according to the seasons
8:00-17:00	Working time in building
17:00-22:00	High load demand from the public grid
22:00-24:00	Low load demand

The 24 hours PV prediction power curves can be calculated according to the equations (2. 20) and (2. 21). The 24 hours' load power is scaled according to the real daily load demand data in the university building from the local electricidal company, and the load power is assumed to be 49 controllable appliances for verifying the load real-time optimization algorithm. It is based on the experience that the load demand respects to a duty-cycle regular change, the load prediction power is assumed to be a little different from the real load power.

The 24 hours PV MPPT power and PV prediction power on June 20th 2018 are shown in Figure 89.

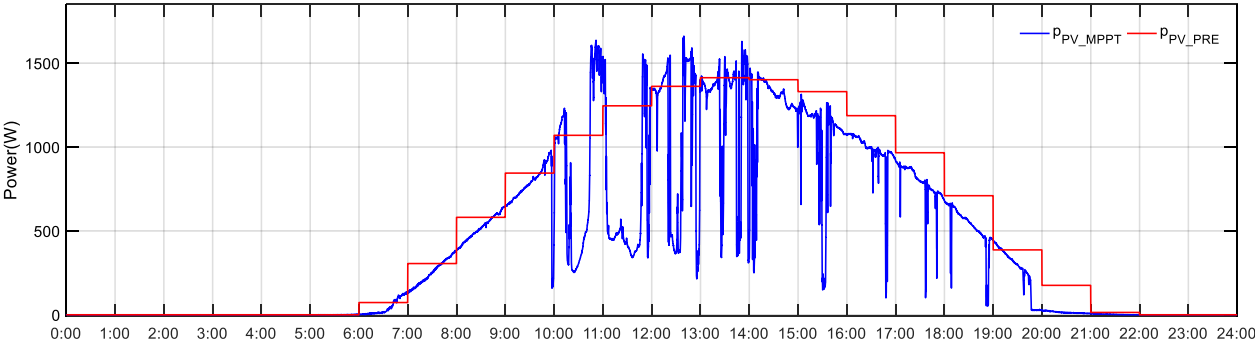


Figure 89. PV MPPT power and PV prediction power curves for June 20th 2018. The load power and load power prediction curves are given in Figure 90 are used.

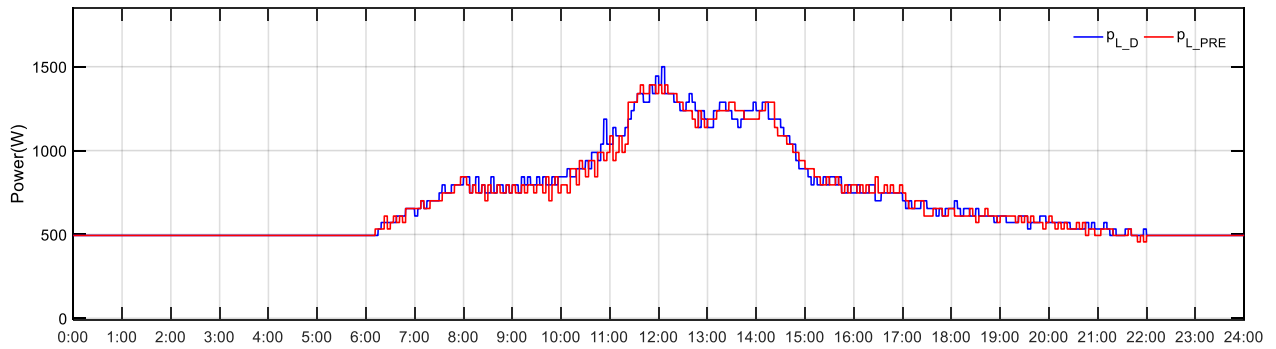


Figure 90. Load power and load power prediction curves.

The 24 hours tariff of the public grid is given according to the TOU method in Table 20, the high tariff is in the period, 10:00-12:00 and 17:00-22:00, the middle tariff is in the period, 6:00-10:00 and 12:00-17:00, the low tariff is in the period, 0:00-6:00 and 22:00-24:00. T_G is the public grid exchanging imposed tariffs for supply and injection.

Table 20. TOU public grid energy tariffs.

Public grid	TOU energy tariffs (€/kWh)			
	0:00-6:00	6:00-8:00	8:00-10:00	10:00-12:00
T_G	0.01	0.1	0.1	0.7

Table 20 bis. TOU public grid energy tariffs.

Public grid	TOU energy tariffs (€/kWh)		
	12:00-17:00	17:00-22:00	22:00-24:00
T_G	0.1	0.7	0.01

Table 21 presents the numerical values of the fixed energy tariffs for 24 hours which is the same as the values given in Table 3. The average O&M tariff $T_{DG_O\&M}$ is assumed to be 0.63 €/h.

Table 21. Fixed energy tariffs

Fixed energy tariffs (€/kWh)	
BS T_{BS}	0.05
PV shed T_{PV_S}	1.5
Load shed T_{L_S}	1.8
DG T_{DG_F}	1.2
SC T_{SC}	0.3

Table 22 presents the simulation period following the different parameters setting, the choice of the additional constraints group 1 and 2, the set of the coefficient k_{L_CRIT} , and public grid power limitation. These configurations are set according to the energy demand of the university building during the week.

Table 22. Period configuration.

Time period	Choose of problem formulation	k_{L_CRIT}	P_{G_MAX}
0:00-6:00	Additional constraints group 2	100%	600W
6:00-8:00	Additional constraints group 1	80%	200W
8:00-17:00	Additional constraints group 1	80%	200W
17:00-22:00	Additional constraints group 1	80%	200W
22:00-24:00	Additional constraints group 2	100%	600W

In Table 22, the 24 hours is divided into five time periods: during 0:00-6:00 and 22:00-24:00 it is assumed that the load demand power is low respecting to the additional constraints group 2, the coefficient k_{L_CRIT} is set to be 100% because all the load demand is critical load that cannot be shedding, and the public grid power is limited to 600W; during 6:00-8:00 the PV energy production is different according the seasons and it is assumed that the additional constraints group 1 is used, the coefficient k_{L_CRIT} is set to be 80%, and the public grid power is limited to 200W; during 8:00-17:00 the load demand varies according to the energy demand of the university building and it is assumed that the power management uses the additional constraints group 1, the coefficient k_{L_CRIT} is set to be 80%, and the public grid power is limited to 200W; during 17:00-22:00 the load demand for tertiary buildings is

low but for residential buildings are very high so that the public grid is highly stressed, therefore, it is assumed that the additional constraints group 1 is used, the coefficient k_{L_CRIT} is set to be 80%, and the public grid power is limited to 200W.

III.1.6. Full microgrid simulation for 24 hours' duration

To solve the full microgrid optimization problem of the economic dispatching, the MILP solver is applied. The weather data set on June 20th 2018 has been introduced in III.1.5. The load power and load prediction power has been provided in III.1.5. The tariff of every electrical component in the full microgrid mode has been given in III.1.5.

The full DC microgrid parameters used for the optimization dispatch layer are presented in Table 23.

Table 23. Parameters for optimization at full microgrid mode.

Parameters	Values	Parameters	Values
P_{BS_MAX}	1000W	P_{DG_MAX}	1500W
SOC_{BS_MIN}	20%	$P_{DG_ON_MAX}$	$(0, P_{DG_MAX}]$
SOC_{BS_MAX}	80%	$P_{DG_ON_MIN}$	$(0, P_{DG_ON_MAX}]$
SOC_{BS_0}	50%	dt_{DG}	1200s
C_{REF}	6.6Ah	k_{L_CRIT}	80%, 100%
P_{PV_STC}	1750W	P_{GF_Limit}	20W/s
P_{G_MAX}	200W, 600W		

In Table 23, the parameters are the same as the parameters in the economics dispatching layer of the grid-connected and off-grid mode above. The DG power limited between $P_{DG_ON_MIN}$ and $P_{DG_ON_MAX}$ when the DG is turned on is the same as the constraints in the economics dispatching layer of the off-grid mode. The $P_{DG_ON_MAX}$ and $P_{DG_ON_MAX}$ is chosen between 0 and P_{DG_MAX} , the $P_{DG_ON_MIN}$ is chosen between 0 and $P_{DG_ON_MAX}$. The k_{L_CRIT} and P_{G_MAX} are set according to the periods in Table 22.

The calculation of the parameters $P_{DG_ON_MIN}$ and $P_{DG_ON_MAX}$ are the same as the parameters in the economics dispatching layer of the off-grid mode. Thus, the appropriate $P_{DG_ON_MIN}$ and $P_{DG_ON_MAX}$ power can be got as the same method depicted in the economics dispatching layer of the off-grid mode.

The full DC microgrid parameters used for the operational algorithm of the operational layer is presented in Table 24.

Table 24. Parameters for the operational algorithm at full microgrid mode.

Parameters	Values	Parameters	Values
P_{BS_MAX}	1000W	v_{SC_Rated}	75V
SOC_{BS_MIN}	20%	$SOC_{SC_MAX_MAX}$	85%
SOC_{BS_MAX}	80%	$SOC_{SC_MAX_MIN}$	75%
SOC_{BS_0}	50%	$SOC_{SC_MIN_MAX}$	45%
C_{REF}	6.6Ah	$SOC_{SC_MIN_MIN}$	35%
P_{PV_STC}	1750W	SOC_{SC_0}	75%
v_{DC}^*	400V	P_{DG_MAX}	1500W
P_{SC_MAX}	1500W	$T_{DG_ON_MAX}$	3600s
T_{SC_MIN}	180s	$T_{DG_OFF_LIM}$	1200s
C_{SC}	94F	k_{L_CRIT}	80%, 100%
P_{G_MAX}	200W, 600W		

In Table 24, the parameters are the same as the parameters in the operational layer of the grid-connected and off-grid mode above.

III.1.6.1. Optimization results

The day-ahead economics optimization results on June 20th 2018 by using PV and load prediction power profiles under the appropriate constant DG power 1050W are shown in Figure 91 and Figure 92.

In Figure 91 and Figure 92, the PV and load prediction power profiles are used, the day-ahead optimization results are shown under the appropriate constant DG power; at the beginning of the optimization results, the PV power is less than the load demand power, the BS is recharging by the public grid because of the low public grid power tariff; at 6:40, the DG is turned on; at 7:00, the DG is turned off, the BS and the public grid provide power to support the load demand power; then the DG is turned on at 21:00.

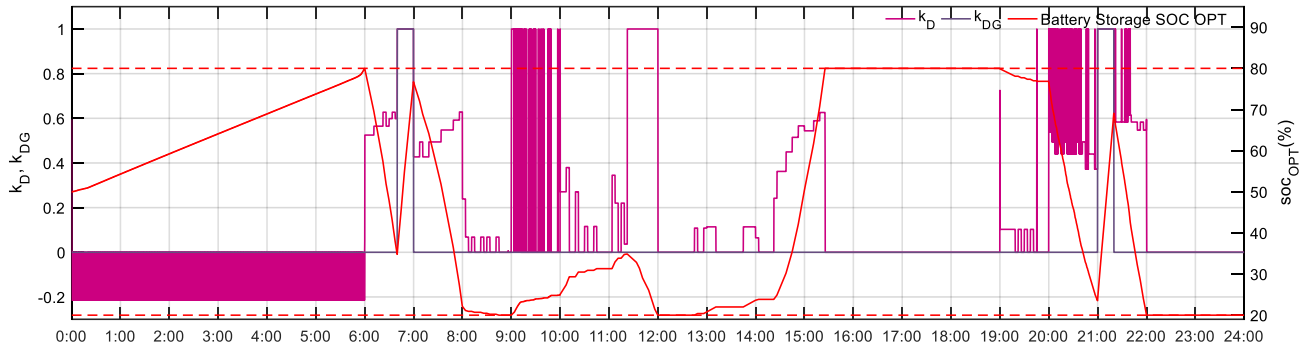


Figure 91. The day-ahead economics optimization results (k_D , k_{DG}) and BS SOC curves at full microgrid mode on June 20th 2018.

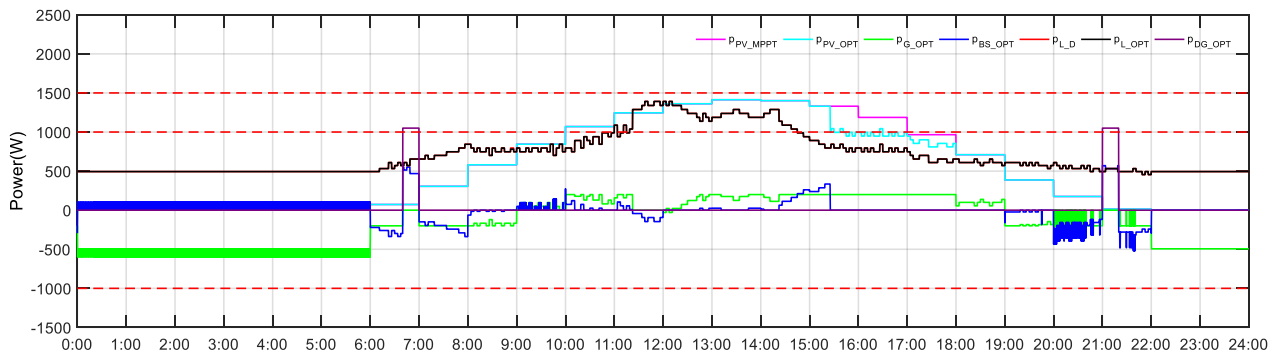


Figure 92. The day-ahead economics optimization results of power curves at full microgrid mode on June 20th 2018.

The day-ahead economics optimization results on June 20th 2018 by using PV and load prediction power profiles under the appropriate DG power range from 850W to 1250W are shown in Figure 93 and Figure 94.

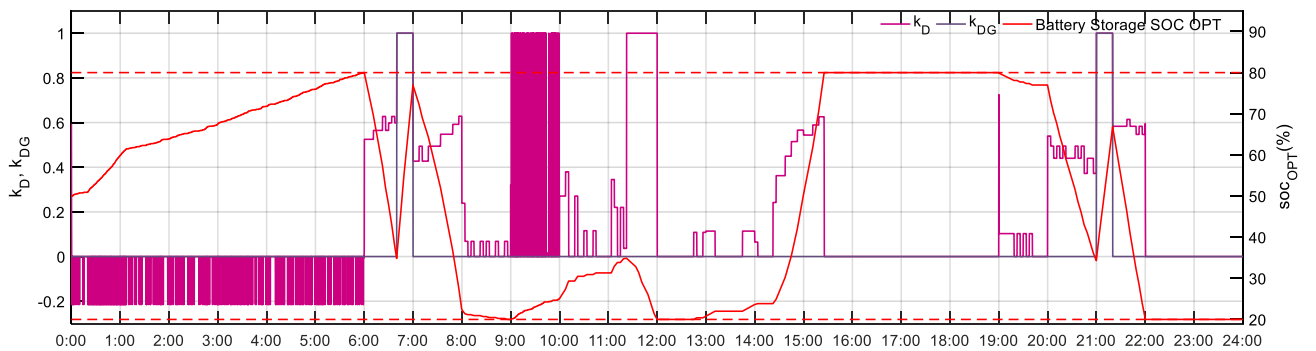


Figure 93. The day-ahead economics optimization results (k_D , k_{DG}) and BS SOC curves at full microgrid mode on June 20th 2018.

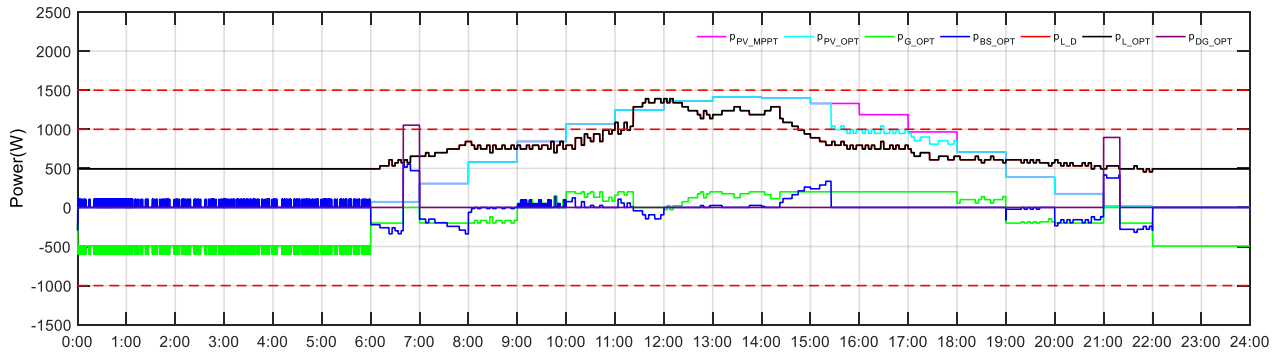


Figure 94. The day-ahead economics optimization results of power curves at full microgrid mode on June 20th 2018.

In Figure 93 and Figure 94, the PV and load prediction power profiles are used, the day-ahead optimization results are shown under the appropriate DG power range, which is almost the same as the results in Figure 91 and Figure 92. The power values of the DG are not the same.

The ideal economics optimization results on June 20th 2018 by using real PV and load power profiles under the appropriate constant DG power 1100W are shown in Figure 95 and Figure 96.

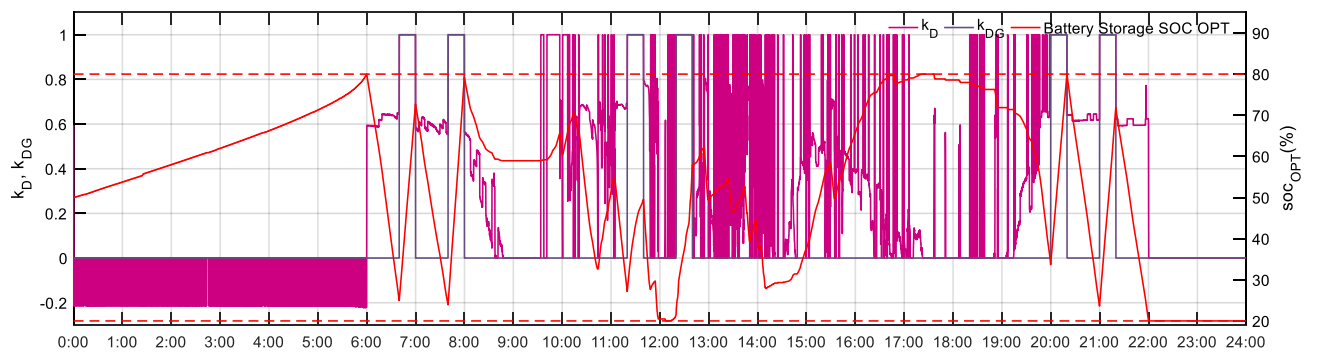


Figure 95. The ideal economics optimization results (k_D , k_{DG}) and BS SOC curves at full microgrid mode on June 20th 2018.

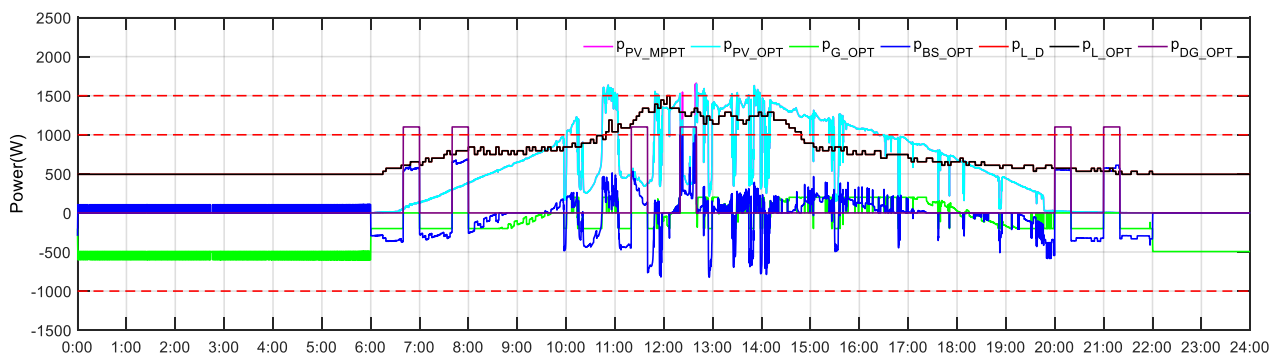


Figure 96. The ideal economics optimization results of power curves at full microgrid mode on June 20th 2018.

In Figure 95 and Figure 96, the real PV and load power profiles are used, the ideal day-ahead optimization results are shown under the appropriate constant DG power; at the beginning of the optimization results, the PV power is less than the load demand power, and the BS is recharging by the public grid because of the low public grid tariff; when the public grid tariff is increased and its power limitation is decreased, the DG is turned on to supply the load demand power and the BS at the constant power in the duty cycle; at 6:40, 7:40, 11:20, 12:20, 20:00, and 21:00.

The ideal economics optimization results on June 20th 2018 by using real PV and load power profiles under the appropriate DG power range from 750W to 1450W are shown in Figure 97 and Figure 98.

In Figure 97 and Figure 98, the real PV and load power profiles are used, the ideal day-ahead optimization results are shown under the appropriate DG power range, which is almost the same as the results in Figure 95 and Figure 96. The DG start-up from 11:00 to 13:00 is different from the results in Figure 97 and Figure 98.

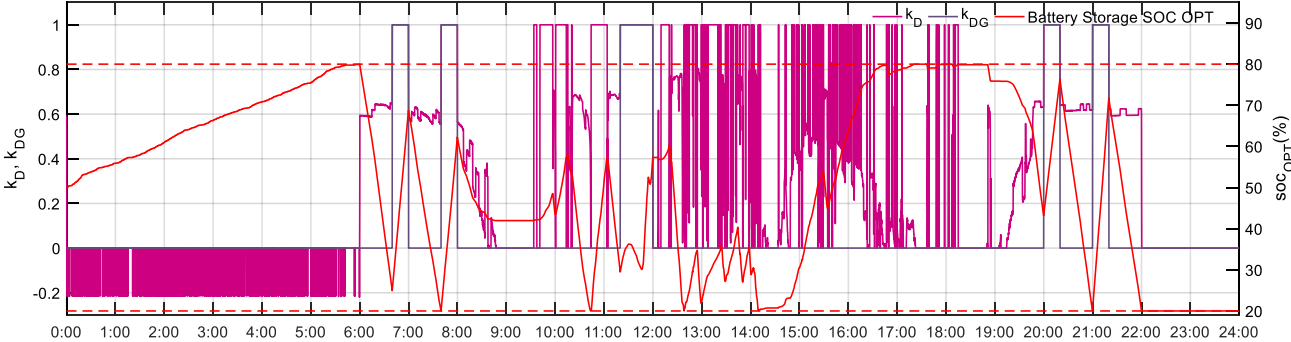


Figure 97. The ideal economics optimization results (k_D , k_{DG}) and BS SOC curves at full microgrid mode on June 20th 2018.

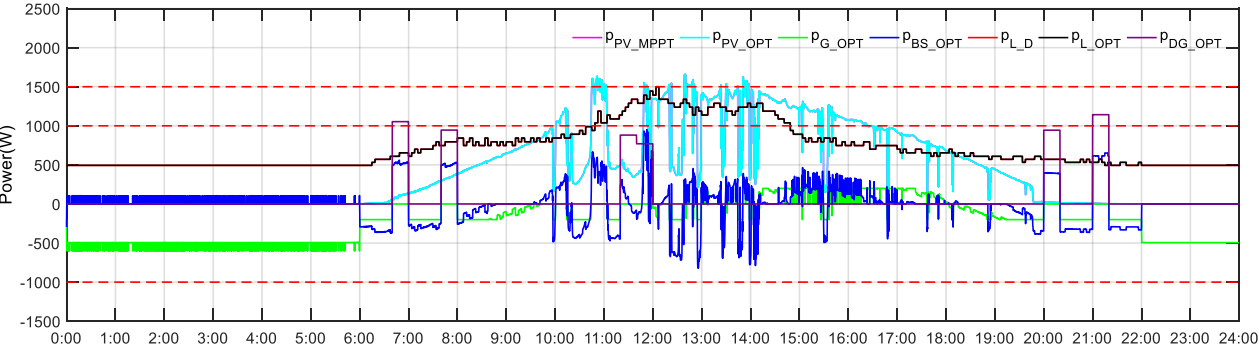


Figure 98. The ideal economics optimization results of power curves at full microgrid mode on June 20th 2018.

III.1.6.2. Real-time results

The following results consider the real-time simulation results of the operational layer. In order to validate the effectiveness of the day-ahead optimization, the real-time simulation result by using the day-ahead optimization will be compared with the real-time simulation result without considering the day-ahead optimization results.

III.1.6.2.1 Real-time result without optimization

Without considering the day-ahead optimization results, the cases under the power management strategy proposed in II.5.4.1. should be used. In order to give a better comparison, the cases when k_D equal to 1, 0.5, 0, -0.5, or -1 are also simulated. The k_D is negative representing the public grid and BS can work at the different power direction, the public grid is selling power while the BS is charging shown in the equations (2. 49).

The simulation cases without considering the day-ahead optimization results are listed to be 15 conditions in Table 25. During 0:00-6:00 and 22:00-24:00, the k_D is set to be 1, 0.5, 0, -0.5, or -1. From 6:00-22:00, the k_D is set to be 1, 0.5, 0.

Table 25. Simulation cases without considering the day-ahead optimization results.

Time period	0:00-6:00 and 22:00-24:00	6:00-22:00
	k_D value	k_D value
Condition 1	1	1
Condition 2	0.5	1
Condition 3	0	1
Condition 4	-0.5	1
Condition 5	-1	1
Condition 6	1	0.5
Condition 7	0.5	0.5
Condition 8	0	0.5
Condition 9	-0.5	0.5
Condition 10	-1	0.5
Condition 11	1	0
Condition 12	0.5	0
Condition 13	0	0
Condition 14	-0.5	0
Condition 15	-1	0

The results under condition 1 when k_D equal to 1 and k_{DG} equal to 0 are shown in Figure 99 and Figure 100.

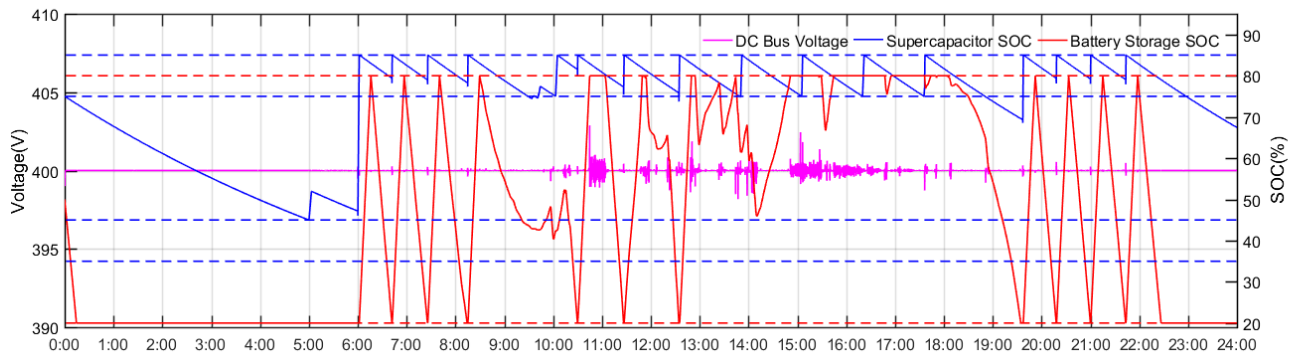


Figure 99. DC bus voltage and BS SOC curves when $k_D = 1$ and $k_{DG} = 0$ at full microgrid mode on

June 20th 2018.

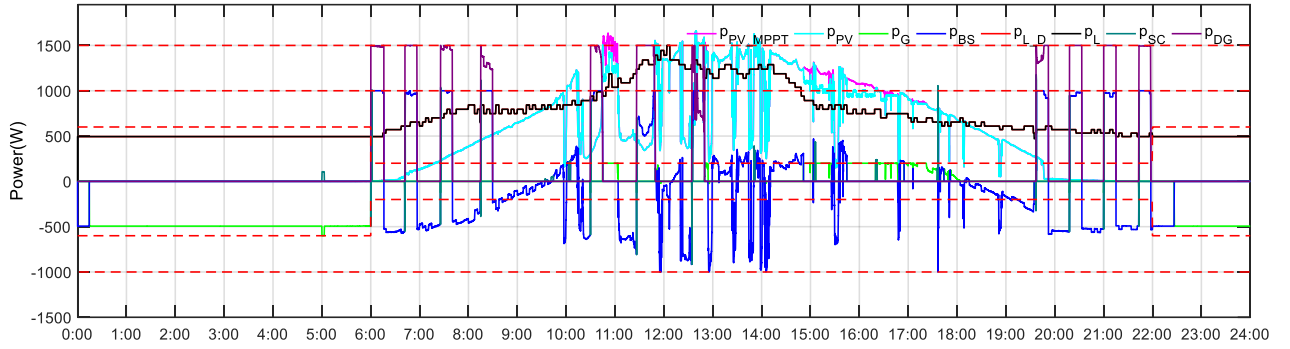


Figure 100. Power curves when $k_D = 1$ and $k_{DG} = 0$ at full microgrid mode on June 20th 2018.

In Figure 99 and Figure 100, the public grid, the BS, and the DG are the controllable sources to support the microgrid, the SC is only used to compensate the start-up of the DG, the public grid and the BS have higher priority than the DG to compensate the power difference between p_{PV_MPPT} and p_{L_D} . The DG is turned on eleven times.

The figures of the other 14 conditions are not shown here. The cost comparison of the 15 conditions will be shown in III.6.6.3.

III.1.6.2.2 Real-time results with day-ahead optimization

Considering the day-ahead optimization results, the cases under the power management strategy proposed in II.5.4.2. should be used. The optimization coefficient k_D and k_{DG} can introduce the day-ahead optimization results in the economic dispatching layer. There are two real-time operational simulations by using the day-ahead economics optimization results under the appropriate constant DG power and the appropriate DG power range showing following; in the same time, there are two real-time operational simulations by using the ideal economics optimization results under the appropriate constant DG power and the appropriate DG power range showing following.

The real-time operational simulation results of the DC microgrid by using the day-ahead economics optimization results under the appropriate constant DG power are shown in Figure 101 and Figure 102.

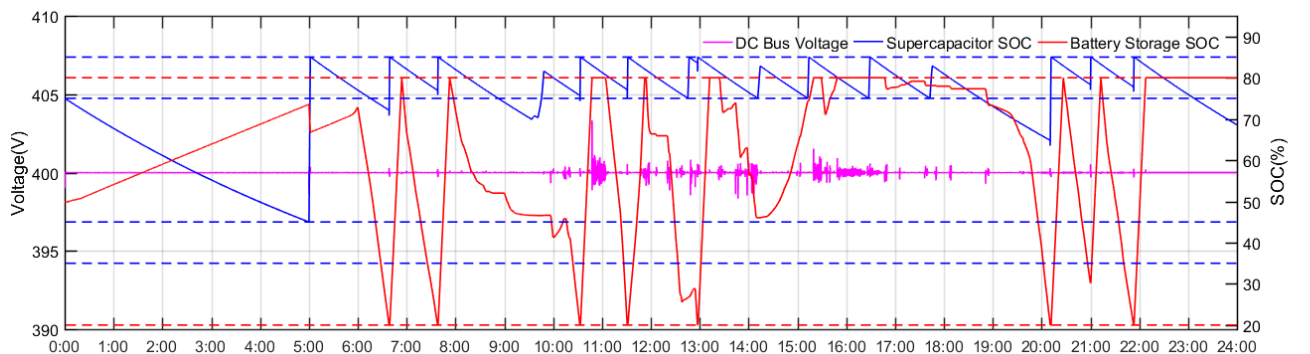


Figure 101. The actual results of DC bus voltage and BS SOC curves at full microgrid mode on June

20th 2018.

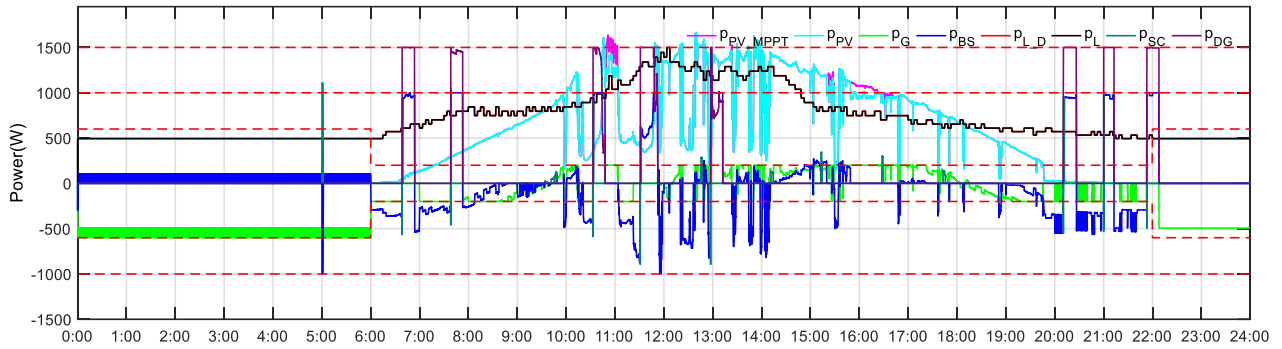


Figure 102. The actual results of power curves at full microgrid mode on June 20th 2018.

In Figure 101 and Figure 102, the day-ahead economics optimization results under the appropriate constant DG power are introduced in the real-time operational layer, it can be seen that the DG is turned on eight times. In the rest of the real-time simulation, the DG is off, the BS is charging and discharging, the public grid is selling and buying power from the microgrid, the BS is recharging by the public grid during the period from 0:00 to 6:00.

The real-time operational simulation results of the DC microgrid by using the day-ahead economics optimization results under the appropriate DG power range are shown in Figure 103 and Figure 104.

In Figure 103 and Figure 104, the day-ahead economics optimization results under the appropriate DG power range are introduced in the real-time operational layer, it can be seen that the DG is turned on eight times. In the rest of the real-time simulation, the DG is off, the BS is charging and discharging, the public is selling and buying power from the microgrid, the BS is recharging by the public grid during the period from 0:00 to 6:00.

To compare the two results before, it can be seen that the results under the appropriate DG power range are the same as the results under the appropriate constant DG power.

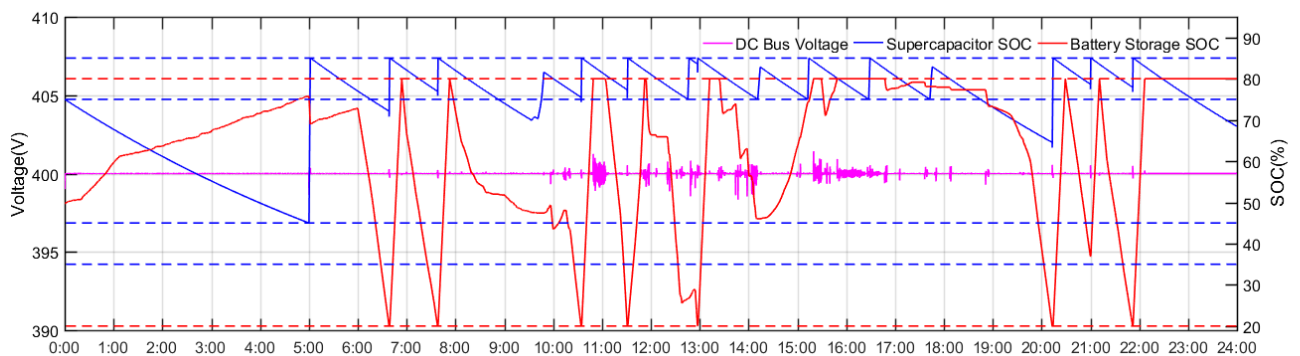


Figure 103. The actual results of DC bus voltage and BS SOC curves at full microgrid mode on June 20th 2018.

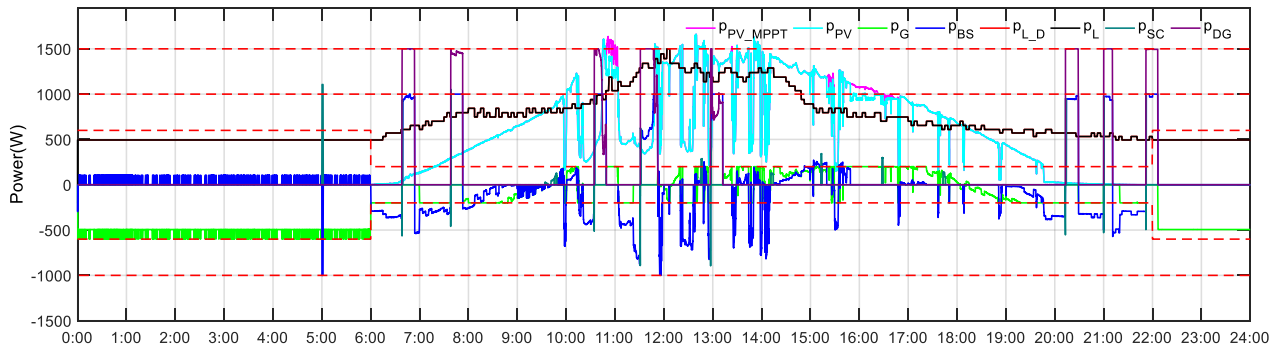


Figure 104. The actual results of power curves at full microgrid mode on June 20th 2018.

The real-time operational simulation results of the DC microgrid by using the ideal economics optimization results under the appropriate constant DG power are shown in Figure 105 and Figure 106.

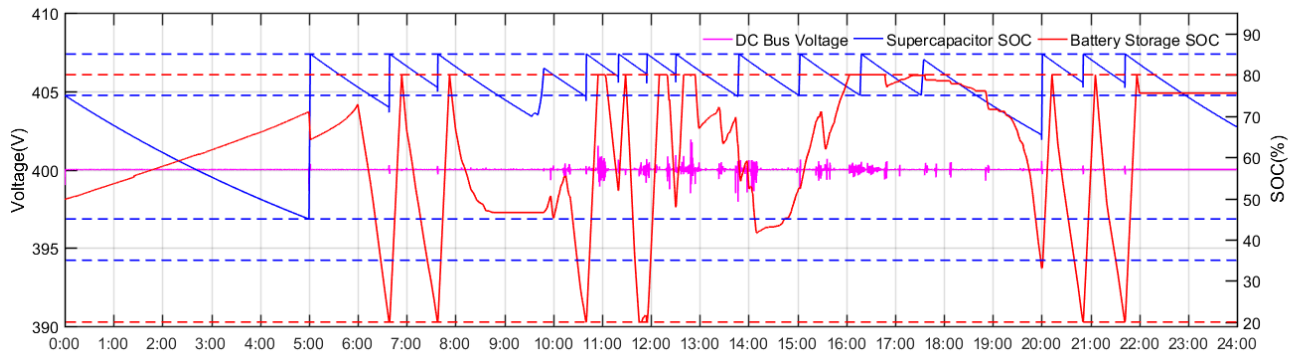


Figure 105. The ideal results of DC bus voltage and BS SOC curves at full microgrid mode on June 20th 2018.

In Figure 105 and Figure 106, the ideal economics optimization results under the appropriate constant DG power are introduced in the real-time operational layer, it can be seen that the DG is turned on nine times. In the rest of the real-time simulation, the DG is off, the BS is charging and discharging, the public is selling and buying power from the microgrid, the BS is recharging by the public grid during the period from 0:00 to 6:00.

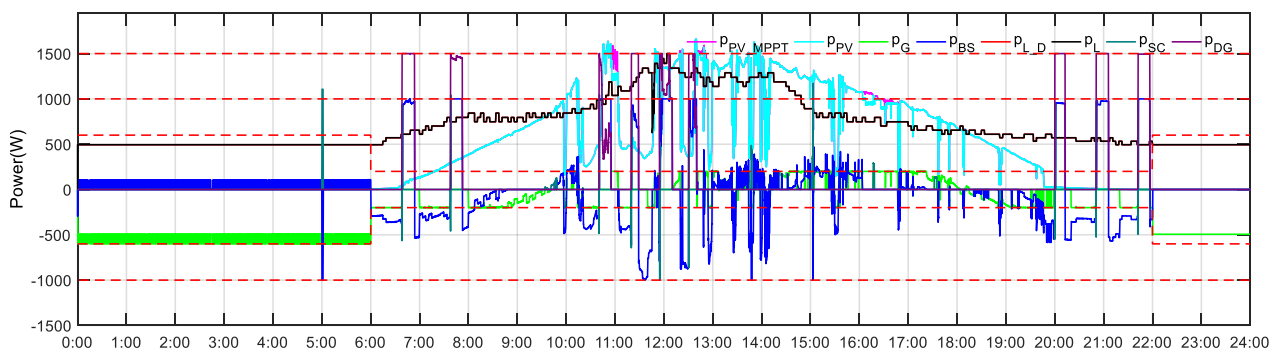


Figure 106. The ideal results of power curves at full microgrid mode on June 20th 2018.

The real-time operational simulation results of the DC microgrid by using the ideal economics optimization results under the appropriate DG power range are shown in Figure 107 and Figure 108.

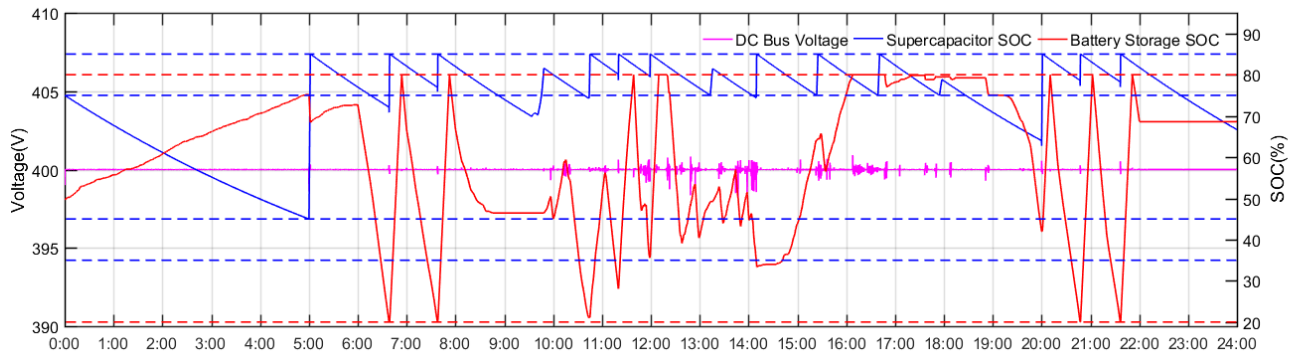


Figure 107. The actual results of DC bus voltage and BS SOC curves at full microgrid mode on June 20th 2018.

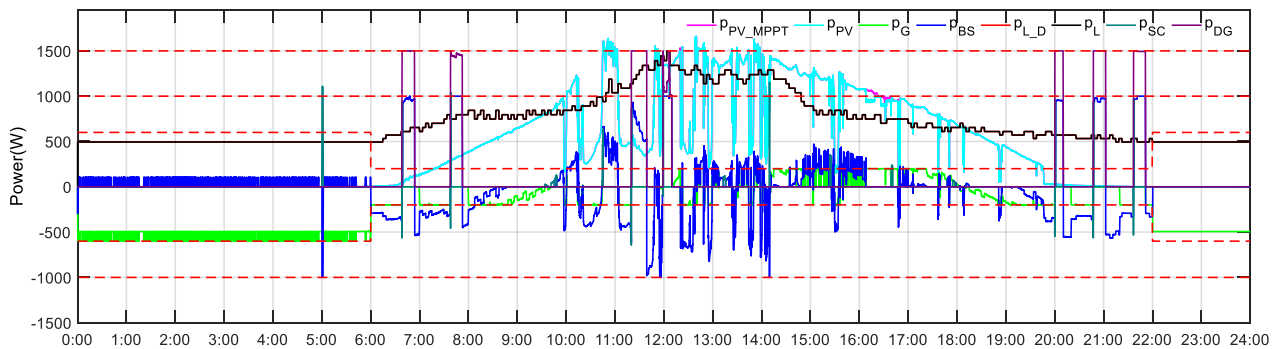


Figure 108. The actual results of power curves at full microgrid mode on June 20th 2018.

In Figure 107 and Figure 108, the ideal economics optimization results under the constant DG power range are introduced in the real-time operational layer, it can be seen that the DG is also turned on only seven times. In the rest of the real-time simulation, the DG is off, the BS is charging and discharging, the public grid is selling and buying power from the microgrid, the BS is recharging by the public grid during the period from 0:00 to 6:00.

To compare the two results before, it also can be seen that the results under the appropriate DG power range are the same as the results under the appropriate constant DG power.

III.1.6.3. Full microgrid simulation results comparison and analysis

Now, it is necessary to give a table that lists the cost of every component from the above simulation results including the optimization results in III.6.6.1. and the real-time operational results in III.6.6.2. The 24 hours simulation results for full microgrid mode on June 20th 2018 is shown in Table 26.

Table 26. Results summary for full microgrid mode June 20th 2018.

Day-ahead optimization	NO				
Condition	1	2	3	4	5
The sum of C_{BS} and C_G (c€)	19.27	19.28	22.92	23.45	23.45
C_{PV_S} (c€)	39.64	39.64	28.81	28.74	28.74
C_{L_D} (c€)	0.70	0.70	3.09	0.84	0.84
C_{DG} (c€)	671.49	671.49	610.86	609.70	609.70
C_{SC} (c€)	4.45	4.45	4.43	4.43	4.43
C_{TOTAL} (c€)	735.58	735.58	670.14	667.18	667.18

Table 26 bis. Results summary for full microgrid mode for June 20th 2018.

Day-ahead optimization	NO				
Condition	6	7	8	9	10
The sum of C_{BS} and C_G (c€)	57.69	57.66	59.07	59.31	59.31
C_{PV_S} (c€)	17.81	17.77	27.37	35.77	35.77
C_{L_D} (c€)	0.01	0.01	0.01	0.01	0.01
C_{DG} (c€)	446.01	446.14	428.81	421.95	421.95
C_{SC} (c€)	4.06	4.06	4.16	4.17	4.17
C_{TOTAL} (c€)	525.61	525.66	519.44	521.23	521.23

Table 26 bis. Results summary for full microgrid mode for June 20th 2018.

Day-ahead optimization	NO				
Condition	11	12	13	14	15
The sum of C_{BS} and C_G (c€)	60.25	60.25	58.77	61.93	61.93
C_{PV_S} (c€)	6.51	6.51	16.12	1.24	1.24
C_{L_D} (c€)	0.01	0.01	0.01	0.01	0.01
C_{DG} (c€)	440.09	440.10	426.04	383.73	383.73
C_{SC} (c€)	4.09	4.09	4.17	4.11	4.11
C_{TOTAL} (c€)	510.97	510.98	505.14	451.04	451.04

Table 26 bis. Results summary for full microgrid mode for June 20th 2018.

Day-ahead optimization	YES			
	Constant DG		Variable DG	
Condition	MILP results	Operational results	MILP results	Operational results
The sum of C_{BS} and C_G (c€)	4.98	54.08	8.08	57.05
C_{PV_S} (c€)	77.45	22.25	77.45	21.53
C_{L_D} (c€)	0.16	0.01	0	0.01
C_{DG} (c€)	126	471.55	119.91	461.58
C_{SC} (c€)	--	4.38	--	4.37
C_{TOTAL} (c€)	208.60	552.28	205.45	544.57

Table 26 bis. Results summary for full microgrid mode for June 20th 2018.

Day-ahead optimization	YES			
	Constant DG		Variable DG	
Condition	Ideal MILP results	Ideal Operational results	Ideal MILP results	Ideal Operational results
The sum of C_{BS} and C_G (c€)	56.69	56.75	63.85	61.60
C_{PV_S} (c€)	1.82	12.23	0	5.20
C_{L_D} (c€)	0	3.53	0	0.01
C_{DG} (c€)	390	453.82	355.45	395.52
C_{SC} (c€)	--	4.42	--	4.17
C_{TOTAL} (c€)	448.52	530.76	419.31	466.52

In Table 26, it can be seen that the total of the 15 conditions without optimization is reduced from condition 1 to condition 15; the DG has a high cost in every condition. By the comparisons in Table 26, the total cost under the condition when the total cost under condition of the operational results is higher than the total cost under the condition of ideal operational results, because the accuracy of PV and load power prediction has a big influence on power dispatching. The total cost under the condition of the operational results is less than the total cost under the condition from 1 to 5, which can give a positive proof that the optimization in the economics dispatching layer can make a good function to reduce the total cost in the real-time simulation in the operational layer on day-ahead. The total cost with variable DG power is less than the results with constant DG power under the condition of MILP results and ideal MILP results due to the loose constraints for DG power. What's more, the total cost under the condition of ideal operational results is less than the total cost under the condition of operational results because of the ideal prediction power.

The simulation results show that the effectiveness of the full microgrid supervision system compared with grid-connected and off-grid operation mode. The full microgrid with proposed supervision system can simultaneously guarantee the stability and reliability of the public grid and prevent the critical load, as long as it is designed according to minimize the overall operation cost. Also, the controlling of the DG is the key point because of its high-power tariff, which accounts for the highest proportion of the total costs. In addition, the 24 hours full microgrid with 24 hours' supervisory system is proposed for

the real case considering the actual situation, the critical load, the low load power demand, and the peak load demand in different time periods. Through the simulation, the full microgrid is proved to be directly applied to the actual system. With the applied of the full microgrid, the overall cost can be reduced with protecting the critical load, and making full use of PV generated power.

III.2. Conclusion

The simulation is designed to valid the studies presented in the chapter II considering the grid-connected mode, off-grid operation mode, and the proposed full microgrid mode with 9 hours' duration and 24 hours' duration.

In this chapter, firstly, the simulation scenario for 9 hours's duration is given, where the simulation cases are designed to separately to grid-connected mode, off-grid mode, and the full microgrid mode which is proposed combining the advantages of grid-connected and off-grid modes. Secondly, in each simulation cases, the condition of the ideal MILP is considered as the reference, which use the real recorded PV and load power profiles to replace the PV and load power production profiles to eliminate the production power error. Then, there are three weather conditions are used to valid the microgrid with different operation modes. In the end, considering the fact of the power grid's continuous operation all day, the full microgrid for 24 hours' simulation is done.

The simulation results prove the superior of the proposed full DC microgrid supervisory system, the load demand is maintained compared to the results of the grid-connected mode, the operation cost is less than the off-grid operation cost. In the full microgrid mode, the proposed supervisory system can be applied to keep the DC microgrid power balance in real-time and to reduce the overall cost by using the day-ahead optimization, as well as considering to make full use of the PV generated power with well considering the peak and valley of the public grid. In addition, a back-up source is used to well prevent the critical load.

Chapter IV. Optimization considering converter efficiency

In a DC microgrid, the converter is the key component to transfer power. Especially, the bidirectional energy converter flexibly adjusts the flow of electrical energy according to the relationship between the supply and demand of electrical energy, providing energy buffering and intelligent management for the DC microgrid. The converter efficiency is one of the important indicators of a DC microgrid. In a datasheet of a converter, the conversion power of a converter is given. If the converter works out of the power range, the power loss is much more as indicated and converter efficiency is low, and the worst case is that the conversion power is less than the power loss. In addition, the intermitted PV power generation leads to the change of the converter efficiency, which reduce the power quality in the DC microgrid with increasing the voltage fluctuation of the DC bus. Thus, it is important to consider the converter power loss for better balancing the power in a DC microgrid management. In addition, if the converter efficiency can be calculated by a mathematical model in advance, then it is convenient to increase the converter efficiency with low power loss.

Generally, the real-time controller does not consider the power loss of a converter in a microgrid. So, most of the power loss in converter shows on the bus of a microgrid. In AC microgrid, the power loss is displayed in the poor quality of the voltage and frequency of bus power. In DC microgrid, the power loss influences the voltage of the microgrid [54]. The poor-quality power increases the regulatory burdens of users' loads, even leads to a reduction in load life, and more serious equipment failure.

In the aspect of the economic cost, a high efficiency of a converter can reduce the operation cost of a microgrid. However, it is impossible to always keep the converters in the microgrid working at the highest efficiency power point because of the intermitted renewable energy sources. The optimized energy flow is constantly changing, which leads to the uncertainty of the energy loss of the microgrid. Therefore, the research and modeling of converter power loss are crucial in energy management and optimization in the microgrid.

IV.1. Description of converter modeling

The problem of power loss in switching devices is always a hotspot of scholars from various countries. The continuous increase of switching frequency makes the modeling analysis of loss largely determine the success of the design. The loss analysis of the power device is based on the switching device model. At present, there are many methods for modeling the loss of switching devices: one is an accurate model based on the specific parameters of the device. Due to the large number of specific

parameters, this model can only use computer simulation to obtain accurate results. Although it is closest to the actual situation, it requires a large amount of calculation and takes a long time. This is also the reason why the accurate model cannot be widely used in engineering. The other is the simplified analytical model of the circuit; indeed, the voltage and current instantaneous expression obtained by approximate fitting is used to express the loss. This model has a small calculation amount and can make the designer quickly concludes, and it is also convenient to analyze the loss of switching devices in different circuit environments. Therefore, it is the most commonly used loss analysis method in engineering. However, because the switching process is greatly simplified during the analysis process, the accuracy of the results obtained by the model is very dependent on the degree of simplification and the reasonableness of assumptions. In [83], a rapid loss estimation equation is proposed to provide computationally simple loss prediction under all operating conditions, where a statistical analysis method is used.

In this chapter, only a simple converter is considered, which is formed by directly connecting the insulated gate bipolar transistor (IGBT) with the surrounding inductors and capacitors, as shown in Figure 109 and Figure 110. The detailed information on the applied IGBT is shown in appendix 5.

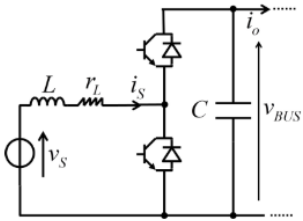


Figure 109. The boost/buck converter.

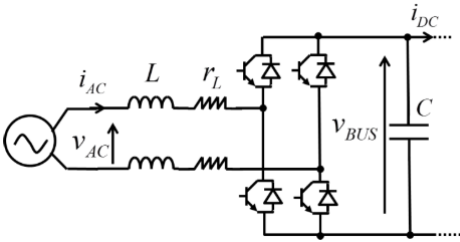


Figure 110. The single-phase full-bridge DC/AC converter.

The power loss compensation circuit, such as a dedicated buffer circuit, a phase-shifted full-bridge soft switch and auxiliary circuit, is not taken into account. The converter of this chapter simplifies the difficulty of mathematical modeling while highlighting the impact of energy conversion efficiency on the operation of the full DC microgrid in chapter II. In Figure 109, the boost/buck converter is shown, and the BS is connected to the DC bus. i_s and v_s are separately the current and voltage of the source; i_o and v_{BUS} are separately the current and voltage of DC bus. Figure 110 shows the single-phase full-bridge DC/AC converter, and the single-phase source is connected to the DC bus. i_{AC} and v_{AC} are

separately the current and voltage of the AC source; i_{DC} and v_{BUS} are separately the current and voltage of DC bus. L is the inductance for boosting voltage and power filtering.

The power losses in power electronic converters are generated in two main parts of the converter in Figure 111. Hence the losses can be divided into two parts as well: the losses in the semiconductors and the losses of the passive components. The losses in semiconductors can also be classified into two categories: the losses of conduction and the switching losses. The driving loss can be neglected because it is relatively small compared with the aforementioned losses.

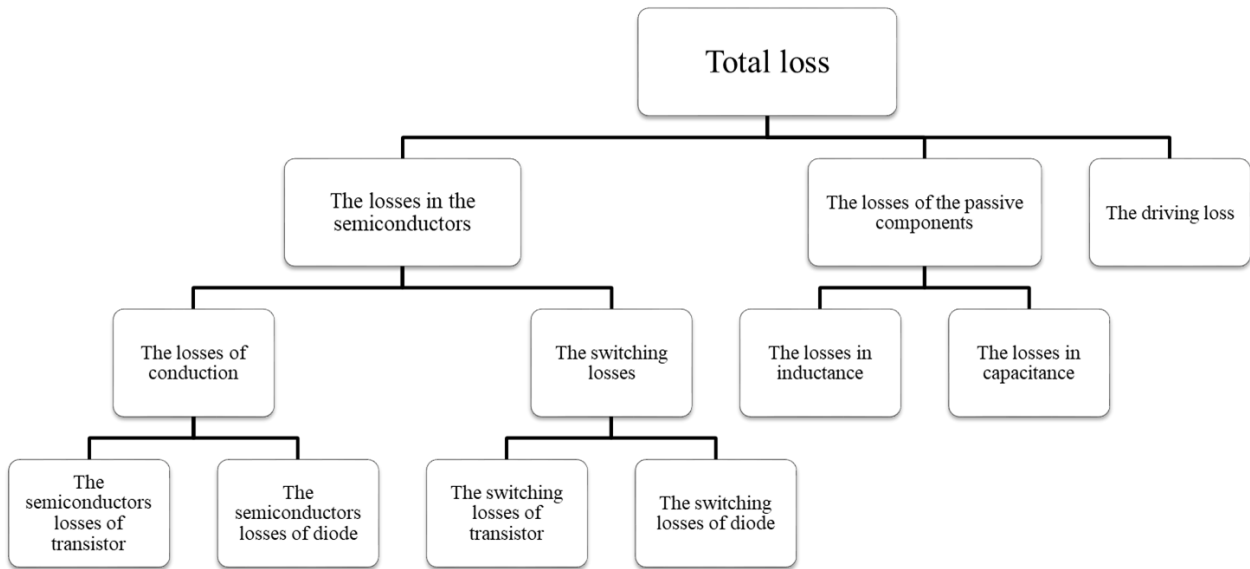


Figure 111. Power loss classification in the converter.

The converters used in the full DC microgrid are DC/DC converters and DC/AC converters. And the modeling of these two kinds of converters is slightly different. The modeling of the converter has been shown in reference [54], and the modeling of the converter is a power average model, where the instantaneous power is not taken into account.

The boost/buck converter is shown in equation (4. 1) and (4. 2). The equation (4. 1) gives the sum of the power loss: p_{condT} is the power loss of conduction in the transistor of IGBT; p_{condD} is the power loss of conduction in the diode of IGBT; p_{comT} is the switching power loss in the transistor of IGBT; p_{comD} is the switching power loss in the diode of IGBT; p_L is the power loss in inductance.

$$P_{loss_sum} = P_{condT} + P_{condD} + P_{comT} + P_{comD} + P_L \quad (4. 1)$$

Equation (4. 2) shows the detailed mathematical model.

$$\left\{ \begin{array}{l} p_{condT} = V_{CE0} \cdot |i_s(t)| \cdot d(t) + r_{CE} \cdot i_s^2(t) \cdot d(t) \\ p_{condD} = V_{F0} \cdot |i_s(t)| \cdot (1-d(t)) + r_F \cdot i_s^2(t) \cdot (1-d(t)) \\ p_{comT} = (a + b \cdot d(t) \cdot |i_s(t)| + c \cdot d(t) \cdot i_s^2(t)) \cdot \frac{V_{cc}(t)}{U_n} \cdot f \\ p_{comD} = \frac{1}{2} f \cdot V_{cc}(t) \cdot Q_{rr} \\ p_L = r_L \cdot i_s^2(t) \end{array} \right. \quad (4.2)$$

where V_{CE0} is the threshold voltage of voltage drop between the collector and the emitter of the transistor, V_{F0} is the threshold voltage of diode forward voltage drop, i_s is the source current, r_{CE} is the resistance between collector and emitter which equivalents to the sum of the resistances in the transistor, r_F is the resistance of diode, a , b , and c are the coefficients of the polynomial, V_{cc} is the direct voltage applied to diode when opening, U_n is the nominal voltage of transistor, f is the switching frequency, Q_{rr} is the reverse recovery charge, r_L is the internal resistance of the inductor coil, and d is the duty cycle of transistor turn-on.

The single-phase converter is shown in equation (4.3) and (4.4). The equation (4.4) gives the detailed mathematical model of the single-phase DC/AC converter.

$$\left\{ \begin{array}{l} \bar{i}_T = \left(\frac{1}{2\pi} + \frac{m \cdot \cos \varphi_{ph}}{8} \right) \cdot i_{ph_eff} \cdot \sqrt{2} \\ \bar{i}_D = \left(\frac{1}{2\pi} - \frac{m \cdot \cos \varphi_{ph}}{8} \right) \cdot i_{ph_eff} \cdot \sqrt{2} \\ i_{T_eff}^2 = \left(\frac{1}{8} + \frac{m \cdot \cos \varphi_{ph}}{3\pi} \right) \cdot i_{ph_eff}^2 \cdot 2 \\ i_{D_eff}^2 = \left(\frac{1}{8} - \frac{m \cdot \cos \varphi_{ph}}{3\pi} \right) \cdot i_{ph_eff}^2 \cdot 2 \end{array} \right. \quad (4.3)$$

$$\left\{ \begin{array}{l} p_{condT} = 2 \cdot (V_{CE0} \cdot \bar{i}_T + r_{CE} \cdot i_{T_eff}^2) \\ p_{condD} = 2 \cdot (V_{F0} \cdot \bar{i}_D + r_F \cdot i_{D_eff}^2) \\ p_{comT} = 2 \cdot \left(\frac{a}{2} + \frac{b}{\pi} \cdot \bar{i}_T + \frac{c}{4} \cdot i_{T_eff}^2 \right) \cdot \frac{V_{cc}(t)}{U_n} \cdot f \\ p_{comD} = \frac{1}{2} f \cdot V_{cc}(t) \cdot Q_{rr} \\ p_L = 2 \cdot r_L \cdot i_{AC_eff}^2(t) \end{array} \right. \quad (4.4)$$

where \bar{i}_T is the average current flowing through transistor, \bar{i}_D is the average current flowing through diode, i_{T_eff} is the effective current of transistor, i_{D_eff} is the effective current of diode, m is the

modulation index, φ_{ph} is the phase angle between current and voltage, i_{ph_eff} is the effective value of single-phase current, i_{AC_eff} is the AC source effective current.

There is an advantage that the parameter of the mathematical model above can be directly found in the datasheet of IGBT as shown in appendix 5, and p_{comT} is obtained by curve fitting in the datasheet of IGBT. The modeling considers the fact that the measured variables, voltage, and current, can only be measured in the side of the sources.

The switching frequency of the converter model is assumed to be fixed. In order to easily consider the power loss in a converter, only loss power is introduced to replace the real current and voltage values of the converter, and the reference [54] of the thesis gives a conclusion that voltage and current have a little influence on the power loss of the converter.

Figure 112 gives the lost power with a variable power in the boost\buck converter used between PV sources and DC bus. The lost power increases with the increased PV power.

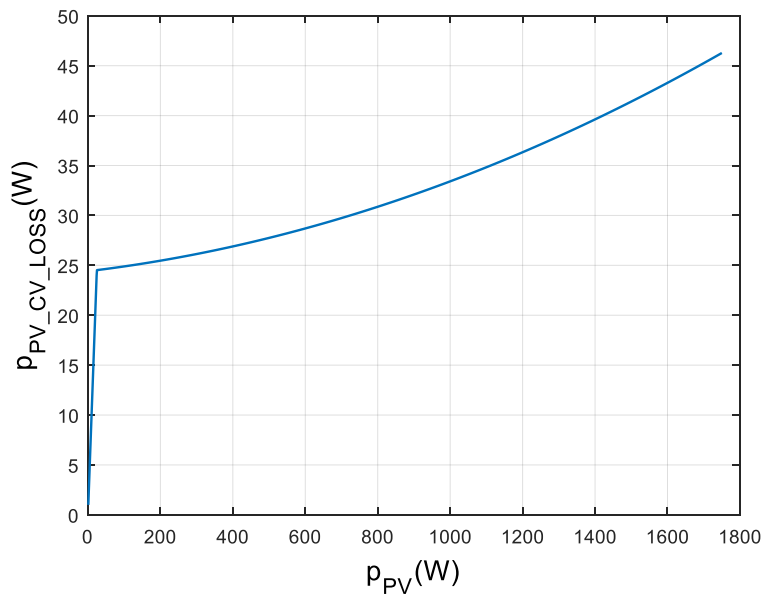


Figure 112. The power loss in the PV boost converter.

Figure 113 shows the corresponding conversion efficiency, η_{PV} , increases with increased PV power, as calculated in equation (4. 5). However, η_{PV} will decrease when the PV power is big enough with a low PV power.

$$\eta_{PV} = \frac{P_{PV} - P_{loss_sum}}{P_{PV}} \quad (4. 5)$$

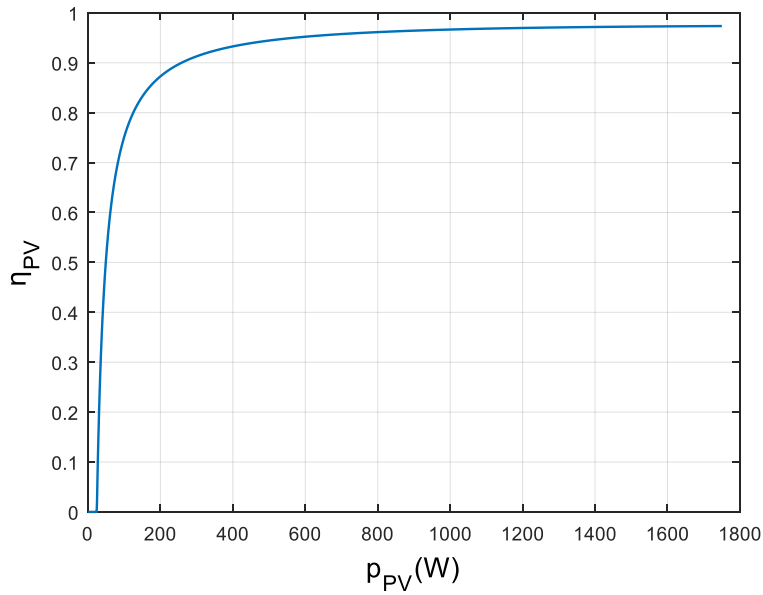


Figure 113. The power efficiency in the PV boost converter.

Though the work in [54], it can be seen that the power average modeling of converter has the sufficient accuracy in the power loss estimation.

IV.2. Power management strategy design

Power management considering the power efficiency of a converter is the key point in a microgrid to keep power balance in real-time and to increase the power quality of a microgrid for keeping the safety of the microgrid operation.

In a microgrid, the converters connect every physical component with the DC bus. So, their power efficiency is important. If the power efficiency of a converter is very low, the microgrid will supply too much more power to the converter that the microgrid is meaningless to be intelligent to manage power flow. However, a converter without power loss is not impossible.

In [84], a centralized power management control strategy that coordinates the parallel operation of grid side converters within a hybrid microgrid is presented, which operating in real-time to considering the constraints of battery and renewable energy sources with DC bus and AC bus. The advanced is that the power quality of the DC/AC bus is achieved by compensating unbalanced and nonlinear loads. Reference [85] proposes a decentralized power management strategy in an islanded microgrid by using a designed multi-loop droop controller. However, the above works do not consider the converter power loss in the controller. Reference [86] presents a comprehensive study on recent achievements of model predictive control algorithms to overcome the challenges in the real-time implementation of power converter control, in which power loss can be reduced by changing the switching frequency. In [87], a temporally coordinated energy management strategy for AC/DC hybrid microgrid considering the

dynamic conversion efficiency of a bidirectional AC/DC converter is proposed. The proposed strategy is divided into two stages: the day-ahead economic energy management stage to minimize the daily operation cost, and the day-ahead schedules of controllable units are adjusted based on intraday ultra-short-term forecast data to suppress the intraday power fluctuations induced by day-ahead forecast errors. In [88], an adaptive droop control strategy to improve the operation efficiency of microgrids under different load profiles, where an optimum solution of efficiency model is derived by Lagrange multiplier method.

In this chapter, it is chosen a converter with a suitable operating range to minimize power loss. In the full DC microgrid, intelligent management allows better control power flow and reduces energy loss.

In Figure 114, a real-time power management strategy is shown [61], where the converter loss model is considered. The real-time power management strategy can search the variable converter efficiency from the designed converter loss model and can send the control signal to the real-time controller to achieve the real-time control considering the power loss in the converter. Thus, the power management strategy not only can keep the real-time balance of the full DC microgrid but also consider the power loss in real-time control.

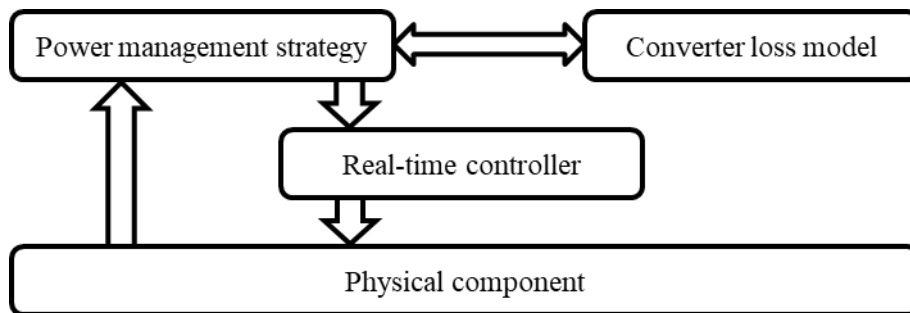


Figure 114. The power loss model in power management strategy.

IV.3. Optimization considering converter dynamic efficiency

Due to the uncertain of the power generation of renewable energy sources and the power consumption of the load demand, optimization is a method to optimize the power flow in a microgrid. However, optimization is constrained to its computation burden and complex of the deigned problem. The real microgrid is a non-linear and complex system. Thus, we need to model the system to be a simple one, or a strong and fast computation method is necessary.

In [89], a power optimization tool is proposed for an industrial microgrid considering a long-term planning and short-term energy management which are coupled via two game-theoretical frameworks. Different long-term and short-term pricing schemes are considered to provide general advice concerning the creation of a new industrial microgrid. The power loss in a microgrid is neglected in [89]. In [87] and [88], the converter power loss is considered in the optimization. The distinction is that a day-ahead

optimization used in [87], and a mathematical method used in [88] to optimize the power flow in real-time.

In this chapter, it is considered that the power loss model of a converter can be integrated into real-time optimization and long-term optimization in the full DC microgrid. However, some computation and mathematical burdens are the blocks to achieve a good result.

IV.3.1. Problem description

The full DC microgrid optimized power flow considering the power loss of the converter is shown in Figure 115. The public grid, the DG, the PV sources, the BS, and a series of DC loads are consisted to be the optimized power flow in the optimization of the full DC microgrid. The converter power loss of the DC/DC and AC/DC are integrated. The converter power loss of the DC load is assumed to be a part of the DC load.

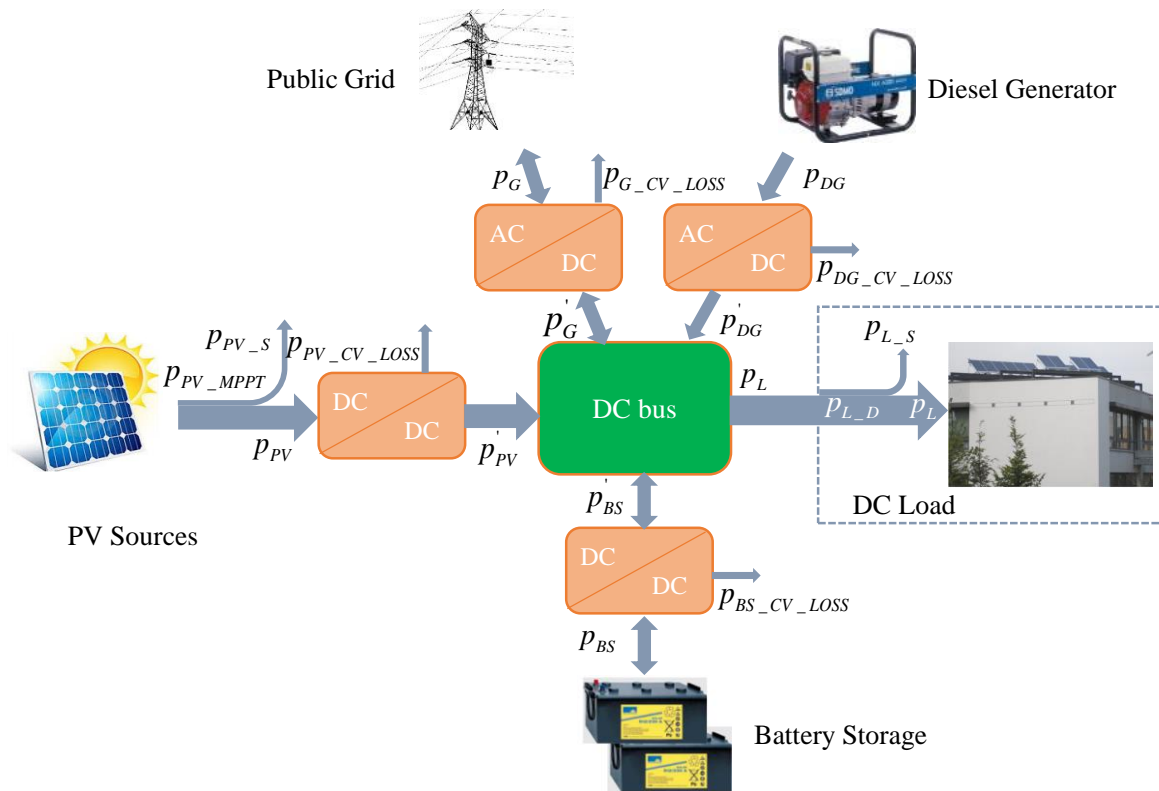


Figure 115. The optimized power flow with the power loss of converter.

The power loss models of converters are described in IV.1, which is a power average model. However, it is not easy to add the model with current and voltage directly in an optimization, which is not convex with a cubic equation. Thus, the power loss model of the converter should be simplified to be a simple function to neglect some precise in the converter model, or the random search algorithm should be applied. The optimization objective could be the real-time power in [88], the total operation cost of the full DC microgrid in [87], the environment pollution, or a multi-objective considering several different objectives to achieve Pareto-optimal [90].

From the power loss model given in IV.1, it can be seen that the total lost power is a quadratic function to the power in a converter, as shown in equation (4. 6), thus, we deal with the quadratic function for a simplified problem.

$$p_{loss}(t) = a \cdot p^2(t) + b \cdot p(t) + c \quad (4. 6)$$

IV.3.2. Problem formulation

The problem formulation should be done considering the optimization objective, and constraints of the full DC microgrid.

The objective is designed to minimize the total cost of the full DC microgrid operation in day-ahead, as shown in equation (4. 7), where the PV shedding cost, the load shedding cost, the BS cost, the public grid cost, and the DG cost are given. The detailed calculation of every cost is shown in equation (4. 8). The power loss of the converter given in equation (4. 6) is not listed here, because it is implicit in the increased energy supply from every source.

$$C_{TOTAL} = C_{PV_S} + C_{L_S} + C_{BS} + C_G + C_{DG} \quad (4. 7)$$

$$\left\{ \begin{array}{l} C_{BS} = \frac{1}{3.6 \times 10^6} \sum_{t_i=t_0}^{t_F} T_{BS}(t_i) \cdot |p_{BS}(t_i)| \cdot \Delta t \\ C_{DG} = \frac{1}{3.6 \times 10^6} \sum_{t_i=t_0}^{t_F} T_{DG_F}(t_i) \cdot p_{DG}(t_i) \cdot \Delta t + \frac{1}{3.6 \times 10^3} \sum_{t_i=t_0}^{t_F} T_{DG_O\&M}(t_i) \cdot \Delta t \cdot (p_{DG}(t_i) > 0) \\ C_{PV_S} = \frac{1}{3.6 \times 10^6} \sum_{t_i=t_0}^{t_F} T_{PV_S}(t_i) \cdot p_{PV_S}(t_i) \cdot \Delta t \\ C_{L_S} = \frac{1}{3.6 \times 10^6} \sum_{t_i=t_0}^{t_F} T_{L_S}(t_i) \cdot p_{L_S}(t_i) \cdot \Delta t \\ C_G = \frac{1}{3.6 \times 10^6} \sum_{t_i=t_0}^{t_F} T_G(t_i) \cdot (-p_G(t_i)) \cdot \Delta t \end{array} \right. \quad (4. 8)$$

The constraints of every component of the full DC microgrid are shown in equation (4. 9), where the power balance, the power constraint of every component, and the energy capacity limits of storage components are formulated. The rules of the power flow in the optimization approach the real-time power management strategy rules in IV.2, and the load shedding and PV shedding are not allowed until the BS is empty or full. The difference rule between real-time power management and the optimization problem is the optimization problem gives a larger solution space than the real-time power management to allow to pre-schedule the power flow in the full DC microgrid.

$$\begin{aligned}
s.t. \quad & \begin{cases} p_{PV}(t_i) + p_{DG}(t_i) - p_{CV_LOSS_SUM}(t_i) = p_L(t_i) + p_{BS}(t_i) + p_G(t_i) \\ p_{CV_LOSS_SUM}(t_i) = p_{PV_CV_LOSS}(t_i) + p_{DG_CV_LOSS}(t_i) + p_{BS_CV_LOSS}(t_i) + p_{G_CV_LOSS}(t_i) \\ \text{if } p_{DG}(t_i) > 0 \text{ then } p_G(t_i) = 0 \\ \text{if } SOC_{BS}(t_i) > SOC_{BS_MIN} \text{ then } p_{L_S}(t_i) = 0 \\ \text{if } SOC_{BS}(t_i) < SOC_{BS_MAX} \text{ and } p_{DG}(t_i) = 0 \text{ then } p_{PV_S}(t_i) = 0 \\ p_{DG}(t_i) = p_{DG}(t_{i-1}) \text{ if } rem(t_i / dt_{DG}) \neq 0 \quad p_{DG}(t_i) \in \{0\} \cup [p_{DG_ON_MIN} \quad p_{DG_ON_MAX}] \\ t_i = \{t_0, t_0 + \Delta t, t_0 + 2\Delta t, \dots, t_F\} \end{cases} \quad (4.9)
\end{aligned}$$

In equation (4. 10), the additional constraints group 1 gives the rules that the critical load cannot be shed and the power in the BS and public grid cannot exchange power when the diesel generating is not turned on.

additional constraints group 1:

$$\begin{aligned}
s.t. \quad & \begin{cases} \text{if } p_{PV_MPPT}(t_i) \geq p_{L_D}(t_i) \text{ then } \begin{cases} p_G(t_i) \geq 0 \\ p_{BS}(t_i) \geq 0 \end{cases} \\ \text{if } p_{PV_MPPT}(t_i) \leq p_{L_D}(t_i) \text{ and } p_{DG}(t_i) = 0 \text{ then } \begin{cases} p_G(t_i) \leq 0 \\ p_{BS}(t_i) \leq 0 \end{cases} \\ p_{L_S}(t_i) \leq (1 - k_{L_CRIT}) \cdot p_L(t_i) \end{cases} \quad (4.10)
\end{aligned}$$

The equation (4. 11) shows the additional constraints group 2, and only the critical load constraint is given, which gives a large solution space including that the power can exchange between the BS and public grid.

additional constraints group 2:

$$s.t. \quad p_{L_S}(t_i) \leq (1 - k_{L_CRIT}) \cdot p_L(t_i) \quad (4.11)$$

The power consumption in the converter is a nonlinear function. And the piecewise function is a good method to linearize the nonlinear function. Therefore, the nonlinear function is decomposed to be a piecewise function in Figure 116 and equation (4. 12).

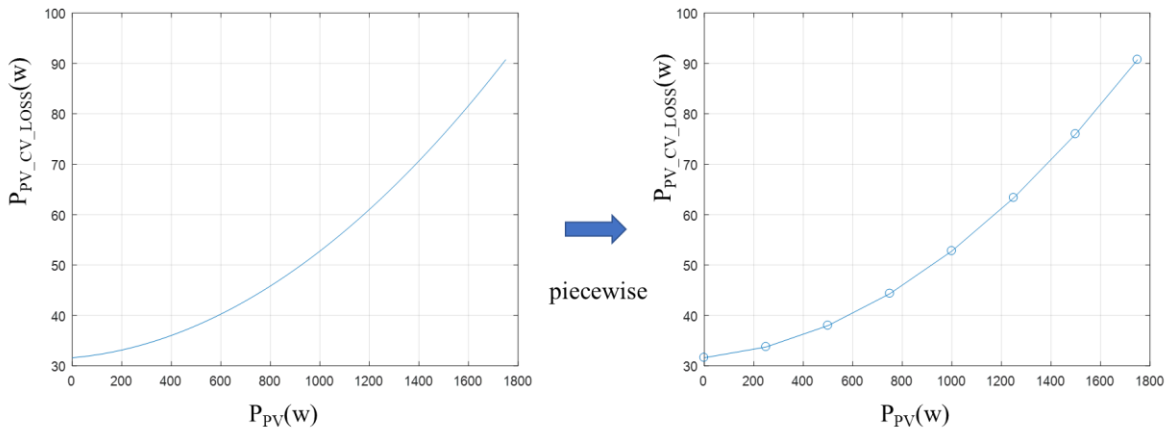


Figure 116. The power loss model in power management strategy.

$$p_{PV_CV_LOSS}(t_i) = \begin{cases} F1 & p_{PV}(t_i) < 250 \\ F2 & 500 > p_{PV}(t_i) \geq 250 \\ F3 & 750 > p_{PV}(t_i) \geq 500 \\ F4 & 1000 > p_{PV}(t_i) \geq 750 \\ F5 & 1250 > p_{PV}(t_i) \geq 1000 \\ F6 & 1500 > p_{PV}(t_i) \geq 1250 \\ F7 & p_{PV}(t_i) \geq 1750 \end{cases} \quad Fi = a_i \cdot p_{PV}(t_i) + b_i, i \in [1, 7] \cap \mathbb{Z} \quad (4. 12)$$

In Figure 116, the piecewise function approaches the original function, where some original function information is neglected. Thus, the function is given in equation (4. 12), where the indicator [71] can be used to easily formulate the function.

However, the cost is to use more indicator constraints to model a nonlinear function, thus, the piecewise function in MILP leads to so much calculation of central processing unit (CPU) that the optimization cannot be solved in a short time for a real-time optimization with data updating in the full DC microgrid. Fortunately, the day-ahead optimization allows enough time to calculate with the piecewise function in MILP.

IV.4. Simulation verification

The simulation of power management is verified in MATLAB/Simulink and the optimization is done by using CPLEX [71] in a personal computer (PC) with intel core i7-6700HQ.

IV.4.1. Simulation scenario

The simulation is designed to show the influence of the converter power loss on the full DC microgrid and give the solution to reduce the influence by using the power loss model of the converter given in IV.2 and IV.3. The parameters of IGBT can be find in appendix 5, and the switching frequency is set to be 12 kHz. There are five cases in the simulation.

The PV MPPT power, PV prediction power, the load power, and load prediction power profiles are given in III.1.5. The simulation parameters are given in III.1.5.

In Table 27, the five cases are listed in the table above based on if the power loss model of the converter is integrated in the simulation, if the power loss model of the converter efficiency is considered in the real-time power management strategy, and if the day-ahead optimization considers the power loss in the converter.

Case 1 simulates the ideal converter, i.e. without power loss. Case 2 simulates the real condition, considering the converter power loss model in the converter. Case 3 uses the converter efficiency in real-time power management based on the case 2. Case 4 uses the optimization results of the day-ahead

optimization without the converter efficiency based on the case 3. Case 5 uses the optimization results of the day-ahead optimization with the converter efficiency based on the case 3.

Case 1 and 2 are applied to show the influence of the power loss of the converter in the full DC microgrid. Case 2 and 3 are compared to show the function of the real-time power management integrated with the converter efficiency. Case 4 and 5 are respectively compared to case 3 to display the influence of the day-ahead optimization with or without the converter efficiency.

Table 27. Simulation cases.

Case	Power loss in converter	Converter efficiency in power management	Day-ahead optimization without converter efficiency	Day-ahead optimization with converter efficiency
1	NO	NO	NO	NO
2	YES	NO	NO	NO
3	YES	YES	NO	NO
4	YES	YES	YES	NO
5	YES	YES	NO	YES

IV.4.2. Simulation results

IV.4.2.1. Optimization results

The day-ahead simulation results without considering the converter loss are shown in Figure 117 and Figure 118.

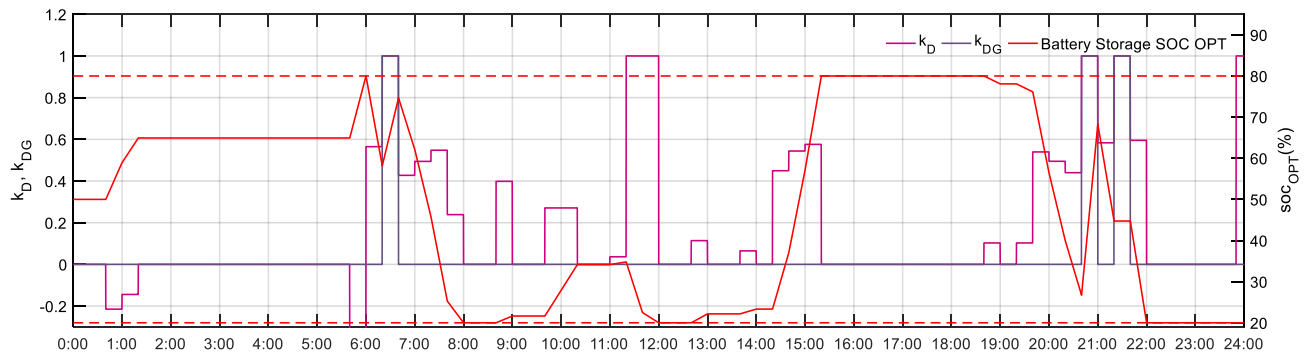


Figure 117. The day-ahead economics optimization results k_D , k_{DG} and BS SOC curves at full microgrid mode on June 20th, 2018 without converter loss.

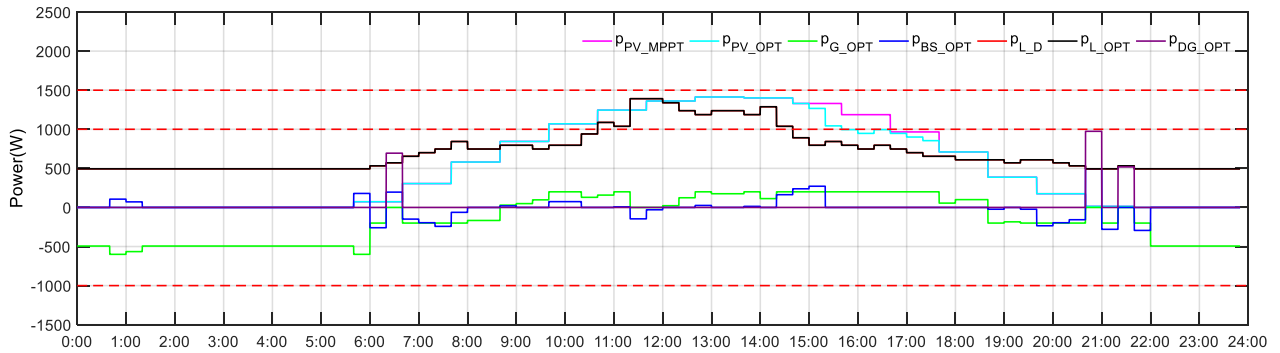


Figure 118. The day-ahead economics optimization results of power curves at full microgrid mode on June 20th, 2018 without converter loss.

In Figure 117 and Figure 118 the PV and load prediction power profiles are used; at the beginning of the optimization results, the PV power is less than the load demand power, and the BS is charged by the public grid because of the low public grid power tariff; at 6:20, the DG is turned on; at 6:40, the DG is turned off, the BS and the public grid provide power to support the load demand power; then the DG is turned on at 20:40 and 21:20. The PV shedding happens at 15:00. At the end of the optimization results, the public grid is only used to supply the load demand.

The day-ahead optimization results with considering the converter loss are shown in Figure 119, Figure 120, and Figure 121. In Figure 119 and Figure 120, the PV and load prediction power profiles are used; at the beginning of the optimization results, the PV power is less than the load demand power, the public grid is used to supply the load, the BS and the rest power of the public grid are used to cancel the power loss in converter; then, at 5:40, the BS is recharged by the public grid because of the low public grid power tariff and PV power; at 6:00, the DG is turned on; at 6:20, the DG is turned off, the BS and the public grid provide power to support the load demand power; then the DG is turned on at 7:00, 17:40, 19:40, 20:40 and 21:20. The load shedding happens at 8:20, 12:00, and 14:00. At the end of the optimization results, the public grid and BS are used to supply the load demand and power loss in the converter of the full DC microgrid.

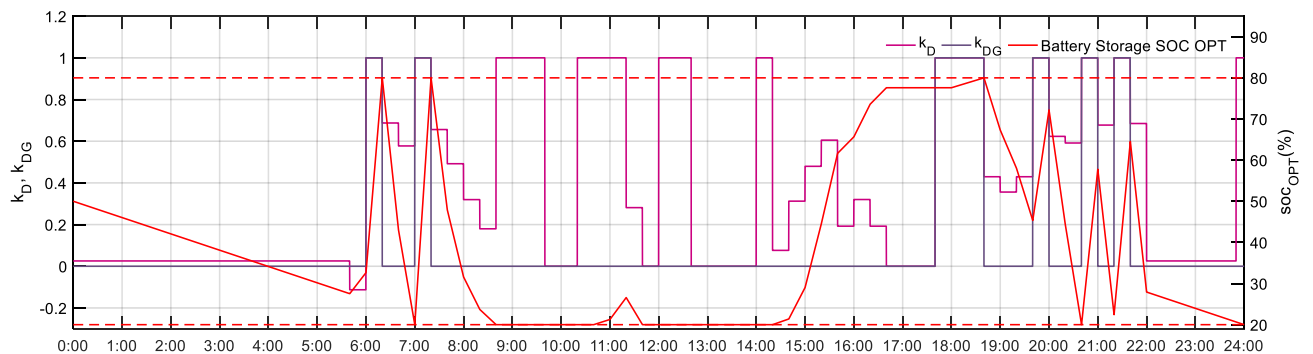


Figure 119. The day-ahead economics optimization results k_D , k_{DG} and BS SOC curves at full microgrid mode on June 20th, 2018 with converter loss.

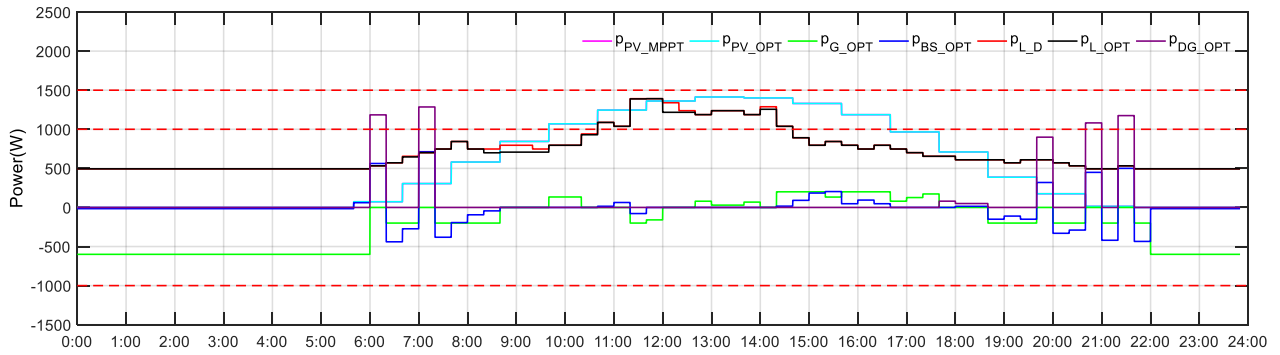


Figure 120. The day-ahead economics optimization results of power curves at full microgrid mode on June 20th, 2018 with converter loss.

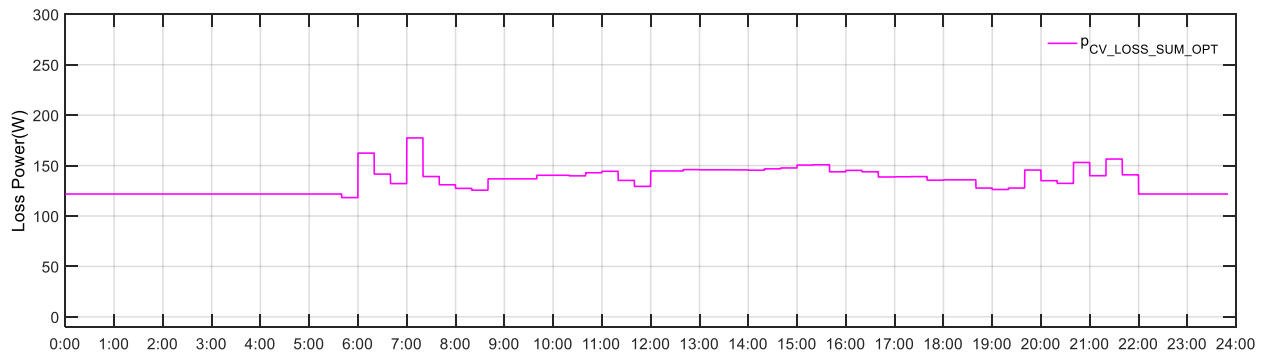


Figure 121. The day-ahead economics optimization results of converter loss power curves at full microgrid mode on June 20th, 2018.

In Figure 121, the sum of the power loss of the converter is shown. The power loss varies with the power of every source.

The day-ahead simulation results are shown in Table 28. In Table 28, it can be seen that the cost of DG in the optimization with the converter loss is more than the cost of DG in the optimization without the converter loss because of the power loss in the converters. Besides, the calculation time increases dramatically due to the power loss model in the day-ahead optimization, because of the introduction of the piecewise function for the power loss in converters. Thus, the optimization with converter loss above cannot be an optimization of real-time data update for a real-time controller in the PC.

Table 28. Simulation results of the day-ahead optimization.

	optimization without converter loss	optimization with converter loss
Cpu time (s)	0.90625	283.281
The sum of C_{BS} and C_G (c€)	11.2146	45.8134
C_G (c€)	4.17044	33.9022
C_{BS} (c€)	7.04412	11.9113
C_{PV_S} (c€)	58.3848	0
C_{L_D} (c€)	0	27.6321
C_{DG} (c€)	150.469	400.243
C_{DG_F} (c€)	87.4692	232.243
$C_{DG_O\&M}$ (c€)	63	168
C_{TOTAL} (c€)	220.069	473.688

IV.4.2.2. Real-time simulation results

The following curves show the real-time simulation results listed in Table 27.

The simulation results of case 1 are shown in Figure 122, Figure 123, and Figure 124. In Figure 122 and Figure 123, the PV and load power profiles are used; at the beginning of the optimization results, the PV power is less than the load demand power, and the public grid is used to supply the load and the BS is recharged by the public grid because of the low public grid power tariff; at 6:25, the DG is turned on; at 6:45, the DG is turned off; then the DG is turned on nine times. The PV shedding happens at 12:50 and 14:55. At the end of the optimization results, the public grid and BS are used to supply the load demand and recharge the BS.

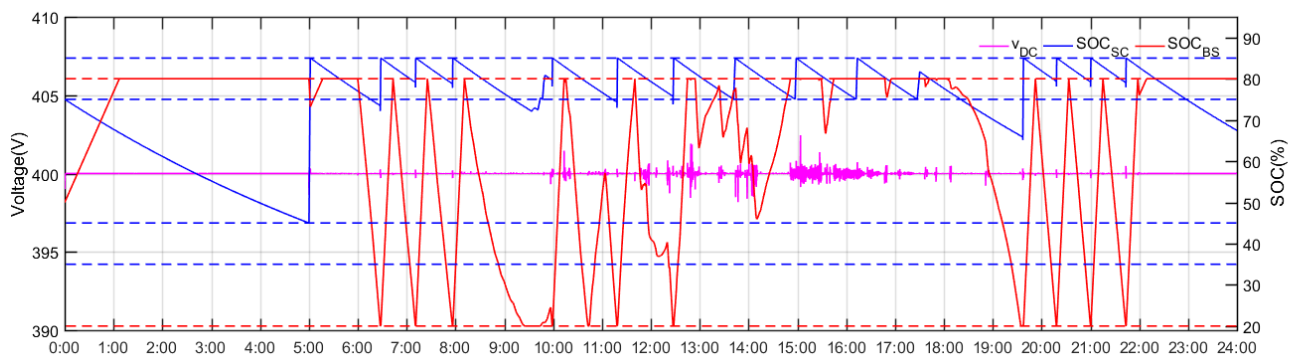


Figure 122. DC bus voltage and BS SOC curves of case 1 at full microgrid mode on June 20th, 2018.

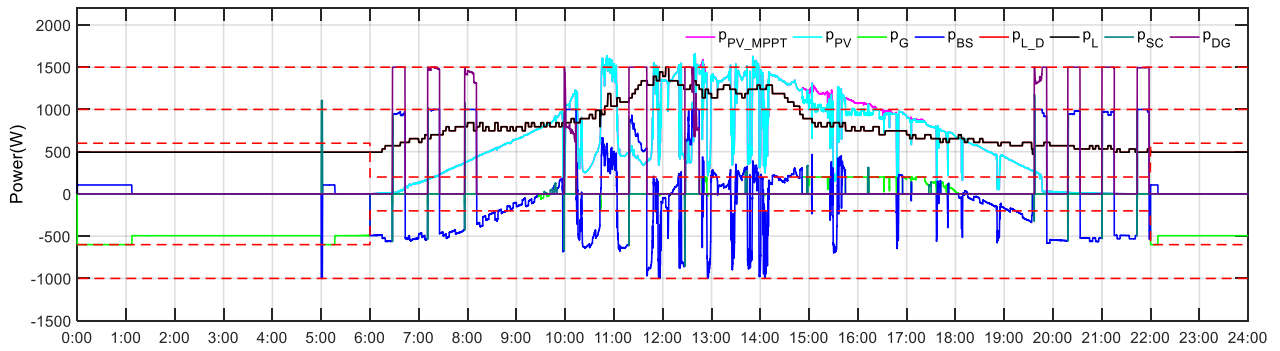


Figure 123. Power curves of case 1 at full microgrid mode on June 20th, 2018.

The simulation results of case 2 are shown in Figure 124, Figure 125, and Figure 126.

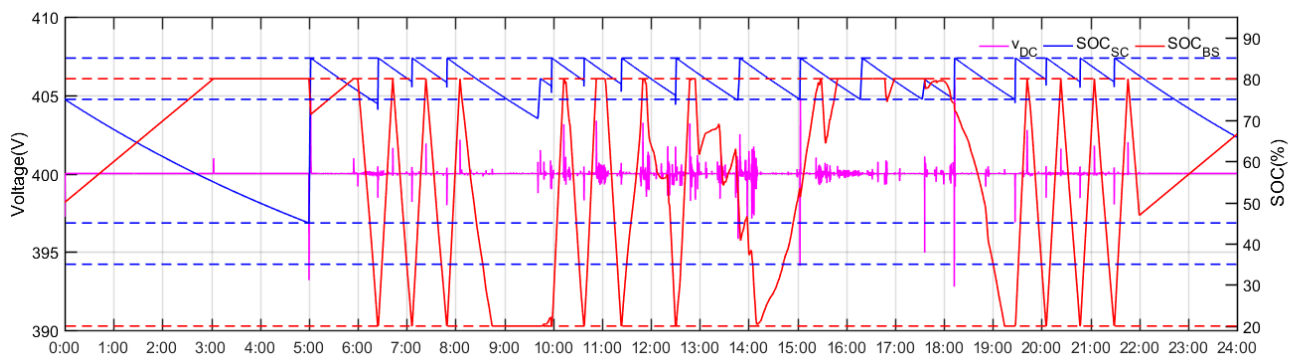


Figure 124. DC bus voltage and BS SOC curves of case 2 at full microgrid mode on June 20th, 2018.

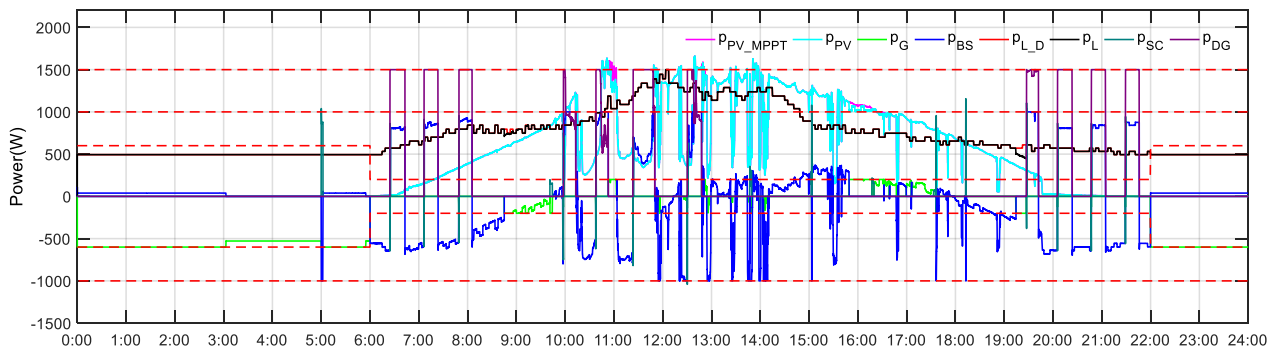


Figure 125. Power curves of case 2 at full microgrid mode on June 20th, 2018.

In Figure 124 and Figure 125, the PV and load power profiles are used; at the beginning of the optimization results, the PV power is less than the load demand power, the public grid is used to supply the load, and the rest power of the public grid is used to cancel the power loss in the converter and charge the BS; then, at 5:00, the SC is recharged by the public grid and the BS; then, the DG is turned on eleven times. The load shedding happens at 8:50 and 19:10. The PV shedding happens at 10:55 and 15:55. At the end of the optimization results, the public grid and BS are used to supply the load demand and power loss in the converter of the full DC microgrid and charge the BS.

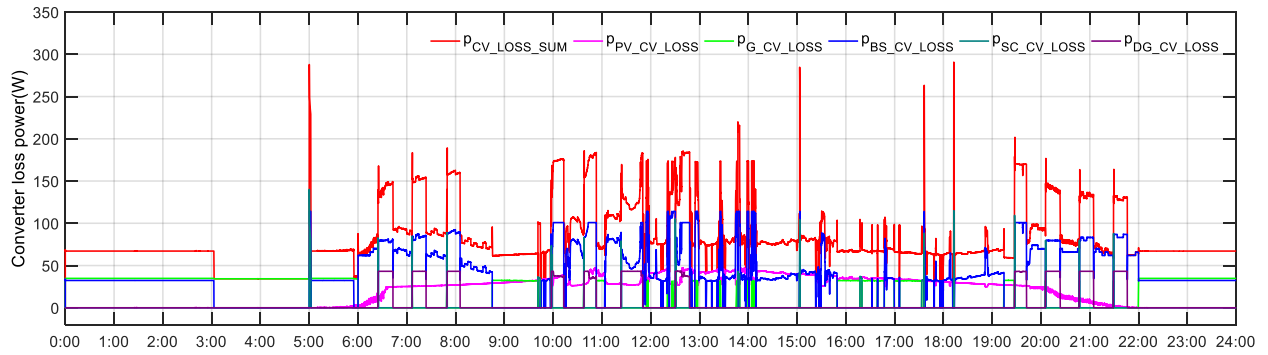


Figure 126. The converter loss power curves of case 2 at full microgrid mode on June 20th, 2018.

In Figure 126, the power loss curves of the converter of case 2 are shown. The power loss varies with the power of every source.

The simulation results of case 3 are shown in Figure 127, Figure 128, and Figure 129.

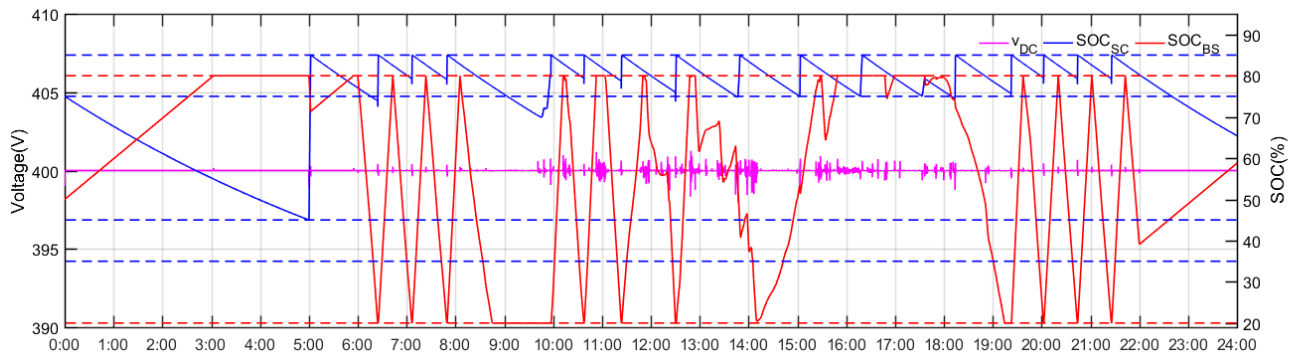


Figure 127. DC bus voltage and BS SOC curves of case 3 at full microgrid mode on June 20th, 2018.

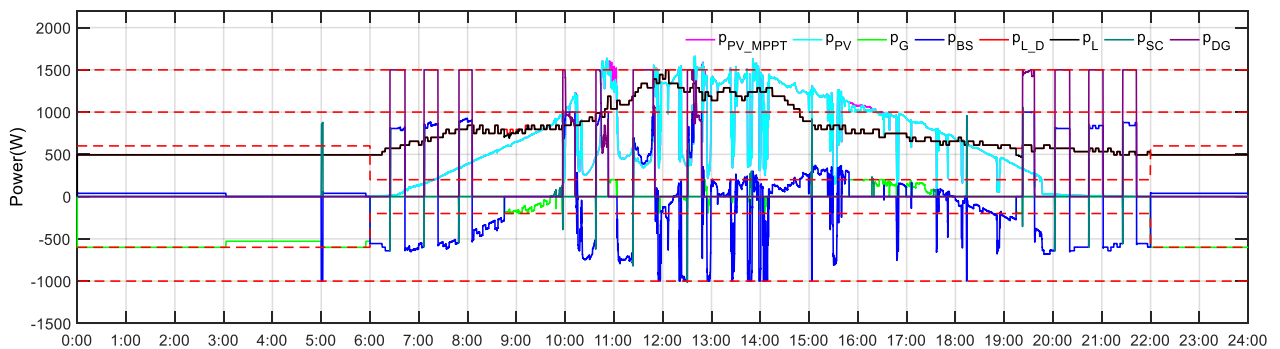


Figure 128. Power curves of case 3 at full microgrid mode on June 20th, 2018.

In Figure 127 and Figure 128, the fluctuation of the voltage of the DC bus is reduced by comparing it with the results in case 2. Compared with the results of Case 2, the power curve and the BS SOC curve have the same trend.

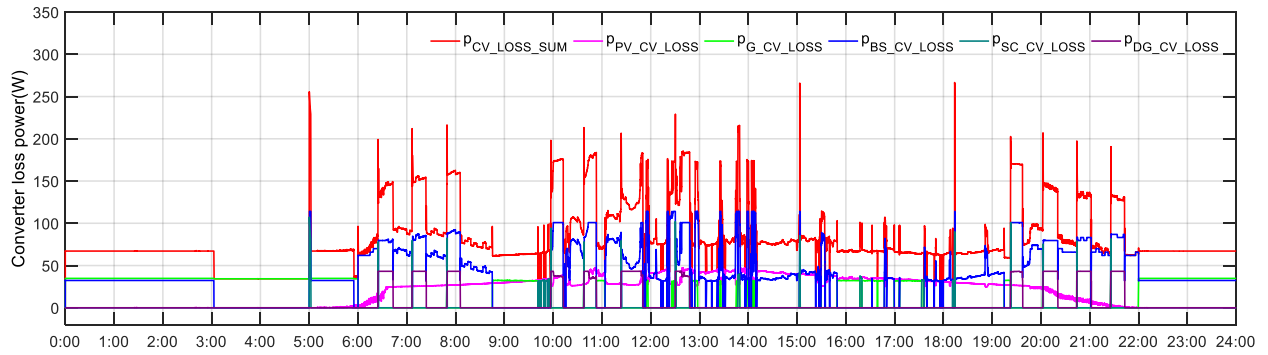


Figure 129. The converter loss power curves of case 3 at full microgrid mode on June 20th, 2018.

In Figure 129, the power loss curves of the converter of case 3 are shown. The power loss varies with the power of every source, which is almost the same as the results in case 2.

The simulation results of case 4 are shown in Figure 130, Figure 131, and Figure 132.

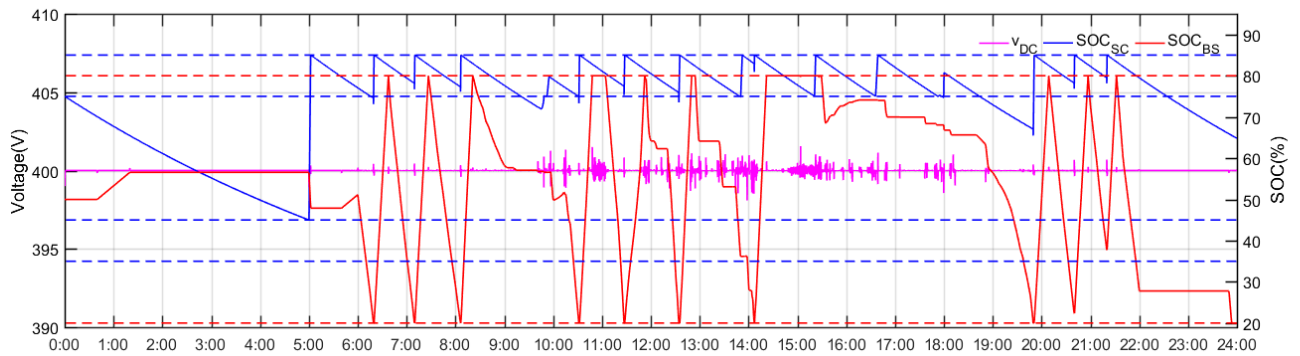


Figure 130. DC bus voltage and BS SOC curves of case 4 at full microgrid mode on June 20th, 2018.

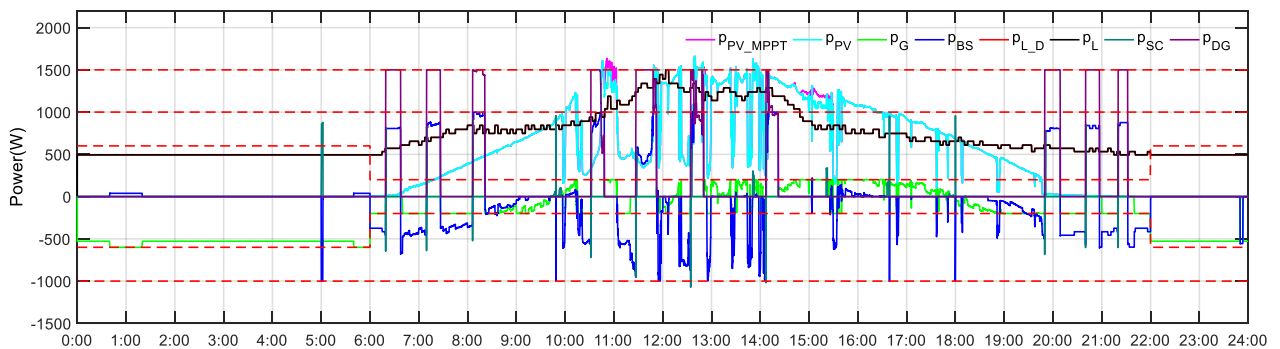


Figure 131. Power curves of case 4 at full microgrid mode on June 20th, 2018.

In Figure 130 and Figure 131, the fluctuation of the voltage of the DC bus is reduced by comparing it with the results in case 2. Compared with the results of Case 2 and case 3, the number of the DG start-up is reduced, and the BS is not recharged after 22:00.

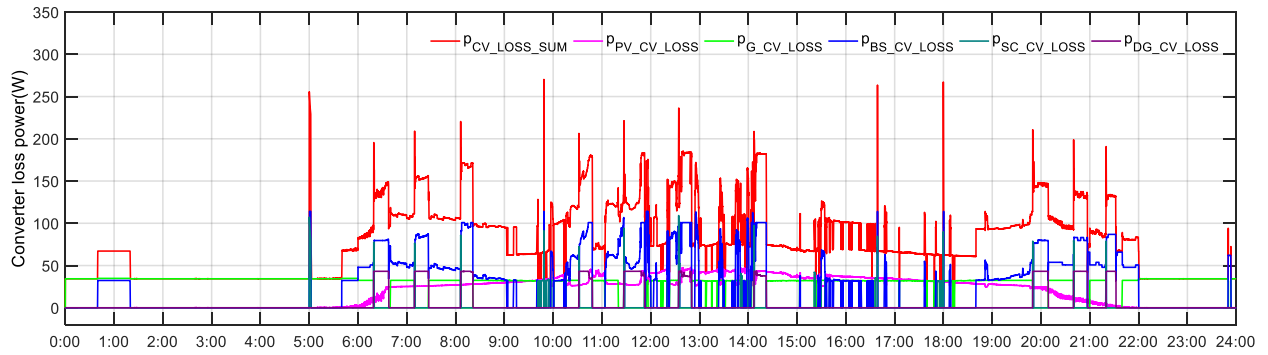


Figure 132. The converter loss power curves of case 4 at full microgrid mode on June 20th, 2018.

In Figure 132, the power loss curves of the converter of case 4 are shown. The power loss varies with the power of every source

The simulation results of case 5 are shown in Figure 133, Figure 134, and Figure 135.

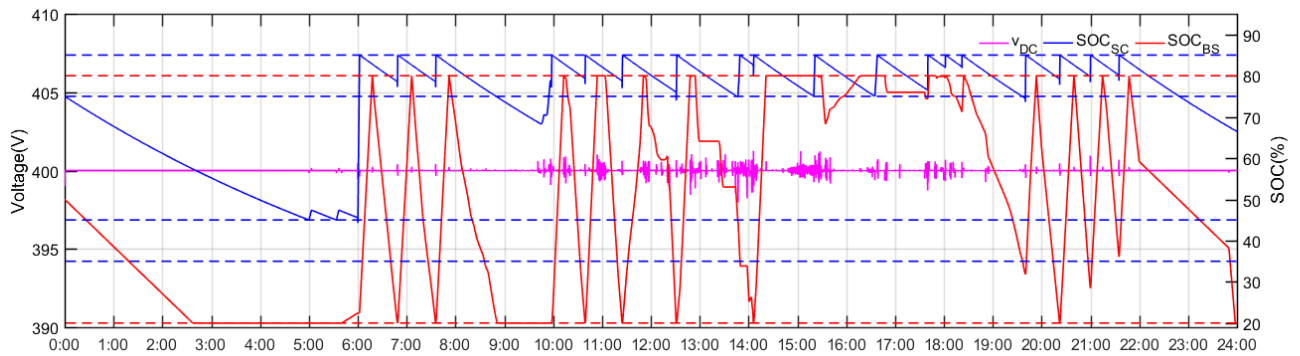


Figure 133. DC bus voltage and BS SOC curves of case 5 at full microgrid mode on June 20th, 2018.

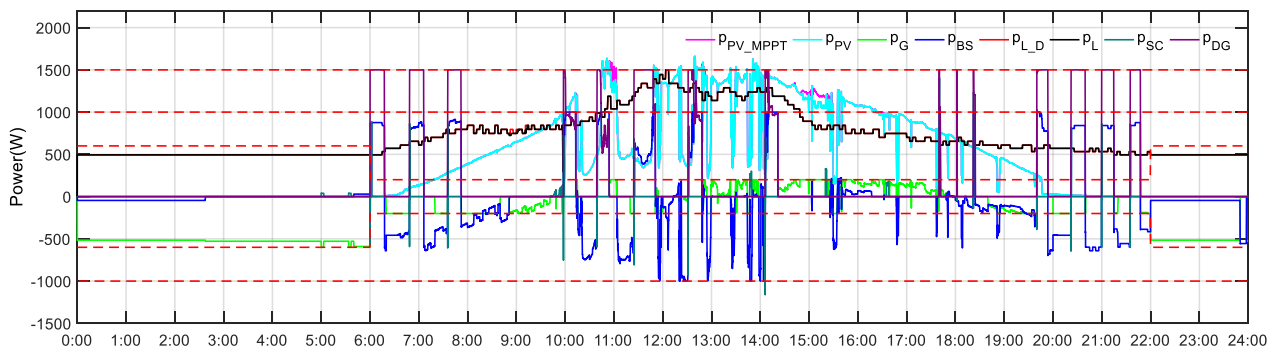


Figure 134. Power curves of case 5 at full microgrid mode on June 20th, 2018.

In Figure 133 and Figure 134, the fluctuation of the voltage of the DC bus is reduced by comparing it with the results in case 2. Compared with the results of case 4, the number of the DG start-up is increased.

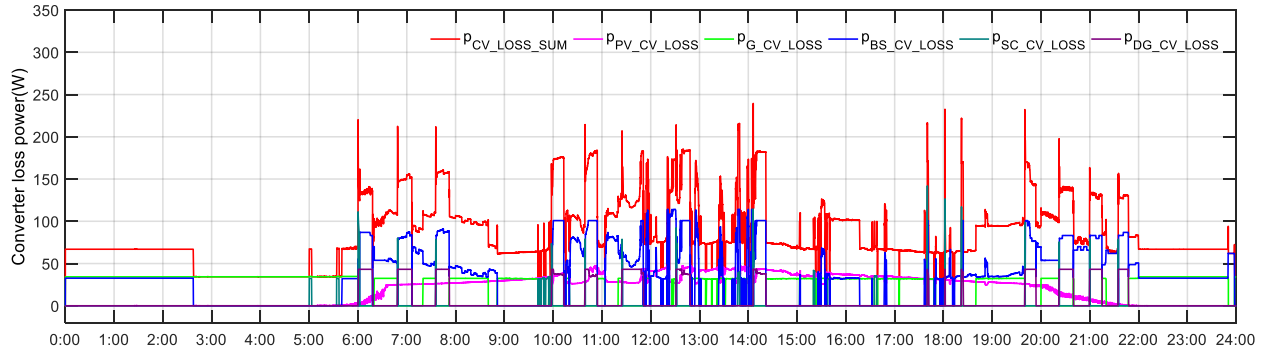


Figure 135. The converter loss power curves of case 5 at full microgrid mode on June 20th 2018.

In Figure 135, the power loss curves of the converter of case 5 are shown. The power loss varies with the power of every source.

IV.4.2.3. Simulation results comparison and analysis

The simulation results of every case are compared through the indexes: the root mean square σ_{V_BUS} , the total energy consumption of the load in the full DC microgrid E_{LOAD} , the total energy loss in all the converter in the full DC microgrid $E_{CV_LOSS_SUM}$, the total supplied energy in the full DC microgrid E_{SUPPLY} , the total cost of the full DC microgrid C_{TOTAL} , and the global efficiency of the full DC microgrid η_{GLOBAL} in Table 29.

Comparing the indexes in Table 29 and Table, the analyzes can achieve the following:

1. Comparing case 1 and case 2, the power loss in the converter can lead to a bad power quality, a high-power cost, and a low global efficiency.
2. The σ_{V_BUS} in case 3 is less than the one in case 2, which proves that the real-time power management with the power loss in the converter can increase the DC bus power quality.
3. Comparing η_{GLOBAL} and C_{TOTAL} in cases 4 within case 3, it proves that the day-ahead optimization without the power loss in the converter can increase the global power efficiency in the full DC microgrid and reduce the total cost. However, a little DC bus power quality sacrificed.
4. The η_{GLOBAL} and C_{TOTAL} in case 5 are worse than the ones in case 3, and the reason is the day-ahead optimization with the power loss in converter leads to a more power supply in the full DC microgrid.

Table 29. Simulation results of the cases.

Case	Date	σ_{V_BUS}	E_{LOAD} (kWh)	$E_{CV_LOSS_SUM}$ (kWh)
1	20062018	0.0440	17.1461	0
2	20062018	0.1847	17.1197	1.9571
3	20062018	0.0487	17.1255	1.9615
4	20062018	0.0651	17.1507	1.9105
5	20062018	0.0585	17.1363	2.0352

Table 29 bis. Simulation results of the cases.

Case	E_{SUPPLY} (kWh)	C_{TOTAL} (c€)	η_{GLOBAL}
1	17.1523	667.1596	0.9996
2	19.0814	793.3408	0.8972
3	19.0917	795.3016	0.8970
4	19.0665	743.3908	0.8995
5	19.1764	839.8600	0.8936

In general, case 4 shows the best results in the simulation above, which proves the effectiveness of the converter efficiency in power management and day-ahead optimization without considering the converter efficiency.

IV.4.3. Simulation analyzes

Based on the simulation above, it can be seen that the character of the conversion efficiency of the power converter can lead to a bad DC bus power quality in the full DC microgrid. The real-time power management considering the conversion efficiency of the power converter can reduce the bad influence of the power consumption in the converter. The day-ahead without considering the conversion efficiency of the power converter can reduce the total cost and increase the global power efficiency of the full DC microgrid. However, the day-ahead optimization with considering the conversion efficiency of the power converter gives a bad result, because the converter power consumption in the day-ahead optimization leads to a more power supply in the full DC microgrid, the most obvious increased power loss occurs at the converter connecting to the DG and the day-ahead optimization with considering the conversion efficiency controls the BS and public grid working at the same time, which also increases the power loss in the converter.

IV.5. Conclusion

The power loss in the converter has a bad influence on the power quality and safety of power supply in a full DC microgrid, and the difficulty of the control algorithm is increased. This chapter provides an effective management algorithm that depends on the accuracy of the model to increase the quality of the power supply in a full DC microgrid. In addition, this chapter proposes an optimization algorithm that considers power loss in a full DC microgrid. The simulation results show that the optimization algorithm that does not consider power loss has a better effect. The reason for this phenomenon is that the power loss of the converter leads to more frequency of the DG start-up. The power loss of the converter increases the calculation complexity in the optimization, which increases in calculation time. Therefore, in future research, a random search algorithm to improve the efficiency of optimization will be applied to considering the non-linear constraints with limited computation time.

Chapter V. PV power prediction model

In a DC microgrid supervisory system, taking into account the complexity of PV power prediction, the laboratory separates PV power prediction from the research of DC microgrid as another research direction. Therefore, this thesis in chapter 2 firstly uses the existing PV power prediction method, which is a simple model using the data directly obtained from website, to construct the full DC microgrid supervision system, and verifies the feasibility of the system. And then, we think increasing the times of optimization and accuracy of power prediction can improve the performance of the supervisory system.

Thus, we conduct research on PV power prediction in chapter 5 to be ready for real-time optimization.

In a DC microgrid, the optimization is very important to achieve intelligent power management in reducing the cost of the microgrid. However, it is highly dependent on the prediction of renewable energy and load [74]. In a building, load forecasting depends on the organization's users or personnel composition and some user or personal habits. Therefore, in the short-term load forecast relative to tertiary buildings development, it can be assumed that the predicted load does not change much from historical load data. The renewable energy prediction like PV power relies mainly on solar irradiation and PV cell temperature. In reference [91], some mathematical models connecting PV cell temperature and air condition are compared. The reference [92] shows some methods to predict the solar irradiation based on different prediction periods, sky images, statistical learning methods, satellite imagery, numerical weather prediction with model output statistics, and climatology. However, the calculation cost will be high to consider the influence of clouds, aerosols, and other atmospheric constituents, and also PV panel efficiency. The reference [93] and [94] give some more mathematic model to predict the solar irradiation based on the solar position and historical data. In reference [95], a simplified clear sky solar irradiation method is provided to be an easy way based on the position of the solar panels relative to the sun. In this chapter, we focus on the simple mathematic model based on the position because the model can be reliably applied in day-ahead [96-98] only with local computation. The day-ahead optimization is considered and used to schedule the power flow as in chapter II and IV. In day-ahead optimization the PV power prediction is an hourly prediction, is not enough for real-time optimization. The real-time optimization [99-101] is applied to manage the power flow in real-time need real-time PV power prediction data update with enough accuracy. In addition, the clear sky solar irradiation method can be used in real-time with the local real-time information, such as: cloud position, real-time atmospheric transmittance, etc.

V.1. Solar irradiation prediction model

V.1.1. Clear sky model

The clear sky model is based on the location of the PV panel. The basic calculation is the conversion between the local time and solar time, which is described as detail in references [93] and [94].

In reference [95] the detailed of the simplified clear sky model is shown. The beam radiation on earth can be simply expressed as equation (5. 1).

$$g_b = g_{sc} \cdot T^n \quad (5. 1)$$

where g_b is the beam radiation on earth, g_{sc} is the extra-terrestrials solar irradiation, T is the atmospheric transmittance for short wave solar irradiance, and n is the air mass coefficient approximately provided in equation (5. 2).

$$n = \frac{1}{\cos(\theta_z)} \quad (5. 2)$$

where θ_z is the local zenith angle.

The beam radiation on a given sloped surface is given as equation (5. 3).

$$g_{bg} = g_b \cdot \cos(\theta) \quad (5. 3)$$

where θ is the angle of incidence between the beam irradiance on the surface and the normal to the surface, which is approximately expressed in equation (5. 4).

$$\cos(\theta) = \begin{cases} \sin(\delta) \cdot \sin(\varphi) \cdot \cos(\beta) - \sin(\delta) \cdot \cos(\varphi) \cdot \cos(\beta) \cdot \cos(\gamma) + \\ \cos(\delta) \cdot \cos(\varphi) \cdot \cos(\beta) \cdot \cos(\omega) + \cos(\delta) \cdot \sin(\varphi) \cdot \sin(\beta) \cdot \cos(\gamma) \cdot \cos(\omega) \\ + \cos(\delta) \cdot \sin(\varphi) \cdot \sin(\gamma) \cdot \sin(\omega) \end{cases} \quad (5. 4)$$

where δ is the declination of the sun at solar noon, φ is local latitude, β is the slope angle between the plane and horizontal, γ is surface azimuth angle, ω is hour angle.

The diffuse radiation is shown in equation (5. 5).

$$g_{dg} = 0.3 \cdot (1 - T^n) \cdot \frac{(1 + \cos(\beta))}{2} g_{sc} \cdot \cos(\theta) \quad (5. 5)$$

Therefore, the total radiation on a surface is the sum of the beam radiation and diffuse radiation in equation (5. 6).

$$g_{tg} = g_{bg} + g_{dg} \quad (5. 6)$$

V.1.2. *Météo France model*

The *Météo France* model makes an hourly forecast several times per day including the accumulated ground solar radiation in J/m^2 . Since the data is free and sometimes the data is missing or cannot be updated in time, this data is suitable for application in day-ahead optimization. The advantage of the *Météo France* model is to save the local computing resources.

V.2. *Supervisory system in a full DC microgrid*

In this chapter, two solar prediction models are compared by applying them into the supervisory system in a full DC microgrid in Figure 136.

In Figure 136. The real-time power management can deal with the real-time power flow to achieve the transient power balance in the full DC microgrid. The optimization can achieve long-term energy schedule in the full DC microgrid to reducing the total operation cost. In the optimization, the real-time optimization concerns the short-time energy management, the day-ahead optimization handles the energy management of the whole day. Besides, the power prediction can give the prediction results for the optimization based on the metadata.

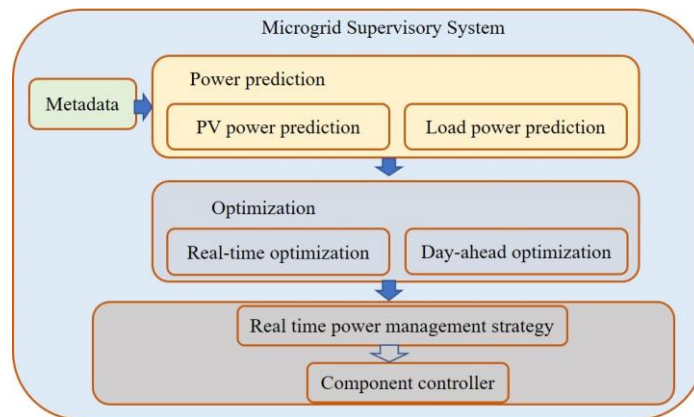


Figure 136. The supervisory system structure in a full DC microgrid with the power prediction model.

V.3. *Simulation verification*

The full DC microgrid simulation based on two solar prediction models is verified in MATLAB/Simulink; note that the optimization is done by using CPLEX [71].

V.3.1. Simulation scenario

The simulation is designed to evaluate the clear sky model by giving a comparison between the clear sky model and the Météo France model on the influence of the operation cost of the full DC microgrid considering the converter efficiency. The quality of the evaluation of the clear sky model should not be limited to only a few months of data. We should use at least one year of data to evaluate the model. As the comparison data from Météo France, the data on some days cannot be got. Thus, we use only the data on the 15th of every month. And the 12 simulation results by using the clear sky model are compared with the 12 results by using the data from Météo France. There are three cases in the simulation, and every case is simulated 24 times in one year.

The PV MPPT is calculated according to the recorded date in solar irradiation sensor installed beside the PV, the PV prediction power profiles are provided in the two models before. The load and load prediction power profiles are assumed to be the same every day given in II.6.5. The simulation parameter is given in II.6.5.

Table 30. Simulation cases.

Case	Power loss in converter	Converter efficiency in power management	Day-ahead optimization without converter efficiency
1	NO	NO	YES
2	YES	NO	YES
3	YES	YES	YES

In Table 30, the three cases are listed in the table above based on if the power loss model of the converter is integrated into the simulation, if the power loss model of the converter efficiency is considered in the real-time power management strategy, and the day-ahead optimization without considering the power loss in the converter.

Case 1 simulates the ideal converter without power loss. Case 2 simulates the real condition, considering the converter power loss model in the converter. Case 3 uses the converter efficiency in real-time power management based on case 2. Among the three cases, the day-ahead optimization without converter efficiency by using the clear sky model and Météo France model are applied.

The three cases are applied to show the influence of the clear sky model and Météo France model in operation cost of the full DC microgrid if considering the power loss of the converter in the full DC microgrid or the real-time power management integrated with the converter efficiency.

V.3.2. Simulation results

The simulation results of the three cases are given in V.3.2.1. The cost of every component in a full DC microgrid is compared below.

V.3.2.1. Cases study results

V.3.2.1.1 Case 1

The following results show the simulation of case 1 listed in Table 31 and Table 32.

In Table 31, the results by using the clear sky model are given. The highest total cost varies as the change of the season. The total cost in winter is higher than the total cost in summer, and the highest total cost is in January, the lowest total cost is in May.

Table 31. Simulation results of case 1 of the clear sky model.

Data	15/08/2018	15/09/2018	15/10/2018	15/11/2018	15/12/2018	15/01/2019
The sum of C_{BS} and C_G (c€)	110.90	111.96	103.21	94.69	100.88	96.96
C_{PV_S} (c€)	0.09	1.51	0	0	0	0
C_{L_D} (c€)	34.80	3.92	0.07	51.10	53.28	48.81
C_{DG} (c€)	1373.39	1061.41	1203.55	1854.75	1817.58	1869.46
C_{SC} (c€)	5.17	5.07	5.14	5.60	5.58	5.58
C_{TOTAL} (c€)	1524.37	1183.89	1311.98	2006.16	1977.33	2020.83

Table 31 bis. Simulation results of case 1 of the clear sky model.

Data	15/02/2019	15/03/2019	15/04/2019	15/05/2019	15/06/2019	15/07/2019
The sum of C_{BS} and C_G (c€)	99.13	101.32	90.22	47.74	74.13	49.28
C_{PV_S} (c€)	0	0	0	30.15	46.40	11.26
C_{L_D} (c€)	0.01	47.64	0.01	0.01	0.65	0.01
C_{DG} (c€)	1238.18	1761.47	517.32	316.08	478.04	390.75
C_{SC} (c€)	5.14	5.39	4.32	4.047	4.50	4.28
C_{TOTAL} (c€)	1342.48	1915.83	611.88	398.05	603.73	455.60

In Table 32, the results by using the Météo France model are given. The highest total cost is in January; the lowest total cost is in May like the results of the clear sky model.

Table 32. Simulation results of case 1 of the Météo France model.

Data	15/08/2018	15/09/2018	15/10/2018	15/11/2018	15/12/2018	15/01/2019
The sum of C_{BS} and C_G (c€)	107.62	109.04	94.50	94.42	99.06	100.90
C_{PV_S} (c€)	0.54	4.08	0	0	0	0
C_{L_D} (c€)	32.76	5.43	0.01	46.17	54.92	53.75
C_{DG} (c€)	1367.35	1043.93	1302.68	1855.32	1834.79	1855.08
C_{SC} (c€)	5.11	4.87	5.33	5.59	5.58	5.50
C_{TOTAL} (c€)	1513.40	1167.37	1402.54	2001.52	1994.37	2015.25

Table 32 bis. Simulation results of case 1 of the Météo France model.

Data	15/02/2019	15/03/2019	15/04/2019	15/05/2019	15/06/2019	15/07/2019
The sum of C_{BS} and C_G (c€)	107.98	97.06	87.15	49.33	65.40	50.03
C_{PV_S} (c€)	0	0	0	5.67	51.20	9.19
C_{L_D} (c€)	0.01	55.93	0.01	1.66	0.41	1.83
C_{DG} (c€)	1204.03	1799.30	530.43	315.84	540.53	388.92
C_{SC} (c€)	5.12	5.54	4.32	4.09	4.60	4.28
C_{TOTAL} (c€)	1317.15	1957.85	621.93	376.62	662.15	454.27

To compare the simulation results, the cost of the PV shedding and the load shedding and the total cost are respectively shown in Figure 137, Figure 138, and Figure 139.

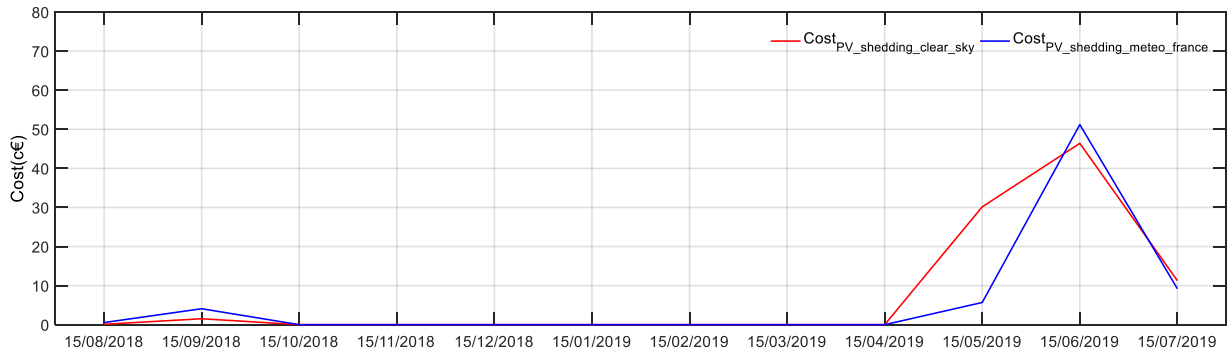


Figure 137. The PV shedding cost comparison between the clear sky model and the Météo France model.

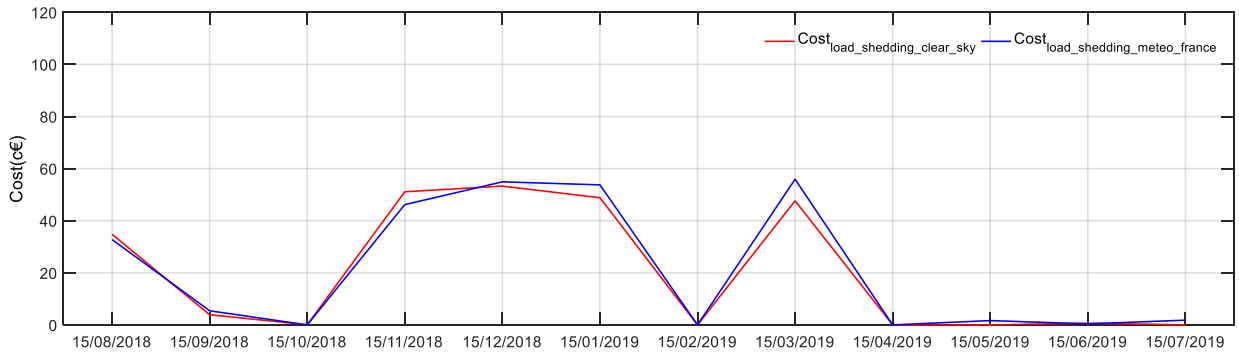


Figure 138. The load shedding cost comparison between the clear sky model and the Météo France model.

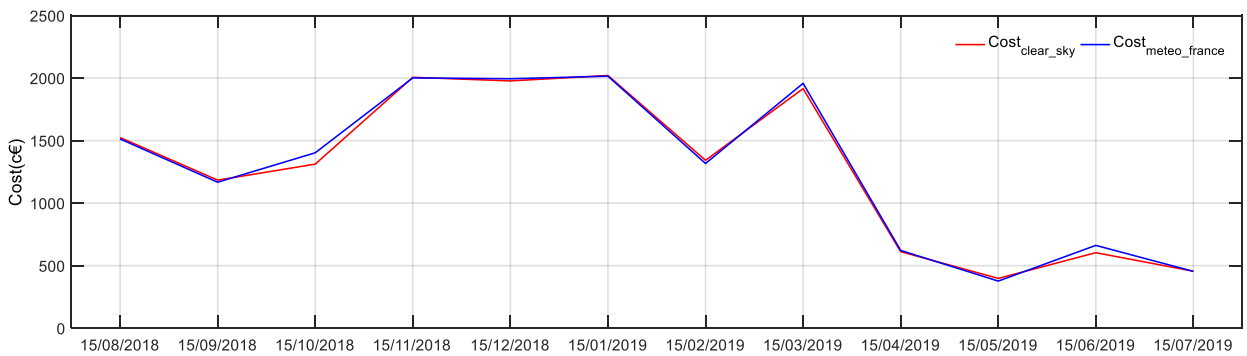


Figure 139. The total cost comparison between the clear sky model and the Météo France model.

In Figure 137, Figure 138, and Figure 139, the results of the clear sky model are similar to the results of the Météo France model. Furthermore, comparing Figure 137 and Figure 139, it can be seen that the cost of PV shedding is high while the total cost is low. And comparing Figure 138 and Figure 139, a similar phenomenon is shown that the cost of load shedding is high while the total cost is high.

V.3.2.1.2 Case 2

The following simulation gives the simulation results of case 2 listed in Table 33 and Table 34. In Table 33, the results by using the clear sky model are given. The highest total cost happens in December, and the lowest total cost happens in May, which also respects the results in case 1.

Table 33. Simulation results of case 2 of the clear sky model.

Data	15/08/2018	15/09/2018	15/10/2018	15/11/2018	15/12/2018	15/01/2019
The sum of C_{BS} and C_G (c€)	104.06	110.24	102.89	83.07	82.00	87.52
C_{PV_S} (c€)	0	0	0	0	0	0
C_{L_D} (c€)	72.28	14.11	28.41	98.65	95.48	97.46
C_{DG} (c€)	1677.94	1394.46	1520.44	2142.27	2182.55	2169.43
C_{SC} (c€)	5.25	5.26	5.33	5.45	5.62	5.48
C_{TOTAL} (c€)	1859.55	1524.08	1657.08	2329.46	2365.66	2359.91

Table 33 bis. Simulation results of case 2 of the clear sky model.

Data	15/02/2019	15/03/2019	15/04/2019	15/05/2019	15/06/2019	15/07/2019
The sum of C_{BS} and C_G (c€)	101.83	96.63	96.41	62.59	77.66	64.93
C_{PV_S} (c€)	0	0	0	0	20.81	0
C_{L_D} (c€)	11.65	68.72	24.51	3.44	0.92	9.03
C_{DG} (c€)	1589.21	2122.70	685.87	452.44	697.32	574.61
C_{SC} (c€)	5.41	5.65	4.36	4.23	4.61	4.49
C_{TOTAL} (c€)	1708.12	2293.70	811.16	522.72	801.34	653.07

In Table 34, the results by using the Météo France model are given. The highest total cost also happens in December, and the lowest total cost happens in May, which is similar to the results in the clear sky model.

Table 34. Simulation results of case 2 of the Météo France model.

Data	15/08/2018	15/09/2018	15/10/2018	15/11/2018	15/12/2018	15/01/2019
The sum of C_{BS} and C_G (c€)	102.17	108.37	94.92	87.18	82.98	94.97
C_{PV_S} (c€)	0	0	0	0	0	0
C_{L_D} (c€)	51.73	28.55	18.74	90.93	93.28	88.51
C_{DG} (c€)	1665.63	1369.93	1620.32	2159.83	2182.45	2155.63
C_{SC} (c€)	5.16	5.22	5.45	5.51	5.62	5.47
C_{TOTAL} (c€)	1824.70	1512.08	1739.44	2343.46	2364.34	2344.59

Table 34 bis. Simulation results of case 2 of the Météo France model.

Data	15/02/2019	15/03/2019	15/04/2019	15/05/2019	15/06/2019	15/07/2019
The sum of C_{BS} and C_G (c€)	96.94	89.30	98.25	63.53	74.78	64.16
C_{PV_S} (c€)	0	0	0	0	33.93	0
C_{L_D} (c€)	11.65	93.59	18.37	5.47	1.28	9.31
C_{DG} (c€)	1607.21	2112.90	730.14	467.95	791.77	568.22
C_{SC} (c€)	5.48	5.58	4.53	4.27	4.88	4.48
C_{TOTAL} (c€)	1721.29	2301.38	851.31	541.23	906.65	646.18

The cost of the PV shedding and the load shedding and the total cost are respectively shown in Figure 140, Figure 141, and Figure 142.

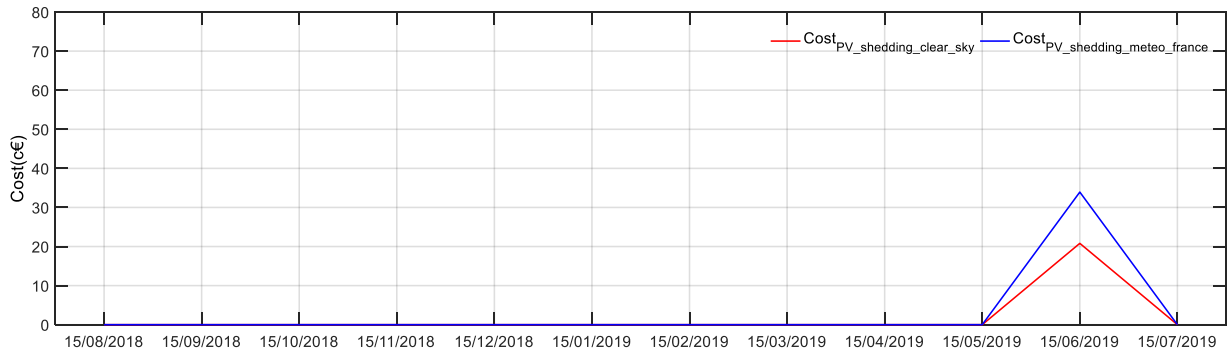


Figure 140. The PV shedding cost comparison between the clear sky model and the Météo France model.

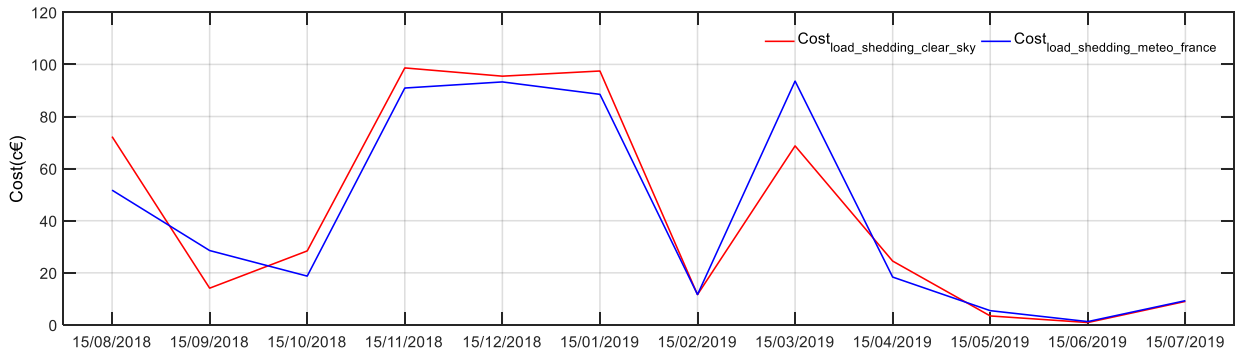


Figure 141. The load shedding cost comparison between the clear sky model and the Météo France model.

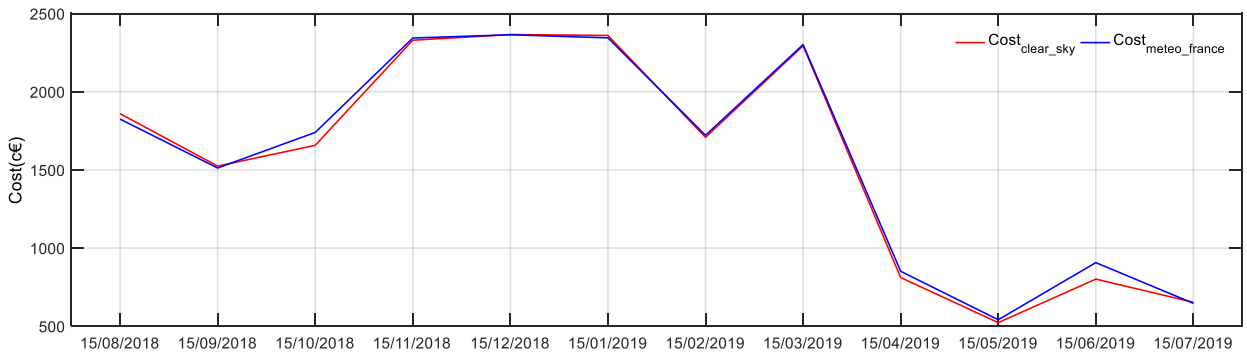


Figure 142. The total cost comparison between the clear sky model and the Météo France model.

In Figure 140, Figure 141, and Figure 142, we can draw similar results like the ones shown in case 1. The difference is that the cost of the PV shedding between the clear sky mode and the Météo France model has a bigger difference than the results in case 1. The load shedding is higher than the results in case 1 because of the power loss in the converter.

V.3.2.1.3 Case 3

The following simulation gives the simulation results of case 3 listed in Table 35 and Table 36. In Table 35, the results by using the clear sky model are given. These results are almost similar to the clear sky model in case 2.

Table 35. Simulation results of case 3 of the clear sky model.

Data	15/08/2018	15/09/2018	15/10/2018	15/11/2018	15/12/2018	15/01/2019
The sum of C_{BS} and C_G (c€)	103.63	109.73	103.74	82.78	82.30	87.44
C_{PV_S} (c€)	0	0.05	0	0	0	0
C_{L_D} (c€)	64.84	14.27	18.52	100.86	96.08	98.89
C_{DG} (c€)	1705.57	1402.80	1540.34	2148.72	2187.67	2175.49
C_{SC} (c€)	5.25	5.28	5.37	5.47	5.63	5.50
C_{TOTAL} (c€)	1879.30	1532.15	1667.97	2337.84	2371.69	2367.32

Table 35. Simulation results of case 3 of the clear sky model.

Data	15/02/2019	15/03/2019	15/04/2019	15/05/2019	15/06/2019	15/07/2019
The sum of C_{BS} and C_G (c€)	101.31	96.57	101.71	61.32	77.84	65.82
C_{PV_S} (c€)	0	0	0	0	22.51	0
C_{L_D} (c€)	11.81	69.53	10.51	5.80	8.04	1.29
C_{DG} (c€)	1592.66	2129.64	684.83	468.38	694.45	601.62
C_{SC} (c€)	5.40	5.65	4.29	4.21	4.61	4.48
C_{TOTAL} (c€)	1711.19	2301.40	801.34	539.73	807.46	673.23

In Table 36, the results by using the Météo France model are given. These results are almost similar to the Météo France model in case 2.

Table 36. Simulation results of case 3 of the Météo France model.

Data	15/08/2018	15/09/2018	15/10/2018	15/11/2018	15/12/2018	15/01/2019
The sum of C_{BS} and C_G (c€)	102.45	107.91	95.51	86.92	83.34	94.94
C_{PV_S} (c€)	0	0	0	0	0	0
C_{L_D} (c€)	51.99	15.74	18.90	93.11	94.26	89.39
C_{DG} (c€)	1671.24	1379.39	1624.72	2165.76	2187.31	2161.72
C_{SC} (c€)	5.18	5.17	5.45	5.52	5.63	5.48
C_{TOTAL} (c€)	1830.88	1508.22	1744.60	2351.32	2370.56	2351.55

Table 36. Simulation results of case 3 of the Météo France model.

Data	15/02/2019	15/03/2019	15/04/2019	15/05/2019	15/06/2019	15/07/2019
The sum of C_{BS} and C_G (c€)	97.80	89.56	96.50	61.83	75.76	60.64
C_{PV_S} (c€)	0	0	0	0	33.00	9.82
C_{L_D} (c€)	11.80	94.41	9.38	8.19	2.01	1.29
C_{DG} (c€)	1614.79	2118.33	732.49	465.83	790.77	612.87
C_{SC} (c€)	5.49	5.59	4.45	4.20	4.79	4.45
C_{TOTAL} (c€)	1729.89	2307.90	842.83	540.06	906.34	689.09

The cost of the PV shedding and the load shedding and the total cost are respectively shown in Figure 143, Figure 144, and Figure 145.

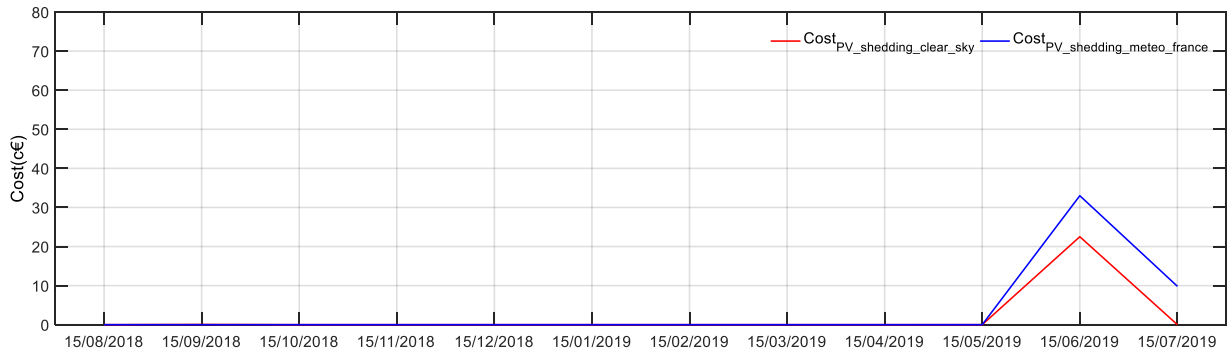


Figure 143. The PV shedding cost comparison between the clear sky model and the Météo France model.

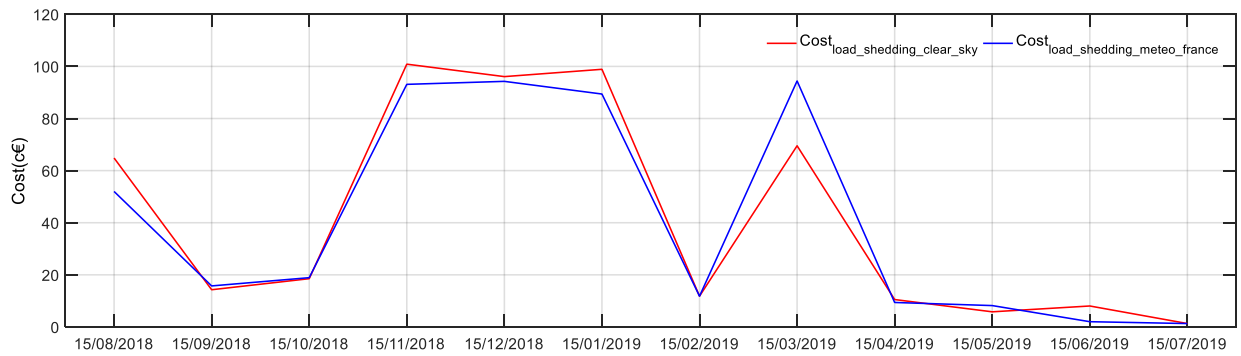


Figure 144. The load shedding cost comparison between the clear sky model and the Météo France model.

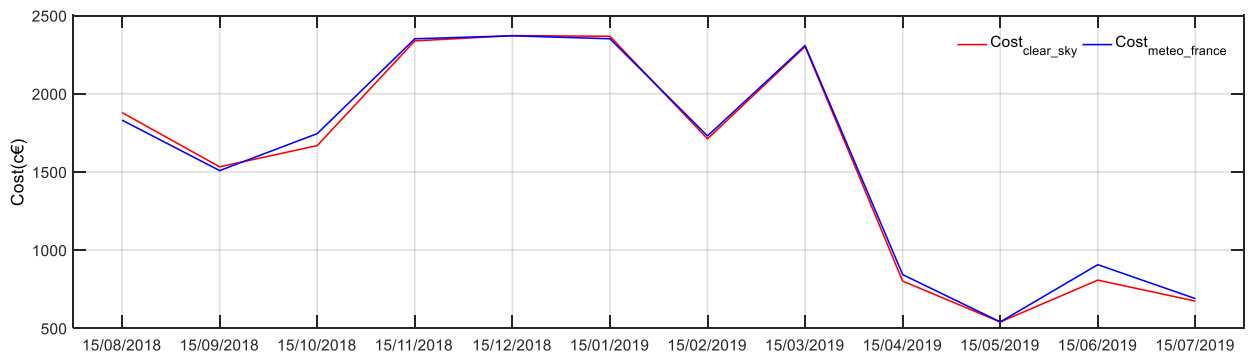


Figure 145. The total cost comparison between the clear sky model and the Météo France model.

In Figure 143, Figure 144, and Figure 145, we can draw similar results like the ones shown in case 2.

V.3.2.2. Simulation results comparison and analysis

The simulation results are compared through the indexes: the average difference of cost AVR , and a percentage of AVR and the average cost of the Météo France model S_{AVR} in Table 37.

Table 37. Simulation results of the cases.

Case	AVR_{PVS} (c€)	AVR_{LDS} (c€)	AVR_{TOTAL} (c€)	$S_{AVR_{PVS}}$	$S_{AVR_{LDS}}$	$S_{AVR_{TOTAL}}$
1	1.56	-1.04	-11.02	0.12%	0.08%	0.85%
2	-1.09	1.10	-17.56	0.06%	0.06%	1.10%
3	-1.68	0.82	-15.21	0.10%	0.05%	0.95%

Comparing the indexes in Table 37, the analyzes can achieve the following:

1. In case 1, we can see that the AVR_{PVS} is positive representing that the clear sky model leads to more cost than the Météo France model in PV power shedding, the AVR_{LDS} is negative representing that the clear sky model achieves less cost than the Météo France model in load power shedding. AVR_{TOTAL} is positive also representing the same results as AVR_{LDS} . However, those cost differences between the clear sky model and the Météo France model are very small shown the indexes, $S_{AVR_{PVS}}$, $S_{AVR_{LDS}}$ and $S_{AVR_{TOTAL}}$.
2. Case 2 and 3 have the same results as case 1, and the AVR_{PVS} and AVR_{LDS} in case 2 and case 3 are opposite to case 1 because of the influence of the power loss in the converters.

V.3.3. Simulation analyzes

The results of the clear sky model are close to the results of the Météo France model. Thus, the results of the two models have no big difference in three conditions, the ideal converter without considering converter efficiency, the conversion efficiency of the power converter, and power management considering the power converter efficiency. Besides, the cost varies as the month, the total cost in winter is higher than the total cost in summer.

V.4. Conclusion

The PV prediction is the key for the optimization of the full DC microgrid, which is deciding the results of the operation cost of the full DC microgrid and can be calculated according to the solar irradiation on the PV panel. Luckily, there are many ways to get solar information for the PV power prediction, this chapter proposes to compare two simple methods, the clear sky model and the Météo France model. The clear sky model is simplified to be suitable for a quick calculation to get the solar irradiation.

In this chapter, firstly, the clear sky model and the Météo France model are introduced. Then the supervisory system of the full DC microgrid is given to valid the two models before. The simulation scenario is designed to be three cases for a comprehensive validation. By comparing the three simulation

cases in one year, we can know that the clear sky model has a similar effect to the Météo France model in the optimization of the full DC microgrid. Meanwhile, we can conclude that the total cost of the full DC microgrid varies with the seasons, and the total cost in winter is higher than the total cost in summer because of the changes in solar irradiation. The clear sky model is a powerful alternative model when there are problems with the Météo France model data acquisition, for example, there is no internet, or the official website does not upload data in time. Also, the clear sky model can be used in the real-time optimization by a model prediction controller with considering the local real-time information, such as: cloud position, real-time atmospheric transmittance, etc.

General conclusions and perspectives

In the long history of the electric power system, the power generation, the power transmission, and the power distribution, have been developing and progressing continuously, integrating modern science and technology, in order to better serve users. Nowadays, with the continuous growth of global electricity consumption, energy demand continues to increase. However, the environmental carrying capacity and natural resources restrict the increase of traditional energy sources with mature technologies. Therefore, the challenge in the energy field has prompted mankind to continuously develop renewable energy. In recent years, the cost of PV energy has been decreasing year by year, prompting the establishment of large-scale renewable energy power plants. However, the collection and utilization of renewable energy requires strong energy management capabilities, and the integrated storage of renewable energy power generation can better ensure the effective use of renewable energy. However, large-scale PV power plants need to take up a large area, and wind power plants may impact the environment, so these large-scale power plants here are more suitable to be built in remote areas. If a large number of renewable energy power plants are built, the transmission of electricity will be a considerable cost. Therefore, the current research believes that the PV energy installed on the roof and locally consumed can effectively reduce the use of public grid energy and relieve the pressure on the public grid. Thus, the microgrid came into being. The wide application of microgrid has reduced the operating pressure of the power grid and increased the penetration and utilization rate of renewable energy. However, the initial investment cost of establishing a microgrid is still considerable. With the continuous development of equipment and devices, people believe that the cost of microgrids will decrease year by year.

Microgrid is becoming more and more mature, and the application of microgrids is becoming more and more widespread. The core of microgrid is the efficient bi-directional power converter, efficient and fast controller, mature energy, and power management system. The DC microgrid is simpler and more efficient with less converter to directly supply the DC appliances for local prosumers than AC microgrid. Thus, in this thesis, the research focuses on the power and energy management system in DC microgrid, which is also called microgrid supervisory system. In the supervisory system, there are many challenges that are required to be solved, such as the intermittency of the PV sources, the efficiency of the bi-directional converter, the controller, the power balance in the microgrid, the physical limitations of the device, the multi-time scale optimization considering multiple optimization objectives of microgrid.

In DC microgrid, there are two main operation models, grid-connected mode, and off-grid mode including islanded mode and isolated mode. Firstly, the thesis is aiming to propose a supervisory system for both grid-connected model and off-grid model, which is called full microgrid supervisory system in this thesis. The supervisory has two main layers and they need to be design, the operational layer, and the optimization layer. In the operational layer of the full DC microgrid, the sources from both grid-

connected model and off-grid model are considered; the renewable sources have the priority to supply the load demand; if the renewable sources cannot deal with the load demand, then the public grid and the BS is used to supply or store the rest power; the back-up sources can supply the load demand if the other components cannot supply the load demand. Therefore, the real-time load demand optimization is introduced in the operational layer. Thus, the power in the full DC microgrid can exchange power with the public grid and the back-up sources can also give a guarantee to the load demand. In the optimization layer, the day-ahead optimization is done considering the constraints of every component. In the day-ahead optimization, the objective is to minimize the total operation cost. Thus, the tariff of the components in the DC microgrid is pre-defined. Then, the day-ahead optimization is formulated considering the almost the same rule as the operational layer in order to make the constraints of the optimization close to the condition as the operational layer. It is important if the supervisory system can operate in 24 hours, which means whether the supervisory system can be applied in actual scenarios. In order to achieve the 24 hours' operation of the supervisory system, the rule of the operational layer and the day-ahead optimization are modified to suitable for the 24 hours' operation.

Then, the thesis is aiming to consider the non-linear constraints of the dynamic efficiency of the converter in the full DC microgrid. If the power loss is not considered, the stability of the system will become lower, and the energy loss of the system may increase. Thus, the thesis is focused on the non-linear constraints in optimization that are difficult to solve with the pure mathematical solver. Thus, we seek new methods to approximate non-linear constraints. The piecewise function is easy method to linearize the non-linear constraints, the disadvantage is that the constraints is increased with new linear constraints which is approximated from the non-linear constraints.

The proposed supervisory system is reliable to the prediction accuracy of the PV power and load demand power. In this thesis, the research is based on a real case of the university building. Before the research of the load demand prediction, the load data and load prediction data of this university are got from the EDF company, which are almost the same with little difference. Thus, in the research of the load demand prediction, it is assumed that the load demand prediction is close to the real load demand. However, in the research of PV power prediction, the PV power is very dependent on the solar irradiation. Thus, to get an accuracy solar irradiation on a surface is the key to calculate the accuracy PV prediction power. Fortunately, it is easy to get the solar irradiation from Meteo France, however it is quite difficult to get accuracy prediction irradiation because of the intermitted PV power. Sometimes, the free solar irradiation cannot be got in some days, which give a bad influence on the DC microgrid cost. Thus, this thesis compares a solar irradiation prediction model, which can work at any time with only the information of the geographic information of the PV panel with a little computation.

After concluding the main research work of this thesis, the originality of this thesis concludes as given below.

Firstly, this thesis considering the advantage of the grid-connected and off-grid model of a DC microgrid, proposed a full DC microgrid. Then, this thesis designed a supervisory system for the full DC microgrid. In the proposed DC microgrid, the real-time load demand optimization is applied, and the SC is used to supply the power deficiency while the DG start-up. Then, in the proposed supervisory system, the day-ahead optimization problem is formulated and solved by CPLEX. Furthermore, the supervisory system can operate in 24 hours. The results show the advanced of the full DC microgrid with the proposed supervisory system. The less load shedding is achieved with a less increased cost. Thus, this full DC microgrid with the proposed supervisory system has a better performance than the DC microgrid only considering the grid-connected model or the off-grid model.

Secondly, this thesis considers the converter efficiency in the DC microgrid supervisory system. The operational layer of the supervisory system can apply the converter model to calculate the power loss of the converter in real-time, which is regarded as the power complementary in converter by using the controller. Then, this thesis also considers the power loss of the converter in the optimization layer of the supervisory system. The day-ahead optimization problem is formulated considering the linearized power loss constraints. The simulation results show the operational layer considering the power loss can reduce the fluctuation of the DC bus voltage, and the day-ahead optimization can reduce the overall operation cost the DC microgrid.

Thirdly, this thesis concentrates on the PV power prediction. Thus, this thesis compares two model for the solar irradiation prediction. The results show that the two have almost the same results in the proposed full DC microgrid.

The accomplished work during this thesis opens up several perspectives, which are also the key points needed to be improved.

Firstly, the real-time power management strategy in the operational layer of the full DC microgrid is too regular that the power management should be modified when the full DC microgrid is changed. Then, in order to formulate the same problem as the power management strategy in the operational layer, the constraints of the day-ahead optimization are too strict. The better way is to formulate the least constraints in ensuring the safety of the DC microgrid, and the new optimization problem can be solved in real-time.

Secondly, it is an improvement to consider the dynamic efficiency of the converter in DC microgrid supervisory system. The simulation results also show the effectiveness of the real-time power management considering the dynamic efficiency of the converter. The drawback is that the results is not good when the day-ahead optimization considering the dynamic efficiency of the converter is used. The reason is that the inconsistent between the real-time power management strategy in the operational layer of the DC microgrid and the day-ahead optimization in the optimization layer. The real-time power management strategy has its rule to optimize the real-time power. However, the rule in the power management strategy is too difficult to formulate in the day-ahead optimization problem. Thus, the day-

ahead optimization is to solve a problem, which is close to the rule in the power management strategy. Furthermore, if the day-ahead optimization cannot solve the problem with non-linear constraints of the dynamic efficiency of the converter in real-time, the results will be improved when the real-time management strategy can introduce the real-time optimization results.

Thirdly, the day-ahead optimization in the DC microgrid is very dependent on the accuracy of the PV power prediction and load power prediction. However, the prediction model cannot give a more accuracy prediction result. Although the CK model can achieve the results close to the results of the MF model with a little computation, the CK model cannot make the accuracy real-time prediction and also does not consider the real environment with cloud and building. Thus, it is necessary to build a better PV prediction model considering the real environment.

To sum up, the thesis proposes a full DC microgrid gathering the advantages of the DC microgrid operating at grid-connected model and the DC microgrid operating at off-grid model. Then, the supervisory system is proposed for the full DC microgrid. In the real-time power management layer of the supervisory system, a rule is used based on the tariff of every component to optimize the power at real-time, and a load demand optimization is applied to optimize the load at real-time. Then, a day-ahead optimization is proposed to optimize the power flow and achieve global minimal cost. In addition, the full DC microgrid can operate for 24 hours with a supervisory system for 24 hours. Then, considering the dynamic efficiency of the converter, the thesis proposes a new supervisory system to reduce the power loss in converter and get more stable DC bus voltage. Then the thesis compares two model to be used in the PV power prediction. The results show the proposed full DC microgrid and supervisory system gives a reference for the application of the DC microgrid.

In future work, an advanced problem for DC micorgrid should be built considering the non-linear constaints in the DC microgrid. The computation of the proposed problem should be fast to satisfy the real-time regularition of the DC microgrid. Furthermore, the decentralized supervisory system is a competitive method with some distributed consensus theory, such as mult-agent system with a negotiation technology. Also, the artificial intelligence can be considered as an advanced modeling method to the DC microgrid to directly build a model for the relationship among variables only considering massive input and output data. In general, an intelligent microgrid with less cost enhanced security, eco-friendly, and easy access is the future power grid.

References

- [1] Jiang W., et al., *A Multiagent-Based Hierarchical Energy Management Strategy for Maximization of Renewable Energy Consumption in Interconnected Multi-Microgrids*. IEEE Access, 2019. **7**: p. 169931-169945.
- [2] Shamshirband S., Rabczuk T., and Chau K.-W., *A Survey of Deep Learning Techniques: Application in Wind and Solar Energy Resources*. IEEE Access, 2019. **7**: p. 164650-164666.
- [3] Elavarasan R.M., et al., *A Comprehensive Review on Renewable Energy Development, Challenges, and Policies of Leading Indian States With an International Perspective*. IEEE Access, 2020. **8**: p. 74432-74457.
- [4] Yi W., et al., *Multiobjective Robust Scheduling for Smart Distribution Grids: Considering Renewable Energy and Demand Response Uncertainty*. IEEE Access, 2018. **6**: p. 45715-45724.
- [5] Masera M., et al., *Smart (Electricity) Grids for Smart Cities: Assessing Roles and Societal Impacts*. Proceedings of the IEEE, 2018. **106**(4): p. 613-625.
- [6] Haghghat H., Karimianfard H., and Zeng B., *Integrating Energy Management of Autonomous Smart Grids in Electricity Market Operation*. IEEE Transactions on Smart Grid, 2020. **11**(5): p. 4044-4055.
- [7] Harmon E., et al., *The Internet of Microgrids: A Cloud-Based Framework for Wide Area Networked Microgrids*. IEEE Transactions on Industrial Informatics, 2018. **14**(3): p. 1262-1274.
- [8] Ren L. and Zhang P., *Generalized Microgrid Power Flow*. IEEE Transactions on Smart Grid, 2018. **9**(4): p. 3911-3913.
- [9] Anoh K., et al., *Energy Peer-to-Peer Trading in Virtual Microgrids in Smart Grids: A Game-Theoretic Approach*. IEEE Transactions on Smart Grid, 2020. **11**(2): p. 1264-1275.
- [10] Arcos-Aviles D., et al., *Fuzzy Logic-Based Energy Management System Design for Residential Grid-Connected Microgrids*. IEEE Transactions on Smart Grid, 2018. **9**(2): p. 530-543.
- [11] Tang Z., Hill D.J., and Liu T., *A Novel Consensus-Based Economic Dispatch for Microgrids*. IEEE Transactions on Smart Grid, 2018. **9**(4): p. 3920-3922.
- [12] Ross M., et al., *Microgrid Economic Dispatch With Energy Storage Systems*. IEEE Transactions on Smart Grid, 2018. **9**(4): p. 3039-3047.
- [13] Xiao J., et al., *Multiobjective optimization model of collaborative dispatch in the microgrids*. in *2019 International Conference on Advanced Mechatronic Systems (ICAMEchS)*. 2019.
- [14] Shuai H., et al., *Stochastic Optimization of Economic Dispatch for Microgrid Based on Approximate Dynamic Programming*. IEEE Transactions on Smart Grid, 2018: p. 1-1.
- [15] Xia H., et al., *Distributed Control Method for Economic Dispatch in Islanded Microgrids With Renewable Energy Sources*. IEEE Access, 2018. **6**: p. 21802-21811.
- [16] Xu Y. and Zhang J., *A two-layer two-stage dispatching strategy for active distribution network with micro-grid considering multiple interactions*. Electric Power Systems Research, 2020. **187**.
- [17] Velasquez M.A., et al., *Hierarchical dispatch of multiple microgrids using nodal price: an approach from consensus and replicator dynamics*. Journal of Modern Power Systems and Clean Energy, 2019. **7**(6): p. 1573-1584.
- [18] Li Y., et al., *Optimization of Dynamic Dispatch for Multiarea Integrated Energy System Based on Hierarchical Learning Method*. IEEE Access, 2020. **8**: p. 72485-72497.
- [19] Chouhan S., et al. *DER optimization to determine optimum BESS charge/discharge schedule using Linear Programming*. in *2016 IEEE Power and Energy Society General Meeting (PESGM)*. 2016.
- [20] Conte F., et al., *Mixed-Integer Algorithm for Optimal Dispatch of Integrated PV-Storage Systems*. IEEE Transactions on Industry Applications, 2019. **55**(1): p. 238-247.
- [21] Makohin D.G., et al. *Design and Implementation of a Flexible Microgrid Controller through Mixed Integer Linear Programming Optimization*. in *2018 9th IEEE International Symposium on Power Electronics for Distributed Generation Systems (PEDG)*. 2018.
- [22] Lara J.D., Olivares D.E., and Cañizares C.A., *Robust Energy Management of Isolated Microgrids*. IEEE Systems Journal, 2019. **13**(1): p. 680-691.

- [23] Zhao B., et al., *Robust Optimal Dispatch of AC/DC Hybrid Microgrids Considering Generation and Load Uncertainties and Energy Storage Loss*. IEEE Transactions on Power Systems, 2018. **33**(6): p. 5945-5957.
- [24] Zhou Y., et al., *Generation Scheduling of Self-generation Power Plant in Enterprise Microgrid with Wind Power and Gateway Power Bound Limits*. IEEE Transactions on Sustainable Energy, 2019: p. 1-1.
- [25] Garcia D.J., Gong J., and You F., *Multi-Stage Adaptive Robust Optimization over Bioconversion Product and Process Networks with Uncertain Feedstock Price and Biofuel Demand*, in *26th European Symposium on Computer Aided Process Engineering*. 2016. p. 217-222.
- [26] Lei X., et al., *A Bi-Layer Multi-Time Coordination Method for Optimal Generation and Reserve Schedule and Dispatch of a Grid-Connected Microgrid*. IEEE Access, 2019. **7**: p. 44010-44020.
- [27] Zhou B., et al., *Optimal Scheduling of Biogas–Solar–Wind Renewable Portfolio for Multicarrier Energy Supplies*. IEEE Transactions on Power Systems, 2018. **33**(6): p. 6229-6239.
- [28] Liu G., Xu Y., and Tomsovic K., *Bidding Strategy for Microgrid in Day-Ahead Market Based on Hybrid Stochastic/Robust Optimization*. Ieee Transactions on Smart Grid, 2016. **7**(1): p. 227-237.
- [29] Choobineh M. and Mohagheghi S., *Robust Optimal Energy Pricing and Dispatch for a Multi-Microgrid Industrial Park Operating Based on Just-In-Time Strategy*. IEEE Transactions on Industry Applications, 2019: p. 1-1.
- [30] Li Y., et al., *Multi-Objective Optimal Dispatch of Microgrid Under Uncertainties via Interval Optimization*. IEEE Transactions on Smart Grid, 2019. **10**(2): p. 2046-2058.
- [31] Li C., et al., *Economic Dispatch for Operating Cost Minimization Under Real-Time Pricing in Droop-Controlled DC Microgrid*. IEEE Journal of Emerging and Selected Topics in Power Electronics, 2017. **5**(1): p. 587-595.
- [32] Xiao J., et al., *Multi-Level Energy Management System for Real-Time Scheduling of DC Microgrids With Multiple Slack Terminals*. IEEE Transactions on Energy Conversion, 2016. **31**(1): p. 392-400.
- [33] Zhao J. and P.L. *Decentralized two-stage control for active power real time dispatch in islanded AC microgrids*. in *2017 IEEE Conference on Energy Internet and Energy System Integration (EI2)*. 2017.
- [34] Maulik A. and Das D., *Optimal power dispatch considering load and renewable generation uncertainties in an AC–DC hybrid microgrid*. IET Generation, Transmission & Distribution, 2019. **13**(7): p. 1164-1176.
- [35] Zhou Q., et al., *Two-Layer Control Scheme for Maintaining the Frequency and the Optimal Economic Operation of Hybrid AC/DC Microgrids*. IEEE Transactions on Power Systems, 2019. **34**(1): p. 64-75.
- [36] Liu S. and Yu W. *Two-time-scale stochastic optimization dispatch of PV-microgrid considering demand side management*. in *2017 36th Chinese Control Conference (CCC)*. 2017.
- [37] Zhaoxia X., et al. *Multiple time-scale optimization scheduling for islanded microgrids including PV, wind turbine, diesel generator and batteries*. in *IECON 2017 - 43rd Annual Conference of the IEEE Industrial Electronics Society*. 2017.
- [38] He X., Zhao Y., and Huang T., *Optimizing the Dynamic Economic Dispatch Problem by the Distributed Consensus-based ADMM Approach*. IEEE Transactions on Industrial Informatics, 2019: p. 1-1.
- [39] Ahmad J., Tahir M., and Mazumder S.K., *Dynamic Economic Dispatch and Transient Control of Distributed Generators in a Microgrid*. IEEE Systems Journal, 2019. **13**(1): p. 802-812.
- [40] Marzband M., et al., *Distributed Smart Decision-Making for a Multimicrogrid System Based on a Hierarchical Interactive Architecture*. Ieee Transactions on Energy Conversion, 2016. **31**(2): p. 644-655.
- [41] Du Y., et al. *Coordinating multi-microgrid operation within distribution system: A cooperative game approach*. in *2017 IEEE Power & Energy Society General Meeting*. 2017.
- [42] Xu Q., et al., *A Decentralized Control Strategy for Economic Operation of Autonomous AC, DC, and Hybrid AC/DC Microgrids*. IEEE Transactions on Energy Conversion, 2017. **32**(4): p. 1345-1355.

- [43] Duan J. and Chow M., *Robust Consensus-Based Distributed Energy Management for Microgrids With Packet Losses Tolerance*. IEEE Transactions on Smart Grid, 2020. **11**(1): p. 281-290.
- [44] Zeraati M., Golshan M.E.H., and Guerrero J.M., *A Consensus-Based Cooperative Control of PEV Battery and PV Active Power Curtailment for Voltage Regulation in Distribution Networks*. Ieee Transactions on Smart Grid, 2019. **10**(1): p. 670-680.
- [45] Li Q., et al., *Consensus-Based Distributed Economic Dispatch Control Method in Power Systems*. IEEE Transactions on Smart Grid, 2019. **10**(1): p. 941-954.
- [46] Nutkani I.U., et al., *Decentralized Economic Dispatch Scheme With Online Power Reserve for Microgrids*. IEEE Transactions on Smart Grid, 2017. **8**(1): p. 139-148.
- [47] Wen Y., et al., *Microgrid Dispatch with Frequency-Aware Islanding Constraints*. IEEE Transactions on Power Systems, 2019: p. 1-1.
- [48] Kong X., et al., *Hierarchical Distributed Model Predictive Control of Standalone Wind/Solar/Battery Power System*. IEEE Transactions on Systems, Man, and Cybernetics: Systems, 2019: p. 1-12.
- [49] Khalid M., *Wind Power Economic Dispatch – Impact of Radial Basis Functional Networks and Battery Energy Storage*. IEEE Access, 2019. **7**: p. 36819-36832.
- [50] Huang B., et al., *Distributed Optimal Economic Dispatch for Microgrids Considering Communication Delays*. IEEE Transactions on Systems, Man, and Cybernetics: Systems, 2019: p. 1-9.
- [51] Dong G. and Chen Z., *Data-Driven Energy Management in a Home Microgrid Based on Bayesian Optimal Algorithm*. IEEE Transactions on Industrial Informatics, 2019. **15**(2): p. 869-877.
- [52] Ma W.-J., et al., *Distributed Energy Management for Networked Microgrids Using Online ADMM With Regret*. IEEE Transactions on Smart Grid, 2018. **9**(2): p. 847-856.
- [53] Sechilariu M. and Locment F., *Chapter 4 - Direct Current Microgrid Power Modeling and Control*, in *Urban DC Microgrid*, Sechilariu M. and Locment F., Editors. 2016, Butterworth-Heinemann. p. 133-170.
- [54] Wu H., Sechilariu M., and Locment F., *Influence of Dynamic Efficiency in the DC Microgrid Power Balance*. Energies, 2017. **10**(10).
- [55] Mariam L., Basu M., and Conlon M.F., *Microgrid: Architecture, policy and future trends*. Renewable and Sustainable Energy Reviews, 2016. **64**: p. 477-489.
- [56] Kumar M. and Tyagi B. *A state of art review of microgrid control and integration aspects*. in *2016 7th India International Conference on Power Electronics (IICPE)*. 2016.
- [57] Alramlawi M. and Li P., *Design Optimization of a Residential PV-Battery Microgrid With a Detailed Battery Lifetime Estimation Model*. IEEE Transactions on Industry Applications, 2020. **56**(2): p. 2020-2030.
- [58] Yin C., et al., *Energy management of DC microgrid based on photovoltaic combined with diesel generator and supercapacitor*. Energy Conversion and Management, 2017. **132**: p. 14-27.
- [59] Yang C., et al., *Dynamic event-triggered robust secondary frequency control for islanded AC microgrid*. Applied Energy, 2019. **242**: p. 821-836.
- [60] Weber L.G., Nasiri A., and Akbari H., *Dynamic Modeling and Control of a Synchronous Generator in an AC Microgrid Environment*. IEEE Transactions on Industry Applications, 2018. **54**(5): p. 4833-4841.
- [61] Bai W., Sechilariu M., and Locment F., *DC Microgrid System Modeling and Simulation Based on a Specific Algorithm for Grid-Connected and Islanded Modes with Real-Time Demand-Side Management Optimization*. Applied Sciences, 2020. **10**(7).
- [62] Ramabhotla S., et al., *Operation and Maintenance Cost Optimization in the Grid Connected Mode of Microgrid*, in *Proceedings 2016 Eighth Annual Ieee Green Technologies Conference*. 2016. p. 56-61.
- [63] Lingamuthu R. and Mariappan R., *Power flow control of grid connected hybrid renewable energy system using hybrid controller with pumped storage*. International Journal of Hydrogen Energy, 2019. **44**(7): p. 3790-3802.
- [64] Sechilariu M. and Locment F., *Chapter 3 - Backup Power Resources for Microgrid*, in *Urban DC Microgrid*, Sechilariu M. and Locment F., Editors. 2016, Butterworth-Heinemann. p. 93-132.

- [65] Meng L., et al., *Microgrid supervisory controllers and energy management systems: A literature review*. Renewable and Sustainable Energy Reviews, 2016. **60**: p. 1263-1273.
- [66] Kotra S. and Mishra M.K., *A Supervisory Power Management System for a Hybrid Microgrid With HESS*. IEEE Transactions on Industrial Electronics, 2017. **64**(5): p. 3640-3649.
- [67] Villalva M.G., Gazoli J.R., and Filho E.R., *Comprehensive Approach to Modeling and Simulation of Photovoltaic Arrays*. IEEE Transactions on Power Electronics, 2009. **24**(5): p. 1198-1208.
- [68] Sechilariu M. and Locment F., *Chapter 2 - Photovoltaic Source Modeling and Control*, in *Urban DC Microgrid*, Sechilariu M. and Locment F., Editors. 2016, Butterworth-Heinemann. p. 35-91.
- [69] Yin C., et al., *Power Management Strategy for an Autonomous DC Microgrid*. Applied Sciences, 2018. **8**(11).
- [70] Trigueiro dos Santos L., Sechilariu M., and Locment F., *Optimized Load Shedding Approach for Grid-Connected DC Microgrid Systems under Realistic Constraints*. Buildings, 2016. **6**(4).
- [71] *IBM ilog cplex optimizer*.; Available from: <http://ibm.com>.
- [72] Houssamo I., *Contribution à l'étude théorique, à la modélisation et à la mise en œuvre d'un système multisource appartenant à un micro-réseau électrique. Considérations sur la qualité de l'énergie*. 2012, UNIVERSITE DE TECHNOLOGIE DE COMPIEGNE.
- [73] Wang B., *Intelligent control and power flow optimization of microgrid : energy management strategies*. 2013, UNIVERSITE DE TECHNOLOGIE DE COMPIEGNE.
- [74] Trigueiro dos Santos L., *Contribution on the day-ahead and operational optimization for DC microgrid building-Integrated*. 2017, UNIVERSITE DE TECHNOLOGIE DE COMPIEGNE.
- [75] Wu H., *Étude et analyse globale de l'efficacité énergétique d'un micro-réseau urbain à courant continu*. 2017, UNIVERSITE DE TECHNOLOGIE DE COMPIEGNE.
- [76] Yin C., *Impact of diesel generator operating modes on standalone DC microgrid and control strategies implying supercapacitor*. 2018, UNIVERSITE DE TECHNOLOGIE DE COMPIEGNE.
- [77] Li R., et al., *A novel time-of-use tariff design based on Gaussian Mixture Model*. Applied Energy, 2016. **162**: p. 1530-1536.
- [78] Dagdougui H., Ouammi A., and Sacile R., *Towards a Concept of Cooperating Power Network for Energy Management and Control of Microgrids*, in *Microgrid*. 2017. p. 231-262.
- [79] Awais M., et al., *Real-Time Pricing with Demand Response Model for Autonomous Homes*, in *2015 Ninth International Conference on Complex, Intelligent, and Software Intensive Systems*. 2015. p. 134-139.
- [80] Wang Y. and Li L., *Critical peak electricity pricing for sustainable manufacturing: Modeling and case studies*. Applied Energy, 2016. **175**: p. 40-53.
- [81] Bin W., et al. *The optimization of CPP strategy based on load data analysis*. in *2016 China International Conference on Electricity Distribution (CICED)*. 2016.
- [82] Wang Z. and Li F. *Critical peak pricing tariff design for mass consumers in Great Britain*. in *2011 IEEE Power and Energy Society General Meeting*. 2011.
- [83] Amyotte M. and Ordonez M., *Power Loss Prediction for Distributed Energy Resources: Rapid Loss Estimation Equation*. IEEE Transactions on Industrial Electronics, 2020: p. 1-1.
- [84] Yallamilli R.S. and Mishra M.K., *Instantaneous Symmetrical Component Theory Based Parallel Grid Side Converter Control Strategy for Microgrid Power Management*. IEEE Transactions on Sustainable Energy, 2019. **10**(2): p. 682-692.
- [85] Mahmood H. and Jiang J., *Decentralized Power Management of Multiple PV, Battery, and Droop Units in an Islanded Microgrid*. IEEE Transactions on Smart Grid, 2019. **10**(2): p. 1898-1906.
- [86] Aghdam M.M., Li L., and Zhu J., *Comprehensive study of finite control set model predictive control algorithms for power converter control in microgrids*. IET Smart Grid, 2020. **3**(1): p. 1-10.
- [87] Wei B., et al., *Temporally coordinated energy management for AC/DC hybrid microgrid considering dynamic conversion efficiency of bidirectional AC/DC converter*. IEEE Access, 2020: p. 1-1.

- [88] Yuan W., et al., *Adaptive Droop Control Strategy of Autonomous Microgrid for Efficiency Improvement*, in *2019 IEEE 10th International Symposium on Power Electronics for Distributed Generation Systems (PEDG)*. Xi'an, China. p. 972-977.
- [89] Stevanoni C., et al., *Long-Term Planning of Connected Industrial Microgrids: A Game Theoretical Approach Including Daily Peer-to-Microgrid Exchanges*. IEEE Transactions on Smart Grid, 2019. **10**(2): p. 2245-2256.
- [90] Lyu Z.L., Wang X.Q., and Yang Z.X. *Optimal dynamic dispatch of pareto frontier for microgrid based on MOIBBO algorithm*. in *2017 IEEE Power & Energy Society General Meeting*. 2017.
- [91] Denoix T., Sechilariu M., and Locment F., *Experimental comparison of photovoltaic panel operating cell temperature models*. Proceedings, IECON 2014 - 40th Annual Conference of the IEEE Industrial Electronics Society, 2015: p. 2089-2095.
- [92] Tuohy A., et al., *Solar Forecasting: Methods, Challenges, and Performance*. IEEE Power and Energy Magazine, 2015. **13**(6): p. 50-59.
- [93] Duffie J.A. and Beckman W.A., *Solar Engineering of Thermal Processes, 4th edn*.
- [94] Kalogirou S.A., *Environmental Characteristics*, in *Solar Energy Engineering*. 2014, Academic Press. p. 51-123.
- [95] Wu H., et al., *Optimal Power Dispatching in the DC Microgrid with Clear Sky Irradiance Model*, in *ELECTRIMACS 2019*, Walter Zamboni G.P., Editor. 2017, Springer: Salerno, Italy.
- [96] Kumar K.P. and Saravanan B., *Day ahead scheduling of generation and storage in a microgrid considering demand Side management*. Journal of Energy Storage, 2019. **21**: p. 78-86.
- [97] Sankar V.C.J., Sreehari P., and Nair M.G. *Day ahead optimal scheduling of an islanded urban micro grid with distributed active generator units*. in *2017 International Conference on Technological Advancements in Power and Energy (TAP Energy)*. 2017.
- [98] Yang M., Wang J., and An J., *Day-Ahead Optimization Scheduling for Islanded Microgrid Considering Units Frequency Regulation Characteristics and Demand Response*. IEEE Access, 2020. **8**: p. 7093-7102.
- [99] Zeinal-Kheiri S., et al., *Real-time energy management in a microgrid with renewable generation, energy storages, flexible loads and combined heat and power units using Lyapunov optimisation*. IET Renewable Power Generation, 2020. **14**(4): p. 526-538.
- [100] Jia Y., et al., *Distributed Economic Model Predictive Control for a Wind-Photovoltaic-Battery Microgrid Power System*. IEEE Transactions on Sustainable Energy, 2020. **11**(2): p. 1089-1099.
- [101] Shi Y., et al., *Model Predictive Control for Smart Grids With Multiple Electric-Vehicle Charging Stations*. Ieee Transactions on Smart Grid, 2019. **10**(2): p. 2127-2136.

Appendices

Appendix 1: Parameters of Solar-Fabrick series SF 130/2

Appendix 2: Parameters of Sonnenschein Solar: S12/6.6A

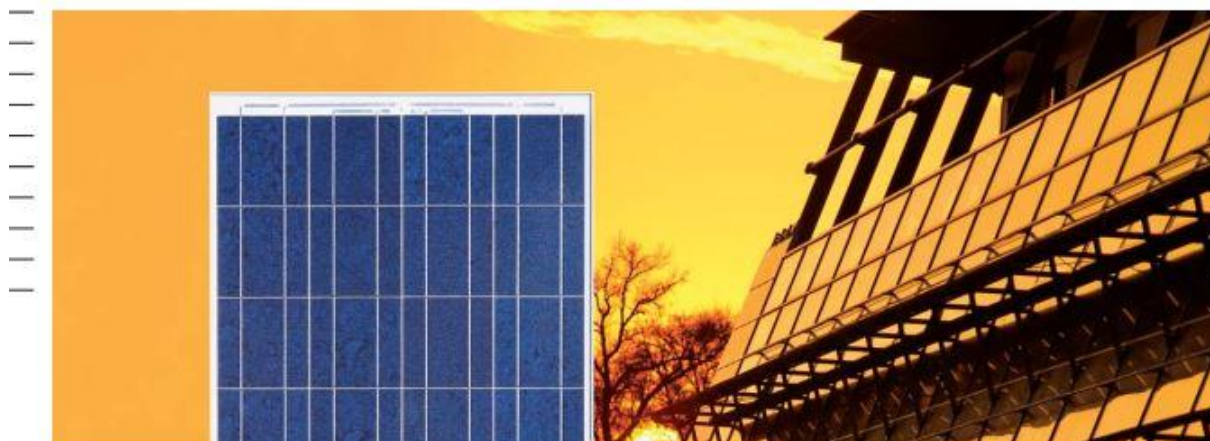
Appendix 3: Parameters of Maxwell 75V modules: BMOD0094 P075 B02

Appendix 4: Parameters of SDMO Technic 6500E AVR

Appendix 5: IGBT Semikron SKM 100GB063D

Appendix 1: Parameters of Solar-Fabrik series SF 130/2

Module Photovoltaïque Solar-Fabrik Série SF 130/2



Une qualité optimale de série:

- Stabilité dans le temps grâce au verre solaire spécial transparent, équipé de filtre UV
- Présélection et tri des cellules à 100 %
- Rendement énergétique élevé grâce à l'utilisation de composants de qualité appairés avec précision (cf. l'étude « Power Check » de l'institut Fraunhofer ISE)
- Techniques de production de pointe et système de gestion de la qualité certifié (ISO 9001), pour la garantie d'une qualité produit « made in Germany »
- Cadre de module en aluminium spécialement développé en option; montage rapide et facile avec le système de fixation breveté Profilink; esthétique avantageuse grâce aux fixations intégrées
- Charge du panneau jusqu'à: 5400 Pa selon la norme IEC 61215
- Critères de tri très sélectifs de seulement +/- 2,5 W (= 1,9 %) pour éviter une première sélection des modules.
- Contrôles réguliers des modules de calibrage pour la mesure de la puissance à l'Institut Fraunhofer de systèmes à énergie solaire (ISE)

Dimensions

Série SF 130/2	Sans cadre	Cadre alu
l x L (mm)	1485 x 663	1491 x 669
Épaisseur (mm)	5	35
Poids (kg)	10,5	12,5

Homologations/Certifications

EN IEC 61215 ed. 2
Classe de protection II
Directive 89/336/CEE (CE)
Directive 73/23/CEE (CE)



Caractéristiques module Solar-Fabrik Série SF 130/2

Type de module	SF 130/2-125	SF 130/2-130	SF 130/2-135
Nombre de cellules (polycristallin)	36	36	36
Tension max. système	840 V	840 V	840 V

Caractéristiques électriques en STC (Standard Test Conditions: 1000 W/m², 25 °C, AM 1,5)

Puissance nominale*	P _{max}	125 W	130 W	135 W
Limites de tri puissance		+/- 2,5 W	+/- 2,5 W	+/- 2,5 W
Tension appr.	U _{MPP}	17,50 V	17,72 V	17,94 V
Tension circuit ouvert appr.	U _{OC}	21,53 V	21,69 V	21,86 V
Courant appr.	I _{MPP}	7,14 A	7,34 A	7,52 A
Courant de court-circuit appr.	I _{SC}	7,84 A	7,96 A	8,08 A

Caractéristiques électriques sous 800 W/m², NOCT, AM 1,5

Puissance en MPP appr.	P _{max}	96 W	100 W	104 W
Tension appr.	U _{MPP}	17,67 V	17,90 V	18,12 V
Tension circuit ouvert appr.	U _{OC}	21,26 V	21,42 V	21,59 V
Courant appr.	I _{MPP}	5,43 A	5,58 A	5,72 A
Courant de court-circuit appr.	I _{SC}	5,88 A	5,97 A	6,07 A

Sous un ensoleillement de 200 W/m² et une température de 25 °C, le rendement diminue de 7 % environ par rapport au rendement en conditions standard STC.

Températures

Coefficient de température tension	T _K (U _{OC})	-72 mV/K
Coefficient de température courant	T _K (I _{SC})	5,45 mA/K
NOCT		45 °C +/- 4K

Autres caractéristiques

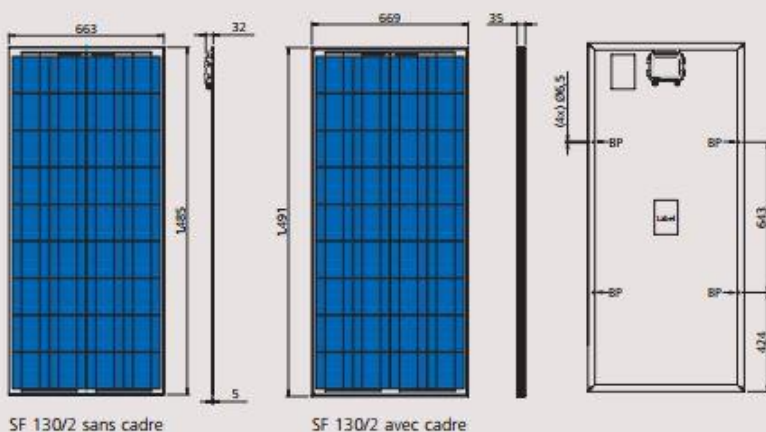
Test haute tension	Tension d'essai 3200 V _{DC} /max. 60µA
Tenue à la grêle **	Jusqu'à 25 mm de diamètre à 23 m/s
Résistance à la tempête **	Vitesse du vent jusqu'à 130 km/h = 800 Pa et facteur de sécurité 3
Charge de neige supportée **	Sans cadre: 2400 Pa Δ 245 kg/m ²
Contrainte testée selon IEC 61215	Avec cadre: 5400 Pa Δ 550 kg/m ²

* (tolérance +/- 5 %)

** en combinaison avec notre système de fixation breveté Profilink installé selon les recommandations (BP) Sous réserve de modifications techniques.

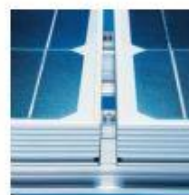
Garantie de puissance: 25 ans conformément à nos conditions de garantie supplémentaires, envoyées sur demande.

Certifié par le VDE (Association des électrotechniciens allemands) selon les normes DIN EN ISO 9001, Reg.Nr. 5002983/QM/11.2003 / DIN EN ISO 14001, Reg.Nr. 5002983/UM/11.2003

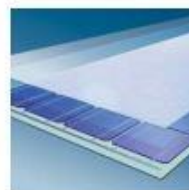


SF 130/2 sans cadre

SF 130/2 avec cadre



Un système de fixation efficace: Profilink



Structure du module: verre spécialement trempé à faible teneur en fer/film vinyl transparent en acétate d'éthyle (EVA)/cellules photovoltaïques/EVA/feuille arrière en Tedlar



Solar-Fabrik AG
Munzinger Straße 10
79111 Freiburg / Allemagne
tél. +49-(0)761-4000-0
fax +49-(0)761-4000-199
www.solar-fabrik.de

État: 15.12.2006, Solar-Fabrik AG
Document n° 0612MD8153

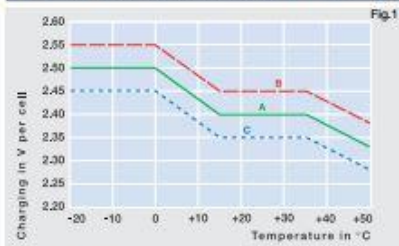
Appendix 2: Parameters of Sonnenschein Solar: S12/6.6A

Solar series



Technical characteristics and data

Type	Part number	Nominal voltage V	Nominal capacity C_{100} 1.8 V/C Ah	Discharge current I_{100} A	Length (l) max. mm	Width (b/w) max. mm	Height up to top of cover (h1) max. mm	Height incl. con- nectors (h2) max. mm	Weight approx. kg	Terminal	Terminal position
S12/6.6 S	NGSO1206D6HS0SA	12	6.6	0.066	151.7	65.5	94.5	98.4	2.6	S-4.8	3
S12/17 G5	NGSO120017HS0BA	12	17.0	0.170	181.0	76.0	-	167.0	6.1	G-M5	1
S12/27 G5	NGSO120027HS0BA	12	27.0	0.270	167.0	176.0	-	126.0	9.7	G-M5	1
S12/32 G6	NGSO120032HS0BA	12	32.0	0.320	197.0	132.0	160.0	184.0	11.2	G-M6	2
S12/41 A	NGSO120041HS0CA	12	41.0	0.410	210.0	175.0	-	175.0	14.8	A-Terminal	1
S12/60 A	NGSO120060HS0CA	12	60.0	0.600	261.0	136.0	208.0	230.0	19.0	A-Terminal	1
S12/85 A*	NGSO120085HS0CA	12	85.0	0.850	353.0	175.0	-	190.0	27.3	A-Terminal	1
S12/90 A	NGSO120090HS0CA	12	90.0	0.900	330.0	171.0	213.0	236.0	31.3	A-Terminal	2
S12/130 A	NGSO120130HS0CA	12	130.0	1.300	286.0	269.0	208.0	230.0	39.8	A-Terminal	4
S12/230 A	NGSO120230HS0CA	12	230.0	2.300	518.0	274.0	216.0	238.0	70.0	A-Terminal	3

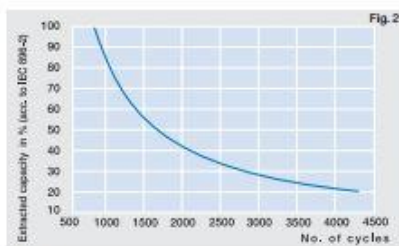
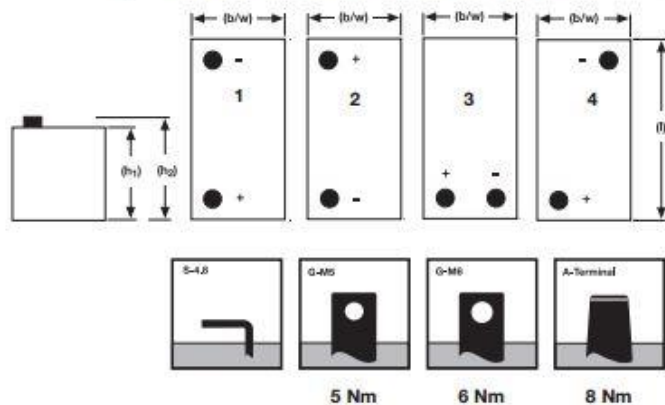


Charge mode (to Fig.1):

- 1.) with switch regulator (two-step controller)
 - charge on curve B (max.charge voltage) for max.2 hrs/day then switch over to continuous charge - curve C
- 2.) Standard charge (without switching) - curve A
- 3.) Boost charge (Equalizing charge with external generator)
 - charge on curve B for max. 5 hrs/month, then switch over to curve C

Type	Capacities $C_1 - C_{100}$ (20°C)				
	C_1 1.70 V/C	C_5 1.70 V/C	C_{10} 1.70 V/C	C_{20} 1.75 V/C	C_{100} 1.80 V/C
S12/6.6 S	2.9	4.6	5.1	5.7	6.6
S12/17 G5	9.3	12.6	14.3	15.0	17.0
S12/27 G5	15.0	22.1	23.5	24.0	27.0
S12/32 G6	16.9	24.4	27.0	28.0	32.0
S12/41 A	21.0	30.6	34.0	38.0	41.0
S12/60 A	30.0	42.5	47.5	50.0	60.0
S12/85 A	55.0	68.5	74.0	76.0	85.0
S12/90 A	50.5	72.0	78.0	84.0	90.0
S12/130 A	66.0	93.5	104.5	110.0	130.0
S12/230 A	120.0	170.0	190.0	200.0	230.0

Drawings with terminal position, terminal and torque



(to Fig. 2)

Endurance in cycles according to IEC 896-2

* S12/85 A = 400 cycles

Not to scale!

Appendix 3: Parameters of Maxwell 75V modules: BMOD0094 P075 B02

DATASHEET
75V MODULE

FEATURES AND BENEFITS*

- Up to 15 year DC life
- 75V DC working voltage
- Resistive cell balancing
- Temperature outputs
- High power density

TYPICAL APPLICATIONS

- Wind turbine pitch control
- UPS systems



PRODUCT SPECIFICATIONS

ELECTRICAL	BMOD0094 P075 B02
Rated Capacitance ¹	94 F
Minimum Capacitance, initial ¹	94 F
Maximum Capacitance, initial ¹	113 F
Maximum ESR _{DC} , initial ¹	13 mΩ
Test Current for Capacitance and ESR _{DC} ¹	100 A
Rated Voltage	75 V
Absolute Maximum Voltage ²	91 V
Absolute Maximum Current	1,900 A
Leakage Current at 25°C, maximum ³	50 mA
Maximum Series Voltage	750 V
Capacitance of Individual Cells ⁹	3,000 F
Maximum Stored Energy, Individual Cell ⁹	3.0 Wh
Number of Cells	32

TEMPERATURE	
Operating Temperature (Cell Case Temperature)	
Minimum	-40°C
Maximum	65°C
Storage Temperature (Stored Uncharged)	
Minimum	-40°C
Maximum	70°C

*Results may vary. Additional terms and conditions, including the limited warranty, apply at the time of purchase. See the warranty details for applicable operating and use requirements.

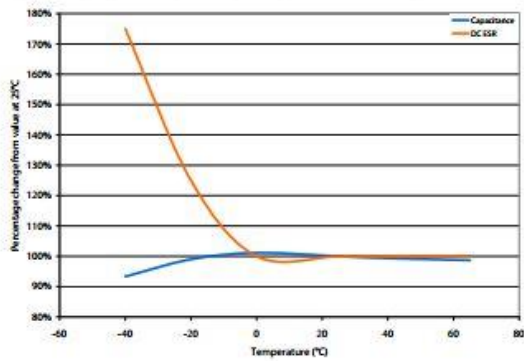
PRODUCT SPECIFICATIONS (Cont'd)

PHYSICAL		BMOD0094 P075 B02
Mass, typical		25 kg
Power Terminals		M8/M10
Recommended Torque - Terminal		20/30 Nm
Vibration Specification		SAE J2380
Shock Specification		N/A
Environmental Protection		IP54
Cooling		Natural Convection
MONITORING / CELL VOLTAGE MANAGEMENT		
Internal Temperature Sensor		RTD
Temperature Interface		Analog
Cell Voltage Monitoring		N/A
Connector		Harting
Cell Voltage Management		Passive
POWER & ENERGY		
Usable Specific Power, P_d^4		2,100 W/kg
Impedance Match Specific Power, P_{max}^5		4,300 W/kg
Specific Energy, E_{max}^6		2.9 Wh/kg
Stored Energy, E_{stored}^7		73 Wh
SAFETY		
Short Circuit Current, typical (Current possible with short circuit from rated voltage. Do not use as an operating current.)		5,800 A
Certifications		RoHS
High-Pot Capability ¹⁰		2,500 VDC

TYPICAL CHARACTERISTICS

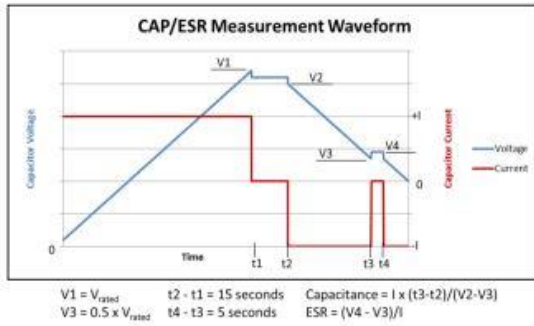
THERMAL CHARACTERISTICS		BMOD0094 P075 B02
Thermal Resistance ($R_{\theta ca}$, All Cell Cases to Ambient), typical ⁸		0.50°C/W
Thermal Capacitance (C_{th}), typical		19,000 J/°C
Maximum Continuous Current ($\Delta T = 15^\circ\text{C}$) ⁸		48 A _{RMS}
Maximum Continuous Current ($\Delta T = 40^\circ\text{C}$) ⁸		78 A _{RMS}
LIFE		
DC Life at High Temperature ¹ (held continuously at Rated Voltage and Maximum Operating Temperature)		1,500 hours
Capacitance Change (% decrease from minimum initial value)		20%
ESR Change (% increase from maximum initial value)		100%
Projected DC Life at 25°C ¹ (held continuously at Rated Voltage)		15 years
Capacitance Change (% decrease from minimum initial value)		20%
ESR Change (% increase from maximum initial value)		100%
Shelf Life (Stored uncharged at 25°C)		4 years

ESR AND CAPACITANCE VS TEMPERATURE



NOTES

1. Capacitance and ESR_{DC} measured at 25°C using specified test current per waveform below.
2. Absolute maximum voltage, non-repeated. Not to exceed 1 second.
3. After 72 hours at rated voltage. Initial leakage current can be higher.
4. Per IEC 62391-2, $P_d = \frac{0.12V^2}{ESR_{DC} \times \text{mass}}$
5. $P_{max} = \frac{V^2}{4 \times ESR_{DC} \times \text{mass}}$
6. $E_{max} = \frac{1/2 CV^2}{3,600 \times \text{mass}}$
7. $E_{stored} = \frac{1/2 CV^2}{3,600}$
8. $\Delta T = I_{RMS}^2 \times ESR \times R_{ca}$
9. Per United Nations material classification UN3499, all Maxwell ultracapacitors have less than 10 Wh capacity to meet the requirements of Special Provisions 361. Both individual ultracapacitors and modules composed of those ultracapacitors shipped by Maxwell can be transported without being treated as dangerous goods (hazardous materials) under transportation regulations.
10. Duration = 60 seconds. Not intended as an operating parameter.



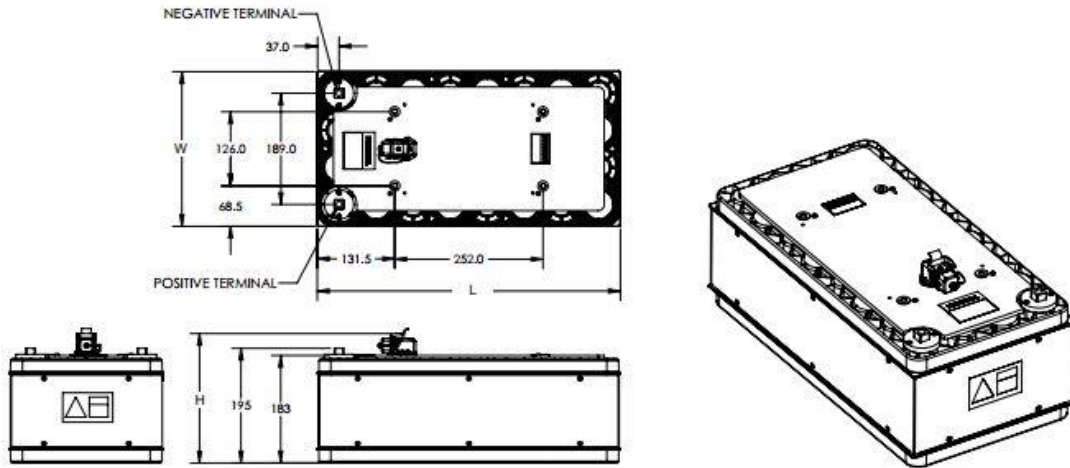
MOUNTING RECOMMENDATIONS

Please refer to the user manual for installation recommendations

MARKINGS

Products are marked with the following information: Rated capacitance, rated voltage, product number, name of manufacturer, positive and negative terminal, warning marking, serial number.

BMOD0094 P075 B02



Part Description	Dimensions (mm)			Package Quantity
	L (±0.3mm)	W (±0.2mm)	H (±0.7mm)	
BMOD0094 P075 B02	515	263	220	1

Product dimensions are for reference only unless otherwise identified. Product dimensions and specifications may change without notice. Please contact Maxwell Technologies directly for any technical specifications critical to application. All products featured on this datasheet are covered by the following U.S. patents and their respective foreign counterparts: 6643119, 7295423, 7342770, 7352558, 7384433, 7440258, 7492571, 7508651, 7791860, 7791861, 7859826, 7883553, 7935155, 8072734, 8098481, 8279580, and patents pending.



Maxwell Technologies, Inc.
Global Headquarters
3888 Calle Fortunada
San Diego, CA 92123
USA
Tel: +1 858 503 3300
Fax: +1 858 503 3301



Maxwell Technologies SA
Route de Montena 65
CH-1728 Rossens
Switzerland
Tel: +41 (0)26 411 85 00
Fax: +41 (0)26 411 85 05



Maxwell Technologies, GmbH
Leopoldstrasse 244
80807 München
Germany
Tel: +49 (0)89 / 4161403 0
Fax: +49 (0)89 / 4161403 99



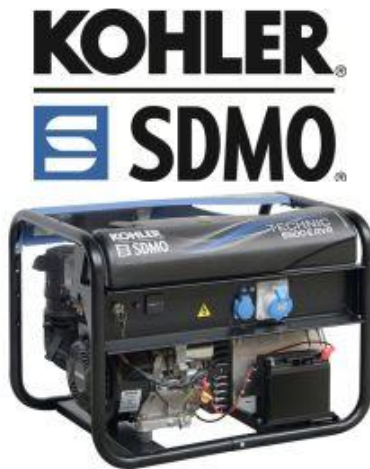
Maxwell Technologies, Inc.
Shanghai Trading Co. Ltd.
Unit A2,C 12th Floor
Huarun Times Square
500 Zhangyang Road,
Pudong New Area
Shanghai 200122,
P.R. China
Phone: +86 21 3852 4000
Fax: +86 21 3852 4099



Maxwell Technologies Korea Co., Ltd.
Room 1524, D-Cube City
Office Tower, 15F #662
Gyeongin-Ro, Guro-Gu,
Seoul, 152-706
South Korea
Phone: +82 10 4518 9829

MAXWELL TECHNOLOGIES, MAXWELL, MAXWELL CERTIFIED INTEGRATOR, ENABLING ENERGY'S FUTURE, BOOSTCAP, C CELL, D CELL and their respective designs and/or logos are either trademarks or registered trademarks of Maxwell Technologies, Inc. and may not be copied, imitated or used, in whole or in part, without the prior written permission Maxwell Technologies, Inc. All contents copyright © 2014 Maxwell Technologies, Inc. All rights reserved. No portion of these materials may be reproduced in any form, or by any means, without prior written permission from Maxwell Technologies, Inc.

Appendix 4: Parameters of SDMO Technic 6500E AVR



TECHNIC 6500 E AVR

PORTABLE POWER
Generating Sets Range TECHNIC

- PRODUCT ADVANTAGES**
- Entire group guaranteed 3 years
 - KOHLER air-cooled industrial engine
 - Connection interface equipped with an hour meter
 - Electric starter with batteries without maintenance
 - AVR : Automatic tension regulation

QUAD CLEAN AIR FILTER The Cyclonic Quad Clean air filters provide 4 levels of filtration which effectively filter out large particles and capture the finest particles. They ensure a continuous supply of clean air to the engine, fuel economies, increase the engine performance and extend its lifetime

AVR By regulating the voltage electronically by $\pm 2\%$, depending on the model, the AVR eliminates all risk of damage to boilers or certain kinds of electronic equipment.

Range TECHNIC
A long run time equipment that can withstand extreme conditions, for daily professional use.

TECHNIC 6500 E AVR

GENERAL SPECIFICATIONS

Range	TECHNIC
Frequency (Hz)	50 Hz
Max power LTP (kW) *	6.50
Nominal voltage (V)	230
Number of Phase	Single phase
Fuel	Petrol
Tank (L)	18
75% cons. (l/h) *	2.60
75% Autonomy (h) *	6.90
Sound power level guaranteed LwA dB(A)	97
Acoustic pressure level @1m in dB(A)	83
Acoustic pressure level @7m in dB(A)	69

ENGINE SPECIFICATIONS

Engine brand	KOHLER
Engine type	CH440E
Distribution	O.H.V.
Start	Electrical Starter
Oil shutdown	Oui
Displacement (cm3)	429
Oil system capacity including filters (L)	1.30

ALTERNATOR SPECIFICATIONS

Technology	Collar and brush
AVR Regulation	Yes
Indication of protection	IP 23
Insulation class	H

PLUGS AND PANEL DESCRIPTIVE

1 230V 10/16A socket - circuit breaker + 1 230V 32A socket - circuit breaker + hour meter

DIMENSIONS AND WEIGHT

Length (cm)	81
Width (cm)	55.50
Height (cm)	59
Dry Weight (kg)	101

PACKAGING

Packaging type	Box
Length (cm)	82
Width (cm)	56.50
Height (cm)	60
Weight (kg)	104
Pallet type	120/80
Number of box by pallet	6
Pallet height (cm)	193
weight of the packaged Pallet (kg)	634



TECHNIC 6500 E AVR - PORTABLE POWER - Generating Sets TECHNIC
 This document is not contractual - The SDMO company reserves the right to modify any of the characteristics stated in this document without notice, in a constant effort to improve the quality of its products. *ISO 8528.
 SDMO Industries • 270 rue de Kerervern • CS 40047 • 29801 Brest cedex 9 - France • Tél. +33 (0)2 98 41 41 41 • www.kohlersdmo.com

Appendix 5: IGBT Semikron SKM 100GB063D

SKM 100GB063D



SEMITRANS[®] 2

Superfast NPT-IGBT Module

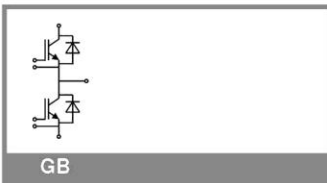
SKM 100GB063D

Features

- N channel, homogeneous Silicon structure (NPT- Non punch through IGBT)
- Low tail current with low temperature dependence
- High short circuit capability, self limiting if term. G is clamped to E
- Pos. temp.-coeff. of V_{CEsat}
- Very low C_{ies} , C_{oes} , C_{res}
- Latch-up free
- Fast & soft inverse CAL diodes
- Isolated copper Bonding Technology without hard mould
- Large clearance (10 mm) and creepage distances (20 mm)

Typical Applications*

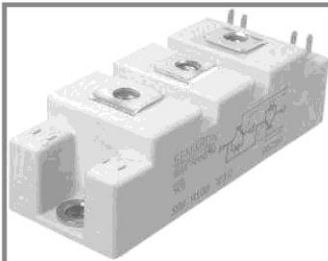
- Switching (not for linear use)
- Switched mode power supplies
- UPS
- Three phase inverters for servo / AC motor speed control
- Pulse frequencies also above 10 kHz



Absolute Maximum Ratings		$T_c = 25^\circ\text{C}$, unless otherwise specified		
Symbol	Conditions	Values	Units	
IGBT				
V_{CES}	$T_j = 25^\circ\text{C}$	600	V	
I_C	$T_j = 150^\circ\text{C}$	130	A	
	$T_{case} = 25^\circ\text{C}$ $T_{case} = 70^\circ\text{C}$	100	A	
I_{CRM}	$I_{CRM} = 2 \times I_{Cnom}$	200	A	
V_{GES}		± 20	V	
t_{psc}	$V_{CC} = 300\text{ V}; V_{GE} \leq 20\text{ V}; T_j = 125^\circ\text{C}$ $V_{CES} < 600\text{ V}$	10	μs	
Inverse Diode				
I_F	$T_j = 150^\circ\text{C}$	$T_{case} = 25^\circ\text{C}$	100	A
		$T_{case} = 80^\circ\text{C}$	75	A
I_{FRM}	$I_{FRM} = 2 \times I_{Fnom}$	200	A	
I_{FSM}	$t_p = 10\text{ ms}; \sin.$	720	A	
Module				
$I_{t(RMS)}$		200	A	
T_{vj}		- 40 ... + 150	$^\circ\text{C}$	
T_{slg}		- 40 ... + 125	$^\circ\text{C}$	
V_{isol}	AC, 1 min.	2500	V	

Characteristics		$T_c = 25^\circ\text{C}$, unless otherwise specified			
Symbol	Conditions	min.	typ.	max.	Units
IGBT					
$V_{GE(th)}$	$V_{GE} = V_{CE}; I_C = 2\text{ mA}$	4,5	5,5	6,5	V
I_{CES}	$V_{GE} = 0\text{ V}; V_{CE} = V_{CES}; T_j = 25^\circ\text{C}$		0,1	0,3	mA
V_{CE0}		$T_j = 25^\circ\text{C}$	1,05		V
		$T_j = 125^\circ\text{C}$	1		V
r_{CE}	$V_{GE} = 15\text{ V}$	$T_j = 25^\circ\text{C}$	10,5		$\text{m}\Omega$
		$T_j = 125^\circ\text{C}$	14		$\text{m}\Omega$
$V_{CE(sat)}$	$I_{Cnom} = 100\text{ A}; V_{GE} = 15\text{ V}$	$T_j = 25^\circ\text{C}_{chiplev.}$	2,1	2,5	V
		$T_j = 125^\circ\text{C}_{chiplev.}$	2,4	2,8	V
C_{ies}	$V_{CE} = 25; V_{GE} = 0\text{ V}; f = 1\text{ MHz}$		5,6		nF
C_{oes}		0,6		nF	
C_{res}		0,4		nF	
Q_G	$V_{GE} = 0\text{ V} - +15\text{ V}$		240		nC
R_{Gint}	$T_j = ^\circ\text{C}$		0		Ω
$t_{d(on)}$	$R_{Gon} = 10\ \Omega$	$V_{CC} = 300\text{ V}$ $I_C = 100\text{ A}$	50		ns
t_t			40		ns
E_{on}	$R_{Goff} = 10\ \Omega$	$T_j = 125^\circ\text{C}$ $V_{GE} = \pm 15\text{ V}$	4		mJ
$t_{d(off)}$			300		ns
t_t			35		ns
E_{off}			3		mJ
$R_{th(j-c)}$	per IGBT			0,27	K/W

SKM 100GB063D



SEMISTRANS® 2

Superfast NPT-IGBT Module

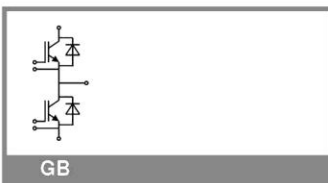
SKM 100GB063D

Features

- N channel, homogeneous Silicon structure (NPT- Non punch through IGBT)
- Low tail current with low temperature dependence
- High short circuit capability, self limiting if term. G is clamped to E
- Pos. temp.-coeff. of V_{CEsat}
- Very low C_{ies} , C_{oes} , C_{res}
- Latch-up free
- Fast & soft inverse CAL diodes
- Isolated copper Bonding Technology without hard mould
- Large clearance (10 mm) and creepage distances (20 mm)

Typical Applications*

- Switching (not for linear use)
- Switched mode power supplies
- UPS
- Three phase inverters for servo / AC motor speed control
- Pulse frequencies also above 10 kHz



Characteristics					
Symbol	Conditions	min.	typ.	max.	Units
Inverse Diode					
$V_F = V_{EC}$	$I_{Fnom} = 100 \text{ A}; V_{GE} = 0 \text{ V}$				
	$T_J = 25 \text{ }^\circ\text{C}_{chiplev.}$		1,55	1,9	V
	$T_J = 125 \text{ }^\circ\text{C}_{chiplev.}$		1,55		V
V_{F0}				0,9	V
	$T_J = 125 \text{ }^\circ\text{C}$				
r_F			8	10	mΩ
	$T_J = 125 \text{ }^\circ\text{C}$				
I_{RRM}	$I_F = 100 \text{ A}$		44		A
Q_{tr}			6		μC
E_{tr}	$V_{GE} = -15 \text{ V}; V_{CC} = 300 \text{ V}$				mJ
$R_{th(j-c)D}$	per diode			0,6	K/W
Module					
L_{CE}				30	nH
R_{CC+EE}	res., terminal-chip	$T_{case} = 25 \text{ }^\circ\text{C}$	0,75		mΩ
		$T_{case} = 125 \text{ }^\circ\text{C}$	1		mΩ
$R_{th(c-s)}$	per module			0,05	K/W
M_s	to heat sink M6		3	5	Nm
M_t	to terminals M5		2,5	5	Nm
w				160	g

This is an electrostatic discharge sensitive device (ESDS), international standard IEC 60747-1, Chapter IX.

* The specifications of our components may not be considered as an assurance of component characteristics. Components have to be tested for the respective application. Adjustments may be necessary. The use of SEMIKRON products in life support appliances and systems is subject to prior specification and written approval by SEMIKRON. We therefore strongly recommend prior consultation of our personal.

SKM 100GB063D



SEMITRANS[®] 2

Superfast NPT-IGBT Module

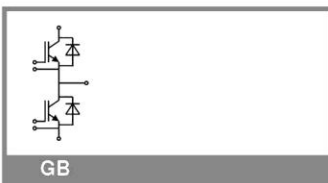
SKM 100GB063D

Features

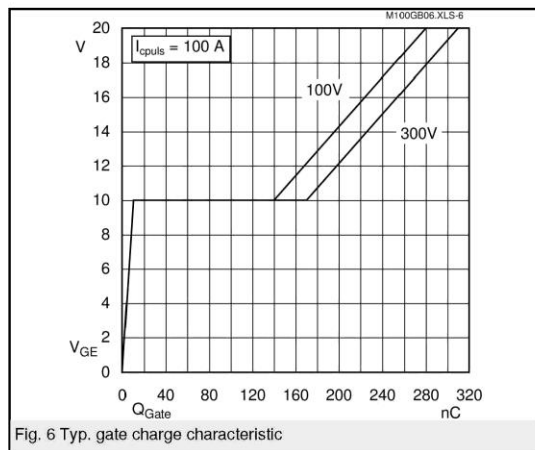
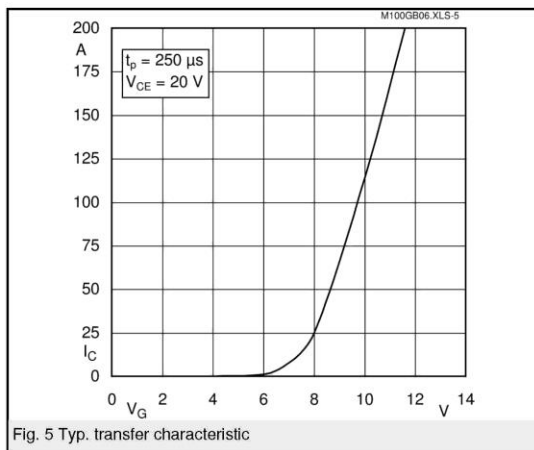
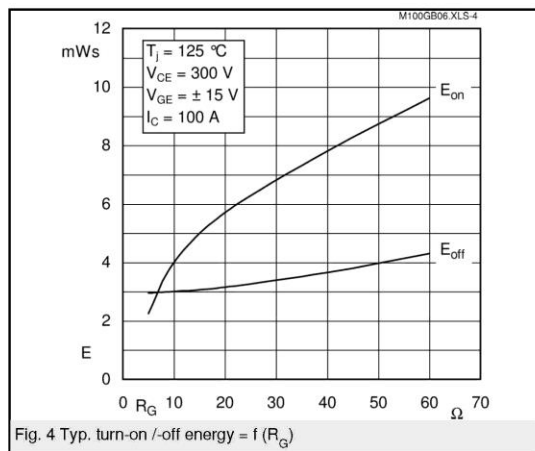
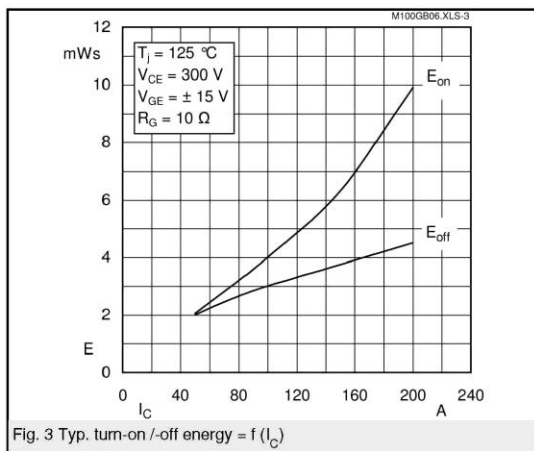
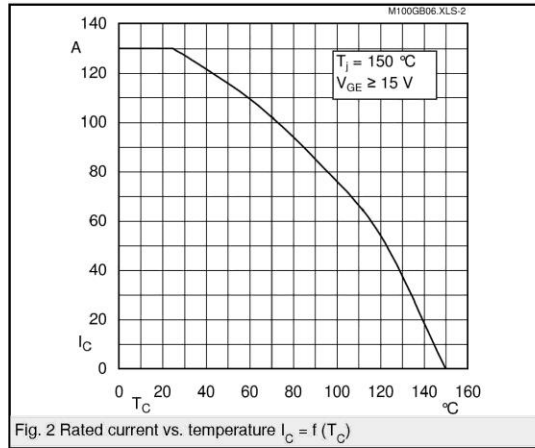
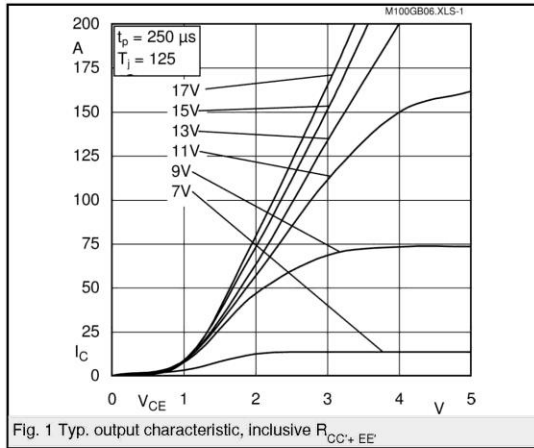
- N channel, homogeneous Silicon structure (NPT- Non punch through IGBT)
- Low tail current with low temperature dependence
- High short circuit capability, self limiting if term. G is clamped to E
- Pos. temp.-coeff. of V_{CEsat}
- Very low C_{ies} , C_{oes} , C_{res}
- Latch-up free
- Fast & soft inverse CAL diodes
- Isolated copper Bonding Technology without hard mould
- Large clearance (10 mm) and creepage distances (20 mm)

Typical Applications*

- Switching (not for linear use)
- Switched mode power supplies
- UPS
- Three phase inverters for servo / AC motor speed control
- Pulse frequencies also above 10 kHz



Z_{th} Symbol	Conditions	Values	Units
$Z_{th(j-c)I}$			
R_{θ}	i = 1	160	mk/W
R_{θ}	i = 2	88	mk/W
R_{θ}	i = 3	18	mk/W
R_{θ}	i = 4	4	mk/W
τ_{ui}	i = 1	0,0447	s
τ_{ui}	i = 2	0,0087	s
τ_{ui}	i = 3	0,0015	s
τ_{ui}	i = 4	0,0002	s
$Z_{th(j-c)D}$			
R_{θ}	i = 1	400	mk/W
R_{θ}	i = 2	165	mk/W
R_{θ}	i = 3	30,5	mk/W
R_{θ}	i = 4	4,5	mk/W
τ_{ui}	i = 1	0,0613	s
τ_{ui}	i = 2	0,0085	s
τ_{ui}	i = 3	0,0045	s
τ_{ui}	i = 4	0,0003	s



SKM 100GB063D

